Alma Mater Studiorum · Università di Bologna

SCUOLA DI SCIENZE
Dipartimento di Fisica e Astronomia
Corso di Laurea Magistrale in Astrofisica e Cosmologia

Exploiting the clustering of cosmic voids as a novel cosmological probe

Presentata da:
Elena Marcuzzo

Relatore:
Prof. Federico Marulli

Correlatori:
Prof. Lauro Moscardini
Dr. Sofia Contarini
Dr. Carlo Giocoli

Sessione I
Anno Accademico 2021/2022

A mamma e papà,
per aver sempre aiutato i miei sogni a prendere forma.

Abstract

The investigations of the large-scale structure of our Universe provide us with extremely powerful tools to shed light on some of the open issues of the currently accepted Standard Cosmological Model, and on its six fundamental parameters. Thanks to the development of both high-precision surveys and numerical simulations, we have been able to achieve progressively tighter constraints. However, this led to the growth of the so-called cosmic tensions, that emerge when comparing high and low redshift probes. In order to disentangle those degeneracies, the ΛCDM model is continuously tested by means of different cosmological probes and their combinations.

Focusing on the largest scales, the volume of the Universe turns out to be almost entirely dominated by the cosmic voids, i.e. large underdense regions among the nodes, filaments, sheets and walls composing the so-called cosmic web. Until recently, constraining the cosmological parameters from cosmic voids was almost infeasible, because the amount of data in void catalogues was not enough to ensure statistically relevant samples. Thus, the constraints from cosmic voids were not competitive with those of other cosmological probes. The increasingly wide and deep fields in present and upcoming surveys have made the cosmic voids emerge in the current cosmological scenario as incredibly promising probes, despite the fact that we are not yet provided with a unique and generally accepted definition of the void radius and inner density. While some properties of the cosmic voids have already been extensively verified and exploited in the literature (see e.g. the void size function), other statistics, such as their auto-correlation function, have never been deployed for cosmological analyses.

In this Thesis, after some necessary theoretical bases of the general properties of our Universe, we address the two-point statistics of cosmic voids, in the very first attempt to model its features with cosmological purposes. To this end, we implement an improved version of the void power spectrum presented by Chan et al., 2014. In particular, we have been able to build up an exceptionally robust method to tackle with the void clustering statistics, by proposing a functional form that is entirely based on first principles. We extract our data from a suite of high-resolution N-body simulations, namely the DUSTGRAIN-*pathfinder*, which account for both the ΛCDM and alternative modified gravity scenarios ($f(R)$ models) in the redshift range $0 \leq z \leq 2$. Since we aim at studying cosmic voids that are traced by both the dark matter particle field and the halo distribution, as a first step of our analysis we extract the halo catalogues by means of a halo finder algorithm. Then, a void finding procedure is employed, and finally the voids are properly cleaned. We do this in order to make the void catalogues consistent with the assumptions used to make reliable predictions of the void size function, i.e. the Vdn model proposed by Jennings et al. (2013). This model, valid for the underlying dark matter field, has been recently extended to the distribution of biased tracers by Contarini et al. (2019) and Contarini et al. (2022).

To accurately compare the data to the theory, we calibrate the model by accounting for a free parameter, which is meant to be a multiplicative factor on the median radius of the analysed void samples. This factor is needed to readjust the theory of the Hard Spheres, which we consider in order to model the void exclusion term. Afterwards, we constrain the cosmological parameters ($\Omega_{\rm m}$ and σ_8, i.e. the matter density parameter and the amplitude of the power spectrum at $z = 0$) by sampling their posterior distributions with Gaussian likelihood and uniform priors. This procedure has been firstly applied to the cosmic voids identified in the dark matter field, within the $\Lambda{\rm CDM}$ cosmological scenario. Furthermore, since we are analysing a suite of simulations designed to study eventual effects of the modified gravity in the large-scale structure of the Universe, we also consider the $f(R)$ cosmologies. Indeed, cosmic voids are proven to be excellent laboratories to test modifications of gravity, thanks to both their shallow gravitational potential and the fact that, within them, the screening mechanism acts only marginally. As far as the modified gravity effects are limited, our auto-correlation model has revealed to be a reliable method to constrain the main $\Lambda{\rm CDM}$ parameters. By contrast, it cannot be used to model the void clustering in those simulations that assume a stronger modification of the gravity, indicating that some additional parameters must be taken into consideration in the model function.

Since the two-point statistics of generic objects depends mainly on the position of their centres, we expect to be able to model the auto-correlation function of voids identified in the halo distribution through the same theoretical formulas as those implemented for the dark matter field, at least at first approximation. However, we have not been able to cross-check our two-point modelling for voids extracted from the halo distribution yet, because the statistics provided by the analysed simulations for samples of voids with large radii is not sufficient to perform a reliable Bayesian analysis.

In future works, we will further develop our analysis on the void clustering statistics, by testing the auto-correlation function model on both larger and higher-resolution simulations, in which the extracted void samples have a definitely better statistical relevance with respect to that of the simulations considered here. One of our further main aims is to apply the whole analysis presented in this Thesis to real data catalogues, in order to provide cosmological constraints from the observed void 2PCF. Finally, we also plan to combine these constraints with the ones provided by other cosmological probes (e.g. void and cluster number counts and density profiles, weak lensing analyses, Ly-α forest, CMB, and many others).

Sommario

Le proprietà della struttura a grande scala del nostro Universo forniscono strumenti estremamente efficaci per fare luce su alcune criticità del Modello Standard, che rappresenta il modello cosmologico attualmente accettato dalla comunità scientifica. Grazie allo sviluppo di campagne osservative e simulazioni numeriche di alta precisione, siamo stati in grado di ottenere vincoli sempre più stretti sui principali parametri del modello ΛCDM. Tuttavia, questo ha portato alla comparsa delle cosiddette tensioni cosmiche, che emergono dal confronto tra *probe* cosmologiche ad alto e basso redshift. Per eliminare queste degenerazioni, il modello ΛCDM viene continuamente testato per mezzo di varie *probe* cosmologiche e loro combinazioni.

Facendo riferimento alle grandi scale, il volume dell'Universo è quasi interamente dominato dai vuoti cosmici, che emergono nella ragnatela cosmica come grandi regioni sottodense. In passato, la quantità di dati presenti nei cataloghi di vuoti non risultava essere sufficiente per garantire dei campioni statisticamente rilevanti e, di conseguenza, non era possibile vincolare i parametri cosmologici per mezzo di questi oggetti. In particolare, questi vincoli non erano competitivi con quelli di altre *probe* cosmologiche. Le campagne osservative e le simulazioni numeriche costruite a campo sempre più ampio e profondo hanno fatto sì che i vuoti cosmici emergessero nell'attuale scenario cosmologico come una *probe* incredibilmente promettente, nonostante non sia ancora stato stabilito un modo univoco per definire e descrivere questi oggetti. Se alcune proprietà dei vuoti cosmici sono già state ampiamente testate e utilizzate in letteratura (per esempio, i conteggi dei vuoti in funzione della loro dimensione), altre statistiche, come la funzione di auto-correlazione, non sono mai state sfruttate in cosmologia.

In questo lavoro di Tesi, dopo aver fornito alcune basi teoriche necessarie per comprendere alcune delle proprietà del nostro Universo, ci siamo occupati della cosiddetta statistica a due punti dei vuoti cosmici, in quello che è il primo tentativo di costruire una modellizzazione affidabile da usare per fini cosmologici. A questo scopo, abbiamo implementato una versione migliore dello spettro di potenza dei vuoti presentato da Chan et al. (2014). Vedremo come, dopo una lunga analisi, siamo riusciti a costruire un metodo eccezionalmente robusto per studiare il *clustering* dei vuoti, proponendo una forma funzionale interamente basata su principi primi. I dati che abbiamo analizzato sono stati estratti nell'intervallo di redshift $0 \leq z \leq 2$ da una serie di simulazioni N-body ad alta risoluzione chiamate DUSTGRAIN-*pathfinder*, costruite assumendo sia la cosmologia del Modello Standard, sia quella legata ai modelli alternativi di gravità modificata (modelli $f(R)$). Poiché il nostro obiettivo è quello di studiare i vuoti cosmici tracciati sia dal campo di particelle di materia oscura sia dalla distribuzione degli aloni, per impostare la nostra analisi abbiamo estratto innanzitutto i cataloghi di aloni tramite un algoritmo implementato con lo scopo di identificarli nel campo totale di materia. In seguito, ci siamo concentrati sull'applicazione di una procedura progettata per la ricerca dei vuoti, sia nei cataloghi di aloni che in quelli di particelle di materia oscura. Infine, i vuoti sono stati opportunamente riscalati secondo il cosiddetto algoritmo di *cleaning*, applicato ai cataloghi di vuoti per renderli consistenti con le assunzioni utilizzate per il calcolo della funzione di distribuzione teorica dei vuoti, secondo il modello Vdn proposto da Jennings et al. (2013). Questo

modello è in realtà valido solo per il campo totale di materia, ma è stato recentemente esteso alla distribuzione dei traccianti affetti da bias da Contarini et al. (2019) e Contarini et al. (2022).

Per un confronto accurato tra i dati e la teoria, abbiamo calibrato il modello considerando un unico parametro libero, da intendersi come un fattore moltiplicativo sul raggio mediano dei vuoti analizzati. Questo fattore è risultato essere necessario per riadattare al caso dei vuoti cosmici la teoria delle *Hard Spheres*, utilizzata allo scopo di modellare il termine di esclusione dei vuoti. A questo punto, abbiamo vincolato i parametri cosmologici ($\Omega_{\rm m}$ e σ_8, ovvero il parametro di densità della materia e l'ampiezza dello spettro di potenza a $z = 0$) tramite il campionamento delle cosiddette distribuzioni a posteriori, assumendo una funzione di verosimiglianza Gaussiana e distribuzioni a priori uniformi. Questa procedura è stata applicata ai vuoti cosmici identificati nel campo di densità della materia oscura nel caso delle simulazioni ΛCDM. Inoltre, avendo a disposizione una serie di simulazioni che comprendono anche scenari cosmologici alternativi di gravità modificata, abbiamo applicato la stessa analisi anche alle cosmologie $f(R)$. In questo modo è stato possibile sfruttare il fatto che i vuoti cosmici sono stati dimostrati essere perfetti laboratori per testare eventuali modifiche della gravità, sia per il loro potenziale gravitazionale poco profondo (e quindi poco variabile in funzione della distanza dal centro), sia perchè al loro interno il meccanismo di *screening* (necessario per ritrovare il comportamento della Relatività Generale sulle piccole scale) agisce solo marginalmente. In questa Tesi abbiamo dimostrato che il nostro modello di auto-correlazione è affidabile per vincolare i principali parametri della cosmologia ΛCDM, e che questo metodo è robusto finchè gli effetti della gravità modificata sono modesti. Al contrario, non può essere utilizzato per modellare il clustering dei vuoti nelle simulazioni che assumono un livello di gravità modificata maggiore e, di conseguenza, in questi casi è necessario introdurre alcuni parametri aggiuntivi nel modello dell'auto-correlazione.

Visto che il clustering di generici oggetti cosmici dipende essenzialmente dalle posizioni dei loro centri, ci aspettiamo, almeno in prima approssimazione, di riuscire modellare accuratamente anche la funzione di auto-correlazione dei vuoti identificati nella distribuzione degli aloni, utilizzando le stesse formule teoriche implementate per il campo delle particelle di materia oscura. Tuttavia, non siamo ancora stati in grado di eseguire un controllo incrociato della nostra modellizzazione sulle misure del clustering ottenute per i vuoti estratti dalla distribuzione degli aloni. Il motivo principale è da ricercarsi nel fatto che la statistica dei cataloghi di vuoti negli aloni, costruiti in accordo con la teoria del modello Vdn, non è sufficiente per eseguire correttamente l'analisi Bayesiana necessaria per vincolare i parametri cosmologici.

Durante lo sviluppo di questa Tesi, abbiamo progettato diversi modi per migliorare l'analisi presentata. In particolare, testeremo il nostro modello di clustering dei vuoti su simulazioni più grandi e a più alta risoluzione, per poter disporre di cataloghi di vuoti con maggiore rilevanza statistica rispetto alle simulazioni considerate in questo lavoro, con l'obiettivo di svilupparne una versione più accurata. Un altro dei nostri obiettivi principali è quello di applicare l'intera analisi presentata in questa Tesi a cataloghi di dati reali, al fine di fornire vincoli cosmologici sfruttando la 2PCF dei vuoti misurata dalle osservazioni. Infine, ci riproponiamo di combinare questi vincoli con quelli forniti da altre *probe* cosmologiche (come, per esempio, i conteggi dei vuoti e degli ammassi, il lensing gravitazionale, la foresta di Ly-α, la CMB, e molte altre).

Contents

Introduction

At present, the Λ-cold dark matter (ΛCDM) concordance model is widely accepted as the Standard Model for our Universe (e.g. Shafieloo and Clarkson, 2010; Heavens et al., 2017). It is based on the existence of the CDM and the dark energy (DE, in the form of the cosmological constant Λ) and it relies on the principles of Einstein's General Relativity. According to this model, the structure formation follows a bottom-up hierarchical scenario resulting in the well known Cosmic Web (van de Weygaert and Schaap, 2009; Cautun et al., 2014; Novosyadlyj and Tsizh, 2017), in which the collapsed structures derive from the positive fluctuations in the primordial density field, while voids are their negative counterpart.

Being these adiabatic perturbations originated by a random process at the end of the inflation[1], the distribution of the initial density contrast is described by a (nearly) Gaussian statistics. As the fluctuations evolve in time going through the nonlinear regime, their distribution looses its Gaussian shape. This results in more bound collapsed structures and an excess of underdense regions. We can use both the overdensities and the underdensities to deal with the main open issues of the ΛCDM model. The clustering of galaxy clusters is related to the nonlinear evolution of the positive perturbations, and the virialization process they undergo erases the memory of the initial conditions. By contrast, voids keep this memory, and this has some important advantages:

- they are just mildly nonlinear,
- they become more spherical as their evolution proceeds,
- in their low-density interiors there are almost no baryons,
- they are extremely sensitive to the diffuse components (i.e. DE and neutrinos) thanks to their emptiness,
- they are severely related to possible modification of gravity (i.e. Modified Gravity) thanks to their shallow gravitational potentials.

Hence, we do think it is important to test potential statistical uses of voids, which are nearly a newborn in the current cosmological framework and, if combined with already well studied probes[2], can help us to unveil the mysteries of our Universe.

[1] The inflation is a period of time in the early stages of the Universe which is supposed to be a fair solution to the main open problems of the ΛCDM model (i.e. the cosmological *flatness*, *horizon* and the *magnetic monopoles* problems).

[2] For example, we refer to galaxy and cluster clustering (e.g. Norberg et al., 2009; Marulli et al., 2012; Castorina et al., 2015; Sereno et al., 2015; Marulli et al., 2017; García-Farieta et al., 2019; Tutusaus et al., 2020), CMB (e.g. Rassat et al., 2014; Planck Collaboration et al., 2020c), Lyman-α forest (e.g. Weinberg et al., 2003; Dijkstra, 2014).

Cosmic voids are large underdense regions among nodes, filaments and walls in the large-scale structure (Coil, 2013) that spatially dominate our Universe[3], since they account for the $90-95\%$ of the whole volume (Platen et al., 2007). Typical void sizes stretch over an extremely wide range of scales going from *minivoids* towards *supervoids*, with linear dimensions of a few to hundreds of megaparsecs (Blumenthal et al., 1992; Tikhonov and Karachentsev, 2006; Szapudi et al., 2015). Traditionally, robust cosmological constraints have been extracted from the high-density regions, firstly because they are observationally favoured and secondly because they have provided the scientific community with higher statistics than voids.

Then the question is *why choosing the cosmic voids?* The reason is that nowadays we are moving towards a very high precision Cosmology thanks to the upcoming wide-field surveys (e.g. DESI[4], Euclid[5], SPHEREx[6], WFIRST[7], LSST[8]; see Pisani et al., 2019 and references therein) which make cosmic voids become competitive as a cosmological probe. Moreover, it is well known that the Universe has recently entered a phase of accelerated expansion (Riess et al., 1998; Schmidt et al., 1998; Perlmutter et al., 1999) and although the Standard Cosmological Model (§1.3) assumes this acceleration is due to the cosmological constant Λ, this raises the two unsolved problems of *fine-tuning* and *coincidence*. To overcome these issues there are mainly two options: considering either the DE equation of state as evolving in time (§1.4.1) or the modified gravity (§1.4.2). As mentioned before, by virtue of their unique properties, cosmic voids are key probes to shed light on these two feasible alternatives.

By considering voids identified both in the DM particle field and in the halo distributions, the main steps we intend to go through are measuring and modelling the void auto-correlation function in order to constrain the cosmological parameters and the void bias. Finally, we also aim at studying the above mentioned void statistics[9] as a mean to disentangle degeneracies among the ΛCDM and the $f(R)$ modified gravity models. To reach our purposes we consider C++ and Python codes, taking advantage in particular of the `CosmoBolognaLib` (§4.1; Marulli et al., 2016) - a set of *free software* libraries for cosmological calculations. Note that we will perform this analysis on simulations in an effort to find methods which can be applied to future observations.

[3] On the other hand, the great majority of the total mass is bounded in the collapsed structures, such as DM haloes, galaxies and galaxy clusters.

[4] Dark Energy Spectroscopic Instrument (DESI): https://www.desi.lbl.gov/.

[5] Euclid: https://www.euclid-ec.org.

[6] SPHEREx: https://spherex.caltech.edu/.

[7] Wide Field Infrared Survey Telescope (WFIRST): https://roman.gsfc.nasa.gov/.

[8] Large Synoptic Survey Telescope (LSST): https://www.lsst.org/.

[9] Other types of void statistics, such as the void size function and the void density profile, have already been studied in e.g. Contarini et al. (2019) and Contarini et al. (2021).

This Master Thesis work is organised as follows:

- in chapter 1 we present a general overview of the cosmological background against which we are working, in order to set the theoretical bases for our analysis;
- in chapter 2 there are the main characteristics of the formation and evolution of cosmic structures, both in the linear and nonlinear regimes;
- in chapter 3 we focus on the cosmic voids as a cosmological probe, providing a detailed description of their definition, identification and relevant statistics;
- in chapter 4 we present the `CosmoBolognaLib`, our simulations and the numerical tools used to produce the void catalogues we analysed;
- in chapter 5 we illustrate step by step the outcomes of our study on the void auto-correlation function, providing an explanation of how we intend to exploit the void clustering statistics in the present cosmological framework;
- in chapter 6 we sum up our main results to draw relevant conclusions and list possible future perspectives of this Thesis, which are necessary to make further steps towards a full cosmological usage of cosmic voids.

Chapter 1

Cosmological framework

Involving the largest scales of the Universe, Cosmology as a research field gives us the perception of the whole in order to figure out the deepest meaning of the physical laws within which we are living. The purpose of the first two chapters is to set the theoretical bases on *(I)* the working principles and models of our Universe, *(II)* the Standard Cosmological Model and its open issues, *(III)* the formation and evolution of the cosmic structures, *(IV)* the large-scale structure of the Universe, namely LSS, *(V)* its statistical properties and *(VI)* the main features of the N-body simulations needed to study the LSS.

Let us underline that we decided to provide some fundamental concepts of Cosmology in order to have the basic requirements needed to understand cosmic voids, their statistical properties and the analyses we have performed (see CHAPTER 3, CHAPTER 4 and CHAPTER 5). The reader who is already familiar with these topics can proceed beyond these first two chapters, by directly approaching the main features of cosmic voids presented in CHAPTER 3.

Nowadays, the favoured cosmological model for our Universe is the so-called ΛCDM. This model is in agreement with the ongoing observations but it is based on two components - the *cold dark matter* and the *cosmological constant* (corresponding to the $\simeq 30\%$ and $\simeq 70\%$ of the total energy budget, respectively) - whose content and behaviour are still far to be fully understood. The Standard Model is built on two milestones:

Gravity. The gravity is the leading force on large scales and it acts following the laws of Einstein's General Relativity (see §1.1).

Cosmological Principle. According to the Cosmological Principle[1] (CP hereafter), on sufficiently large scales (at least hundreds of Megaparsec) the Universe is both *homogeneous* and *isotropic*. This means that both preferred positions and directions do not exist in an average sense. The scientific community trusts this principle because the great majority of present observational data ensure a level of around 10^{-5} for the large scale anisotropy (Coles and Lucchin, 2002)[2].

[1] In the XX century the cosmological investigations were not yet supported by satisfactory observational data and the scientists of that time needed some guiding principle to move the first hesitant steps on their way to define a global theory for the Universe.

[2] These data concern, for example, the Cosmic Microwave Background, the clusters of galaxies and the radiogalaxies. Note that even if the currently adopted concordance model is based on this principle, there is some

1.1 General Relativity and metric definition

As mentioned before, the gravity is the only force to be considered when constructing cosmological models to describe the largest scales of our Universe, at least at first approximation. The gravitational interaction is well characterized by the Einstein's General Relativity[3] (GR hereafter; see Einstein, 1915), a theory that totally transformed the idea of gravity from an interacting force between two massive bodies to a natural outgrowth of the curvature of the spacetime[4]. Indeed, the GR is based on the existence of a **four-dimensional spacetime** where every point is seen as an *event* defined by a four-vector x^μ, with $\mu = 0, 1, 2, 3$. In this context, the geometry is represented by the *metric tensor*[5] $g_{\mu\nu}$, through which we can define the minimum separation between two points in spacetime as follows:

$$\mathrm{d}s^2 = g_{\mu\nu}\mathrm{d}x^\mu \mathrm{d}x^\nu = g_{00}\mathrm{d}t^2 + 2g_{0i}\mathrm{d}t\mathrm{d}x^i + g_{ij}\mathrm{d}x^i\mathrm{d}x^j \ , \tag{1.1}$$

where $\mathrm{d}s^2$ is the so-called *mean square distance* (invariant length), $g_{00}\mathrm{d}t^2$ is the temporal component, $g_{ij}\mathrm{d}x^i\mathrm{d}x^j$ are the spatial components and $2g_{0i}\mathrm{d}t\mathrm{d}x^i$ are the mixed components.

Being the geometry of the spacetime the mirror image of the metric tensor $g_{\mu\nu}$, it is an essential ingredient of the *Einstein Field Equation*:

$$R_{\mu\nu} - \frac{1}{2}g_{\mu\nu}R = \frac{8\pi G}{c^4}T_{\mu\nu} \ , \tag{1.2}$$

where G and c are constants, the *gravitational constant* and the *speed of light*, respectively; $R_{\mu\nu}$ is the *Ricci tensor* and R is the *Ricci scalar*, both defined by means of the *Riemann tensor* $R^\sigma_{\lambda\mu\nu}$; $T_{\mu\nu}$ is the *energy-momentum tensor*. Equation (1.2) is the fundamental equation of the GR theory, and it argues that the curvature of the spacetime is a function of the matter density, energy and pressure content enclosed in our Universe. The left-hand-side (LHS, hereafter) of the equation defines the *Einstein tensor* $G_{\mu\nu}$, which represents the geometry of the spacetime and therefore is sensitive to potential modifications of gravity. By contrast, the right-hand-side (RHS) is characterized by the energy-momentum tensor $T_{\mu\nu}$, which is linked to the matter and energy budget of the Universe and, as a consequence, it depends on possible hidden forms of DE.

Typically, the cosmological models are built by considering the solutions of the Einstein Field Equation valid within the aforementioned Cosmological Principle. It is possible to obtain a general form for the metric starting from the mean square distance between two points in

more recent evidence (e.g. Beisbart, 2009; Schwarz, 2009; Secrest et al., 2021; Nadolny et al., 2021) against the CP. Anyway, we will see in §2.1 that, if verified, the inflation process could provide itself the homogeneity and isotropy of the Universe, without seeking help from the CP *ab initio*.

[3] As a first step, since Albert Einstein noticed the impossibility to reconcile the classical mechanics with the electromagnetism, he gave birth to the theory of Special Relativity in order to get rid of this incompatibility. This theory led to a novel definition of time, which was no longer consistent with the concept of universality. Gravity was later added and the GR theory was developed in a scientific process that lasted more than 10 years.

[4] According to Misner et al. (1973) and Wheeler and Ford (1998), *"spacetime tells matter how to move; matter tells spacetime how to curve"*.

[5] The metric tensor is interpreted as the potential of gravitational forces.

the spacetime as defined in equation (1.1) and ensuring:

- the isotropy (for the essential validity of the CP) by imposing the mixed terms equal to zero, i.e. $g_{0i} = 0$;
- that the light travels at the speed of light c, which means that the RHS equals the distance covered with speed c, i.e. $\mathrm{d}s^2 = 0 \rightarrow g_{00} = c^2$.

This leads to the general metric:

$$\mathrm{d}s^2 = c^2\mathrm{d}t^2 - g_{ij}\mathrm{d}x^i\mathrm{d}x^j = (c\mathrm{d}t)^2 - \mathrm{d}l^2 \,, \tag{1.3}$$

where x^i and x^j are two sets of (spatial) *comoving coordinates*, at rest with respect to the frame of the expanding Universe; t is the *proper time*, defined as the temporal coordinate measured by a clock at rest with respect to the expansion of Universe.

1.1.1 The Friedmann-Lemaître-Robertson-Walker metric

Focusing on the spatial term, to define properly the explicit formula of g_{ij} we need to look for a metric in the three-dimensional space which satisfies the CP we are assuming. Mathematics tells us that there are only three possibilities for a 3D geometry to be consistent with the homogeneity and the isotropy of the CP: *flat*, *spherical* and *hyperbolic* Universe. Hence, in order to obtain a generalized formula for the spatial[6] element $\mathrm{d}l^2$, we

- refer to spherical coordinates (ρ, θ, ϕ) with $0 \leq \rho < \infty$, $0 \leq \theta < \pi$ and $0 \leq \phi < 2\pi$;
- define the *solid angle* as $\mathrm{d}\Omega^2 = \mathrm{d}\theta^2 + \sin^2\theta\,\mathrm{d}\phi^2$;
- consider $\rho \equiv ar$, where $a = a(t)$ is the *cosmic scale factor* and has the dimension of a length, while r is a dimensionless variable ($0 \leq r < \infty$).

Under these assumptions we can write:

$$\mathrm{d}l^2 = a^2\left[r^2\mathrm{d}\Omega^2 + \frac{\mathrm{d}r^2}{1-\kappa r^2}\right] = a^2\left[r^2(\mathrm{d}\theta^2 + \sin^2\theta\,\mathrm{d}\phi^2) + \frac{\mathrm{d}r^2}{1-\kappa r^2}\right], \tag{1.4}$$

where (r, θ, ϕ) are the dimensionless comoving coordinates and κ is the *curvature parameter*. κ is a discrete and adimensionless parameter, which can assume three different values according to the geometry of the space: $\kappa = 0$ flat Universe, $\kappa = 1$ spherical (closed) Universe, $\kappa = -1$ hyperbolic (open) Universe. This parameter is related to the matter and energy density content and it can be used, together with the cosmic scale factor a, to define the *Gaussian curvature* $C_G = \kappa/a^2$.

Finally, sticking together the terms of time and space in the limit of the validity of the CP, we get the Friedmann-Lemaître-Robertson-Walker metric (FLRW hereafter) for the 4D spacetime:

$$\mathrm{d}s^2 = c^2\mathrm{d}t^2 - a^2(t)\left[\frac{\mathrm{d}r^2}{1-\kappa r^2} + r^2(\mathrm{d}\theta^2 + \sin^2\theta\mathrm{d}\phi^2)\right]. \tag{1.5}$$

[6] To describe the metric we take into account the 3D Riemann tensor R_{ijkl} and the Ricci scalar R which determine, the curvature of the 3D space and the scalar curvature, respectively. Assuming the validity of the CP, R_{ijkl} does not depend on $g_{\mu\nu}$ derivatives and R does not depend on $g_{\mu\nu}$ and so it is constant. Thanks to the symmetry of the Riemann tensor, it is possible to define the FLRW metric (eq. 1.5) from equation (1.1) of the general metric.

It is also possible to rewrite the FLRW metric redefining the spatial term $\mathrm{d}l^2$ (eq. 1.4) with the set of coordinates (χ, θ, ϕ), by linking the functional forms of χ to different values of κ in the following way:

$$\chi = F(r) \equiv \int \frac{\mathrm{d}r}{\sqrt{1-\kappa r^2}} = \begin{cases} r & \text{for} \quad \kappa = 0 \\ \sin^{-1}(r) & \text{for} \quad \kappa = +1 \\ \sinh^{-1}(r) & \text{for} \quad \kappa = -1 \end{cases} \tag{1.6}$$

and equation (1.4) becomes:

$$\mathrm{d}l^2 = a^2 \left[\mathrm{d}\chi^2 + f^2(\chi)(\mathrm{d}\theta^2 + \sin^2\theta \mathrm{d}\phi^2) \right], \tag{1.7}$$

where

$$f(\chi) = \begin{cases} \chi & \text{for} \quad \kappa = 0 \\ \sin(\chi) & \text{for} \quad \kappa = +1 \\ \sinh(\chi) & \text{for} \quad \kappa = -1 \end{cases} \tag{1.8}$$

Note that while the spherical closed Universe has a finite volume which can be defined analytically as $V = 2\pi^2 a^3$, the flat and the hyperbolic ones have infinite volumes.

As already noticed before, the CP we assumed to carry on this analytical description of the FLRW metric is reliable on large scales, although there are few evidence that possibly question it (see e.g. Secrest et al., 2021). Of course, both the homogeneity and the isotropy cease to apply when we consider small scales, where the gravitational attraction dominates and the homogeneity is replaced by clumps of collapsed objects spaced out by empty regions. When we consider such small volumes, the Universe does not appear the same in every position we look at it.

1.1.2 Distances, Redshift and Hubble Flow

Due to the well-known expansion, enclosed in the cosmic scale factor $a(t)$, the spatial part of the Universe changes its size as the time flows. There are several possible ways to compute the distance between two points in the spacetime depending on what we need to deal with.

It is important to clarify such different definitions of distance, since it is a crucial quantity when performing cosmological analyses. Let us specify that in this Thesis work we will refer both to the *comoving* separations and the redshift.

Proper Distance. The simplest possible concept of distance is the one we are commonly used to consider, the *proper distance*, that is the real distance between two objects. It can be measured by taking into account a fixed scale factor $a = a(t) = const$, i.e. to a given time t corresponds a certain value of the cosmic scale factor. Let us consider two points $\vec{p}$ and $\vec{q}$ in the spacetime, for example the observer and an external galaxy, at $t = const$ i.e. $\mathrm{d}t = 0$. We make an additional assumption, by aligning the reference frame considered with the distance we are measuring; as a consequence, $\mathrm{d}\theta = \mathrm{d}\phi = 0$. To compute the proper distance between

those points in the context of the FLRW metric we can use the following formula:

$$d_{\rm pr} = a(t) \int_0^r \frac{{\rm d}r'}{\sqrt{1-\kappa r'}} = a(t) F(r) \ , \tag{1.9}$$

where $F(r)$ (eq. 1.6) depends on the curvature describing the geometry of the Universe.

Comoving Distance. This kind of distance is independent of the expansion of the Universe and it is known as the proper distance measured at today's time $t = t_0$, i.e. the proper distance re-scaled for the ratio of the scale factor at today's time to the scale factor at the time t:

$$d_{\rm c} \equiv d_{\rm pr}(t_0) = a(t_0) F(r) = \frac{a(t_0)}{a(t)} d_{\rm pr} \ , \tag{1.10}$$

where the third equivalence can be justified multiplying and dividing by $a(t)$ and considering the definition of $d_{\rm pr}$ (eq. 1.9). The word *comoving* refers to the fact that by definition $d_{\rm c}$ follows the variation of the scale factor, as if the expansion of the Universe was erased.

Hubble-Lemaître Law. The proper distance as defined in equation (1.9) varies and, given the dependence on time through $a(t)$, it means that there is a velocity to take into account. This radial velocity has to be intended as the global motion followed by all the objects inside the cosmos, which is known as the *Hubble flow*. It is obtained by deriving $d_{\rm pr}$ with respect to time[7] t:

$$v_{\rm r} = \frac{\rm d}{{\rm d}t} d_{\rm pr} = \frac{\rm d}{{\rm d}t} \Big[a(t) F(r) \Big] = H(t) d_{\rm pr} \ . \tag{1.11}$$

This is the *Hubble-Lemaître Law*, an equation expressing the velocity at which the points in the spacetime drift apart because of the expansion of the Universe; $H(t) \equiv \frac{\dot{a}}{a}$ is defined as *Hubble parameter*, i.e. a function of time that has the same value everywhere in the Universe at a given cosmic time. Its present value $H(t_0) = H_0$ is a crucial cosmological parameter which establishes the time-distance scales of the Universe; we refer to it as *Hubble Constant*. Commonly, its units of measure is $[{\rm km\ s^{-1}\ Mpc^{-1}}]$, which shows that it has the dimension of the inverse of a time $[s^{-1}]$; in fact, if we assume the expansion rate of our Universe to be constant for its whole history, $\tau_H = H_0^{-1}\ [s]$ (namely *Hubble time*) is an estimate for the age of the Universe or, for the sake of accuracy, for the amount of time passed since when the expansion started. However, this assumption is absolutely inaccurate and τ_H can be seen just as a rough over-estimate at first approximation (see fig. 1.1).

It was Edwin Hubble who found out the expansion of the Universe by measuring the radial velocities of some distant galaxies. By means of their observations he was able to build the *distance - radial velocity* relation for the first time (Hubble, 1929), discovering that the more a galaxy is distant from the observer the more it moves away with a higher velocity. His resulting measure of the Hubble constant was $H_0 \simeq 500\ {\rm km\ s^{-1}\ Mpc^{-1}}$, a value which corresponds to an age of $\tau_H \simeq 2\ {\rm Gyr}$. Of course, our present knowledge tells us that this is not the right value for τ_H since, assuming a flat ΛCDM model, the proven age of our Universe is around

[7] Note that $F(r)$ is time-independent.

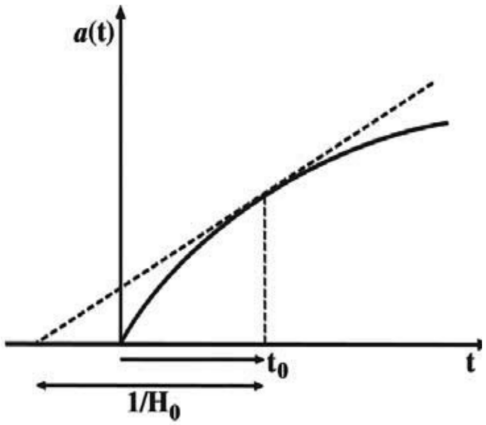

Figure 1.1: Graphic representation of the comparison between the true age of the Universe t_0 and the one resulting from $1/H_0$. Credits to: Coles and Lucchin (2002).

14 Gyr from more recent estimates[8] of the Hubble constant ($H_0 \simeq 70$ km s^{-1} Mpc^{-1}).

It is common to redefine the Hubble parameter through an adimensional parameter $h(t)$ as follows:

$$H(t) \equiv 100\, h(t)\, [\mathrm{km\ s^{-1}\ Mpc^{-1}}]\,. \tag{1.12}$$

This helps to overcome the uncertainties that affect the value of H_0: we generally express the relevant cosmological lengths in units of $h = h(t)\left[h^{-1}\mathrm{Mpc}\right]$ because with this method we are able to describe theoretical models despite the tensions on the true value of the Hubble parameter. However, there are some arguments against using this unit of measure; for example, Sánchez (2020) suggests to abandon the $\left[h^{-1}\mathrm{Mpc}\right]$ units, and replace σ_8 with σ_{12}. Note that σ_8 and σ_{12} are defined as the mass variance σ_M filtered on a scale radius of $8\ h^{-1}\mathrm{Mpc}$ and $12\ h^{-1}\mathrm{Mpc}$, respectively. These quantities represent two possible ways to express the amplitude of the power spectrum $P(k)$.

Redshift. Why is the concept of redshift relevant in the cosmological context? As a consequence of the *Hubble flow*, the more an object is distant from us and the more its spectrum is affected by the redshift phenomenon. This effect is something similar to the *Doppler shift* towards longer wavelengths and can be defined through the following formula:

$$z \equiv \frac{\lambda_{\mathrm{obs}} - \lambda_{\mathrm{em}}}{\lambda_{\mathrm{em}}} = \frac{\Delta\lambda}{\lambda_{\mathrm{em}}}\,, \tag{1.13}$$

where λ_{obs} is the observed wavelength, while λ_{em} is the emitted one. We consider to have an emitting source at a distance r from us which radiates a photon of true wavelength λ_{em} at the instant of time t_{em}, and an observer (located where we are) that receives the same photon of wavelength λ_{obs} at the instant of time t_{obs}. Starting from the FLRW metric (eq. 1.5) and imposing

[8] Nowadays, the scientific community is dealing with some statistical tensions (see §1.4 for further details); one of them is related to the value of the Hubble constant, which is measured with more and more precision as both the instruments and the techniques are improved.

- $\mathrm{d}s^2 = 0$, since a photon is a massless particle which follows the light-like geodetics;
- $\mathrm{d}\theta = \mathrm{d}\phi = 0$ because we align the reference frame with the distance the photon travels along for simplicity

we have:

$$0 = c^2\mathrm{d}t^2 - a^2(t)\frac{\mathrm{d}r^2}{1-\kappa r^2} \,. \tag{1.14}$$

Let us separate the variables (r, t) and then integrate the *temporal* part from the instant in which the photon leaves to the instant in which it reaches the observer and the *spatial* part along the line of sight. Equation (1.14) turns into:

$$\int_{t_{\rm em}}^{t_{\rm obs}} \frac{c\,\mathrm{d}t}{a(t)} = \int_0^r \frac{\mathrm{d}r'}{\sqrt{1-\kappa r'^2}} = F(r) \,. \tag{1.15}$$

Likewise, we now pretend to have another photon emitted by the same source at $t_{em} + \delta t_{em}$ and caught by the observer at $t_{obs} + \delta t_{obs}$. Since the radial distance travelled is the same as before, we write:

$$\int_{t_{\rm em}+\delta t_{\rm em}}^{t_{\rm obs}+\delta t_{\rm obs}} \frac{c\,\mathrm{d}t}{a(t)} = \int_0^r \frac{\mathrm{d}r'}{\sqrt{1-\kappa r'^2}} = F(r) \,. \tag{1.16}$$

Given that $F(r)$ is the same in both the previous equation, we can equal the temporal integrals of (1.15) and (1.16). By doing this and assuming that $\delta t_{\rm em}$ and $\delta t_{\rm obs}$ are very small, i.e. the cosmic scale factor $a(t)$ is constant at the time in which it is computed, we have:

$$\frac{\delta t_{\rm obs}}{a(t_{\rm obs})} = \frac{\delta t_{\rm em}}{a(t_{\rm em})} \,. \tag{1.17}$$

Finally, moving from times and wavelengths to frequencies $\left(\nu = \frac{1}{\delta t}\,;\nu = \frac{c}{\lambda}\right)$ and considering t as the generic time at which the photon is emitted and t_0 (i.e. today's time) as the instant at which the photon is received by the observer, we obtain the definition of the *cosmological redshift*:

$$1 + z = \frac{a_0}{a(t)} \,. \tag{1.18}$$

The cosmological redshift is not to be understood as a Doppler effect because nothing is moving with its proper velocity; it is just an effect due to the fact that objects are embedded in a sort of expanding fluid which fills up the Universe.

Other cosmological distances

As disclosed at the beginning of §1.1.2, in Cosmology there is not a unique way to define the notion of distance. We have seen the proper distance, the comoving distance and the redshift. Observationally, it is also possible to exploit either the flux or the angular diameter of the cosmic sources.

Luminosity distance. In order to give a definition of the luminosity distance we must appeal to the so-called *standard candles*, cosmic objects whose intrinsic luminosity is known[9]. Therefore, we can use their observed flux f to measure their distance $d_{\rm L}$:

$$\begin{cases} f = \dfrac{L}{4\pi d^2} \ , \\ d_{\rm L} = \left(\dfrac{L}{4\pi f}\right)^{1/2} \ . \end{cases} \tag{1.19}$$

The key point here is that considering a fixed absolute luminosity L, if we move the standard candle further from the observer, the flux decreases because the photons are distributed over a larger spherical surface, i.e. a surface corresponding to a larger radius and, as a consequence, the photon number density is lower. In the context of GR, there are many aspects to be taken into account:

- the *cosmological redshift* underwent by the cosmic source (i.e. the energy displacement towards the red part of its emission);
- the *time dilation* due to the delay of an emitted photon that reaches the observer, i.e. $\delta t_{\rm obs} = (a_0/a(t))\delta t_{\rm em}$, which has to be considered since $L \equiv {\rm d}E/{\rm d}t$;
- the *photon-surface growth* as a consequence of the expansion of the Universe itself, i.e. $4\pi r^2 \xrightarrow{\text{becomes}} 4\pi a^2(t_0) r^2$.

All the above considered, we can reformulate the flux and luminosity distance definitions (eq. 1.19) as follows:

$$\begin{cases} f = \dfrac{L}{4\pi a_0^2 r^2 (1+z)^2} \ , \\ d_{\rm L} = a_0 r (1+z) \ . \end{cases} \tag{1.20}$$

Angular diameter distance. Another observational method to estimate the distance of cosmic objects is based on sources characterized by a known angular diameter, namely the *standard rulers*[10]. For this kind of objects, the angle under which we see them in the sky is used as a measure of their distance. Starting from the usual FLRW metric, let us consider a standard ruler perfectly perpendicular to our line of sight, i.e. ${\rm d}\phi = 0$. Moreover, the proper dimension $D_{\rm pr}$ of the source is fixed and the measure is performed at a given instant of time so that, respectively, ${\rm d}r = 0$ and ${\rm d}t = 0$. Taken these conditions into account, we can write the FLRW metric (eq. 1.5) as:

$${\rm d}s^2 = D_{\rm pr}^2 = a^2(t) r^2 {\rm d}\theta^2 \ . \tag{1.21}$$

Now, since an angular diameter distance is generally computed as $d_{\rm A} = \frac{D_{\rm pr}}{{\rm tg}\theta} \approx \frac{D_{\rm pr}}{\theta}$, where the last approximation is justified in the limit of small angles, we can define the *angular diameter*

[9] For example, the Supernovae Ia are phenomena with the same intrinsic luminosity, regardless of their progenitor or their location in the spacetime, thus they are used as standard candles.

[10] For example, the BAO feature which manifests itself with a peak at $\simeq 150$ Mpc $\simeq 100\ h^{-1}$Mpc on either the CMB or the clustering signal at late times.

distance using the following formula:

$$d_{\mathrm{A}} = a(t)r \ . \tag{1.22}$$

It is also possible to establish a way to link the luminosity distance (eq. 1.20) and the angular distance (eq. 1.22):

$$\frac{d_{\mathrm{L}}}{d_{\mathrm{A}}} = (1+z)^2 \ , \tag{1.23}$$

which is called *distance duality relation*, historically associated with the Etherington's *reciprocity theorem* (Etherington, 1933). This relation is an efficient tool to perform validity tests on cosmological models, on the nature of their spacetime and their assumptions (especially homogeneity and isotropy; see e.g. Li et al., 2011 and Liao, 2019). From eq. (1.23) it follows that if we could measure both these distances for the same source[11], we would find out $d_{\mathrm{L}} > d_{\mathrm{A}}$.

To sum up, we must be aware there are different ways to determine cosmic distances. The physical limit at which $d_{\mathrm{pr}} \sim d_{\mathrm{c}} \sim d_{\mathrm{L}} \sim d_{\mathrm{A}}$ is $r \to 0$ and $t \to t_0$, i.e. considering small scales in the local Universe where we can trust on the validity of the Euclidean laws.

1.2 Friedmann universes

In this section we outline the whole range of cosmological models derived from the Einstein Field equation and the subsequent Friedmann equations, with the aim of exploring the major components of our Universe and their evolution through its history.

The Friedmann cosmological model and its equations rely on the homogeneity and isotropy assumptions of the CP and set their bases on GR through the aforementioned Einstein Field Equation. Starting from equation (1.2), let us make two hypotheses on its terms:

- we assume the FLRW metric (see §1.1.1) for the geometric term (LHS);
- we define the energy-momentum tensor $T_{\mu\nu}$ in the limit of a perfect fluid[12], formalised as $T_{\mu\nu} = -pg_{\mu\nu} + (p + \rho c^2)u_\mu u_\nu$, where p is the pressure, $g_{\mu\nu}$ the metric tensor, ρc^2 the energy density and $u_{\mu,\nu}$ are the four-velocities (i.e. the temporal derivatives of the four-vectors).

With these two assumptions, it is possible to derive the Friedmann equations from the GR field equation[13]:

$$\text{[I]} \qquad \ddot{a} = -\frac{4\pi}{3}G\left(\rho + \frac{3p}{c^2}\right)a \ , \tag{1.24}$$

[11] This is the case of e.g. massive galaxy clusters since we can measure both their angular and luminosity distances via Sunyaev-Zel'dovich effect and X-Ray observations.

[12] The validity of the perfect-fluid approximation is guaranteed by the fact that the mean free path of a particle (i.e. the average distance travelled by a particle of the fluid before modifying its direction as a consequence of a collision with another particle) is smaller than the typical scales of structure formation and evolution across the Universe.

[13] Note that going through GR principles is really challenging, but we can take advantage of the *Newtonian Approximation*. This can be done because there are some theorems valid both in classical mechanics and in General Relativity; for example, the Birkhoff theorem needed to obtain the Friedmann equations in GR is equivalent to the Gauss theorem in Newtonian mechanics.

$$[\mathrm{II}] \qquad \dot{a}^2 + \kappa c^2 = \frac{8\pi}{3} G\rho a^2 \,, \tag{1.25}$$

These are the only two (of sixteen) independent equations of the system resulting from the Einstein Field Equation (eq. 1.2); they provide a full description of the temporal evolution of the cosmic scale factor $a(t)$, telling us how does the Universe dynamically expand.

Equations (1.24) and (1.25) can be linked by the *adiabatic condition*[14] $\mathrm{d}\mathcal{U} = -p\mathrm{d}V$, which can be expressed in cosmological terms as follows:

$$\mathrm{d}(\rho c^2 a^3) = -p\mathrm{d}a^3 \,, \tag{1.26}$$

where $\mathcal{U} = \rho c^2 a^3$ is the *internal energy* (i.e. the product of the energy density and the volume), p is the pressure and $V = a^3$ is the volume of the Universe. Moreover, be aware that in eq. (1.26) and later on, ρ and p have to be interpreted as the total sum of density and pressure for all the components that make up our Universe.

Since when equations (1.24) and (1.25) were suggested by Friedmann (1922) as solutions of the Einstein's system of field equations (1.2), many efforts have been made to study their behaviour and analytic solutions. This leads to the development of several viable cosmological models.

Einstein static model. Friedmann's dynamic equations emerged in the early twentieth century, when people - e.g. Albert Einstein - were stuck in the belief that the universe was *static*, i.e. $\dot{a} = \ddot{a} = 0$. The dilemma is that under this condition the first equation (eq. 1.24) turns into

$$\rho = -\frac{3p}{c^2} \,, \tag{1.27}$$

which would be difficult to explain, since both density and pressure cannot be negative for ordinary matter. Hence, Einstein in 1917 modified his own equations by introducing the *Cosmological Constant* Λ, so that equation (1.2) becomes (Einstein, 1917):

$$R_{\mu\nu} - \frac{1}{2} g_{\mu\nu} R - \Lambda g_{\mu\nu} = \frac{8\pi G}{c^4} T_{\mu\nu} \,, \tag{1.28}$$

or

$$R_{\mu\nu} - \frac{1}{2} g_{\mu\nu} R = \frac{8\pi G}{c^4} T_{\mu\nu} + \Lambda g_{\mu\nu} \,. \tag{1.29}$$

These equations are mathematically indistinguishable, but the physical meaning can have different interpretations:

- adding Λ in the LHS means modifying the GR encoded in the spatial term, i.e. considering the *Modified Gravity* (MG hereafter) in the structure formation scenario, which is based on the gravitational instability;
- including it in the RHS implies a modification of the energy-momentum tensor definition, i.e. considering the *Dark Energy* (DE hereafter) in the total energy budget.

[14] The adiabatic condition is valid as far as our Universe is akin to a closed system which evolves without exchanging energy or heat with the external environment.

Let us take the path of the DE, rewriting equation (1.29) as

$$R_{\mu\nu} - \frac{1}{2} g_{\mu\nu} R = \frac{8\pi G}{c^4} \tilde{T}_{\mu\nu} \,, \tag{1.30}$$

where $\tilde{T}_{\mu\nu} = T_{\mu\nu} + \frac{\Lambda c^4}{8\pi G} g_{\mu\nu}$ is called *effective energy-momentum tensor*. Now, applying the already defined energy-momentum tensor for a perfect fluid (see the beginning of §1.2), i.e. $\tilde{T}_{\mu\nu} = -\tilde{p} g_{\mu\nu} + (\tilde{p} + \tilde{\rho} c^2) u_\mu u_\nu$, we obtain a new characterization for both the pressure and the density:

$$\begin{cases} \tilde{p} = p - \dfrac{\Lambda c^4}{8\pi G} \,, \\ \tilde{\rho} = \rho + \dfrac{\Lambda c^2}{8\pi G} \,. \end{cases} \tag{1.31}$$

Equations (1.31) show how in $\tilde{p}$ the cosmological constant contributes negatively to the ordinary pressure p, while in $\tilde{\rho}$ it has a positive contribution with respect to the ordinary density ρ. From some considerations on the *effective density* and assuming that the pressure of matter is negligible if compared to that of radiation, it is possible to infer that the Einstein's Universe is *static*, *spherical* and filled with matter, where the static condition is based on a unique value of the cosmological constant (i.e. $\Lambda = \Lambda_E \equiv \frac{4\pi G \rho}{c^2}$).

A few years later, the expansion of the Universe was proven by Edwin Hubble (see §1.1.2) and Einstein finally abandoned the static idea of the Universe, getting rid of his correction and going back to the normal Friedmann models.

Lemaître-de Sitter model. Actually, in the following years, scientists proceeded by trial and error, including or removing the cosmological constant depending on the physical problem they were dealing with. For example, in 1927 it has been developed the Lemaître flat Universe, based on the de Sitter model (see de Sitter, 1917 and Mohajan, 2017). This Universe is flat ($\kappa = 0$, Euclidean geometry), empty of matter ($p = 0$, $\rho = 0$) but entirely filled up with the cosmological constant, so that the equations (1.31) becomes:

$$\begin{cases} \tilde{p} = -\dfrac{\Lambda c^4}{8\pi G} \,, \\ \tilde{\rho} = +\dfrac{\Lambda c^2}{8\pi G} \,, \end{cases} \tag{1.32}$$

and, as a consequence, $\tilde{p} = -\tilde{\rho} c^2$. Furthermore, according to this model, the second Friedmann equation (1.25) tells us that the scale factor $a(t)$ varies following an exponential growth, while the Hubble parameter $H(t) = H$ is here time-independent: the expansion rate is exponential and constant throughout the history of the Universe. Finally, looking at the first equation (1.24), it is evident how $\ddot{a}$ should be negative, since $p \geq 0$ and $\rho > 0$ by definition for normal matter. In this context, the cosmological constant helps explaining the observed accelerated expansion of the Universe ($\ddot{a} > 0$, through type Ia SNae), given that it plays the role of a negative pressure.

1.2.1 Friedmann general models

Having introduced the context in which the Friedmann Universes are embedded, our aim now is to find the analytic solutions of the Friedmann equations. To reach this purpose, as a first step we perform a function study assuming that there is only one[15] component of unknown nature in the Universe. Then we will consider the more realistic case of three components.

One-component model

Taking into account the adiabatic condition (1.26), we focus on the second Friedmann equation to derive the *density parameter* $\Omega(t)$ as a function of the *curvature parameter* κ. First of all, let us define two essential cosmological quantities which are necessary for the following analysis: the *critical density* and the *density parameter*.

The critical density $\rho_{crit}(t)$ is the density value that our Universe must recover to be characterized by a flat geometry:

$$\rho_{crit}(t) \equiv \frac{3H^2(t)}{8\pi G} \,. \tag{1.33}$$

Its value at today's time ($\rho_{crit}(t_0) = \rho_{crit,0}$) is fixed and, since its definition (1.33), it can be computed simply through the measure of Hubble constant H_0 expressed as in (1.12): $\rho_{crit,0} = 1.9 \cdot 10^{-29}\, h^2 \left[\mathrm{g\ cm^{-3}}\right]$.

The density parameter $\Omega(t)$ is a dimensionless parameter defined by means of a density ratio:

$$\Omega(t) \equiv \frac{\rho(t)}{\rho_{crit}(t)} \quad \longrightarrow \quad \Omega_0 = \frac{\rho_0(t)}{\rho_{crit,0}} \,. \tag{1.34}$$

As we will soon notice, by measuring Ω_0 (i.e. the density parameter at today's time), we can infer the geometry of our Universe. The formulas describing the evolution of $\Omega(t)$ tell us that it is sufficient to evaluate this parameter at $t = t_0$ because the geometry of the Universe cannot change: if it is flat today, it was born flat and the same is valid for all the other cases.

Moving on with our analysis, we divide eq. (1.25) by a_0^2 (i.e. the squared cosmic scale factor computed at today's time t_0) and, rewriting it in a convenient way, we have:

$$\left(\frac{\dot{a}}{a_0}\right)^2 - \frac{8\pi}{3} G\rho \left(\frac{a}{a_0}\right)^2 = -\frac{\kappa c^2}{a_0^2} \,, \tag{1.35}$$

where in the RHS the curvature parameter κ can assume three possible values (see §1.1.1). Now, taking into account eq. (1.33) and recalling the definition of the Hubble parameter as a function of the cosmic scale factor $a(t)$ and its derivative, eq. (1.35) becomes:

$$H_0^2 \left(1 - \frac{\rho_0}{\rho_{crit,0}}\right) = -\frac{\kappa c^2}{a_0^2} \,. \tag{1.36}$$

This relation regulates the evolution of the cosmic scale factor a and it can be computed at any

[15] Note the advantage in this case is that we have only one relation between pressure and density, i.e. between the quantities that, together with the cosmic scale factor $a(t)$, represent the dependencies of the Friedmann equations.

time, hence we choose $t = t_0 \rightarrow a = a_0$. Equation (1.36) let us infer that:

- $\kappa = 0$ (flat) $\iff \rho_0 = \rho_{crit,0}$ and $\Omega_0 = 1$;
- $\kappa = +1$ (spherical) $\iff \rho_0 > \rho_{crit,0}$ and $\Omega_0 > 1$;
- $\kappa = -1$ (hyperbolic) $\iff \rho_0 < \rho_{crit,0}$ and $\Omega_0 < 1$.

Three-component model

Since that the present Standard Cosmological Model (see §1.3) accounts for the existence of three components[16] (i.e. matter, radiation and cosmological constant), the following analysis is more realistic than the previous one, which was just for preparatory purposes.

In order to solve the Friedmann equations (eqs. 1.24 and 1.25) for more that one component, let us define the *equation of state* (EoS, hereafter) for a generic component which permeates the Universe in the limit of the perfect-fluid approximation:

$$p = w\rho c^2 \,, \tag{1.37}$$

where w is a variable related to the *sound speed* definition as follows:

$$c_s = \left(\frac{\partial p}{\partial \rho}\right)^{1/2}_{S=const} = c\sqrt{w} \,. \tag{1.38}$$

To ensure the physical validity of this equation, w must belong to the so-called *Zel'dovich interval*, i.e. $0 \leq w < 1$, where the lower limit reflects the natural domain of the square root function $[0; +\infty)$, while the upper limit is due to the fact that nothing can travel at speed larger or equal to the speed of light ($v < c$ always). It is in the Zel'dovich range that the ordinary components of our Universe, namely the matter and the radiation, exist. By contrast, the cosmological constant is called "extra-ordinary component" since its w value does not fit this interval. It is possible to assign a specific value to the variable w for each constituent of our Universe starting from their well-known EoS:

- *Radiation* (photons and relativistic matter, such as massive neutrinos) $\rightarrow$ the EoS of a generic relativistic fluid is defined as follows:

$$p_r = \frac{1}{3}\rho_r c^2 \,, \tag{1.39}$$

  so that, to recover the general equation (1.37), $w = \frac{1}{3}$.

- *Matter* (non-relativistic) $\rightarrow$ assuming a perfect gas composed by N particles, each having the mass of a proton, the EoS can be written as:

$$p_m = \frac{k_B T}{m_p c^2}\rho_m c^2 \simeq 0 \,, \tag{1.40}$$

[16] Of course, each component takes part to the energy budget of our Universe and this can be formalised by interpreting the energy-momentum tensor in the RHS of the Einstein equation (eq. 1.2) as $T_{\mu\nu} = \sum_{i=0}^{N} T^{(i)}_{\mu\nu}$, where N is the total number of components and (i) stands for the i-th component.

where $k_B = 1.38 \cdot 10^{-16} [\mathrm{erg\ K^{-1}}]$ is the Boltzmann constant, T is the temperature of the gas and ρ_m is the matter density. The last equivalence argues that p_m vanishes and this is because the amount of energy due to the particle mass ($m_p c^2$) is negligible with respect to the thermal energy ($k_B T$). As a consequence, the pressure associated to the matter component is totally insignificant if compared with that of the radiative component. For eq. (1.40) to be verified, we need w to be equal to zero.

- *Cosmological constant* → from the brief description we gave on the Lemaître-de Sitter universe (in §1.2), we know that for the cosmological constant the EoS is:

$$p_\Lambda = -\rho_\Lambda c^2 \,, \tag{1.41}$$

thus it follows that $w = -1$.

On the adiabatic evolution of our Universe. Blending the adiabatic condition (1.26) with the general expression for the EoS (1.37), we come across the following relation, which tells us how the density of the various components evolves in time:

$$\rho \propto a^{-3(1+w)} \propto (1+z)^{3(1+w)} \,, \tag{1.42}$$

The consequence of this mathematical statement is that the distinct constituents of the Universe prevail over the others in different cosmic epochs, since their temporal[17] density trends depend on their value of w. In fact, starting from eq. (1.42) and making it explicit for each component, we can write the following relations:

$$\begin{cases} \rho_\mathrm{r} \propto \rho_{0,\mathrm{r}}\, a^{-4} = \rho_{0,\mathrm{r}}\, (1+z)^4 \,, \\ \rho_\mathrm{m} \propto \rho_{0,\mathrm{m}}\, a^{-3} = \rho_{0,\mathrm{m}}\, (1+z)^3 \,, \\ \rho_\Lambda \propto \rho_{0,\Lambda}\, a^{0} = \rho_{0,\Lambda}\, (1+z)^0 = const \,. \end{cases} \tag{1.43}$$

For example, the radiation density decreases faster than the matter density and the consequence is that in the early stages of the Universe (i.e. small values of a) the radiative component dominates, while the situation reverses at more recent times (see fig. 1.2). At today's time the situation is a bit complicated since we are living in what is called a *dual epoch*, where matter and cosmological constant coexist with competitive percentages. Moreover, notice that we can also define cosmic times in which the components are perfectly balanced, namely *equivalence times*, through the combination of the different relations in eq. (1.43).

Proceeding with some other useful considerations, let us start from the first Friedmann equation (1.24) and replace the pressure therein with the general EoS (eq. 1.37) to get:

$$\ddot{a} = -\frac{4}{3}\pi G \rho (1+3w) a \,. \tag{1.44}$$

It is evident that in the case of the ordinary components (i.e. with $0 \leq w < 1$) $\ddot{a}$ can only be negative, this implying that the concavity of $a(t)$ is downwards. However, as Riess et al. (1998) and Perlmutter et al. (1999) demonstrated, the Universe has recently entered a phase of

[17] The cosmic time is embedded in $a = a(t)$ and $z \propto \frac{a_0}{a(t)}$.

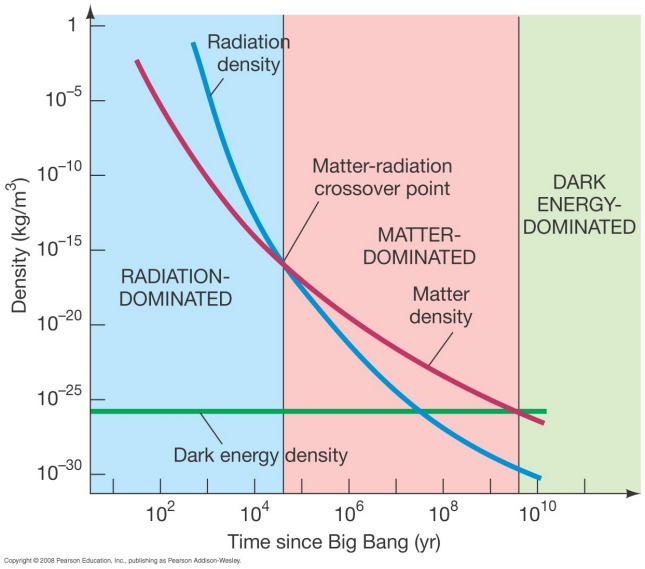

Figure 1.2: Density trends in time of radiation, matter and cosmological constant (DE in the plot): the prevailing component changes over epochs because of the different dependencies seen in eqs. (1.43). Credits to: https://pages.uoregon.edu/jimbrau/astr123/Notes/ Chapter27.html.

accelerated expansion ($\ddot{a} > 0$, upwards concavity) and we need an extra-ordinary component ($w < -1/3$) coming into play to recover this trend. The cosmological constant can help in this context, since it is described by $w = -1$. Furthermore, if its value was large enough, it could not only explain today's accelerated expansion at $t = t_0$, but it could also avoid the Big Bang by introducing an upwards concavity close to $t = 0$. Anyway, our perspective up to now is that of the normal Friedmann models which, by construction of the Friedmann equations, naturally imply the divergence[18] of temperature, density and Hubble parameter at $t = 0$.

Now, let us consider the second Friedmann equation (1.25) in order to achieve a relation describing the evolution of the Hubble parameter $H(t)$, the density parameter $\Omega(t)$ and the redshift z, i.e. the variables that are more strongly associated with observational properties of our Universe. Applying the definitions of the critical density (eq. 1.33) and of the Hubble parameter $H(t) \equiv \frac{\dot{a}}{a}$ to this equation, after some lines of simple algebra we can rewrite it as:

$$H^2(z) = H_0^2(1+z)^2\left[\left(1 - \sum_i \Omega_{0,i}\right) + \sum_i \Omega_{0,i}(1+z)^{1+3w_i}\right]. \tag{1.45}$$

In these equations, $\sum_i$ represents the sum over each component i so that $\sum_i \Omega_{0,i} = \Omega_{\rm TOT}$ is the total density parameter as defined in eq. (1.34) but for a multi-component universe. In particular, $\Omega_{\rm TOT}(t) = \Omega_{\rm r}(t) + \Omega_{\rm m}(t) + \Omega_\Lambda(t)$ and, their definition taken into account, the

[18]This divergence, namely the Big Bang, represents the open physical *origin problem*, one of the big gaps in cosmological knowledge (Coles and Lucchin, 2002).

single density parameters can be made explicit in this way:

$$\begin{cases} \Omega_{\rm r}(t) = \dfrac{8\pi G}{3H^2(t)}\rho_{\rm r}(t)\ , \\ \Omega_{\rm m}(t) = \dfrac{8\pi G}{3H^2(t)}\rho_{\rm m}(t)\ , \\ \Omega_{\Lambda}(t) = \dfrac{8\pi G}{3H^2(t)}\rho_{\Lambda}(t) = \dfrac{\Lambda c^2}{3H^2(t)}\ , \end{cases} \tag{1.46}$$

where the last equivalence concerning the cosmological constant Λ is explained through eqs. (1.32).

Finally, let us emphasize that in eq. (1.45) the term $1-\sum_i \Omega_{0,i} = \Omega_{\rm c}$ is labelled as *curvature density parameter*[19] and it is related to the geometry of the space: for a flat universe $\Omega_{0,\rm TOT} = 1$ and $\Omega_{\rm c} = 0$; for a spherical universe $\Omega_{0,\rm TOT} > 1$ and $\Omega_{\rm c} < 0$; for a hyperbolic universe $\Omega_{0,\rm TOT} < 1$ and $\Omega_{\rm c} > 0$.

1.2.2 Flat versus curved models

Being the Friedmann general model outlined, we now move to the analysis of its descendants, i.e. models with the same basis but whose main characteristics are settled by the specific geometry of the space. Moreover, note that we will proceed by taking into consideration only one component for ease; this is justified since we already shown how in each cosmic epoch, if sufficiently far from the equivalence times, we can assume that one component prevails over the others at least at first approximation.

Einstein-de Sitter flat model

The EdS universe relies on the following hypotheses:

- flat geometry, i.e. $\kappa = 0$ and $\Omega_{\rm TOT} = 1$;
- generic mono-component fluid described by the general EoS (eq. 1.37);
- $\dot{a}_0 > 0$, since we know that the Universe is expanding at $t = t_0$.

Applying these assumptions to eq. (1.45), we get:

$$H(z) = H_0(1+z)^{\frac{3(1+w)}{2}}\ , \tag{1.47}$$

and it is from this relation, after some maths, that we can obtain some relevant dependencies[20] of the EdS parameters (see tab. 1.1 for a schematic recap). In this table, q is the *deceleration parameter* defined through the cosmic scale factor and its derivatives as $q \equiv -\ddot{a}a/\dot{a}^2$.

It is noticeable how the estimates for the age of the Universe through the Hubble constant H_0 are different for the matter-dominated and the radiation-dominated Universe, being

[19] We can define this parameter with both $\Omega_{0,\rm TOT}$ or $\Omega_{\rm TOT}(t)$ because the geometry of the Universe cannot change once defined, as we already pointed out in §1.2.1.

[20] Note that from the relations reported in tab. 1.1 it is possible to achieve all the other dependencies such as, for example, $t(a)$, $\rho(a)$, $\rho(z)$ etc.

w	$w=0$	$w=1/3$
$a(t)=a_0\left(\frac{t}{t_0}\right)^{\frac{2}{3(1+w)}}$	$a(t)\propto t^{2/3}$	$a(t)\propto t^{1/2}$
$t(z)=t_0(1+z)^{-\frac{3(1+w)}{2}}$	$t(z)\propto(1+z)^{-3/2}$	$t(z)\propto(1+z)^{-2}$
$\rho=\frac{1}{6\pi G(1+w)^2}\frac{1}{t^2}$	$\rho=\frac{1}{6\pi G}\frac{1}{t^2}$	$\rho=\frac{3}{32\pi G}\frac{1}{t^2}$
$H(t)=\frac{2}{3(1+w)}\frac{1}{t}$	$H(t)=\frac{2}{3}\frac{1}{t}$	$H(t)=\frac{1}{2}\frac{1}{t}$
$t_0=\frac{2}{3(1+w)}\frac{1}{H_0}$	$t_0=\frac{2}{3}\frac{1}{H_0}$	$t_0=\frac{1}{2}\frac{1}{H_0}$
$q=\frac{1+3w}{2}$	$q=\frac{1}{2}$	$q=1$

Table 1.1: Trends of the parameters for the EdS universe depending on w, i.e. on the nature of the dominant component. **Left**: generic value for w; **centre**: matter-dominated EdS universe; **right**: radiation-dominated EdS universe.

$t_{0,\mathrm{m}}=\frac{2}{3}\frac{1}{H_0}$ and $t_{0,\mathrm{r}}=\frac{1}{2}\frac{1}{H_0}$, respectively. As a consequence, the universe evolves differently according to the kind of fluid which dominates the energy budget. In fact, an increasing pressure corresponds to a greater level of deceleration. Going from a matter-dominated condition with $w=0$ and $P=0$ to a radiation-dominated one with $w=1/3$ and $P>0$, the universe is more decelerated, in agreement with the fact that $t_{0,\mathrm{r}}<t_{0,\mathrm{m}}$. This can be explained starting from the first Friedmann equation that we recall here for convenience:

$$\ddot{a}=-\frac{4\pi}{3}G\left(\rho+\frac{3p}{c^2}\right)a\,.$$

Here the pressure contribution is added to that of the density enhancing the deceleration.

Curved models

Now let us investigate the non-flat models for our Universe since their comprehension will be useful to clearly understand some details on both the structure formation and evolution and the large-scale structure (see CHAPTER 2). The curved models set their basis on the following assumptions:

- hyperbolic geometry, i.e. $\kappa=-1$ and $\Omega_{\mathrm{TOT}}<1$, for the open universe; spherical geometry, i.e. $\kappa=+1$ and $\Omega_{\mathrm{TOT}}>1$, for the closed universe.
- generic mono-component fluid described by the general EoS (eq. 1.37);

We focus on the RHS of eq. (1.45) and we recall that the curvature density parameter $1-\sum_i\Omega_{0,i}$ is constant. The second term in the square brackets varies with a: the lower the cosmic scale factor is, the closer we are to the Big Bang and the more this term raises. This means that we can define a critical value a^* below which, or a value z^* above which, this second term prevails

over the curvature one. We can formalise it as follows:

$$|1-\Omega_0| = \Omega_0 \left(\frac{a_0}{a^*}\right)^{1+3w} , \tag{1.48}$$

or, analogously (see eq. 1.18),

$$|1-\Omega_0| = \Omega_0 (1+z^*)^{1+3w} . \tag{1.49}$$

At early times the curved universes behaves like a flat Universe, since it is as if they do not feel their curvature; in other words, we can assume an EdS universe for much of its evolutionary history. Everything taken into account, for $z \gg z^*$ (i.e. $a \ll a^*$) we neglect Ω_c and eq. (1.45) turns into:

$$H(z) = H_0 \sqrt{\Omega_0} (1+z)^{\frac{3(1+w)}{2}} . \tag{1.50}$$

By comparing this equation with eq. (1.47) derived for the EdS model, we can demonstrate how the flat approximation is reliable at the early stages of our Universe. By contrast, if $z < z^*$ or $a > a^*$, the curvature becomes significant and what happens next in terms of expansion depends on the sign of Ω_c: we need to distinguish open and closed universes.

Starting from the **open** models (i.e. $\kappa = -1$ and $\Omega_{\rm TOT} < 1$), Ω_c is always positive and therefore the square bracket in eq. (1.45) never vanishes. As a consequence, we are facing an infinite expansion. We can assume $\dot{a}(t) > 0 \; \forall t$, because it is known from observations that today $\dot{a}(t = t_0) \equiv \dot{a}_0 > 0$, and the sign simply cannot change. If we stand in the limit $z \ll z^*$ or $a \gg a^*$, we can rewrite the equation of $H(z)$ preserving only the term of curvature in the square brackets[21]:

$$H(z) = H_0 (1+z)(1-\Omega_0)^{1/2} , \tag{1.51}$$

which in terms of a (through the definitions of the cosmic redshift and the Hubble parameter) turns into:

$$\dot{a} = a_0 H_0 (1-\Omega_0)^{1/2} . \tag{1.52}$$

This equation states that $\dot{a} = const$, since all the terms in the RHS are constant themselves. Moreover, from $\dot{a} = \frac{{\rm d}a}{{\rm d}t}$ we get $a \propto t$ (i.e. $H \propto t^{-1}$); thus, in an open model with hyperbolic geometry the cosmic scale factor has a linear growth in time, providing an infinite expansion which will lead the universe to its thermal death, namely the *Big Freeze*.

Moving to the **closed** models (i.e. $\kappa = +1$ and $\Omega_{TOT} > 1$), Ω_c is always negative and therefore the square brackets in eq. (1.45) can vanish. In particular, if $z \ll z^*$ or $a \gg a^*$, there exists a value of the cosmic scale factor $a = a_{\rm max}$ that marks the moment at which $\dot{a} = 0$ (maximum). After this time $t = t_{\rm max}$, the evolution of the scale factor reverses its trend and $\dot{a} < 0$. As a result, for the closed models the expansion is not infinite. By setting the square

[21] The second term in the square brackets of eq. (1.45) depends on $(1+z) \sim a^{-1}$, hence it tends to unity for $z \ll z^*$ or $a \gg a^*$.

brackets of eq. (1.45) equal to zero, we derive the following relation:

$$1 - \Omega_0 = \Omega_0 \left(\frac{a_0}{a_{max}} \right)^{1+3w} , \tag{1.53}$$

and hence,

$$\begin{cases} a_{max} = a_0 \left(\dfrac{\Omega_0}{\Omega_0 - 1} \right)^{\frac{1}{1+3w}} , \\ \rho_{min} = \rho_0 \left(\dfrac{a_0}{a_{max}} \right)^{3(1+w)} = \rho_0 \left(\dfrac{\Omega_0 - 1}{\Omega_0} \right)^{\frac{3(1+w)}{1+3w}} . \end{cases} \tag{1.54}$$

The destiny of a closed universe is to collapse again in the same conditions of the initial Big Bang, reducing itself to a point at $t = 2t_{max}$ in the so-called *Big Crunch*[22].

Finally, let us just point out that analytical solutions of the Friedmann equations exist only for the flat-EdS universe case; for the curved universes we must take into account parametric equations built on trigonometric functions.

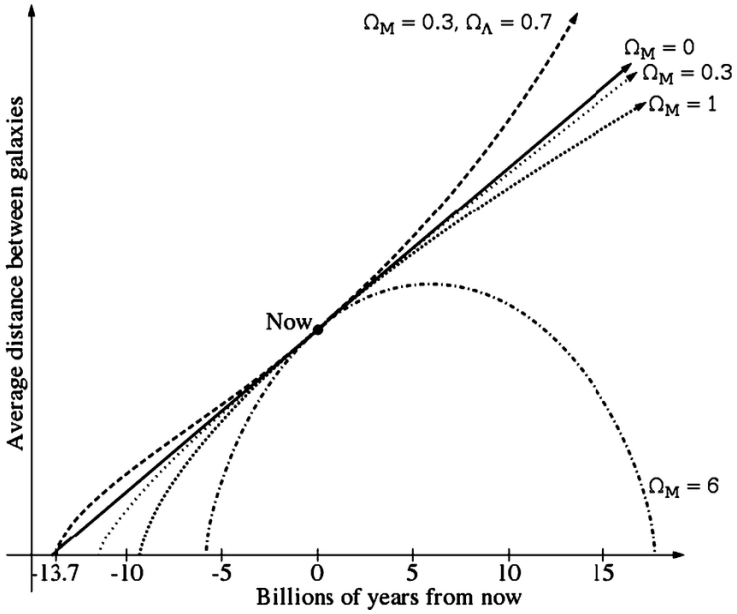

Figure 1.3: Time evolution of the cosmic scale factor for different cosmological parameters: flat Universe if $\Omega_\mathrm{m} = 1$, closed if $\Omega_\mathrm{m} > 1$, open if $\Omega_\mathrm{m} < 1$. The case corresponding to $\Omega_\mathrm{m} = 0.3$ and $\Omega_\Lambda = 0.7$ represents the ΛCDM Universe. Credits to: Casado (2020).

[22]Note that one of the ideas related to the closed universe is what we call *pulsating universe*; it means that after the Big Crunch the universe could start its expansion again and then re-collapses. This concept of infinite universe in disguise had been thought as a possible solution to avoid the Big Bang and the related *origin problem*.

1.3 The ΛCDM Standard Cosmological Model

As discussed in the introduction, the *flat*-ΛCDM model is currently established as the standard paradigm of the actual cosmological framework. This model for our Universe emerges as a natural consequence of the Friedmann equations (eqs. 1.24 and 1.25) in the context of GR and under the assumptions of the Cosmological Principle in the perfect-fluid approximation. Contrary to the models analysed above (see §1.2.2), this one more accurate since it takes into account the existence of more than one component; by doing that, it allows us to give a more realistic description of the Universe we are living in. In fact, it is well known that at first approximation we can consider a mono-component fluid just in some specific cosmic times in the history of our Universe, while at today's time we have observational evidence that we are living in a dual epoch where the matter and the dark energy are of the same order. The bedrocks of the concordance model can be summarised as follows:

- validity of GR[23];
- flat geometry, i.e. $\kappa = 0$ and $\Omega_{\rm TOT} = 1$;
- three-component fluid, i.e. cosmological constant, matter and radiation (in order of predominance at the present time).

The evolution in redshift, from the Big Bang to the present days, is known as *thermal history*, since its regulation is strictly linked to the temperature level through cosmic epochs. At $t_{\rm P} \simeq 10^{-43}$ s, namely the *Planck time*[24], the temperature of our Universe was extremely high, around 10^{32} K; then, it has decreased by thirty orders of magnitude in the subsequent 13.8 Gyr of age of the Universe, reaching 2.7255 ± 0.0006 K as reported in Planck Collaboration et al. (2020). This is the temperature of the photons that make up the so-called *Cosmic Microwave Background* (hereafter CMB), whose existence is well foreseen by the concordance model. Note that it is one of the best proofs of the Big-Bang family of models.
The ΛCDM model bears the name of its main components at $t = t_0$ or $z = 0$, i.e. the cosmological constant (Λ), which represents the DE in its simplest form, and the cold dark matter (CDM). The radiative component is negligible today but it must be considered in order to build an accurate model. It follows a brief description of both the observational properties and the abundances of the three ingredients of our Universe.

Radiation. The great majority of the radiation density is due to CMB photons, while the radiation emitted by stars and gas is negligible. Since this background radiation is at thermal

[23] There is tangible evidence of the validity of the GR in the local Universe. Over the last decades, many tests have been made in order to better understand the behaviour of the matter and energy content in our Universe. The most famous *classical tests* are: the precession of Mercury perihelion (Vankov, 2010), the deflection of light in the Sun's potential well (Will, 2015), the gravitational redshift (Delva et al., 2018) and now also the gravitational waves (Mukherjee et al., 2021).

[24] To describe the Universe from $t = 0$ to $t = t_{\rm P}$ we must call into play the *quantum physics*, i.e. a kind of physics that is derived from the *Heisenberg's uncertainty principle* but for which there is not yet a well developed unified theory. The Planck time is defined as the moment at which the *Schwarzschild scale* (gravity) and the *Compton scale* (quantum mechanics) coincide. Moreover, at $t = t_{\rm P}$, our Universe is supposed to be described by the following quantities: $T_{\rm P} \simeq 10^{32}$ K, $E_{\rm P} \simeq 10^{19}$ GeV, $a_{\rm P} \simeq 10^{-33}$ cm, $\rho_{\rm P} \simeq 10^{93}$ g cm^{-3}, $m_{\rm P} \simeq 10^{-5}$ g and $\sigma \simeq 1$; where T is the temperature, E the energy, a the cosmic scale factor, ρ the density, m the mass, σ the adimensional entropy, while the subscript P stands for "Planck".

equilibrium, it can be described by a perfect *black body*, so that we can estimate its energy density from its temperature through the following relation:

$$\rho_{\rm r} c^2 = \sigma T_{\rm r}^4 \,, \tag{1.55}$$

which, at today's time and considering $T_{0,\rm r} \simeq 2.73$ K , gives us $\rho_{0,\rm r} \simeq 10^{-34}$ g cm^{-3} . It is also possible to compute the radiation energy density parameter by means of eq. (1.34): if we consider $\rho_{0,\rm crit} \simeq 10^{-29}$ g cm^{-3} we get $\Omega_{0,\rm r} \approx 10^{-5}$, which tells us how the radiative contribution to the total energy budget of the Universe is actually negligible at $t = t_0$. This can be justified by means of the density trends we mentioned in §1.2.1: since the radiation density evolves by taking into account also the radiative pressure as a^{-4}, it passes from being dominant in the early stages of the Universe to being totally insignificant at later times (see fig. 1.2).

Matter. This category includes both baryonic and non-baryonic matter (i.e. the DM), hence the total energy density can be expressed as $\Omega_{0,\rm m} = \Omega_{0,\rm b} + \Omega_{0,\rm DM}$. The difference between the ordinary matter and the DM is basically related to the way they interact: the baryonic matter undergoes both gravitational and electromagnetic interactions[25], while the DM today only undergoes weak gravitational interactions. As a consequence, baryons are direcly observable but the DM is not. How can we estimate their abundances? The baryonic energy density can be evaluated by means of the *galaxy luminosity function*, the *primordial nucleosynthesis* and the *CMB*. By constrast, since the DM experiences only gravitational interactions, to measure its contribution we rely on gravitational effects, such as e.g. the *gravitational lensing*, and the *cluster dynamics*. From these methods we obtained $\Omega_{0,\rm m} \simeq 0.3$ and $\Omega_{0,\rm b} \simeq 0.05$, so that the total matter energy density is almost entirely dominated by the dark matter.

Cosmological constant. Last but not least, we now deal with the third constituent of our Universe, the first one in order of abundance today. From the CMB standard ruler we know that the Universe is flat and thus $\Omega_{0,\rm TOT} = 1$. Since we have just stated that $\Omega_{0,\rm m} \simeq 0.3$ and that the radiation today is negligible, there must be some missing component, i.e. $\Omega_{0,?} \simeq 0.7$: *what could it be?* Before the discovery of the accelerated expansion of the Universe, scientists tried to fill this gap with the potential presence of hidden black holes. But soon after it was clear that to have $\ddot{a} > 0$, recovering the accelerated expansion, it should have been added a not-ordinary term with $w < -1/3$ in the Friedmann equations. Einstein relied on the cosmological constant Λ ($w = -1$, the simplest representation of the so-called dark energy component) and the first equation had been rewritten as follows:

$$\ddot{a} = -\frac{4}{3}\pi G \rho_{\rm m} a + \frac{1}{3}\Lambda c^2 a \,, \tag{1.56}$$

from which it is evident that for sufficiently high values of Λ, the RHS reverses its sign, going from being negative to positive. The relevance of the cosmological constant can be pointed out by means of the deceleration parameter q, starting from its definition and applying some

[25] The baryons interact both with the gas through fluid dynamics and micro-physics processes and with the observable electromagnetic radiation.

mathematical passages:

$$q \equiv -\frac{\ddot{a}(t)a(t)}{\dot{a}(t)^2} = -\frac{\ddot{a}}{a}\frac{1}{H^2} = \frac{4}{3}\pi G\frac{\rho_{\rm m}}{H^2} - \frac{\Lambda c^2}{3H^2} = \frac{\Omega_{\rm m}}{2} - \Omega_\Lambda \, . \tag{1.57}$$

The second equivalence is obtained by multiplying and dividing by $a(t)$; the third by replacing $\ddot{a}$ with its expression in equation (1.56); the fourth by considering $\Omega_{\rm m} = \rho_{\rm m}/\rho_{0,\rm crit}$ and $\Omega_\Lambda = \Lambda c^2/(3H^2)$. Equation (1.57) tells us that if Ω_Λ is large enough it can change the sign of the deceleration parameter, giving an explanation for the quite unexpected accelerated phase. In particular, to get $q < 0$ it must be true that

$$\Omega_\Lambda > \Omega_m/2 \, , \tag{1.58}$$

and this condition is indeed satisfied in our Universe; in fact, $q \simeq -0.55$ at $t = t_0$. As already discussed in §1.2, the basic Friedmann equations only allow the possibility of a decelerated Universe: $\ddot{a} < 0$, i.e. downward concavity of the function $a(t)$. In order to invert this trend and recover the upward concavity we must introduce an inflection point ($\ddot{a} = 0$) as seen in fig. 1.3, which represents the evolution of $a(t)$ in different models of universe. Let us now estimate the position in redshift of this inversion by taking into account the density trends in the system of equations (1.43) applied to the acceleration condition (1.58):

$$1 + z_{\rm infl} = \left(\frac{2\,\Omega_{0,\Lambda}}{\Omega_{0,\rm m}}\right)^{\frac{1}{3}} \xrightarrow[\Omega_{0,\Lambda}\simeq 0.7]{\Omega_{0,\rm m}\simeq 0.3} z_{\rm infl} \simeq 0.7 \, . \tag{1.59}$$

The inflection is very close to today's time, hence we can conclude that $\Omega_{0,\Lambda} \simeq 0.7$ is large enough to explain the recent acceleration phase of our Universe but not enough to avoid the Big Bang as we speculated in §1.2.1. Furthermore, the accelerated expansion caused by the cosmological constant happens before the dominance of the cosmological constant itself on the matter component; indeed, $z_{\rm infl} > z_{\rm eq,m-\Lambda} \simeq 0.32$ or, likewise, $t_{\rm infl} < t_{\rm eq,m-\Lambda}$.

Finally, we must keep in mind that the cosmological constant leads to the two unsolved problems of

- *coincidence*, i.e. we are living in a transition epoch during which both the cosmological constant and the matter are relevant, one with an evolution totally different from the other;
- *fine-tuning*, i.e. the fact that the supposed self-regulation of the Universe has strangely made the cosmological constant assume a negligible but non-vanishing value (Weinberg, 1989).

Cosmic Microwave Background.

We refer to the chronological growth of our Universe as the *thermal history*, since its temperature has been mostly decreasing from the Big Bang to today's time, across many different epochs[26]. Nowadays, the average radiation temperature is around 2.73 K.

[26]The Big Bang corresponding time is the so-called Planck time, when the temperature was $T_P \simeq 10^{32}$K, and it is the starting point of the following phases: *GUT transition* ($T_{\rm GUT} \simeq 10^{28-29}$K), *Electro-Weak transition*

What is the origin of this thermal pool? As the decline of the temperature proceeds, about 20 seconds after the BB, the Universe undergoes the $e^+ - e^-$ annichilation and enters the *Radiative Era*, where two crucial processes occur: the *Primordial Nucleosynthesis*[27] 200-300 seconds after the BB, the *Hydrogen Recombination* at $z_{\rm REC} \simeq 1500$ and the *Decoupling Matter-Radiation* at $z_{\rm DEC} \simeq 300$. Note that the Primordial Nucleosynthesis takes place in the Radiative Era, while both the last two processes occur in the Matter Era.

The decoupling between matter and radiation is strongly related to the so-called *last-scattering surface* at $z_{\rm LS} \simeq 1100$, i.e. the time at which the photons do not experience the scattering mechanism anymore and, as a consequence, they are free to escape from the plasma particles. By doing that, the photons start to propagate towards the present days, evolving with a decreasing temperature. At $t = t_0$, since $T_{\rm CMB,0} \simeq 2.73$ K, such ensemble of photons can be seen in the microwave band, that is the reason why we refer to it as *Cosmic Microwave Background*. Together with the Primordial Nucleosynthesis, this is one of the most relevant predictions of the Hot Big Bang Model.

Dark matter.

Many efforts have been made to understand the nature of this invisible[28] form of matter that constitutes the great majority of the total matter component, since there is no standard particle which corresponds to a viable candidate for the DM. Therefore, in order to explain its behaviour, over the last century scientists have looked for alternative competitors, such as primordial black holes (Carr and Kuhnel, 2021), ultra-light particles (i.e. the so-called *fuzzy DM*; see e.g. Hu et al., 2000 and Dentler et al., 2021), weakly interacting massive particles (WIMPs[29], Roszkowski et al., 2018), massive astrophysical compact halo objects (MACHOs[30], Bai et al., 2020) and some others.

Although the DM is still unknown, there is plenty of evidence of its existence, going from the rotation curves of disk galaxies (Fuchs, 2000) to the velocity dispersion of galaxies in clusters (Zwicky, 1937), passing through the microlensing and lensing measurements (Paczyński, 1996; Ellis, 2010).

($T_{\rm EW} \simeq 10^{15}$K), *Quark-Hadron transition* ($T_{\rm QH} \simeq 10^{12}$K), *Hadronic Era* ($T_{\rm HE} \simeq 10^{12}$K), *Leptonic Era* ($T_{\rm LE} \simeq 5 \times 10^9$K), *Radiative Era* ($T_{\rm RE} \simeq 10^9$K $\rightarrow 10^4$K) and *Matter Era* ($T_{\rm ME} < 4000$K).

[27] The Primordial Nucleosynthesis establishes the creation of light elements up to ^{4}He under some necessary assumptions. The chain of reactions stops with the formation of the Helium because at this stage of the Universe the densities are too low to allow the creation of ^8Be (stable).

[28] As we previously pointed out, the DM differs from the baryonic matter since it has not electromagnetic interactions but only gravitational ones.

[29] The WIMPs, together with the MACHOs, represent the most accredited DM candidates. They are not-ordinary particles with energy-masses that span from about 10 GeV to 1 TeV.

[30] The MACHOs are represented by black holes, neutron stars, brown dwarfs and white dwarfs, i.e. extremely compact cosmic structures made of ordinary matter and characterized by no or very faint observable emission.

1.4 Discussing the validity of the ΛCDM model

The cosmological parameters that characterise the ΛCDM model are the following:

- H_0, the *Hubble constant* (see §1.1.2);
- $\Omega_{\rm m} = \Omega_{\rm DM} + \Omega_{\rm b}$, the total *matter density parameter*, where $\Omega_{\rm DM}$ is the *dark-matter density parameter* and $\Omega_{\rm b}$ is the *baryonic-matter density parameter*;
- $\Omega_{\rm DE}$ or Ω_Λ, the *dark-energy* or *cosmological constant density parameter*;
- $\mathcal{A}_{\rm s}$ and σ_8, the first indicating the power spectrum *initial scalar amplitude*, the latter the mass variance σ_M filtered on a scale radius of $8\ h^{-1}{\rm Mpc}$, which is linked to the power spectrum *normalisation* at $z = 0$;
- $n_{\rm s}$, the *spectral index* of the primordial power spectrum;
- τ, the *Thomson scattering optical depth* at the epoch of Reionization[31].

Over the years, scientists have been improving the statistical methods[32] to constrain the values of these ΛCDM parameters (see e.g. Planck Collaboration et al., 2020c). Thanks to the increasing precision of developed techniques, it has been possible to set tight constraints on the cosmological parameters. However, this arose some discrepancies that led to statistical tensions in the Standard Cosmological Model. Indeed, according to the aforementioned paper of the Planck Collaboration $H_0 = 67.4 \pm 0.5\ {\rm km\ s^{-1}\ Mpc^{-1}}$, but other low-redshift measurements provided quite different results; see e.g. Riess et al. (1998), Komatsu et al. (2011), Mandelbaum et al. (2013) and Kobayashi et al. (2017). Furthermore, there exist degeneracies among the parameters, such as $\Omega_{\rm m} - \sigma_8$; however, many of them can be faced by combining different probes. Lastly, note that from the observational point of view, there are many open issues related to both the geometry and the age of the Universe, which arise especially when comparing low- and high-redshift probes.

In this flickering ΛCDM scenario, we must also deal with the theoretical problems of fine-tuning and coincidence linked to the cosmological constant Λ seen as the reason of the late-time accelerated expansion. Several alternative models have been developed in order to address the concordance model and soothe the statistical stress (Pan et al., 2019; Di Valentino et al., 2021). For example, dynamical DE (DDE) models and modified gravity (MG) models have been proposed as viable alternative frameworks. A brief description follows in the next subsections, respectively §1.4.1 and §1.4.2; an exhaustive discussion of these topics can be found in Amendola et al. (2018).

In this context, it is important to mention that some of the effects produced by these DDE and MG models are degenerate with possible effects produced by the presence of neutrinos (see e.g. Lorenz et al., 2017; Baldi et al., 2014; Giocoli et al., 2018), which are another component of our Universe - beyond radiation, matter and cosmological constant presented in §1.3 - that is not fully understood yet. As a consequence, neutrinos could help to reduce the tensions within the ΛCDM Cosmology (see e.g. Lambiase et al., 2019; Sakstein and Trodden, 2020). Note that

[31] The Reionization is a phase in which the Universe ceases to be neutral since the cosmic structures begin to form; this happens about 400 Million years after the BB.

[32] There are many powerful probes in the actual cosmological framework, for example: the CMB angular power spectrum, the gravitational lensing, the Ly-α forest, the clustering and so on, including their combinations.

even though the Standard Model of particle physics describes them as massless particles, there is evidence that they are actually massive (see e.g. Fukuda et al., 1998).

Since in CHAPTER 5 we will test alternative cosmological models to the ΛCDM in an effor to give our contribution in alleviating the above introduced cosmic tensions, let us briefly introduce here both the DDE and MG models.

1.4.1 *Dynamical dark energy* models

Modifying the energy momentum tensor $T_{\mu,\nu}$ in the RHS of the Einstein Field Equation (eq. 1.2) implies a redefinition of the DE component. The attribute *dynamical* means that in this cathegory of models the DE equation of state (eq. 1.41) evolves in time through the w parameter, which becomes a function of redshift, written as:

$$w \equiv w(z) = w_0 + w_a \, f(z) \, . \tag{1.60}$$

These cosmological scenarios are commonly referred to as *quintessence models*, where the *quintessence* corresponds to the DE and is thought to be an unknown fifth component in addition to radiation, baryons, DM and neutrinos.

According to Tsujikawa (2013) and references therein, the *quintessence* is a scalar field Φ which is minimally coupled[33] to gravity. Being this category of DDE the simplest existing scalar-field models that do not lead to theoretical problems, they are crucial in the actual cosmological panorama. The underlying theory supposes that the slow-rolling of the scalar field along a certain potential $V(\Phi)$ should provide a phase of acceleration of the Universe, as needed. Note that this process is similar to the *inflation*[34] of the early Universe. Assuming spatial homogeneity, the above mentioned scalar field Φ evolves via the following equation:

$$\frac{\partial^2 \Phi}{\partial t^2} + 3H \frac{\partial \Phi}{\partial t} + \frac{\partial V(\Phi)}{\partial \Phi} = 0 \, , \tag{1.61}$$

from which we can derive the *pressure* and *density* of the scalar field:

$$\begin{cases} p_\Phi = \dfrac{1}{2}\left(\dfrac{\partial \Phi}{\partial t}\right)^2 - V(\Phi) \, , \\ \rho_\Phi = \dfrac{1}{2}\left(\dfrac{\partial \Phi}{\partial t}\right)^2 + V(\Phi) \, , \end{cases} \tag{1.62}$$

and hence we are able to define the w parameter as $w_\Phi \equiv p_\Phi / \rho_\Phi$.

Among the tensions of the concordance model, the so-called H_0 and σ_8 tensions are the most prominent ones, showing significant discrepancies of the ΛCDM predictions with respect to cosmological observations. Replacing the cosmological constant with the DDE models can help us to alleviate these tensions (see e.g. Sola Peracaula et al., 2016).

[33] See Davari et al. (2019) for details on *minimally* and *non-minimally coupled* scalar fields.
[34] See §2.1.

1.4.2 *Modified gravity* models

The key point of these models is to explain the Universe's recent acceleration by exploiting potential modifications of gravity, whose effects are embedded in the LHS of the Einstein Field Equation (eq. 1.2). With respect to the ΛCDM scenario, whether a MG model is viable depends on two main facts:

- it differs on how the gravitational instability makes the density perturbations dynamically evolve;
- but it must show nearly the same expansion history as the ΛCDM.

In addition, since it has been proved that the GR is valid in the Solar System, the MG model must include what is called a *screening mechanism* (see e.g. Brax and Valageas, 2013), in order to recover the GR predictions in our surroundings or, generalising, at small scales.

f(R) models

The simplest way to include MG in our models is modifying the *Einstein-Hilbert action* by the introduction of a function $f(R)$:

$$S = \int d^4x \sqrt{-g}\left(\frac{R + f(R)}{16\pi G}\right) + \mathcal{L}_{\rm m} \,, \tag{1.63}$$

where R is the *Ricci scalar* and $\mathcal{L}_{\rm m}$ is the Lagrangian density of the total matter field. As already underlined, a MG model described by equation (1.63) must provide the same expansion history of the cosmological constant; with this purpose, Hu and Sawicki (2007) proposed the following functional form for $f(R)$:

$$f(R) = -m^2 \frac{c_1 \left(\frac{R}{m^2}\right)^n}{c_2 \left(\frac{R}{m^2}\right)^n + 1} \,, \tag{1.64}$$

where $m \equiv H_0^2\sqrt{\Omega_{\rm m}}$ is the mass scale, c_1 and c_2 are positive or, at least, vanishing parameters. Assuming $c_2(R/m^2)^n \gg 1$, after some mathematical steps, equation (1.64) turns into:

$$f_{\rm R} \approx -n\frac{c_1}{c_2^2}\left(\frac{m^2}{R}\right)^{n+1} \,. \tag{1.65}$$

Now, by choosing $c_1/c_2 = 6\Omega_\Lambda/\Omega_{\rm m}$ and $n = 1$, at first approximation we find out that these models depend just on the parameter $f_{\rm R0}$, whose value refers to today's time:

$$f_{\rm R0} = -\frac{1}{c_2}\frac{6\Omega_\Lambda}{\Omega_{\rm m}}\left(\frac{m^2}{R_0}\right)^2 \,. \tag{1.66}$$

As fig. 1.4 shows, the higher the absolute value of $f_{\rm R0}$ is and the more the $f(R)$ model moves away from the ΛCDM, being its power spectrum[35] described by a higher normalization at small physical scales, i.e. large k values in the Fourier space.

[35] See §2.4.1 for further details on the power spectrum $P(k)$.

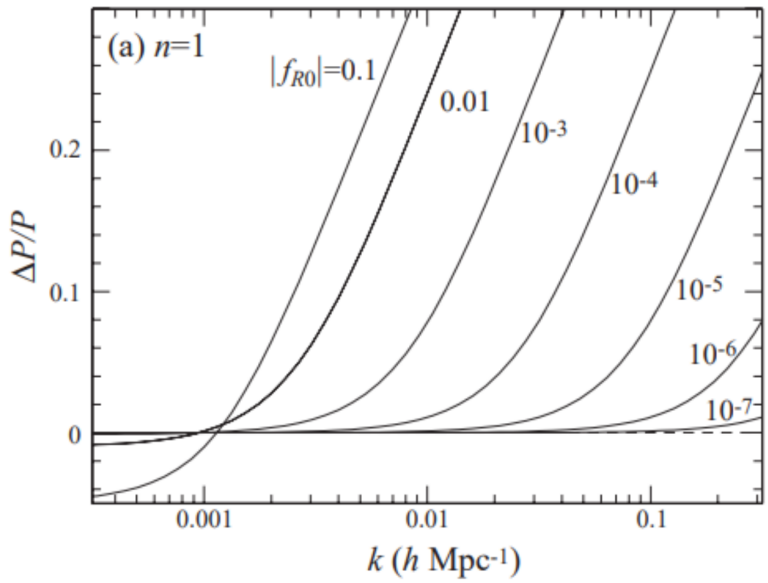

Figure 1.4: Relative power spectrum of the $f(R)$ models with respect to the ΛCDM, depending on the $f_{\rm R0}$ parameter absolute value at fixed $n = 1$. Credits to: Hu and Sawicki (2007).

Notice that the MG models are particularly suited to alleviate the so-called S_8 tension of the ΛCDM model (see e.g. de Cruz Pérez, 2021), where $S_8 \equiv \sigma_8 \sqrt{\Omega_{\rm m}/0.3}$.

Chapter 2

Structure Formation and Evolution

The main aim of this Thesis work is to exploit the clustering statistics of cosmic voids for cosmological purposes. Hence, let us provide in this chapter some theoretical bases on the large-scale structure of our Universe, and on the processes through which it has originated.

We refer to the large-scale structure of the Universe as *Cosmic Web*, i.e. a well built system of voids, filaments, walls and nodes. This recursive network has formed from the primordial fluctuations originated at the end of the inflation (see §2.1) at very high redshift (Snedden et al., 2015; Bacon et al., 2021). According to the Standard Cosmological Model, the formation of cosmic structures follows a bottom-up scenario in which the DM particles collapse in DM haloes, providing the potential wells where the baryons can then fall in (*baryon catch-up*). Small DM haloes and baryonic structures appeared first and then larger ones were built by aggregation. Let us define the *density contrast* as:

$$\delta \equiv \frac{\delta\rho}{\rho} = \frac{\rho - \bar{\rho}}{\bar{\rho}} = \frac{\rho}{\bar{\rho}} - 1 \,, \tag{2.1}$$

where ρ is the local density while $\bar{\rho}$ is the mean density of the Universe. Today (at $z = 0$), the measured density contrast inside virialized cosmic structures is around $100 - 1000$, while at $z \simeq 1100$ it was about 10^{-5}. The goal of Cosmology is to provide an explanation for this growth. Note that we know the amplitude of δ at the *last-scattering surface* redshift from the CMB angular power spectrum and maps of temperature. Under the adiabatic condition (1.26) we can then write $\delta T/T \simeq \delta\rho/\rho \simeq 10^{-5}$, where $T = T_{0,\mathrm{CMB}} \simeq 2.3\,\mathrm{K}$ is the CMB temperature at present time (i.e. the black body radiation temperature).

The formation and evolution of the cosmic structures strongly depend on the cosmological parameters, in which both the geometry and the constituents of the Universe are embedded. As a consequence, the large-scale structure statistics provides extremely powerful probes that supports us on the path to the understanding of the Universe in which we live. In this chapter we will go through both the linear (§2.2) and nonlinear (§2.3) evolution of the cosmic structures, from a brief description of the inflation as a valid method to create perturbations (§2.1) to the statistical properties of the large-scale structure today and over times (§2.1). Finally, in §2.5 we will present the key features of numerical simulations, a robust tool involved in the investigation of the physical properties of our Universe through the computational reproduction of several occurring phenomena.

2.1 Inflation and origin of primordial fluctuations

As already mentioned in the introduction, the inflation is crucial in the actual cosmological framework since it could solve three annoying issues of the Hot Big Bang model: *flatness*, *horizon* and *magnetic monopoles* problems. Moreover, most significantly, inflation provides the initial conditions to solve the Einstein-Boltzmann equations describing the evolution of cosmic structures.

Let us now present the physical concepts behind the inflationary process, from its genesis to the creation of the initial perturbations needed for the formation of the very first cosmic structures. The basic idea of the first inflationary models is strongly related to the theory of the *phase transition*. Hence, in the next paragraph we provide a brief introduction about this topic. Then, it follows a description of the models based on the physics of phase transitions (i.e. the *Guth Models*, see §2.1.1).

Phase Transitions. According to classic Physics, there exist four fundamental forces, namely *gravitational*, *electromagnetic*, *weak* and *strong nuclear* forces. Retracing back in time the history of the primordial Universe, the four forces reunify through three phase transitions called (following an anti-chronological order) *Quark-Hadron*, *Electro-Weak* and *GUT*; finally, the *Theory of Everything* is expected to be required to describe the unified interaction at the Planck time.

A phase transition is defined here as the change from a disordered stage to a situation where a certain order is set. To understand how the idea of phase transition can be introduced in the inflationary models, let us define the *free energy* F as:

$$F = \mathcal{U} - TS \,, \tag{2.2}$$

where $\mathcal{U}$ is the internal energy, T is the temperature and S is the entropy. This equation tells us that $\forall T > 0$, the entropy makes whichever system stabilize by going towards the lowest free-energy state. If we now introduce the *order parameter* Φ, we can rewrite equation (2.2) as follows:

$$F = F_0 + \alpha\Phi^2 + \beta\Phi^4 + \gamma(\Phi^2)^{3/2} \,, \tag{2.3}$$

where Φ is a scalar field that we will call *inflaton*. It refers to how much the system is ordered when it reaches the equilibrium: if $T > T_\mathrm{c}$, where T_c is defined as the *crytical temperature* of the system, the equilibrium is reached for $\Phi = 0$ (totally disordered phase); while if $T < T_\mathrm{c}$ the equilibrium is achieved for $\Phi = \Phi_0 \neq 0$ (ordered phase). Something else that must be mentioned here is that, according to the values of the parameters in eq. (2.3), there are two classes of phase transition:

- first order, i.e. the transition is not instantaneous but happens when $T \ll T_\mathrm{c}$ so that a finite free-energy gap, ΔF, called *latent heat* is present;
- second order, i.e. the transition is instantaneous and can already take place at $T < T_\mathrm{c}$, with the production of an infinitesimal ΔF.

The Guth inflation sticks to the GUT transition ($t_\mathrm{GUT} \simeq 10^{-37}\mathrm{s}$, $T_\mathrm{GUT} \simeq 10^{15}\mathrm{GeV}$), which represents a suitable mechanism that can conduct the Universe to the inflationary acceleration.

Moreover, the energy corresponding to the GUT temperature and associated to the scalar field Φ is high enough to create particles and achieve the amount of entropy needed to solve the ΛCDM open problems. By contrast, the chaotic inflation only assumes the existence of an extremely energetic scalar field, so that it relies on the same energy of the GUT transition but without all the implications of a phase transition.

2.1.1 Guth models and chaotic inflation

Let us associate the *inflaton* Φ to the following Lagrangian density:

$$\mathcal{L}_\Phi = \frac{1}{2}\dot{\Phi}^2 - V(\Phi, T) \,, \tag{2.4}$$

where $\dot{\Phi}$ is the time derivative of the scalar field and $V(\Phi, T)$ is a generic potential that depends on both the scalar field and the temperature. In terms of density and pressure we have:

$$\begin{cases} \rho_\Phi = \dfrac{1}{2}\dot{\Phi}^2 + V(\Phi, T) \,, \\ P_\Phi = \mathcal{L}_\Phi = \dfrac{1}{2}\dot{\Phi}^2 - V(\Phi, T) \,. \end{cases} \tag{2.5}$$

By means of these two last equations it is also possible to define the momentum-energy tensor as $T_{\Phi,ij} = -P_\Phi g_{ij} + (P_\Phi + \rho_\Phi)u_i u_j$.

The dynamic of Φ is regulated by the Friedmann equations (eqs. 1.24 and 1.25) just by adding the terms of its pressure and density introduced in the previous systems of equations. Hence, considering the *Euler-Lagrange equation*

$$\frac{\mathrm{d}}{\mathrm{d}t}\frac{\partial}{\partial\dot{\Phi}}(\mathcal{L}_\Phi a^3) - \frac{\partial}{\partial\Phi}(\mathcal{L}_\Phi a^3) = 0 \,, \tag{2.6}$$

we obtain the formula that regulates the dynamics of the inflaton:

$$\ddot{\Phi} + 3H\dot{\Phi} + \frac{\partial V}{\partial\Phi} = 0 \,, \tag{2.7}$$

where $\ddot{\Phi}$ is the acceleration, while $3H\dot{\Phi}$ is the friction that slows the response of the acceleration to the acting force ($\partial V/\partial\Phi$, i.e. the force per unit mass).

The Guth models (Guth, 2004) are split in two classes:

- **Old Inflation.** This class of models are embedded in first order transitions, hence there is some latent heat that leads to the creations of particles. However, this model has then been excluded since it predicts a too small dimension of our Universe today.
- **New Inflation.** These models assume second order transitions, and thus do not have an amount of latent heat available for particle creation. We can deal with this problem by imposing $\mathrm{d}V/\mathrm{d}\Phi \approx 0$, but this leads to a *fine-tuning problem*.

The current paradigm on which the inflation relies is called *Chaotic Inflation*. Being completely disconnected from the concept of phase transition but keeping the same energy, it is

based on the existence of a highly energetic scalar field Φ in the primordial Universe. What this model does is considering equation (2.7) together with the following rewriting of the second Friedman equation (eq. 1.25)

$$H^2 = \frac{8\pi}{3}\left(\frac{1}{2}\dot{\Phi}^2 + V\right), \tag{2.8}$$

in order to develop the theoretical formulas of the inflationary period. This goal is achieved under the assumption of the so-called *slow rolling conditions* for a generic potential V:

$$\begin{cases} |\ddot{\Phi}| < 3H\dot{\Phi} \\ |\dot{\Phi}^2| \ll V \end{cases} \iff \begin{cases} |V''/V| \ll 1 \\ |V'/V|^2 \ll 1 \end{cases} \tag{2.9}$$

where the dots are time derivatives while the primes are derivatives with respect to Φ. *Slow rolling* means that the inflation must last enough to solve the three already mentioned problems of the ΛCDM model, i.e. flatness, horizon and magnetic monopoles. In this way any inhomogeneity or anisotropy is erased (i.e. the so-called *No Cosmic Hair* theorem).

The three main stages of this process' evolution are the *fall on the attractor*, the *inflation* and the *graceful exit*. In the last phase, with a process of spiraling, the particles are created through the energy loss of the inflaton. For further details on this topic see Linde (2007).

2.2 Linear Evolution

At the end of the inflationary phase (§2.1), the Universe was filled with fluctuations of temperature and density that, when measured at the last-scattering redshift, are about 10^{-5} as a order of magnitude. Until the density perturbations are small enough (i.e. $\delta\rho/\rho \ll 1$) we can rely on the linear evolution, firstly described by Sir James Hopwood Jeans in 1902. His perturbation theory is based on the concept of *gravitational instability*, a model in which the overdensities (i.e. small positive fluctuations) tend to attract matter to grow. By doing that, vast regions of Universe are emptied, resulting in today's cosmic voids.

The cosmic structure evolution is a perpetual competition between the small-scale gravitational attraction and the global gravitational expansion of the Universe: the former favouring the collapse and hence the formation of the cosmic structures, while the latter acting in the opposite direction, making the matter-particles move away from each other as the space expands. As a result, the slower the expansion rate is and the more the gravitational collapse is favoured since the small-scale attraction turns up to be more effective than the global space expansion. By contrast, if the Universe grows rapidly (e.g. open models, see §1.2.2) the formation of structures is less effective.

In the next sections we will see how we can theoretically recover the observed fluctuations of the density field ($\delta\rho/\rho \simeq 100 - 1000$) by combining the linear and nonlinear evolution, respectively in §2.2.2 and §2.3.

Jeans Theory. The Jeans theory describes the dynamical evolution of a self-gravitating gaseous sphere, providing us with analytical solutions valid across the linear regime, and thus applicable only at the beginning of the structure formation process. According to this

approach, the gaseous sphere must exceed the Jeans radius and mass (R_J, M_J)[1] in order to collapse; analogously, a perturbation must be larger than the so-called *Jeans length* (λ_J). There are several ways to define this crucial scale:

- kinetic-potential energy balance:

$$E_{kin} = E_{pot} \quad \rightarrow \quad \frac{1}{2}Mv^2 = -\frac{GM^2}{R} \quad \rightarrow \quad R_J = \frac{v}{\sqrt{2G\rho}}\,, \tag{2.10}$$

- gravitational-pressure force balance:

$$F_g = F_p \quad \rightarrow \quad \frac{GM}{R^2} = -\frac{PR^2}{M} \quad \rightarrow \quad R_J = \frac{v}{\sqrt{G\rho}}\,, \tag{2.11}$$

- freefall-crossing time balance:

$$\tau_{ff} = \tau_{cross} \quad \rightarrow \quad \frac{1}{\sqrt{G\rho}} = \frac{\lambda}{v} = \frac{2R}{v} \quad \rightarrow \quad R_J = \frac{v}{2\sqrt{G\rho}}\,, \tag{2.12}$$

where $G = 6.67428 \times 10^{-8}\ \mathrm{cm^3 g^{-1} s^{-2}}$ is the *gravitational constant*, ρ is the density, M is the mass of the self-gravitating gas while R is its radius, P is the pressure and $\lambda = 2R$ is the diameter of the sphere. Finally, it is remarkable that v is a velocity and it is synonymous either of the *sound speed* (v_s) for the baryons or of the *velocity dispersion* (σ) for the dark matter.

2.2.1 Static Universe

Let us define the system of *fluid-dynamics equations*, which will be crucial in order to trace the evolution of the self-gravitating gaseous sphere:

$$\begin{cases} \dfrac{\partial \rho}{\partial t} + \vec{\nabla}(\rho \vec{v}) = 0 \\ \dfrac{\partial v}{\partial t} + (\vec{v} \cdot \vec{\nabla})\vec{v} = -\dfrac{1}{\rho}\nabla P - \nabla \Phi \\ \nabla^2 \Phi = 4\pi G \rho \\ P = P(\rho, S) = P(\rho) \end{cases} \tag{2.13}$$

where, apart from the variables defined above, Φ is the potential and S is the entropy. The second equivalence of the last equation in the system (2.13) is justified for *adiabatic* models and it means that the entropy is constant, i.e. $\mathrm{d}S/\mathrm{d}t = 0$. Under this approximation it is possible to introduce the sound speed as follows:

$$v_s^2 = \left(\frac{\partial P}{\partial \rho}\right)_{S=cost} \approx \frac{P}{\rho} \quad \rightarrow \quad P = v_s^2 \rho\,. \tag{2.14}$$

[1] The Jeans mass can be expressed as a function of the Jeans radius through $M_J = \frac{4}{3}\pi R_J^3 \rho_b$.

Assuming to know the unperturbed solution of the system of equations (2.13), we add to this solution small perturbations $\delta x/x \ll 1$ (i.e. $\rho = \rho_B + \delta\rho$, $P = P_B + \delta P$, $\Phi = \Phi_B + \delta\Phi$ and $v = v_B + \delta v = \delta v$, where the subscript B stands for *background* and refers to constant quantities; an exception is $v_B = 0$ because we are considering a static Universe). By doing this and neglecting the unperturbed terms since they already satisfy the system (2.13) and the second order terms as they are out of the boundaries of the linear theory, the equations become:

$$\begin{cases} \dfrac{\partial \delta\rho}{\partial t} + \rho_B \nabla \delta v = 0 \\ \dfrac{\partial \delta v}{\partial t} + (\vec{v}\cdot\vec{\nabla})\vec{v} = -v_s^2 \dfrac{\nabla\delta\rho}{\rho_B} - \nabla\delta\Phi \\ \nabla^2\delta\Phi = -4\pi G\delta\rho \end{cases} \tag{2.15}$$

This is what we call the system of *linearized* equations. In order to proceed, we now assume our solutions to be plane waves, hence described by the following:

$$\begin{cases} \delta\rho = \delta\rho_{\vec{k}}\, e^{i\vec{k}\cdot\vec{r}+i\omega t} \\ \delta\Phi = \delta\Phi_{\vec{k}}\, e^{i\vec{k}\cdot\vec{r}+i\omega t} \\ \delta v = \delta v_{\vec{k}}\, e^{i\vec{k}\cdot\vec{r}+i\omega t} \end{cases} \tag{2.16}$$

where $\vec{k} = 2\pi/\lambda$ is the wavelength vector. Considering that the derivatives of these solutions with respect to time and space are

$$\frac{\partial f}{\partial t} = i\omega f \qquad , \qquad \nabla f = i\vec{k} f \ , \tag{2.17}$$

and imposing the determinant of the system (2.15) to vanish, we get the so-called *Dispersion Relation*:

$$\omega^2 = k^2 v_s^2 - 4\pi G\rho_B \ , \tag{2.18}$$

which can be set equal to zero in order to obtain the Jeans wavenumber and the Jeans scale:

$$k_J = \frac{\sqrt{4\pi G\rho_B}}{v_s} \qquad , \qquad \lambda_J = \frac{\sqrt{\pi} v_s}{\sqrt{G\rho_B}} \ .$$

There are two possible outcomes of equation (2.18):

- if $\lambda < \lambda_J$ i.e. $k > k_J \ \rightarrow \ \omega^2 > 0$ and ω can be written as

$$\omega = \pm k v_s \left[1 - \left(\frac{\lambda}{\lambda_J}\right)^2\right]^{1/2} \tag{2.19}$$

  where $c_s \equiv \omega/k$; for $\lambda \rightarrow 0$ we have $c_s \rightarrow v_s$, while for $\lambda \rightarrow \lambda_J$ we can write $c_s \rightarrow 0$;

- if $\lambda > \lambda_J$ i.e. $k < k_J \rightarrow \omega^2 < 0$ and ω takes the following form:

$$\omega = \pm i\sqrt{4\pi G\rho_B}\left[1 - \left(\frac{\lambda_J}{\lambda}\right)^2\right]^{1/2} \tag{2.20}$$

  hence, if $\lambda \rightarrow \lambda_J$, $\omega^2 = 0$ and $\tau_{ff} \sim \omega^{-1} \rightarrow \infty$; if instead $\lambda \rightarrow \infty$, $\omega^2 = -4\pi G\rho_B$ and $\tau_{ff} \sim \omega^{-1} \simeq (G\rho_B)^{-1/2}$.

Therefore, when $\lambda < \lambda_J$ the perturbations propagate as waves, while for $\lambda > \lambda_J$ the amplitude of the density fluctuations undergoes an exponential growth[2].

Before moving on, it should be noted that there is an inconsistency in the static-Universe scenario: $\Phi_B = const$ as a background quantity and this implies that the Poisson equation (third equation of 2.13) is valid for $\rho_B = 0$, i.e. the system is unstable: a self-gravitating gaseous sphere must have $v \neq 0$, expanding or collapsing. However, this physical tension is easily erased by replacing the static hypothesis with a non-static Universe in §2.2.2.

2.2.2 Expanding Universe

In order to perform the Jeans analysis in an expanding Universe, we first need to introduce three essential quantities:

- the *cosmological horizon* sets the length over which only the gravity matters, leading to the simple collapse of the perturbations, and below which the microphysics phenomena must be considered too, together with the *causal connection*[3]; we can write it as:

$$R_{\rm H}(t) = a(t)\int_0^t \frac{c\,{\rm d}t'}{a(t')}\,; \tag{2.21}$$

- the *Jeans length* discriminates which perturbations can grow forming the cosmic structures from the ones which cannot, resulting in a plane-wave propagation; hence, $R_{\rm J}$ is meaningful just if defined (see eqs. 2.10, 2.11 or 2.12) inside the cosmological horizon $R_{\rm H}$;
- the *dissipation length* refers to the fact that, among the perturbations which cannot grow, the ones even smaller than $R_{\rm DIS}$ are dissipated or, in other words, erased.

Notice that the already mentioned scales are listed depending on their relative size, i.e. $R_{\rm H} > R_{\rm J} > R_{\rm DIS}$, and all of them depend on time. Let us then point out three fundamental times necessary to describe the evolution of the primordial fluctuations in the context of an expanding Universe:

- the *equivalence time* ($t_{\rm eq}$) signs the moment in which the radiative era leaves its place to the matter one and, since the radiation is no longer dominant, and its opposition to collapse is increasingly less efficient, the perturbation growth is favoured;

[2] In fact, considering the definition of ω in eq. (2.20), the first equation of (2.16) gives the following functional form for the density contrast evolution: $\delta = \delta\rho/\rho_{\rm B} = \delta_{\vec{k}}\ \exp(\pm|\omega|t)\ \exp(i\vec{kr})$, i.e. an exponential growth in time.

[3] The cosmological horizon can be thought as a radius that defines the spherical volume of the Universe in which it is in causal connection with the observer. $R_{\rm H}$ represents the distance travelled by the light from the Big Bang to the time t.

- the *decoupling time* ($t_{\rm DEC}$) refers to the baryons-radiation decoupling, i.e. the time at which the baryonic matter and the photons take different paths in the thermal history of the Universe. The more its value is smaller, the more the structure formation is favoured;
- the *de-relativisation time*[4] ($t_{\rm DR}$) marks the moment before which the matter is relativistic and, as a consequence, it must be included in the EoS of the radiative component ($w = 1/3$).

As already mentioned, the formation history of the cosmic structures depends on the background Cosmology, and therefore our models must take into account the expansion of the Universe (i.e. the Hubble flow, see §1.1.2), which acts against the small-scale gravitational collapse. We will then consider an EdS model as the background Universe and a small closed Universe (see §1.2.2) to mimic a spherical perturbation. The expansion is taken into account by means of the term of the background velocity: from $v_B = 0$ in the static Universe to $v_B = Hr \neq 0$.

We treat separately the perturbations λ *greater* and *smaller* than the cosmological horizon (eq. 2.21) as beyond its boundaries the gravity is the only acting force and we can neglect gas physics and electromagnetic interactions. We obviously cannot do the same on causally connected scales.

Scales with $\lambda > \mathbf{R_H}$

For such perturbations we do not need the system of hydrodynamic equations (2.13) since the radiative component is ineffective on scales which are not causally connected. Let us rewrite the second Friedmann equation (eq. 1.25) divided by a and express it for both the background-flat Universe ($\kappa_B = 0$) and for the spherical perturbation ($\kappa_p = +1$):

$$H^2 = \frac{8\pi}{3} G\rho - \frac{\kappa c^2}{a^2} \quad \longrightarrow \quad \begin{cases} H_B^2 = \dfrac{8\pi}{3} G\rho_b \\ H_p^2 = \dfrac{8\pi}{3} G\rho_B - \dfrac{c^2}{a^2} \end{cases} \tag{2.22}$$

We proceed by synchronizing the two solutions at the same time through their Hubble parameter ($H_B^2 = H_p^2$) and we obtain the formulas that regulate the perturbation amplitude and the background density evolution:

$$\begin{cases} \delta \propto a^{-2} \rho_B^{-1} \, , \\ \rho_B \propto a^{-3(1+w)} \, . \end{cases} \tag{2.23}$$

Outside the cosmological horizon all perturbations grow, and how fast their growth is depends on the dominant component:

- before the equivalence, i.e. $t < t_{\rm eq}$, the Universe is going through the radiative era, so that the dominant component has $w = 1/3$:

$$\rho_B = \rho_{\rm r} \propto a^{-4} \quad \longrightarrow \quad \delta \propto a^2 \, ; \tag{2.24}$$

[4] Note that we can discriminate between hot and cold dark matter depending on when this de-relativisation time occurs with respect to the decoupling time. In particular, $t_{\rm DR} > t_{\rm DEC}$ implies HDM while if $t_{\rm DR} < t_{\rm DEC}$ the CDM is called into play. As a consequence, the Jeans mass associated to the HDM ($10^{15-16} \mathrm{M}_\odot$) is much greater than that of CDM ($10^{5-6} \mathrm{M}_\odot$) and this results respectively in a *top-down* or *bottom-up* scenario of structure formation.

- after the equivalence, i.e. $t > t_{\rm eq}$, the matter prevails and $w = 0$:

$$\rho_B = \rho_{\rm m} \propto a^{-3} \quad \longrightarrow \quad \delta \propto a \; . \tag{2.25}$$

The proportionality relations (2.24) and (2.25) can be also expressed as a function of time by considering the trends $a = a(t) \propto t^{\Gamma}$, where the values of Γ can be read in table 1.1.

Scales with $\lambda < \mathbf{R_H}$

Inside the horizon the perturbations have to deal with micro-physics processes. We start from the equations in (2.13) but defining the velocity as $\vec{u} = H\vec{r} + \vec{v}$, where Hr is the Hubble flow and $\vec{v}$ is the velocity field:

$$\begin{cases} \dfrac{\partial \rho}{\partial t} + \vec{\nabla}(\rho \vec{u}) = 0 \\ \dfrac{\partial \vec{u}}{\partial t} + (\vec{u} \cdot \vec{\nabla})\vec{u} = -\dfrac{1}{\rho}\nabla P - \nabla \Phi \\ \nabla^2 \Phi = 4\pi G \rho \\ P = P(\rho, S) = P(\rho) \end{cases} \tag{2.26}$$

The easiest way to perform the calculations when taking into account the expansion of the Universe is through the *comoving coordinates* (see §1.1.2), which naturally encode the effect of the cosmic scale factor, being the frame of reference "comoving" with the Hubble flow. In this regard, we recall the following changes of coordinates:

$$r = a\mathrm{X} \quad \Longleftrightarrow \quad k_{\rm com} = a \, k_{\rm phys} \; . \tag{2.27}$$

In order to develope this analysis, we need to define ρ_B: in fact, the background density has a different evolution in time, depending on the prevailing component (see eqs. 2.24 and 2.25). We focus on the solutions of the matter era since this is the most relevant phase for the evolving matter perturbations.

Matter Era. Since $w = 0$, $\rho_B \propto \rho_{\rm m} \propto a^{-3}$ and we can assume $P_{\rm m} = 0$. It is found that, in physical coordinates, the dispersion relation is:

$$\ddot{\delta}_k + 2\frac{\dot{a}}{a}\dot{\delta}_k + \delta_k \Big[k^2 v_s^2 - 4\pi G \rho_B \Big] = 0 \; , \tag{2.28}$$

and we search for solutions in the form $\delta_k = t^{\alpha}$. In this equation, the second term encodes the expansion of the Universe, while the third term describes the competitive effects of the velocity dispersion and the gravitational potential; the cosmological parameters are embedded in these two terms. As long as the matter prevails, the following relations are valid in an EdS

background Universe (tab. 1.1):

$$\begin{cases} a \propto t^{2/3} \quad \longrightarrow \quad H = \dfrac{\dot{a}}{a} \propto \dfrac{2}{3t} \, , \\ \rho_B \propto \dfrac{1}{6\pi G t^2} \, . \end{cases} \tag{2.29}$$

Putting all the above together, after some mathematical passages we get both the Jeans wavenumber and length:

$$k_J = \frac{5}{v_s}\sqrt{\frac{\pi G \rho_B}{6}} \qquad , \qquad \lambda_J = v_s \sqrt{\frac{24\pi}{25 G \rho_B}} \, .$$

If $\lambda < \lambda_J$ or $k > k_J$, the solution δ_k are imaginary, and therefore the perturbations do not grow but propagate as waves. If instead $\lambda > \lambda_J$ or $k < k_J$, they grow towards the cosmic structure formation; in the limit $\lambda \gg \lambda_J$ we derive the following trends:

$$\delta_- \propto t^{-1} \propto a^{-3/2} \qquad , \qquad \delta_+ \propto t^{2/3} \propto a \, ,$$

where the growing solution is δ_+ and it is valid if and only if the component considered is decoupled from radiation; this means that since the DM-radiation decoupling takes place at very high redshift, it can start to collapse immediately, while the baryons begin this process at $z_{\rm DEC} \simeq 300$. It should be noted that in an EdS Universe the density contrast at $z \simeq 1100$ on the last-scattering surface should be $\delta\rho/\rho \simeq 10^{-3}$ in order to achieve the nonlinear observed regime (i.e. $\delta\rho/\rho \sim 1$) at low redshift. However, we know that perturbations are smaller at least of two orders of magnitude. A possible alternative to cope with this problem is to replace the EdS background Universe with a closed model, in which the expansion is reduced and the growth of the perturbations enhanced. Actually, since there is strong evidence on the flatness of the Universe (see e.g. Efstathiou and Gratton, 2020), this hypothesis is not justified. What is likely to happen is that, by starting first its collapse, the DM prepares the potential wells in which the baryon fall is then favoured; this is what is known as *baryon catch-up*.

In the previous analysis, a flat EdS Universe has been considered, but we can even apply the Jeans theory to a curved background Universe. The generic solutions are:

$$\begin{cases} \delta_-(t) = H(t) \\ \delta_+(t) = H(t) \displaystyle\int \frac{\mathrm{d}t}{H^2(t) a^2(t)} \quad i.e. \quad \delta_+ \propto H(z) \int_{-\infty}^{z} \frac{\mathrm{d}z}{a^2} \frac{1+z}{H^2(z)} \end{cases} \tag{2.30}$$

In particular, the growing solution δ_+ of a *closed Universe* has a time evolution faster than in the EdS model; by contrast, the growth process is slower in an *open Universe*. It is noticeable that the integral form of δ_+ is well approximated by means of the following formula:

$$f \equiv \frac{\mathrm{d}\ln\delta_+}{\mathrm{d}\ln a} = \Omega_{\rm m}^{0.55} + \frac{\Omega_\Lambda}{70}\left(1 + \frac{1}{2}\Omega_{\rm m}\right) , \tag{2.31}$$

where f is known as *growing factor*, $\Omega_{\rm m}$ and Ω_Λ are the matter and the dark energy density parameters respectively. Equation (2.31) can be used for tomographic analyses that allow us

to set constraints on the cosmological parameters in two possible ways:

- we can measure f to test the GR: if the exponent of $\Omega_{\rm m}$ is not equal to 0.55, the GR is no longer valid;
- assuming the validity of GR, we can test the cosmological models since an increasing $\Omega_{\rm m}$ is responsible for a more efficient growth of the perturbations.

For the sake of argument, in the previous **Radiative Era** an EdS model is a proper approximation for the primordial phases of our Universe; $w = 1/3$ and $\rho_B \propto \rho_{\rm r} \propto a^{-4}$. Therefore we can perform the same analysis as before but accounting for the *radiative pressure* due to the dominant relativistic component in eqs. (2.26). As a consequence, the Jeans scale of the radiative component is greater than the cosmological horizon, i.e. $\lambda_J > R_{\rm H}$. Since λ_J makes sense only inside the horizon, this means that the relativistic component cannot grow at any scale ($\delta_{\rm r} = 0$): the propagation of the waves is so fast ($c/\sqrt{3}$) that there are not radiative fluctuations at $t < t_{\rm eq}$. In the meanwhile, the DM perturbations included in the cosmological horizon ($\lambda < R_{\rm H}$) undergo the *Meszaros effect*, i.e. the stagnation of the DM growth (Meszaros, 1974). Notice that the reason why perturbations can or cannot grow lies on the comparison between the *free-fall time* $\tau_{\rm ff}$ and the *Hubble time* $\tau_{\rm H}$, defined as:

$$\begin{cases} \tau_{ff} \propto \dfrac{1}{\sqrt{G\rho}} \,, \\ \tau_{H} \propto \dfrac{1}{H(t)} \,. \end{cases} \tag{2.32}$$

In fact, if $\tau_{ff} < \tau_H$ (i.e. $t > t_{eq}$) the gravitational collapse is effective, while it is ineffective otherwise (i.e. $t < t_{eq}$) since the process in this case would last longer than the lifetime of the Universe at the time considered.

Finally, the baryons cannot grow in the radiative era, since they are coupled with radiation and $\delta_{\rm baryons} \sim \delta_{\rm r} \sim 0$; the baryonic matter must wait until the decoupling matter-radiation in the following matter era, when it is free to fall rapidly in the DM potential wells through the *baryon catch-up*.

2.3 Nonlinear Evolution

The Jeans theory provides us with analytical solutions valid across the linear regime. Therefore, it can be applied only at the beginning of the formation process; when the value of δ reaches the unit, a nonlinear theory becomes necessary. There are several ways to develop a theory for the nonlinear regime, such as:

- the *Zel'dovich approximation* and the *spherical collapse model* (see §2.3.1 and §2.3.2);
- higher-order perturbative theories, obtained by starting from the already mentioned eqs. (2.26) and considering terms of order higher[5] than the first;

[5]The greater the order considered is and the more the result is valid for larger density constrasts δ.

- the *peaks theory* (for further details see e.g. Young and Musso, 2020), which applies the peak properties in Gaussian fields to the perturbative theory; the peaks have to be intended as the regions where structures are most easily formed;
- the *lognormal models* (Coles and Jones, 1991), where the assumed density field is the Gaussian distributed natural logarithm of δ; this is an acceptable approximation for density contrast whose value is not too high;
- the N-body simulations[6] (see §2.5), which can trace gravity and how it acts in the evolution of the cosmic structures.

In the next sections we will focus on the description of the Zel'dovich approximation (§2.3.1), the spherical collapse model (§2.3.2) and the N-body simulations (§2.5). Let us underline that the last two will be extensively used to properly construct both halo and void catalogues (chapter 4), and to analyse the void clustering statistical properties (chapter 5).

2.3.1 Zel'dovich approximation

The theory proposed by Zel'dovich (1970) is a Lagrangian non-analytic theory developed as a function of the initial displacement field $G(\vec{q}) = -\nabla_{\vec{q}}\,\phi(\vec{q})$, where $\vec{q}$ is the initial Lagrangian position. The Lagrangian coordinates $\vec{q}$ can be transformed into the Eulerian coordinates $\vec{r}$ through the following relation:

$$\vec{r}(\vec{q},t) = a(t)\,\vec{q} + F(\vec{q},t)\,, \tag{2.33}$$

where $a(t)\vec{q}$ refers to the expansion of the Universe, while $F(\vec{q},t)$ is the displacement; hence, the final position depends on the initial position and on the amount of time passed since when the particles start to move. Let us separate the formula into its two dependencies (i.e. $F(\vec{q},t) = f(t)\,G(q)$), so that equation (2.33) becomes:

$$\vec{r}(\vec{q},t) = a(t)\,\vec{q} + f(t)G(\vec{q}) = a(t)\,\vec{q} + a(t)b(t)G(\vec{q}) = a(t)\Big[\vec{q} + b(t)G(\vec{q})\Big]\,, \tag{2.34}$$

where the second equivalence is to impose that the linear solution is recovered for small perturbations: $b(t) = \delta_+(t)$.

In this approximation the peculiar velocity field is assumed to be irrotational. This means that the trajectories never change: the particles do not feel the mutual interaction and their trajectories cross each other (*shell-crossing problem*). This is the great limit of the Zel'dovich approach; in fact, in a typical N-body simulation the displacement term has to be computed any time a particle moves from the initial position $\vec{q}$ to another position $\vec{q}\,'$.

Defining the differential of the mass in both Lagrangian (eq. 2.35) and Eulerian (eq. 2.36) coordinates as:

$$\mathrm{d}M = \bar{\rho}\mathrm{d}^3\vec{q}\,, \tag{2.35}$$

$$\mathrm{d}M = \rho(\vec{r},t)\mathrm{d}^3\vec{r}\,, \tag{2.36}$$

[6] There are even the *hydrodynamic simulations*, which, beyond gravity, take into account the effects of the physics related to baryons. This definitely complicates the construction of such simulations.

and recalling the *mass conservation principle*, we can combine the two previous equations to get the formula which regulates the density evolution:

$$\rho(\vec{r},t) = \bar{\rho}\,\frac{\mathrm{d}^3\vec{q}}{\mathrm{d}^3\vec{r}}\,. \tag{2.37}$$

Let us now rewrite the Zel'dovich formula (eq. 2.34) as follows:

$$\frac{\mathrm{d}^3\vec{r}}{\mathrm{d}^3\vec{q}} = J\left(\frac{\partial\vec{r}}{\partial\vec{q}}\right) = a^3\left(\delta_{i,j} - b(t)\frac{\partial^2\Phi}{\partial q_i \partial q_j}\right)\,, \tag{2.38}$$

where $\delta_{i,j}$ is the Dirac delta, $\frac{\partial^2\Phi}{\partial q_i \partial q_j}$ is the *deformation tensor*, while J is the Jacobian of the transformation. Since J is symmetric, it can be diagonalized, giving three eigenvalues ($\lambda_1 > \lambda_2 > \lambda_3$); equation (2.37) becomes:

$$\rho(\vec{r},t) = \frac{\bar{\rho}}{a^3}\left[1 - b(t)\lambda_1(\vec{q})\right]^{-1}\left[1 - b(t)\lambda_2(\vec{q})\right]^{-1}\left[1 - b(t)\lambda_3(\vec{q})\right]^{-1}\,. \tag{2.39}$$

For $\lambda_i > 0$ the square brakets vanish and $\rho \to \infty$ (shell crossing), thus the collapse proceeds along the axis on which the diagonalization of the deformation tensor has been made; the higher the positive value is and the more the collapse is effective in that direction and starts before[7]. By contrast, for $\lambda_i < 0$ as the value becomes more negative the density decreases.

2.3.2 Spherical collapse model

The theory exposed in Gunn and Gott (1972) is one of the few analytical solutions existing in the nonlinear regime, and it sets the basis for the *Mass Function*[8] models.

Below we describe the so-called spherical evolution of both the *overdensities* and the *underdensities*, under the validity of the CP and thus by means of the Friedmann equations (see chapter 1). Three crucial assumptions necessary for the following treatment are the following: a spherical[9] perturbation ($\Omega_p > 1$); a null peculiar velocity ($v_p = 0$); an EdS background Universe ($\Omega_\mathrm{B} = 1$), since we focus on on high-redshift perturbations from $t > t_\mathrm{eq}$, where the subscript "eq" stands for the matter-radiation equivalence.

Positive fluctuations

In §2.2.2 it has been shown how a fluctuation grows or decreases in the matter-dominated epoch. The linear theory enables us to express the initial perturbation δ_i as a combination of

[7] If $\lambda_1 = \lambda_2 = \lambda_3$ the collapse is isotropic.

[8] The idea of the spherical collapse can be used to write the Mass Function (see forthcoming §2.4.3), i.e. the prediction of cosmological models on the number of structures with a certain mass at a fixed time or, equivalently, a fixed redshift.

[9] This model is limited to the perfectly spherical case and it is not trivial to generalize it to the more realistic ellipsoidal collapse.

the two solution modes in the following way:

$$\delta_i = \delta(t_i) = \delta_+(t_i)\left(\frac{t}{t_i}\right)^{\frac{2}{3}} + \delta_-(t_i)\left(\frac{t}{t_i}\right)^{-1} , \tag{2.40}$$

and by time-deriving this equation, if we consider the aforementioned hypotheses of null peculiar velocity, we obtain:

$$\delta_+ = \frac{3}{5}\delta_i , \tag{2.41}$$

which means that three-fifths of the initial perturbation grow, while the two-fifths left decay.

It is also possible to write the perturbation at the initial time t_i as a function of the density parameter as:

$$\Omega_p(t_i) = \frac{\rho_p(t_i)}{\rho_{\rm crit}(t_i)} = \frac{\rho(t_i)\cdot(1+\delta_i)}{\rho_{\rm crit}(t_i)} = \Omega(t_i)(1+\delta_i) > 1 , \tag{2.42}$$

where the last inequality is justified since $\Omega_p(t_i) > 1$, i.e. the assumption of closed-Universe perturbations[10]. It follows that

$$\delta_i > \frac{1-\Omega(t_i)}{\Omega_{t_i}} . \tag{2.43}$$

Finally, if we recall that the density parameter evolution in the Friedmann Universes is

$$\Omega(z) = \frac{\Omega_0(1+z)^{1+3w}}{(1-\Omega_0)+\Omega_0(1+z)^{1+3w}} , \tag{2.44}$$

imposing $w = 0$, because of the matter-dominated epoch, equation (2.43) becomes:

$$\delta_+(t_i) = \frac{3}{5}\delta_i > \frac{3}{5}\frac{1-\Omega_{0,B}}{\Omega_{0,B}(1+z)} . \tag{2.45}$$

Hence, for closed or EdS background universes (i.e. $\Omega_{0,B} \geq 1$) any $\delta_i > 0$ can collapse; while for open universes (i.e. $\Omega_{0,B} < 1$) the initial density contrast must be greater than a critical value which verifies the inequality (2.45) in order to make the perturbation grow.

Moving on to the evolution of a spherical perturbation, let us rewrite the second Friedmann equation (eq. 1.25)[11] as follows:

$$\left(\frac{\dot{a}}{a_0}\right)^2 = H_0^2\left[\Omega_0\left(\frac{a_0}{a}\right)^{1+3w} + (1-\Omega_0)\right] , \tag{2.46}$$

which, for $a_0 \to a_i$ and $w = 0$, becomes:

$$\left(\frac{\dot{a}}{a_i}\right)^2 = H_i^2\left[\Omega_i\left(\frac{a_i}{a}\right) + (1-\Omega_i)\right] . \tag{2.47}$$

[10] Looking at fig. 1.3 it is evident how the closed universes are the only ones which can collapse.

[11] Note that in agreement with the spherical collapse model the Friedmann equations are exact; thus, unlike the Zel'dovich Approximation (§2.3.1), this is no longer an approximation.

This equation defines three fundamental stages of the spherical evolution:

- $t_{\rm M}$ (**turn-around**) is the time at which the perturbation reaches its maximum size; assuming the mass conservation and taking into account the solution of the closed universes (see §1.2.2) we can compute its density at $t = t_{\rm M}$ as:

$$\rho_p(t_{\rm M}) = \frac{3\pi}{32 G t_{\rm M}^2} \,. \tag{2.48}$$

  On the other hand, the background density of the EdS Universe (see §1.2.2) is:

$$\rho_B(t_{\rm M}) = \frac{1}{6\pi G t_{\rm M}^2} \,. \tag{2.49}$$

  By combining these two definitions, it is possible to obtain the growing mode of the perturbations:

$$\delta_+(t_M) = \frac{\rho_p(t_M)}{\rho_B(t_M)} - 1 \simeq 4.6 \,. \tag{2.50}$$

  Note that such a value for the density contrast means that the nonlinear regime is already achieved at the time of the maximum expansion of the perturbation, sooner than the effective collapse. As a consequence, applying the linear theory would be a mistake; in fact, it would imply $\delta_{+,\rm lin}(t_{\rm M}) \simeq 1.07$, i.e. a smaller value of the density contrast at the time of maximum expansion.

- $t_{\rm C} \simeq 2t_{\rm M}$ (**collapse**) is the moment in which all the matter should collapse in a geometric point, even if this does not actually happen because of both the baryonic pressure and the DM velocity dispersion. At this time we find:

$$\delta_+(t_{\rm C}) = \frac{\rho_p(t_{\rm C})}{\rho_B(t_{\rm C})} - 1 = 8\frac{\rho_p(t_{\rm M})}{\rho_B(t_{\rm M})}\left(\frac{t_{\rm C}}{t_{\rm M}}\right)^2 - 1 \simeq 180 \,, \tag{2.51}$$

  while in the linear theory $\delta_{+,\rm lin}(t_{\rm C}) \simeq 1.68$.

- $t_{\rm vir} \simeq 3t_{\rm M}$ (**virialization**) is the time when the structure reaches the equilibrium, keeping the same dimension as it had at $t = t_{\rm C}$. The density contrast of the increasing mode is:

$$\delta_+(t_{\rm vir}) = \frac{\rho_p(t_{\rm vir})}{\rho_B(t_{\rm vir})} - 1 = 8\frac{\rho_p(t_{\rm M})}{\rho_B(t_{\rm M})}\left(\frac{t_{\rm vir}}{t_{\rm M}}\right)^2 - 1 \simeq 400 \,, \tag{2.52}$$

  which turns to $\delta_{+,\rm lin}(t_{\rm vir}) \simeq 2.2$ in the linear regime. Hence, linearity is increasingly wrong as the collapse of the perturbation proceeds.

Finally, note that it is possible to compute the size on which the structure has settled at $t = t_{\rm vir}$. For this purpose, let us assume the *virial theorem* and the *mass conservation* between the maximum time and the virialization time:

$$2\mathcal{T} + \mathcal{V} = 0 \quad \longrightarrow \quad E = \mathcal{T} + \mathcal{V} = -\mathcal{T} \,, \tag{2.53}$$

where $\mathcal{T}$ and $\mathcal{V}$ are the kinetic and the potential energy respectively. E is the total energy and

can be written as:

$$\begin{cases} E_{\rm TOT}(t_{\rm M}) = -\dfrac{3}{5}\dfrac{GM^2}{R_{\rm M}} \\ E_{\rm TOT}(t_{\rm vir}) = -\dfrac{1}{2}\dfrac{3}{5}\dfrac{GM^2}{R_{\rm vir}} \end{cases} \tag{2.54}$$

and setting $E_{\rm TOT}(t_{\rm M}) = E_{\rm TOT}(t_{\rm vir})$ we get an expression for the virial radius as a function of the maximum radius:

$$R_{\rm vir} = \frac{1}{2}R_{\rm M} \tag{2.55}$$

where $R_{\rm M} = R(t_{\rm M})$ is the maximum radius. It is equation (2.55) that justifies the factor 8 (i.e. 2^3, to convert the radius into volume) in the previous eqs. (2.51) and (2.52).

Negative fluctuations

Spherical underdensities undergo an opposite evolution with respect to their positive counterparts: as the overdensities tend to reduce their size through the gravitational collapse and form the *cosmic structures*, the underdensities tend to become larger and form the *cosmic voids*. In order to describe the spherical evolution of the negative perturbations, let us refer to an inverse top-hat spherically symmetric underdensity composed by several shells with same center but different radii. The radial expansion of the shells is greater as the mean density contrast $\Delta(r,t)$ is lower; hence, the inner shells are more accelerated than the outer ones since a void is more underdense in its very center. In the Newtonian regime, where $\dot{r} \ll c$ and $r \ll c/H$, this acceleration can be formalized as follows:

$$\frac{{\rm d}^2 r}{{\rm d}t^2} = -\frac{GM}{r} = -\frac{4\pi G}{3}\rho_B(1+\Delta)r \ . \tag{2.56}$$

Note that according to this equation $\frac{{\rm d}^2 r}{{\rm d}t^2} \propto M \propto \Delta$, where $M = M(r)$ is the mass at a given radius. The mass and the mean density contrast at the initial time $t = t_i$ can be defined in the following way:

$$\begin{cases} M_i = \dfrac{4}{3}\pi\rho_B(1+\Delta_i)r_i^3 \\ \Delta_i = \dfrac{3}{r_i^3}\displaystyle\int_0^{r_i} \delta_i(r) r^2 {\rm d}r \end{cases} \tag{2.57}$$

The analytic solution of (2.56) can be found by assuming a specific parametrization to define the mean density contrast so that we can write:

$$1 + \Delta(r,t) = \frac{\rho(r,t)}{\rho_B(r,t)} = \frac{9}{2}\frac{(\sinh\theta - \theta)^2}{(\cosh\theta - 1)^3} \ , \tag{2.58}$$

where θ is a parameter defined such as its differential ${\rm d}\theta$ is the *conformal time*[12]. Starting from the previous equations it has been demonstrated that the mean density contrast in the linear

[12] We refer to the dimensionless conformal time as $\eta = \eta(t)$, and ${\rm d}\eta \equiv \frac{c{\rm d}t}{a(t)}$; see e.g. Steiner (2007) for further details.

regime is:

$$\Delta_i^L(\theta) = -\left(\frac{3}{4}\right)^{2/3} \frac{3}{5}(\sinh\theta - \theta)^{2/3} \,. \tag{2.59}$$

As already pointed out, the inner shells have a larger outward acceleration than the outer layers, hence the former gradually reach the latter. This results in the *shell-crossing* phenomenon, a physical condition that can explain the observed filaments of the large-scale structure, since collapsed objects tend to be placed on the edge of cosmic voids. Beyond the shell-crossing, the void radius increases as a self-similar expanding shell. Furthermore, note that when the shell-crossing occurs, we can associate to a void a specific Hubble parameter, i.e. a function of the Hubble parameter of the Universe computed at the shell-crossing time:

$$H_{sc} = \frac{4}{3} H(t_{sc}) \,. \tag{2.60}$$

This relation tells us that the expansion process is more effective for the underdensities than for the Universe as a whole. Moreover, from eq. (2.59) computed at the shell-crossing time ($\theta = \theta_{sc}$) we can obtain the following value for the negative density contrast in the nonlinear regime:

$$1 + \delta_v^{NL} \simeq 0.205 \quad \Longleftrightarrow \quad \delta_v^{NL} \simeq -0.795 \,, \tag{2.61}$$

while its linear counterpart is:

$$\delta_v^L \simeq -2.71 \,. \tag{2.62}$$

2.4 Large-scale structure

Once the linear and nonlinear evolution regimes have been outlined, we can proceed towards an exhaustive description of the large-scale structure of the Universe. In this section we will outline the evolution history of cosmic structures with the aim of summarising the statistical properties of our Universe, from the linear primordial perturbations to the nonlinear evolved structures.

The theory included in this entire section is of great importance for the analysis presented in chapter 4 and chapter 5. In particular, we provide some basic concepts on the two-point statistics, the tracer bias and the mass function.

2.4.1 Statistical properties of the primordial Universe

The inflation (§2.1) originates adiabatic primordial fluctuations from a stochastic process, which implies that the density contrast distribution has a nearly-Gaussian statistics. As a consequence, we can assume the *ergodic hypothesis*, and the statistical mean on several realizations turns into the mean computed on several spatially divided subsets of our Universe. This assumption is strongly connected to the *fair-sample hypothesis*, since the chosen volumes to be analysed must be a faithful representation of our Universe as a whole.

In this context, the Gaussian probability distribution of the density contrast can be written

as:

$$\mathcal{P}\left(\delta \equiv \frac{\delta\rho}{\bar{\rho}}\right) = \frac{1}{\sqrt{2\pi\sigma^2}}\ \exp\left[-\frac{\delta^2}{2\sigma^2}\right], \tag{2.63}$$

since the mean m is zero for the nature of the density contrast. Furthermore, we can also introduce a new definition of the density contrast (eq. 2.64) and its Fourier Transform (eq. 2.65):

$$\delta(\vec{x}) = \frac{1}{(2\pi)^3}\int_0^\infty \hat{\delta}(\vec{k})\ \exp\Big[i\vec{k}\cdot\vec{x}\Big]\,\mathrm{d}^3\vec{k}\,, \tag{2.64}$$

$$\hat{\delta}(\vec{k}) = \int \delta(\vec{x})\ \exp\Big[-i\vec{k}\cdot\vec{x}\Big]\,\mathrm{d}^3\vec{x}\,, \tag{2.65}$$

where $\delta(\vec{x})$ is dimensionless, while $\delta(\vec{k})$ has volumetric units. $\vec{k} = 2\pi/\lambda$ is called *wavenumber*.

Two-Point Correlation Function

In real space, the *two-point (auto-)correlation function* (2PCF) is defined as:

$$\xi(r) \equiv \langle \delta(\vec{x})\ \delta(\vec{x}+\vec{r})\rangle\,, \tag{2.66}$$

where the 2PCF, $\xi(r)$, is a dimensionless quantity which does not depend on the direction, under the validity of the CP; r is the comoving distance between the two points considered, $\vec{x}$ and $\vec{x}+\vec{r}$.

Assuming a discrete homogeneous distribution of objects with mean numerical density $\bar{n}$, the probability of having an object in any given volume element is:

$$\mathrm{d}P = \bar{n}\,\mathrm{d}V\,, \tag{2.67}$$

and the probability of having two distinct objects in two independent volumes simultaneously is:

$$\mathrm{d}^2P = \bar{n}^2\,\mathrm{d}V_1\,\mathrm{d}V_2\,, \tag{2.68}$$

where $\mathrm{d}V$, $\mathrm{d}V_1$ and $\mathrm{d}V_2$ are volume elements. By contrast, if those volumes are correlated eq. (2.68) becomes:

$$\mathrm{d}^2P = \bar{n}^2\,\mathrm{d}V_1\,\mathrm{d}V_2\Big[1+\xi(r)\Big]\,. \tag{2.69}$$

Thus, the 2PCF can be practically defined as the probability excess or lack of finding couples with respect to a random distribution. Note that a natural consequence of the last equation is that $\xi(r) \geq -1$, since the probability must be non-negative by definition.

Lastly, it is essential to highlight that in order to have a complete description of the counts we must know all the moments of the distribution. Let us define the *mean* and the *variance* as:

$$\begin{cases} \langle N\rangle_V = \sum\limits_i \langle n_i\rangle = \bar{n}\,V \\ \langle N^2\rangle_V = \sum\limits_{i=j}\langle n_i^2\rangle + \sum\limits_{i\neq j}\langle n_i n_j\rangle = \bar{n}V + \bar{n}^2V^2 + \bar{n}^2\int \mathrm{d}V_1\,\mathrm{d}V_2\,\xi \end{cases} \tag{2.70}$$

where N is the number of objects of the sample considered, $\bar{n}$ is its mean number density, $\bar{n}V$

is a statistical noise known as *shot noise* and ξ is the 2PCF. While a Gaussian distribution is entirely described by eqs. (2.70), a generic distribution has non-null higher-order moments, such as the *skewness* $\langle N^3 \rangle_V$, the *kurtosis* $\langle N^4 \rangle_V$, etc. This means extending the concept of 2PCF to more than two points, i.e. respectively, the three-point correlation function (3PCF), the four-point correlation function (4PCF), etc. However, the signal is mainly contained in lower-order clustering functions. Therefore, current cosmological analyses generally rely on 2PCF and 3PCF. The latter is defined as the probability excess or lack of finding triplets with respect to a random distribution; notice that the already considered pairs of the 2PCF enhance the probability of having a triplet, and we can derive the following relation:

$$\xi_3 = \xi(r_{1,2}) + \xi(r_{1,3}) + \xi(r_{2,3}) + \zeta(r_{1,2}, r_{1,3}, r_{2,3}) \,, \tag{2.71}$$

where ζ is called *reduced* or *connected* 3PCF.

Both the 2PCF and the 3PCF have their analogue in the Fourier space: the *power spectrum* $P(k) \propto \langle |\delta_k|^2 \rangle$ and the *bispectrum* $B(k_1, k_2) \propto \langle |\delta(k_1)\delta(k_2)\delta(k_1 - k_2)| \rangle$ respectively.

Power Spectrum

In Fourier space, the 2PCF is transformed into the so-called *power spectrum*, $P(k)$, through

$$\langle \delta(\vec{k})\, \delta^*(\vec{k'}) \rangle \equiv (2\pi)^3\, \delta_D^{3D}(\vec{k} - \vec{k'}) P(k) \,, \tag{2.72}$$

where the complex conjugate of $\delta(\vec{k})$ is defined as $\delta^*(\vec{k}) = \delta(-\vec{k})$, since the density field is real. $\delta_D^{3D}(\vec{k} - \vec{k'})$ is the 3-dimensional *Dirac delta function*. The power spectrum quantifies the contribution of the scale $\vec{k}$ on the total density field in Fourier space. Note that if $\vec{k} = \vec{k'}$, $P(k) \approx |\delta(\vec{k})|^2$, i.e. the power spectrum measures the square mean amplitude of $\delta(\vec{k})$, where $\delta(\vec{k})$ is the amplitude of the wave which corresponds to the wavenumber k in Fourier space. It is possible to link $\xi(r)$ to $P(k)$ through the Fourier formalism:

$$\xi(r) = \frac{1}{(2\pi)^3} \int \mathrm{d}^3\vec{k}\; P(k)\; \exp\left[i\vec{k} \cdot \vec{r} \right] \,, \tag{2.73}$$

which is known as the *Wiener-Khintchine theorem*. Lastly, let us just point out that in the density contrast $\delta_{\vec{k}}$, $\vec{k}$ is a vector, while $P(k)$ depends only on its module.

A relevant quantity related to the power spectrum is the *pointwise variance* σ^2, which is obtained from eq. (2.72) as the appropriate integral of $P(k)$:

$$\sigma^2 = \frac{1}{(2\pi)^3} \int_{-\infty}^{+\infty} \mathrm{d}^3\vec{k}\; P(k) \quad \xrightarrow[\text{coordinates}]{\text{in spherical}} \quad \sigma^2 = \frac{1}{2\pi^2} \int_0^{+\infty} \mathrm{d}k\; k^2\; P(k) \,. \tag{2.74}$$

When performing cosmological analyses we cannot access the density value in each single point of the Universe, but we need to average on volumes. Thus, it is physically more appropriate referring to the *mass variance* instead, which is defined as:

$$\sigma_{\mathrm{M}}^2 \equiv \langle \delta^2 \rangle = \frac{1}{(2\pi)^3} \int \mathrm{d}^3\vec{k}\; P(k)\; \hat{W}_V^2(\vec{k}, R) \,, \tag{2.75}$$

where $\hat{W}_V^2(\vec{k}, R)$ is the Fourier transform of the window function, which acts as a low-pass filter on the scales $\vec{k}$ depending on its filtering radius R or, equivalently, on its filtering mass M. In particular, $\hat{W}$ erases the perturbations on small physical scales ($\lambda < R$); the larger the filter is the more scales are cancelled out. Therefore, if $R \to 0$ the mass variance recovers the pointwise variance (i.e. $\sigma_{\rm M}^2 \to \sigma^2$); if instead $R \to \infty$ what happens is that the density field reduces to the mean density (i.e. $\sigma_{\rm M}^2 \equiv \delta^2 \to 0$).

The shape of the primordial power spectrum describes the amplitude distribution of the Gaussian initial perturbations, hence it must be scale-free, described by a generic power-law:

$$P(k) = \mathcal{A}\, k^n \,, \tag{2.76}$$

where n is the *spectral index*. The fluctuations generated by inflation (§2.1) are *metric fluctuations*, i.e. of the *gravitational potential*. Therefore, on a generic scale R it can be proven that:

$$\delta\Phi_{\rm R} \propto \frac{G\delta M}{R} \propto \sigma_{\rm V} R^2 \propto \sigma_{\rm M} M^{2/3} \propto M^{\frac{1-n}{6}} \propto M^0 \,, \tag{2.77}$$

where the last proportionality relation is justified by the fact that the spectrum of the gravitational fluctuations is commonly referred to as *white noise*, i.e. it is not only scale-free but also scale-invariant, i.e. at each scale it has the same amplitude. As a consequence, what the inflation predicts is $n \simeq 1$, giving rise to the so-called *Zel'dovich spectrum* for the density fluctuations:

$$P(k) = \mathcal{A}\, k \,. \tag{2.78}$$

Finally, note that while the inflation predicts the value of the spectral index n, the initial normalization $\mathcal{A}$ has to be inferred through observations (e.g. CMB; Planck Collaboration et al., 2020c).

On the time evolution of the power spectrum. Let us introduce two fundamental times to consider in the evolution of $P(k)$: $t_{\rm H}$ as the time at which a given perturbation enters the cosmological horizon and $t_{\rm eq}$ as the equivalence matter-radiation time. From the cosmological horizon definition (2.21) it follows that the smallest scales turn out to be inside $R_{\rm H}$ before the greatest ones. As a consequence, the former are more likely to undergo the *stagnation* (Meszaros, 1974) than the latter. Moreover, note that if a scale is large enough to enter the cosmological horizon at $t > t_{\rm eq}$, it grows following the dependencies seen in §2.2.2, without stagnation.

The Meszaros effect is such that the equivalence power spectrum shows a peak at the scale corresponding to the horizon at $t = t_{\rm eq}$, identified as $k_{\rm H,eq}$. Indeed, for lower wavenumbers (i.e. larger physical scales) there are not signs of stagnation, while for higher wavenumbers (i.e. smaller physical scales) there can be found the typical shape induced by this effect. What drives the size of the horizon scale at the time of equivalence (i.e. $k_{\rm H,eq}$) is the matter density parameter $\Omega_{\rm m}$:

$$\rho_{\rm m}(t_{\rm eq}) = \rho_{\rm r}(t_{\rm eq}) \quad \to \quad \rho_{0,\rm m}\, a_{\rm eq}^{-3} = \rho_{0,r}\, a_{\rm eq}^{-4} \quad \to \quad a_{\rm eq} = \frac{\rho_{0,\rm r}}{\rho_{0,\rm m}} = \frac{\Omega_{0,\rm r}}{\Omega_{0,\rm m}} \,, \tag{2.79}$$

where $\Omega_{0,\rm r}$ is fixed by $T_{\rm CMB} \simeq 2.73$ K. From these relations it follows that the higher $\Omega_{0,\rm m}$ is and the earlier the matter-radiation equivalence is achieved. Furthermore, there is a second

order effect due to the presence of massive neutrinos; in fact, if they are relativistic they are part of the radiative component, otherwise they join the matter component. Before the peak, $P(k) \propto k^n \simeq k$; after the peak, $P(k) \sim k^{n-4} \sim k^{-3}$ asymptotically. These trends can be formalized by means of a *transfer function* $T(k)$ as follows:

$$P(k, t_{\rm eq}) = P(k, t_i)\, T^2(k)\ , \tag{2.80}$$

where

$$T(k) \propto \begin{cases} k^0 & \text{for} \quad k < k_{\rm H,eq}\ , \\ k^{-2} & \text{for} \quad k > k_{\rm H,eq}\ . \end{cases} \tag{2.81}$$

At $t = t_{\rm eq}$, it is just the DM component that can grow since the baryons are not yet decoupled from radiation. In this context, it is important to mention the so-called *free-streaming*, a phenomenon which acts at different scales on cold and hot dark matter. This effect occurs on scales that are smaller than the Jeans scale, where the wave propagation can take place. When the DM decouples from radiation it starts to move freely, responding to the mean density field of the Universe. It is because of this free propagation that small-scales perturbations are erased. In fact the so-called *free-streaming scale* ($\lambda_{\rm FS}$) is strongly linked to the Jeans scale. As mentioned before, the HDM Jeans scale is greater than the CDM one (or, equivalently, $k_{\rm FS,HDM} < k_{\rm FS,CDM}$), and hence more scales are cancelled in the HDM scenario (see fig. 2.1, which shows the free-streaming effects in presence of either CDM or HDM). The consequence of this phenomenon is that in HDM-dominated universes the formation of the cosmic structures follows a top-down process, while the CDM-dominated universes are described by a bottom-up structure formation[13].

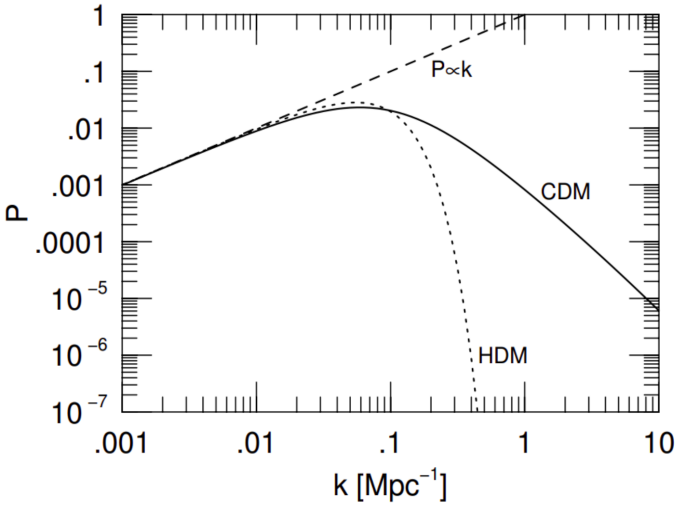

Figure 2.1: Comparison between the power spectrum at the equivalence time for HDM (dotted line) and CDM (solid line) dominated Universe. Credits to: Ryden (2016).

[13]We recall that if in the top-down scenario the larger structures are formed first and then the smaller by disaggregation, in the bottom-up scenario the smaller structures form first and then the biggest ones are created by aggregation.

From the equivalence to later times (i.e. in the matter era), the power spectrum amplitude grows as $\delta_+^2 \propto a^2$ as long as the linear theory is valid. Then, the smaller a physical scale is, the earlier it becomes nonlinear; when this happens, the growth rate is enhanced with respect to the linear regime.

Finally, note that the dependencies of the transfer function $T(k)$ given in eq. (2.81) are valid for the CDM scenario; considering the HDM instead, $T(k) \propto k^{n'}$ for $t > t_{\rm eq}$, where $n' < -2$, i.e. the slope is steeper than that of CDM.

2.4.2 Bias

In order to analyse the matter distribution of a given volume of our Universe, we need to consider the tracer objects (e.g. galaxies, galaxy clusters and voids), since the DM particle field is not directly observable[14]. One of the main aims of cosmologists is finding an accurate relation to link the distribution of tracers to that of the underlying DM; in fact, the luminous matter is not a faithful representation of the underlying DM. The simplest existing parametrisation to account for this discrepancy has been introduced by Kaiser (1984) by means of a local and non-stochastic bias model, valid in the linear regime (i.e. on very large scales):

$$\delta_{\rm tr} \equiv \frac{N_{\rm tr}(V) - \bar{N}_{\rm tr}(V)}{\bar{N}_{\rm tr}(V)} = \frac{\delta N_{\rm tr}(V)}{\bar{N}_{\rm tr}(V)} = \frac{\delta M(V)}{\bar{M}(V)} = b\,\delta_{\rm m}\,, \tag{2.82}$$

where b is the linear bias, $\delta_{\rm tr}$ represents the fluctuations of the number of tracers in a volume V and $\delta_{\rm m} = \delta \otimes W(V)$ is the matter density field filtered on a volume V, e.g. convolved with a top-hat filter of volume V. Equation (2.82) can be expressed in terms of both the power spectrum and the 2PCF as well:

$$\begin{cases} P_{\rm tr}(k) = b^2\, P_{\rm m}(k)\,, \\ \xi_{\rm tr} = {\rm FT}\Big[P_{\rm tr}(k)\Big] = b^2\,\xi_{\rm m}\,, \end{cases} \tag{2.83}$$

where FT stands for *Fourier transform* (see eq. 2.73). It is clear that the higher the linear bias is, the more the distribution of the tracers considered differs from the underlying matter distribution. Note that if $P_{\rm m}$ and $\xi_{\rm m}$ can be derived from the theory by means of the *Boltzmann solvers* (e.g. CAMB), $P_{\rm tr}$ and $\xi_{\rm tr}$ must be computed by observations or simulations through the so-called *clustering estimators* (see §3.2.3).

The tracer bias has been extensively studied in the literature. For instance, one of the most popular functional forms for the DM halo bias was introduced by Mo and White (1996):

$$b(M,z) = 1 + \frac{1}{\delta_c}\left(\frac{\delta_c^2}{\sigma_M^2\,\delta_+^2(z)} - 1\right)\,, \tag{2.84}$$

which was obtained by means of the *excursion-set formalism* (see §3.2.1). From this equation we understand how the linear bias of the tracers is always positive and directly proportional to both the mass M and the redshift z.

[14] Note that the DM distribution can be reconstructed only by means of gravitational effects, such as the gravitational lensing, which probes the image distortions of background sources.

The aforementioned biased tracers play a crucial role in the cosmic void definition. We must take into account that they are affected by a bias factor too, which depends on the redshift and the void radius; see §3.2.3 for further details on the *void bias* and its theoretical definition.

2.4.3 Halo mass function

As anticipated in §2.3.2, it is possible to exploit the spherical collapse model in order to build a model for the halo mass function (HMF, hereafter), which is defined as the number of haloes per unit comoving volume (i.e. the halo comoving number density) as a function of their mass, at a given redshift. The HMF emerges in the cosmological framework as an extremely powerful statistics to investigate the properties of the large-scale distribution of cosmic structures[15]. A theory for the HMF was proposed for the first time by Press and Schechter (1974) (PS, hereafter), in a theoretical formulation that considers DM haloes as spherically symmetric objects[16].

From §2.4.1 we know that the initial distribution of primordial fluctuations is nearly Gaussian (eq. 2.63). As the time evolution of the probability distribution $\mathcal{P}$ proceeds in linear theory (i.e. at high redshift or on very large scales), it holds its Gaussian shape and it is described by the same integral (i.e. subtended area)[17], but lower peak height and larger variance. When the nonlinear regime starts, the growth of the perturbations fastens and the Gaussianity is broken because of the physical barrier $\delta = -1$. This limit emerges from eq. (2.1), since a density must be positive by definition.

Ideally, the HMF could be obtained by applying the spherical collapse model to the nonlinear shape of the probability distribution of the density fluctuations. In practice, the results provided us from the spherical collapse theory (i.e. $\delta_+(t_\mathrm{C}) \simeq 180$) depend on the properties of the background universe, and we do not even know the exact functional form that describes the evolved $\mathcal{P}(\delta)$. Therefore, Press and Schechter (1974) proposed to map the nonlinearity in the corresponding linear regime by considering $\delta_+(t_\mathrm{C}) \simeq 1.686$ and a Gaussian $\mathcal{P}(\delta)$. The probability of having a mass perturbation δ_M that exceeds the critical value δ_C forming a collapsed object of mass M is defined as:

$$\mathcal{P}_{>\delta_\mathrm{C}}(M) = \int_{\delta_\mathrm{C}}^{+\infty} \mathcal{P}(\delta_\mathrm{M}) \mathrm{d}\delta_\mathrm{M}. \tag{2.85}$$

In the PS theory it is supposed that all those fluctuations that reach a density contrast $\delta_\mathrm{M} = \delta_\mathrm{C}$ in linear theory collapse and form the cosmic structures. On these assumptions, the PS mass function can be expressed as:

$$n(M) M \mathrm{d}M = 2\bar{\rho}_\mathrm{m} [\mathcal{P}_{>\delta_\mathrm{C}}(M) - \mathcal{P}_{>\delta_\mathrm{C}}(M + \mathrm{d}M)] \,, \tag{2.86}$$

[15] Let us specify that the analogue of the halo mass function for the underdense counterpart (i.e. the so-called *void size function*) will be discussed in CHAPTER 3, when describing cosmic voids and their main statistical properties.

[16] The theory of PS was then extended in later papers (see e.g. Sheth and Tormen, 2002), which also accounted for the presence of non-spherical haloes by means of ellipsoidal models.

[17] Accounting for both positive and negative fluctuations, $\mathcal{P}$ is equal to unity for the definition of probability itself.

where $\bar{\rho}_{\rm m}$ is the matter average density, $n(M)$ is the comoving number density of haloes with a mass ranging from M and $M + \mathrm{d}M$, and $n(M)M$ is then their total mass. Note that the factor 2 has to be intended as a correction to eq. (2.85). In fact, $M \to 0$ (i.e. $\sigma_{\rm M} \to +\infty$) would imply $\mathcal{P}_{>\delta_{\rm C}} \to 1/2$, but it should result $\mathcal{P}_{>\delta_{\rm C}} = 1$, since no filtering is applied. If we now rewrite the mass variance for a power law power spectrum as $\sigma_{\rm M} = (M/M_0)^{-\alpha}$, where M_0 is the characteristic mass that an object assumes at a certain redshift and $\alpha = (n+3)/6$, from eq. (2.86) we get:

$$n(M) = \sqrt{\frac{2}{\pi}} \frac{\alpha \bar{\rho}_{\rm m}}{M_*^2} \left(\frac{M}{M_*}\right)^{\alpha-2} \exp\left[-\left(\frac{M}{M_*}\right)^{2\alpha}\right] . \tag{2.87}$$

In this equation, M_* is called *cut-off mass* and it represents the mass scale at which the mass variance equals the collapse critical value at a given redshift, i.e. $\sigma(M_*, z) = \delta_{\rm C}(z)$. For example, at redshift $z = 0$ the cut-off mass equals the typical mass of galaxy clusters (i.e. $10^{14} - 10^{15}\ M_\odot$). M_* can be expressed as follows:

$$M_* = M_0 \left(\frac{2}{\delta_{\rm C}}\right)^{\frac{1}{2\alpha}} . \tag{2.88}$$

It is noticeable that, being the HMF based on theoretical principles, it is extremely sensitive to the cosmological parameters and, hence, a powerful cosmological probe.

Since the development of this very first mass function model, many increasingly sophisticated alternatives have been proposed in the literature (see e.g. Jenkins et al., 2001; Tinker et al., 2008; Crocce et al., 2010; Despali et al., 2016). In order to develop our analysis on the DM haloes (see forthcoming CHAPTER 4) we relied on one of the most popular models of halo abundance, i.e. the Tinker et al. (2008) theoretical mass function, which is formalised as follows:

$$\frac{\mathrm{d}n}{\mathrm{d}M} = f(\sigma_{\rm M}) \frac{\bar{\rho}_{\rm m}}{M} \frac{\mathrm{d} \ln \sigma_{\rm M}^{-1}}{\mathrm{d}M} , \tag{2.89}$$

where $f(\sigma_{\rm M})$ is called *multiplicity function*, and it is expected to be universal to the changes in either redshift or cosmology. In agreement with Tinker et al. (2008), it can be defined through the following parametrisation:

$$f(\sigma_{\rm M}) = A \left[\left(\frac{\sigma_{\rm M}}{b}\right)^{-a} + 1\right] \exp\left(-\frac{c}{\sigma_{\rm M}^2}\right) , \tag{2.90}$$

where A, a, b and c are constant parameters to be calibrated with simulations, while $\sigma_{\rm M}$ is the mass variance computed by eq. (2.75) in spherical coordinates.

2.5 N-body simulations

As already pointed out in the previous sections, in the linear or mildly nonlinear regimes there exist suitable analytical solutions which can be used to describe the formation and evolution of cosmic structures. At very high redshift, these scenarios properly represent our Universe

at all scales. By contrast, we must take advantage of *numerical simulations* in order to cope with the totally nonlinear regime, since at lower redshift the values of the evolved density contrasts are much higher. In particular, the smallest physical scales (i.e. greater k modes) are the first to break the linearity. As a consequence, the collapsed structures form in a highly nonlinear regime and numerical simulations help to model their complex dynamics and general properties by simulating the Universe, possibly with a huge amount of particles. Indeed, these systems of particles are hard to be studied through approximate analytical models.

The main characteristic of a simulation is its *spatial resolution*, a quantity that depends on both the volume and the number of particles. If in the past there were only few-hundred-particle simulations, nowadays they are provided with billions of particles thanks to the improvement of computational performances. For a given number of particles, large volumes (i.e. low resolutions) are needed to investigate the statistical properties of the large-scale structures in Cosmology. By contrast, small volumes are needed to study the galaxy formation and evolution with high resolution. Dealing with both these aspects is not trivial, since we should use big high-resolution simulations, which require a number of particles that could be unattainable with current techniques.

There are two main classes of numerical simulations: *(i)* the *N-body simulations*, which only take into account the effect of gravity among the DM particles; *(ii)* the *hydrodynamic simulations*, which trace also the dynamics of baryons. Since our results are based on the analysis of a set of cosmological N-body simulations (i.e. the DUSTGRAIN-*pathfinder*, see §4.2), we now focus on the description of this category[18].

Let us consider an ensemble of N particles with mass m_i, where $i = 1, ..., N$. The N-body simulations are built starting from the following system of dynamical equations:

$$\begin{cases} \vec{F}_i = G\, m_i \sum_{i \neq j} \dfrac{m_j}{r_{ij}^2}\, \hat{r}_{ij} \\ \ddot{\vec{x}}_i = \dfrac{\mathrm{d}\vec{v}_i}{\mathrm{d}t} = \dfrac{\vec{F}_i}{m_i} \\ \dot{\vec{x}}_i = \dfrac{\mathrm{d}\vec{x}_i}{\mathrm{d}t} = \vec{v}_i \end{cases} \tag{2.91}$$

where $\vec{F}_i$ is the gravitational force which acts on the *i*-th particle, $\vec{x}_i$ represents the comoving coordinates, $\vec{v}_i$ is the peculiar velocity of the *i*-th particle and $\hat{r}_{ij}$ stands for the direction of the distance between the *i*- and *j*-th particles. Then, a certain Cosmology is assumed, through the setting of the cosmological parameters, and the simulation runs mimicking the evolution of the Newtonian equations (2.91), so that the Euler equation of motion (2nd eq. in 2.26) becomes:

$$\frac{\mathrm{d}\vec{v}_i}{\mathrm{d}t} + 2\frac{\dot{a}}{a}\vec{v}_i = -\frac{1}{a^2}\nabla\Phi = -\frac{G}{a^3}\sum_{i \neq j} m_j \frac{\vec{x}_i - \vec{x}_j}{|\vec{x}_i - \vec{x}_j|^3} = \frac{\vec{F}_i}{a^3}\,. \tag{2.92}$$

Furthermore, by taking into account the second Friedmann equation (eq. 1.25) we can rewrite

[18] See e.g. Coles and Lucchin (2002) for further details on the hydrodynamics side.

the Poisson equation (third eq. in 2.26) as follows:

$$\nabla^2\Phi = 4\pi G\bar{\rho}a^2\delta = \frac{3}{2}H_0^2\Omega_0\frac{\delta}{a}\,, \tag{2.93}$$

where $\bar{\rho} = \bar{\rho}(t)$ is the average density of the non-relativistic matter, H_0 is the Hubble parameter, Ω_0 is the density parameter of the non-relativistic matter, δ is the local density contrast and a is the cosmic scale factor. These equations are evolved through an iterative time integration over intervals δt, i.e. $t \to t+\delta t$, under the effect of the gravitational force; for each time-step[19] we obtain $\vec{F}_i(t)$ from eq. (2.91), $\vec{x}_i(t)$ and $\vec{v}_i(t)$ from (2.92), defining a set of *snapshots* (i.e. the spatial distribution of the particles in a volume V at each δt).

A cosmological simulation can be developed through different techniques, depending both on the technological efficiency and on the specific characteristics required for it. In the following list we introduce the most employed methods to calculate the gravitational force among particles:

- *Particle-Particle* (PP): at each time-step this technique considers the total gravitational force acting on the *i*-th particle as the sum of all the forces generated by every single particle on it. Providing us with a direct measurement of $\vec{F}_i$, this is the most accurate existing method but also the most expensive in terms of computational time; there are $N(N-1)/2$ couples of particles to be computed, which means that the necessary number of operations scales as $\mathcal{O}(N^2)$.
- *Particle-Mesh* (PM): instead of looking at every particle individually, the volume is sampled with a grid and $\vec{F}_i$ is computed in each cell. Although this method is faster than the PP being described by $\mathcal{O}(N\log N)$, it is less accurate. Note that here N is the number of cells, not the number of particles anymore. See Hockney and Eastwood (1981) for further details.
- *Hybrid methods*: a combination of different methods effective at different scales. As an example, we can mention the P^3M method (Efstathiou et al., 1985), which is based on PM but adding the PP, since it computes the direct force among particles at small scales, within a sphere of radius R around each particle. The accuracy is higher than in PM but the computational time increases to $\mathcal{O}(\tilde{N}^2)$, where $\tilde{N}^2$ is the number of close objects (i.e. with separations below a given threshold scale). In this context, the so-called *adaptive mesh* has been introduced with the aim of speeding up the process through a redefinition of the spatial resolution of the denser regions.
- *Hierarchical Tree* (HT): this is another method to make the PP faster. The technique performs a separation of the simulation in cells with a certain hierarchical order. Every cell has its own center of mass: at small distances from this point the force is directly computed among particles through PP; at big distances the force is computed as if it is generated by each subregions from its center of mass, without the necessity of considering the particles individually. The computational time goes as $\mathcal{O}(N\log N)$. For further details see e.g. Barnes and Hut (1986).

[19] The value of δt can be determined by several criteria, for example: the total energy conservation, the final positions and velocities to be convergent and the initial conditions to be reproducible. See Bagla and Padmanabhan, 1997 for further details.

Chapter 3

Cosmic voids

Being both the cosmological framework and the structure formation outlined, in this chapter we are finally going to describe the main topic of this Thesis: the *cosmic voids*. In recent years, the interest in these huge empty regions of the Universe has increased thanks also to scientific achievements reached by the present and upcoming redshift surveys[1], both deeper and wider with respect to the past. The development of these observational surveys together with the improvement of both numerical simulations[2] (see §2.5) and theoretical models have made voids become competitive as a cosmological probe[3]. Resulting from the evolution of the primordial underdensities (see §2.3.2), cosmic voids represent the negative counterpart of the already extensively studied clusters of galaxies. Indeed, void statistics gives us the chance to disentangle cosmological degeneracies (see §1.4) through the combination of totally orthogonal probes. A great potential of the underdense Universe lies in the fact that voids have not been extensively exploited yet, hence the contribution of these objects to the current cosmological panorama can still be enormous.

As already mentioned in the Introduction, cosmic voids have some important advantages: *(I)* when the linearity is broken by the growing fluctuations, the voids only experience a mildly nonlinear evolution, alleviating all the problems raised by the fully nonlinear regime of structure evolution; *(II)* there is a tendency towards sphericity as their evolution proceeds (Icke, 1984); *(III)* baryonic physics has almost no influence on their life history; *(IV)* voids are extremely sensitive to both diffuse components (DE and neutrinos) and MG thanks to their emptiness and shallow gravitational potentials, respectively.

By contrast, the greatest disadvantage of voids is related to both their definition and identification. In fact, not only we are not yet provided with a unique and generally accepted

[1] See e.g. BOSS (Baryon Oscillation Spectroscopic Survey; Dawson et al., 2013), WFIRST or NGRST (NASA Nancy Grace Roman Space Telescope 2; Green et al., 2012), LSST (Vera C. Rubin Observatory 3; LSST Dark Energy Science Collaboration, 2012) and Euclid (Laureijs et al., 2011; Amendola et al., 2018; Euclid Collaboration et al., 2020).

[2] There exist several numerical simulations depending on the case study considered. See e.g. IllustrisTNG (Nelson et al., 2019), Magneticum (Dolag, 2015) and EAGLE (Schaye et al., 2015) for the hydrodynamic simulations. See e.g. DUSTGRAIN-*pathfinder* (Giocoli et al., 2018) and CoDECS (Baldi, 2012) among the N-body simulation used to study alternative cosmologies. Finally, the Quijote (Villaescusa-Navarro et al., 2020) are extremely suitable for machine learning techniques.

[3] As indicated in the Introduction, for a brief but almost complete overview of this emerging context see Pisani et al. (2019) and references therein.

definition of the void radius and inner density, but we do not even have the possibility to detect these objects straight away. This happens because cosmic voids are widely extended underdense structures that do not emit directly. Therefore, we must recover the void shape and spatial distribution from the luminous tracers through rather challenging techniques.

In the following sections we will introduce some definitions of cosmic voids adopted by different void finding algorithms (§3.1) and then outline the statistics of cosmic voids (§3.2) as a cosmological probe. We will focus more on the 2PCF, since the aim of this Thesis is to calibrate statistical methods to derive constraints on the cosmological model by means of void clustering properties.

3.1 Void finding and definition

Over the last years, different *void finders* have been developed by the scientific community in order to search for cosmic voids in the tracer fields. According to Lavaux and Wandelt (2010), there exist three main categories of void finding algorithms, each one relying on a different criteria of void identification:

- **Geometrical criterion.** The geometrical-based algorithms look for local density minima in a reconstructed continuous 3D density field. According to this class of criteria, cosmic voids are defined as geometrical underdense regions that assume the shape of spherical cells or polyhedra (Platen et al., 2007; Neyrinck, 2008; Sutter et al., 2015b).

- **Density criterion.** Voids are considered to be regions empty of tracers or, analogously, regions where the local density is lower than the fixed mean density (see e.g. Elyiv et al., 2013; Micheletti et al., 2014). The tracers are classified as *wall tracers* and *field tracers* depending on the density of the surrounding environment: the first category is represented by tracers in high density regions (i.e. the walls), while the last refers to tracers in low density regions (i.e. the cosmic voids). It follows that inside voids the so-called wall tracers cannot be present.

- **Dynamical criterion.** These void finders identify cosmic voids as regions from which the matter is removed, following a radial velocity field pointing outwards with respect to the void centers (Forero-Romero et al., 2009; Elyiv et al., 2015). Unlike the two previous cases, here the tracers are used to reconstruct the velocity field.

There also exist 2D void finders, which are based on the described criteria but with the 3D space projected along the line of sight. This kind of finder is suitable especially for weak lensing investigations around voids (see e.g. Sánchez et al., 2016; Cautun et al., 2018; Davies et al., 2021a).

Indeed, from the different void definitions resulting from the criteria outlined above, we can conclude that to different finding algorithms correspond different void sizes and distributions. The void finding algorithm employed in our work is known as VIDE (Void IDentification and Examination toolkit; Sutter et al., 2015b), a public toolkit based on a *geometrical criterion* that we will present extensively in the forthcoming section §4.3.1. Finally, we anticipate that in

section §4.3.2 we will present a further definition of cosmic void that descends from the application of the so-called *cleaning algorithm* on the void catalogues produced by the finding procedures (Ronconi and Marulli, 2017). We will understand that since the cleaning is based on theoretical principles, it makes our statistical analysis more robust.

3.2 Void statistics

Since a relatively short time, cosmologists have developed several possible strategies towards the exploitation of cosmic voids to set the best possible constraints on the cosmological scenario. The zero-order statistics of cosmic voids are the *size function* and the *density profile* (see the forthcoming subsections §3.2.1 and §3.2.2, respectively). However, since the void clustering properties have not been extensively addressed yet, we chose to perform our analysis on the auto-correlation function of cosmic voids (§3.2.3).

3.2.1 Size function

The void size function (VSF hereafter) is defined as the comoving number density of voids as a function of their radii, and represents the simplest existing void statistics that can be used to constrain the cosmological parameters. The VSF can be thought as the analogous of the halo mass function (§2.4.3) but describing the underdense structures. Being these objects devoid of matter, the mass is replaced by the void radius.

Excursion-set formalism

Let us now briefly introduce the excursion-set formalism[4] in the context of cosmic voids, since it allows us to analytically model the VSF by linking the linear and the nonlinear theories. The accuracy of this formalism is limited to the case of an underlying matter density field that is Gaussian distributed. Recalling eq. (2.64), in the linear regime we can write the density contrast field smoothed by a filter W of radius R as:

$$\delta(\vec{x}, R) = \frac{1}{(2\pi)^3} \int_0^\infty \hat{\delta}(\vec{k})\, W(\vec{k}, R) \exp\left[i\vec{k}\cdot\vec{x}\right] \mathrm{d}^3\vec{k}\ , \tag{3.1}$$

where $\delta(\vec{x})$ is the density contrast defined in eq. (2.1) and $\hat{\delta}(\vec{k})$ is its Fourier transform. From this equation, together with the definition of mass variance in eq. (2.75), it is possible to determine a trajectory $\delta[\vec{x}, \sigma^2(R)]$ by varying the scale R of the window function W. If W is considered to be a top-hat filter, the trajectory turns out to be a *random walk*.

Due to the large sizes of cosmic voids, their hierarchy is much more complicated than that of the high-density structures. As a consequence, if for the overdensities exists a threshold $\delta_\mathrm{c}^\mathrm{L}$ that must be reached to form the DM haloes, for the underdensities it is not sufficient to similarly set a threshold $\delta_\mathrm{v}^\mathrm{L}$. Hence, in the former case the excursion-set formalism is exploited to solve the *one-barrier problem*, while for the underdensities it deals with the more challenging

[4]The excursion-set approach was presented in Bond et al. (1991) with the aim of overcoming the *cloud-in-cloud* problem related to the overdensities, i.e. that the smallest perturbations can be erased by the collapse of the biggest ones.

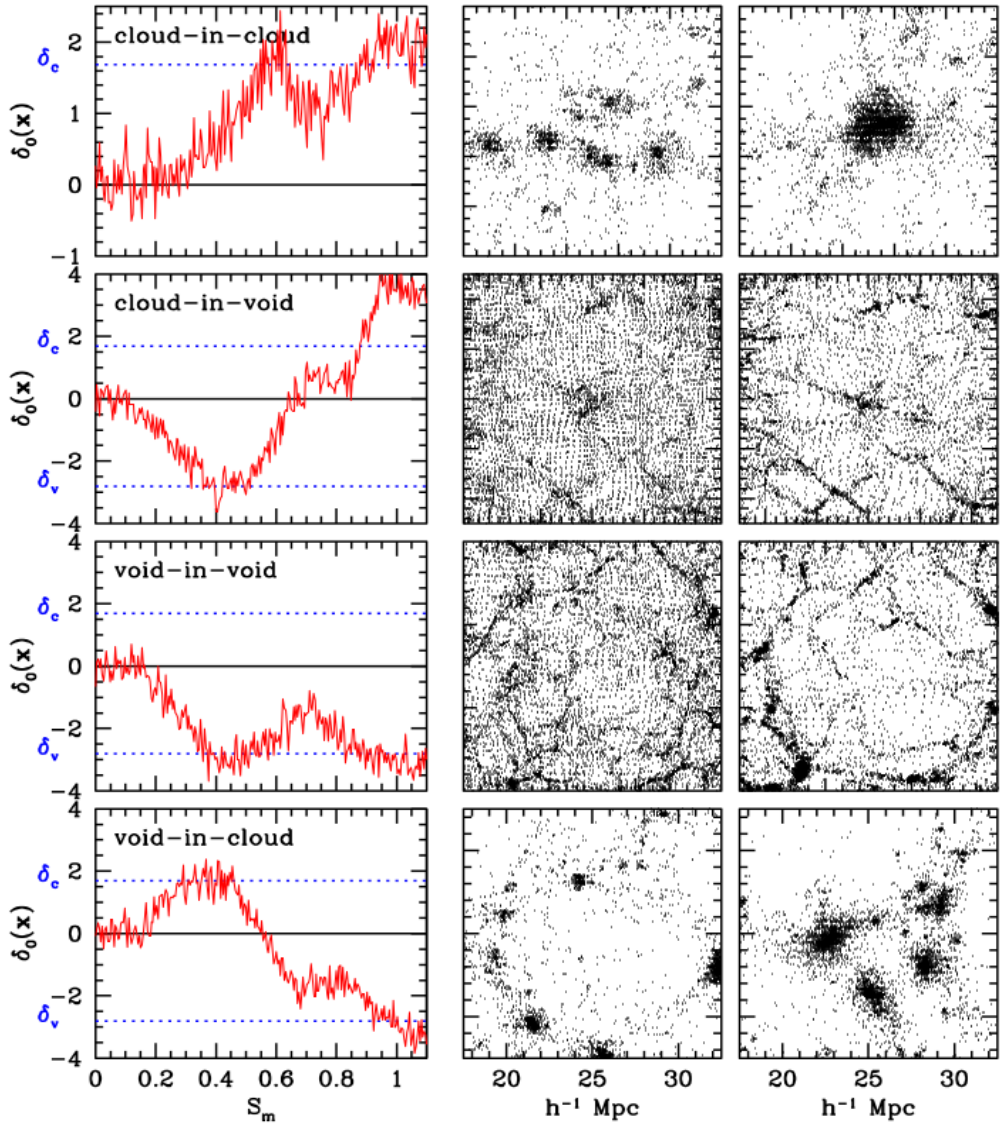

Figure 3.1: Graphic representation of the cloud-in-cloud (top), cloud-in-void, void-in-void and void-in-cloud (bottom) processes of the hierarchical clustering, identified as the four modes of the excursion-set formalism. The trajectories of a local density perturbations $\delta_0(x)$ as a function of the mass resolution $S_\mathrm{m} = \sigma^2(M)$ are shown in the left panels. The dotted horizontal blue lines indicate the barriers considered in the one-barrier and two-barriers problem: δ_c refers to the collapse of the overdensities, while δ_v refers to the void formation. The central and rightmost panels show the evolution of the particles when the barriers are crossed at small (i.e. earlier times) and large (i.e. later times) scales respectively. Note that as S_m increases, the cosmological scales considered decrease. Credits to: Sheth and Weygaert (2004).

two-barrier problem. In fact, when analysing cosmic voids we must account for the *void-in-void* and *void-in-cloud* problems: the first one is the analogue of the *cloud-in-cloud* process of the overdensities mentioned before, i.e. the need to consider void mergers in order to avoid double counts; the second one takes into account that voids embedded in high-density collapsing regions are doomed to vanish. Finally, let us introduce also the *cloud-in-void* process, which refers to an opposite situation with respect to the void-in-cloud: if a small overdense region is embedded in a large void, the formation of high-density collapsed structures is disfavoured. Note that the cloud-in-void and the void-in-cloud processes are asymmetric since in the former the overdensity inside the void survives, while in the latter the void embedded in a high density region is destroyed. The result of this asymmetry is that the Gaussianity of the distribution of primordial fluctuations is no longer valid.

In fig. 3.1 there is a schematic representation of the the above mentioned both halo- and void-formation processes addressed by the excursion-set formalism. As already pointed out, the excursion-set theory is needed in order to develop the theoretical model of the VSF, which is described in the next paragraph.

Void size function theoretical model

The theoretical VSF predicts the comoving number density of voids as a function of their size. A model for the VSF was proposed by Sheth and Weygaert (2004) by means of the *excursion-set formalism*, implemented for the underdensities through the following formula:

$$f_{\ln\sigma} = 2\sum_{j=1}^{\infty} j\pi x^2 \sin(j\pi\mathcal{D}) \exp\left[-\frac{(j\pi x)^2}{2}\right] , \tag{3.2}$$

where $f_{\ln\sigma}$ is called *multiplicity function* and expresses the fraction of Universe filled by cosmic voids. Furthermore, in this formula, the quantities x and $\mathcal{D}$ are defined as:

$$x \equiv \frac{\mathcal{D}}{|\delta_{\rm v}^{\rm L}|}\sigma \qquad ; \qquad \mathcal{D} \equiv \frac{|\delta_{\rm v}^{\rm L}|}{\delta_{\rm c}^{\rm L} + |\delta_{\rm v}^{\rm L}|} , \tag{3.3}$$

with σ the square root of the mass variance filtered on a radius R, $\delta_{\rm v}^{\rm L}$ the negative linear threshold required for the void formation, $\delta_{\rm c}^{\rm L}$ the critical density contrast for an overdensity to collapse ($1.06 \leq \delta_{\rm c}^{\rm L} \leq 1.686$, where the former is related to the turn-around while the latter representing the effective collapse of DM haloes; see §2.3.2).

Equation (3.2) leads to the functional form of the VSF in linear theory proposed by Sheth and Weygaert (2004) (SvdW hereafter) and expressed as:

$$\frac{{\rm d}n^{\rm L}}{{\rm d}\ln r^{\rm L}} = \frac{f_{\ln\sigma}(\sigma)}{V(r^{\rm L})}\frac{{\rm d}\ln\sigma^{-1}}{{\rm d}\ln r^{\rm L}} , \tag{3.4}$$

where $V(r^{\rm L}) = \frac{4}{3}\pi(r^{\rm L})^3$ is the volume of the perturbation, i.e. a sphere with radius $r^{\rm L}$. In order to move from the linear to the nonlinear theory, the authors assumed that the total number of cosmic voids is conserved. We know from the theory of the spherical collapse (§2.3.2) that, since at the shell-crossing a negative perturbation has increased its volume by a factor $a \propto \delta_{\rm v}^{\rm L}$,

a corrective factor must be taken into account on the linear radius definition:

$$\left.\frac{\mathrm{d}n}{\mathrm{d}\ln r}\right|_{\mathrm{SvdW}} = \frac{\mathrm{d}n}{\mathrm{d}\ln\left[a^{-3}\, r^{\mathrm{L}}\right]} \,. \tag{3.5}$$

The relation linking the linear and nonlinear radii can be made explicit as follows:

$$\frac{r}{r^{\mathrm{L}}} = \left(\frac{\bar{\rho}}{\rho_{\mathrm{v}}}\right)^{1/3} , \tag{3.6}$$

where $\bar{\rho}$ is the mean density of the Universe and ρ_{v} is the average density within the void considered.

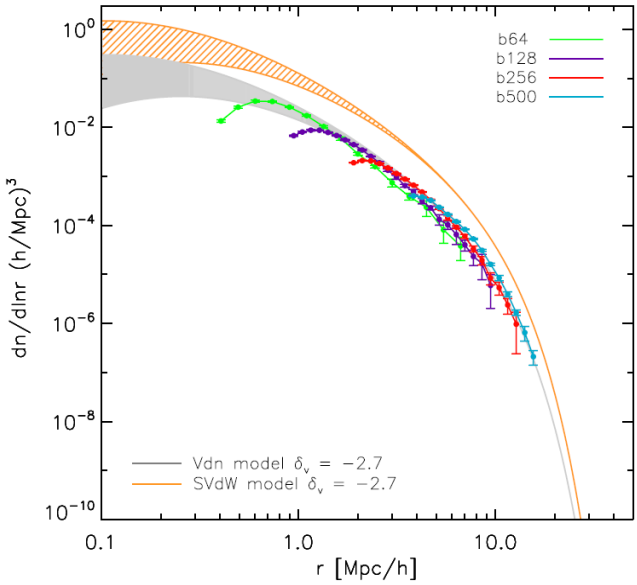

Figure 3.2: Fitting of the measured VSF with both the SvdW and Vdn model predictions, assuming $\delta_{\mathrm{c}}^{\mathrm{L}} = [1.06 - 1.686]$ and $\delta_{\mathrm{v}}^{\mathrm{L}} = -2.7$. It is evident how the data are consistent with the grey-shaded Vdn model, but not with the orange SvdW one. The void counts (green, purple, red and light blue lines) are extracted from the DM density field in ΛCDM simulations with different box sizes ($64h^{-1}$Mpc, $128h^{-1}$Mpc, $256h^{-1}$Mpc and $500h^{-1}$Mpc, respectively). Credits to: Jennings et al. (2013).

The SvdW model only includes the *void-in-cloud* process through the definition of the parameter $\mathcal{D}$ but the *void-in-void* problem is not taken into account. As a consequence, the resulting volume occupied by cosmic voids is greater than the total volume of our Universe and this leads to an overestimation of the void number density. Hence, Jennings et al. (2013) proposed a correction of the SvdW model, which is based on the volume conservation of the voids when moving from the linear to the nonlinear regime, the so-called *volume conserving model* (Vdn model, hereafter):

$$\left.\frac{\mathrm{d}n}{\mathrm{d}\ln r}\right|_{\mathrm{Vdn}} = \frac{\mathrm{d}n}{\mathrm{d}\ln r^{\mathrm{L}}}\frac{V(r^{\mathrm{L}})}{V(r)}\frac{\mathrm{d}\ln r^{\mathrm{L}}}{\mathrm{d}\ln r} \,. \tag{3.7}$$

We show in fig. 3.2 the improvement of the Vdn model over the previous one: the data are well modelled by the Vdn model, while the SvdW model does not show consistency with the measurements of the void abundances.

3.2.2 Density profile

As mentioned before, cosmic voids can be identified through the distribution of tracers (i.e. galaxies, galaxy clusters, DM haloes and DM particles)[5]. The void density profile (i.e. the density contrast as a function of the distance from the void center) can be expressed as follows:

$$u_{\rm v}(r) \equiv \frac{n_{\rm v,tr}(r)}{\langle n_{\rm tr}\rangle} - 1 = \frac{\rho_{\rm v}(r)}{\bar{\rho}} - 1 \ , \tag{3.8}$$

where, if we consider a sphere centered in the centre of a void with a radius corresponding to the void radius, $n_{\rm v,tr}(r)$ is the number density of tracers at each radius r and $\langle n_{\rm tr}\rangle$ is the mean number density of tracers, while ρ_v and $\bar{\rho}$ are the corresponding mass densities, respectively. Note the second equivalence is achieved by considering all tracers with the same mass.

In recent years, several models for the void density profile have been suggested by the scientific community, which are generally divided into two categories: the *phenomenological* models (see e.g. Nadathur et al., 2015) and the *theoretically motivated* models (see e.g. Finelli et al., 2016); the former have the aim to develop suitable functional forms to fit the void density profile, while the latter are based on theoretical laws. One of the most popular formulas for the void density profile was presented by Hamaus et al. (2014). It belongs to the category of phenomenological models and can be expressed as follows:

$$u_{\rm v}(r) = \delta_{\rm c}^{\rm L} \frac{1-(r/r_{\rm s})^{\alpha}}{1+(r/r_{\rm v}^{\rm L})^{\beta}} \ , \tag{3.9}$$

where $\delta_{\rm c}^{\rm L}$ is the density contrast at $r = 0$ (i.e. in the void center), $r_{\rm s}$ is the scale at which the void density equals the tracer mean density $\langle n_{\rm tr}\rangle$ and $r_{\rm v}^{\rm L}$ is the linear void radius. α and β are introduced as free parameters to model the inner and outer density profile slopes, respectively. Fig. 3.3 shows how the functional form of eq. (3.9) properly models the stacked density profiles of cosmic voids divided into different radius bins.

We now focus on some peculiar features of the void density profiles emerging from fig. 3.3. The profile of these objects typically exhibits an underdense central region and an overdense ridge of matter (also called *compensation wall*), with a negative and positive density contrast, respectively. After the compensation wall, which generally appears at about one void radius, the profiles settle at $\delta = 0$ (i.e. at the mean density contrast of the Universe). Something else that should be noted from this figure is that for relatively small voids the density profile is sharp, showing a deep underdense core and a high compensation wall. By contrast, to large voids correspond shallower profiles, with less underdense interiors and nearly invisible ridges of matter.

In this context, let us now briefly explain the origin of such profiles describing the void density contrast. In agreement with §2.3.2, the innermost void density decreases as the time-

[5]Note that in the next chapters we will mostly deal with voids identified in the unbiased DM-particle field. Of course, this kind of analysis can only be performed when simulations are considered.

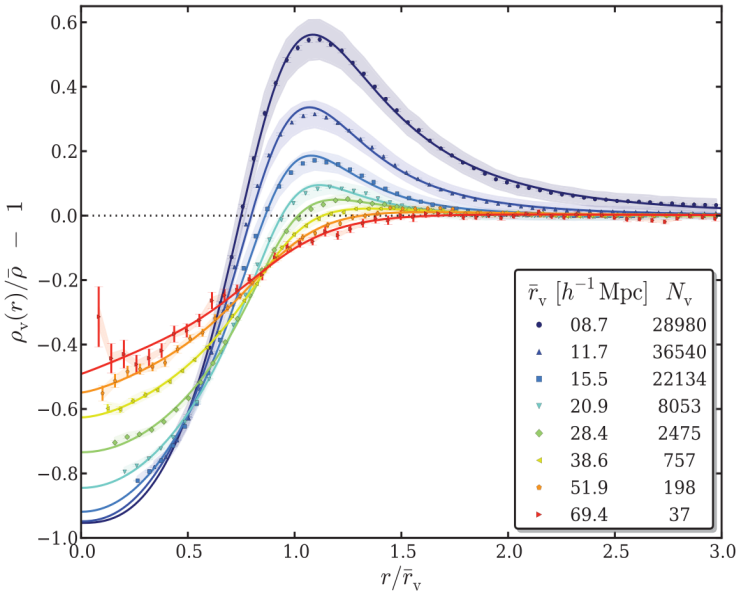

Figure 3.3: Stacked real-space density profiles of voids traced by mock galaxies at $z = 0$. The solid lines are the best fits of eq. (3.9) corresponding to different radius bins: moving from the blue line to the red line, increasing void radii are considered. Note that the x-axis represents the void radii re-scaled by the mean void radius of each bin. The first column of the legend indicates the mean void radii of the different intervals, while the total number of objects in each bin is written in the second column. Credits to: Hamaus et al. (2014b).

evolution of the primordial underdensities proceeds. This is essentially due to their expansion, which is greater in the centre, where the density contrast Δ is lower. As a consequence of this differential expansion, it emerges a ridge of matter where the shell-crossing phenomenon occurs. Moreover, there is a second-order process to be considered when analysing the shape of the void density profile. Indeed, the growth of overdense structures arranged at the edge of the voids causes a further fraction of matter to be removed from the void interiors by means of gravitational attraction. Of course, this effect contributes in both the lowering-density history of void inner regions and the creation of the ridge of matter around them.

3.2.3 Two-point correlation function and void bias

Since the clustering of both the cosmic structures and voids depends on the geometric and dynamic cosmological parameters of our Universe, the two-point statistics is an extremely powerful probe to constrain the cosmological model. In this Thesis work we will focus on the auto-correlation function computed between void centers, and its Fourier transform (i.e. the void power spectrum, see §2.4.1). At the end of this subsection we will also provide a brief description of the cross-correlation function computed between void and tracer centers. Note that to analyse properly the 2PCF statistics we must account for both its measure and modelling.

Auto-correlation estimators

Once the void identification is completed in the distribution of mass tracers of either a redshift survey or a cosmological simulation, we can measure their two-point clustering properties through different *estimators*, which are divided in two main categories according to Kerscher et al. (2000): the *pairwise* and the *geometric* estimators. Let us now concentrate on the first category, in which the estimator chosen for this Thesis work is enclosed. See the above mentioned paper and references therein for further details on the geometric side.

With the aim of estimating the 2PCF of a dataset, let us build a random catalogue[6] with the same geometry and density evolution of our sample. The pairwise estimators allow us to measure the 2PCF by counting pairs between data-data, random-random, and data-random centers; these counts can be expressed as a function of the distance between the couples (i.e. $\mathrm{dd}(r)$, $\mathrm{rr}(r)$ and $\mathrm{dr}(r)$, respectively), normalised by the total number of object pairs considered (i.e. $N_\mathrm{D}(N_\mathrm{D}-1)$, $N_\mathrm{R}(N_\mathrm{R}-1)$ and $N_\mathrm{D}N_\mathrm{R}$, respectively):

$$\mathrm{DD}(r) = \frac{\mathrm{dd}(r)}{N_\mathrm{D}(N_\mathrm{D}-1)} \quad , \quad \mathrm{RR}(r) = \frac{\mathrm{rr}(r)}{N_\mathrm{R}(N_\mathrm{R}-1)} \quad , \quad \mathrm{DR}(r) = \frac{\mathrm{dr}(r)}{N_\mathrm{D}N_\mathrm{R}} \ . \tag{3.10}$$

A highly accurate pairwise estimator that is widespread among the cosmological community was proposed by Landy and Szalay (1993) as:

$$\hat{\xi}_\mathrm{LS}(r) = \frac{\mathrm{DD}(r) - 2\mathrm{DR}(r) + \mathrm{RR}(r)}{\mathrm{RR}(r)} \ , \tag{3.11}$$

which, for $N_\mathrm{R} \to \infty$ i.e. minimum variance, provides us with an unbiased estimation of the 2PCF. Known as *Landy-Szalay estimator*, eq. (3.11) is obviously suitable for both the cosmic voids and collapsed structures.

For the sake of argument, let us point out that another commonly used estimator, known as *natural estimator*, was introduced by Peebles and Hauser (1974). It can be written as follows:

$$\hat{\xi}_\mathrm{N}(r) = \frac{\mathrm{DD}(r)}{\mathrm{RR}(r)} - 1 \ . \tag{3.12}$$

However, it has been demonstrated that such estimator suffers from low accuracy on large scales because the samples of data we are provided with are not continuous but discrete.

Auto-correlation modelling

Concerning cosmic voids, while the 2PCF measurements can be found in the literature[7], the 2PCF modelling is far to be completely understood because theoretical studies of void clustering have only recently begun to be developed. It is in this current scenario that our Thesis work has originated, with the main aim of exploiting the void auto-correlation with cosmological

[6] Note that, typically, the catalogue of random objects is characterised by a greater number of objects than the void catalogue one wants to investigate. This is done in order to enhance the precision on the clustering measurements. In our analyses, $N_\mathrm{R} = 10N_\mathrm{D}$: the number of random objects is ten times higher than the number of data (i.e. the number of cosmic voids in our catalogues).

[7] See e.g. Massara et al. (2015), Clampitt et al. (2016) and Kreisch et al. (2019).

purposes (i.e. to provide constraints on the ΛCDM parameters) for the very first time.

In order to fit the auto-correlation function with a proper model, we decided to start from the power spectrum model proposed by Chan et al. (2014). According to this paper, the VSF assumes the functional form of the SvdW model. In this regard, let us point out that in §3.2.1 we learnt how the Vdn model is more accurate than the SvdW, since it accounts not only for the void-in-cloud phenomenon, but also for the void-in-void process. Here it lies the sensitivity of the void definition adopted to construct the void catalogue of which the VSF is computed: Jennings et al. (2013) found good agreement with the Vdn model by considering voids as sperical non-overlapping regions of density $0.2\bar{n}$ at the ridge between them, where $\bar{n}$ is the mean particle number density of the sample considered; by contrast, Chan et al. (2014) found a better match with the SvdW model, since they accounted only for large parent[8] voids.

In CHAPTER 5 we will present our model for the void auto-correlation function, born as a fusion of the two methods in the above cited papers: the Vdn formula for the VSF and the power spectrum definition adopted in Chan et al. (2014). Since the Vdn model has already been introduced in eq. (3.7), here we present the modelling of the power spectrum of cosmic voids $P_{\rm v}(k)$, which can be expressed as follows:

$$P_{\rm v}(k) = b_1^2 P_{\rm m}(k) + P_{\rm excl}(k) \ . \tag{3.13}$$

In this equation, $P_{\rm m}$ is the dark matter power spectrum and it can be computed through a so-called *Boltzmann solver*[9], the b_1 term is the *linear bias*, while $P_{\rm excl}$ is a corrective power spectrum which accounts for the void exclusion. We will now focus on these latter two terms, giving a more detailed description of both of them.

In order to define b_1, let us write the void mass function in analogy with its better studied counterpart, i.e. the halo mass function, as:

$$\frac{{\rm d}n}{{\rm d}\ln M} = \frac{\bar{\rho}_{\rm m}}{M} \nu \mathcal{F}(\nu, \delta_{\rm v}, \delta_{\rm c}) \frac{{\rm d}\ln \nu}{{\rm d}\ln M} \ , \tag{3.14}$$

where n is the void number density, $\bar{\rho}_{\rm m}$ is the mean dark matter density, M is the mass, $\nu = \frac{|\delta_{\rm v}|}{\sigma_{\rm M}}$ is referred to as *peak height* or *significance*, $\sigma_{\rm M}$ is the root-mean-squared density fluctuation smoothed with a top-hat window of size $R_{\rm L}$ (i.e. the Lagrangian size of the void) and $\mathcal{F}(\nu)$ is the same as eq. (3.2) but considering also a dependence on the quantity ν. Lastly, $\delta_{\rm v}$ and $\delta_{\rm c}$ are the critical density contrasts required for the void formation and the halo formation, respectively. Let us underline that these quantities in linear theory are exactly the same on which the theoretical VSF is built. Hence, it is through these fixed density contrasts that we accounted for the whole theory of the VSF in our model while performing the analysis on the void clustering. Proceeding with the characterisation of the theoretical bias, Sheth and Tormen (1999) argue that the mass function (eq. 3.14) alone is enough to define the large-scale bias by means of the *peak background split* (PBS) model. Thus, it has been shown that the bias

[8] There are two possible outcomes of the VIDE finding procedure that we will address in §4.3.1: the so-called *trimmed* and *untrimmed* catalogues. In the first case the sub-voids (or *child voids*) are removed and only the major voids (or *parent voids*) are considered, while in the latter case both these categories of objects are taken into account.

[9] See e.g. EISENSTEIN-HU (Eisenstein and Hu, 1998) and CAMB (Lewis et al., 2000).

parameters in Eulerian space are:

$$b_i = \frac{1}{n_0}\frac{\partial^i}{\partial\delta^i}\Big[(1+\delta)n(\delta_{\rm L})\Big]\Big|_{\delta=0} \,, \tag{3.15}$$

where n_0 and $n(\delta_{\rm L})$ refer to the void mass function of zero and $\delta_{\rm L}$ background perturbations respectively, while the factor $(1+\delta)$ encloses the transition from the void mass function in the Lagrangian space to the Eulerian space. In agreement with Bernardeau (1994), the relation between δ e $\delta_{\rm L}$ can instead be written through the spherical collapse as follows:

$$\delta_{\rm L} = \delta - \nu_2\delta^2 + \nu_3\delta^3 + \dots \,, \tag{3.16}$$

where $\nu_2 = 12/21$ and $\nu_3 = 341/567$ are constant factors needed to account for the second and third nonlinear orders. Since we will refer to the *linear*[10] order for the whole analysis, this equation becomes $\delta = \delta_{\rm L}$. From eq. (3.15) it is possible to derive the linear bias parameter[11] b_1:

$$b_1(R_{\rm v}) = 1 + \frac{\nu^2-1}{\delta_{\rm v}} + \frac{\delta_{\rm v}\mathcal{D}}{4\delta_{\rm c}^2\nu^2} \,, \tag{3.17}$$

where $R_{\rm v}$ is the void radius. The trend of the bias as a function of the void radius is shown in fig. 3.4. Note that the theoretical bias that we will refer to in our analysis (see the forthcoming CHAPTER 5) corresponds to a fixed linear density contrast $\delta_{\rm v}^{\rm L} = -2.7$, in agreement with the theory of the VSF, as anticipated.

Finally, notice that it is also possible to define the so-called *effective bias* by weighting the PBS linear bias with the theoretical VSF, through the following ratio of integrals computed over the radii considered by the VSF:

$$b_{\rm v,eff} = \frac{\int \frac{{\rm d}n}{{\rm d}R_{\rm v}} b_{\rm v}(R_{\rm v}){\rm d}R_{\rm v}}{\int \frac{{\rm d}n}{{\rm d}R_{\rm v}}{\rm d}R_{\rm v}} \,. \tag{3.18}$$

Let us now move to the description of the exclusion term $P_{\rm excl}$. From the literature, it is known that a term of *halo exclusion* must be considered when identifying haloes, since every halo finding algorithm must decide which structures are parent haloes and which ones are sub-haloes of larger haloes. This choice is referred to as *percolation* and it is of fundamental importance as, depending on the chosen percolation, the statistical properties of the halo catalogues can vary considerably (see e.g. García and Rozo, 2019). As previously clarified, cosmic voids are much more extended than haloes and this results in a more complex hierarchical structure. Therefore, a theoretical principle of void exclusion to classify parent voids and child voids is even more necessary than for haloes in order to properly model the void power spectrum.

To this end, the *hard-sphere* (HS) approximation[12] can be adopted. Let us then consider a

[10] We chose the linear approach because it has been demonstrated that the nonlinear higher-order terms do not improve the analysis up to a significant level (see e.g. Chan et al., 2014).

[11] Actually, this functional form for the linear bias was previously presented in Sheth and Weygaert (2004), but there was a typo that in (3.17) has been corrected.

[12] The HS approximation is commonly employed in statistical mechanics to describe simple liquids and non-

sample of identical hard spheres of diameter D and mean number density $\bar{n}_{\rm v}$, assuming the system in equilibrium. The clustering properties are well-described by the so-called *Percus-Yervick equation*, whose corresponding power spectrum can be expressed as follows:

$$P_{\rm HS}(k) = \frac{c(k)}{1-(2\pi)^3\bar{n}_{\rm v}c(k)} \ , \tag{3.19}$$

with

$$\begin{cases} c(k) = -\frac{D^3}{2\pi^2 q^3}\Big\{a_1(\sin q - q\cos q) + \frac{6\eta a_2}{q}\Big[2q\sin q + (2-q^2)\cos q - 2\Big] + \\ \qquad\qquad + \frac{\eta a_1}{2q^3}\Big[4q(q^2-6)\sin q - (24-12q^2+q^4)\cos q + 24\Big]\Big\} \ , \\ \eta = \frac{\pi\bar{n}D^3}{6} \ , \\ a_1 = \frac{(1+2\eta)^2}{(1-\eta)^4} \ , \\ a_2 = \frac{(1+\eta/2)^2}{(1-\eta)^4} \ , \end{cases} \tag{3.20}$$

where $q = kD$ and η is referred to as *packing fraction*. The exclusion power spectrum must be added to $b_1^2 P_{\rm m}$ (in eq. 3.13) to make voids (i.e. very extended structures) behave like hard spheres, so as to reconstruct a proper functional form that describes the power spectrum of these objects. It can be noticed from fig. 3.5 that the exclusion term has two main effects: it introduces oscillations at small physical scales (i.e. large k scales) due to the sines and cosines in $c(k)$ (see eqs. 3.20), and lowers the $b_1^2 P_{\rm m} = P_{1,1}$ term at large physical scales (i.e. small k scales).

ideal gases (see e.g. Torquato, 2001 and Hansen and McDonald, 2006).

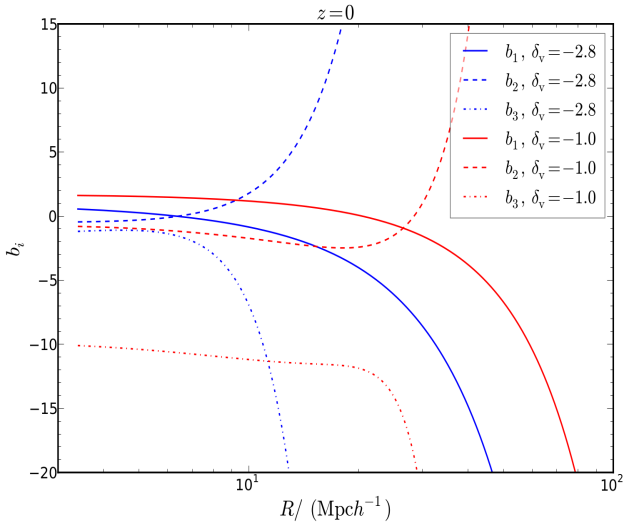

Figure 3.4: The first three orders of the PBS bias parameter emerging from eq. (3.15) at redshift $z = 0$. The blue lines represent a density contrast $\delta_v = -2.8$, while the red ones $\delta_v = -1.0$. The solid lines correspond to the linear bias b_1, while the dashed and dotted lines stand for the second and third order nonlinear bias, respectively. Credits to: Chan et al. (2014).

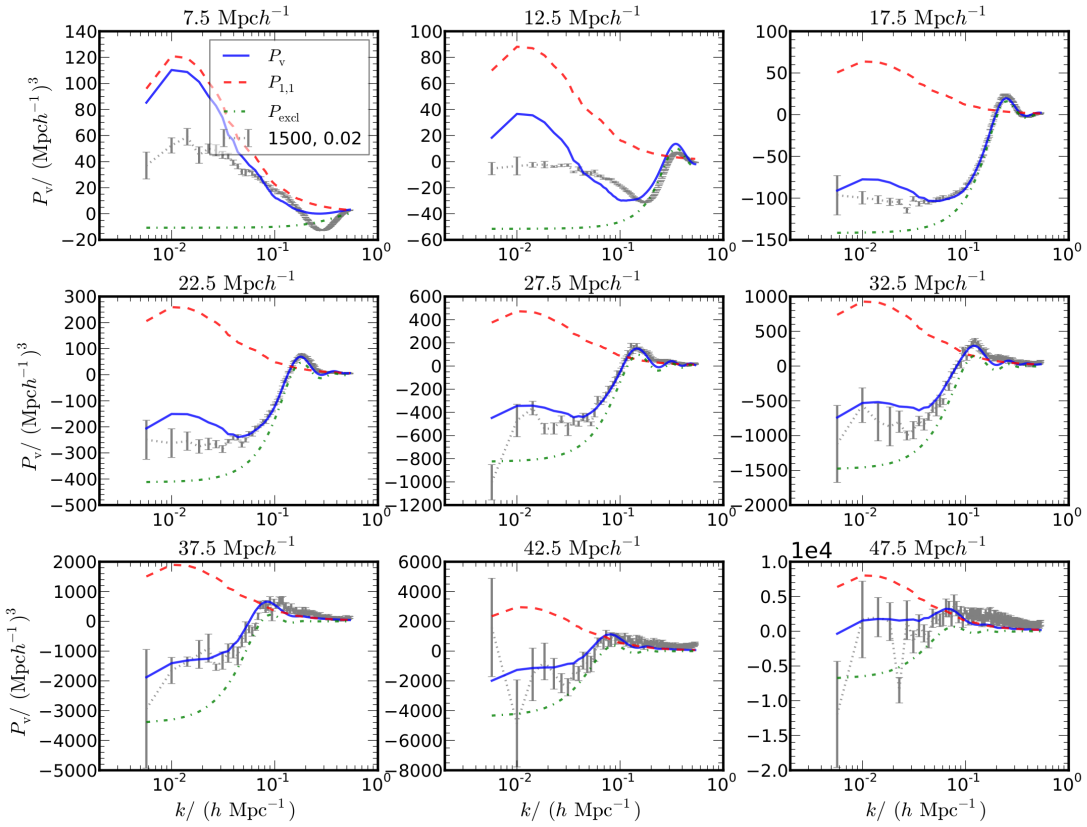

Figure 3.5: Model of the power spectrum implemented as eq. 3.13. The blue line represents the void power spectrum, achieved as the sum of $P_{1,1} = b_1^2 P_m$ (red dashed line, i.e. the DM power spectrum multiplied by the squared linear bias) and $P_{excl} = P_{HS}$ (dotted-dashed green line, i.e. the term of void exclusion). Credits to: Chan et al. (2014).

Void-tracer cross-correlation function

The clustering properties of cosmic voids can not only be computed by means of the above depicted auto-correlation function, but also with the so-called *cross-correlation function* computed for both voids and overdensity tracers simultaneously. To cross-correlate two data samples means to count pairs between void and tracer centers against a distribution of random points. Note that the random catalogue is built with the same characteristics of one of the two catalogues, analogously to what we do for the auto-correlation measurement. The most commonly used estimator for the cross-correlation function was introduced by Szapudi and Szalay (1998) in the context of the N-point correlation definition. The *Szapudi-Szalay estimator*, can be expressed through the following formula:

$$\hat{\xi}_{\rm SS}(r) = \frac{\mathrm{D_1D_2}(r) - \mathrm{D_1R}(r) - \mathrm{D_2R}(r) + \mathrm{RR}(r)}{\mathrm{RR}(r)} \,, \tag{3.21}$$

where D_1 and D_2 are the centers corresponding to the first and the second catalogue respectively, while R are points of the random catalogue. Note that the terms in this equations are defined analogously to eq. (3.10).

Concerning the modelling of the cross-correlation function, its knowledge is slightly more advanced than that of the auto-correlation function; there exist several models that can be found in literature (see e.g. Hamaus et al., 2014c and 2015).

The void-tracer cross-correlation $\xi_{\rm v,tr}$ is directly linked to the void density profile presented is §3.2.2. In fact, since it reflects the probability of finding a tracer inside a sphere centered on the void center at a comoving radial distance r, it can be written by means of the appropriate integral of the void density profile $u_{\rm v}(r)$ as

$$\xi_{\rm v,tr}(r) = \frac{1}{3r^2}\frac{\mathrm{d}}{\mathrm{d}r}\Big[r^3\Delta(r)\Big] \,, \tag{3.22}$$

where

$$\Delta(r) = \frac{3}{r^3}\int_0^{R_{\rm v}} u_{\rm v}(r) r^2 \mathrm{d}r. \tag{3.23}$$

Furthermore, it is possible to define the void-tracer cross-correlation through the auto-correlation of tracers $\xi_{\rm tr}(r)$ in the following way:

$$\xi_{\rm v,tr}(r) \simeq b_{\rm v}\, b_{\rm tr}\, u_{\rm v}(r)\, \xi_{\rm m}(r) \,, \tag{3.24}$$

where $b_{\rm v}$ and $b_{\rm tr}$ are the void bias and the tracer bias, respectively. The typical overdensity tracers used in observations are galaxies and galaxy clusters, while in N-body simulations the DM particles and haloes are also considered. In eq. (3.24), the DM particle correlation $\xi_{\rm m}$ is known from theory, and the tracer bias $b_{\rm tr}$ has been studied extensively in the literature (see e.g. Desjacques et al., 2018). By contrast, both the void bias and density profile are not yet fully understood. Note that one of the aims of our analysis is the validation of the theoretical void bias presented in §3.2.3.

3.3 A novel cosmological probe

Scientists are much further behind in understanding voids than the collapsed structures. Since cosmic voids are quite extended structures, a cosmological exploitation of these objects requires huge amounts of data, both in redshift surveys and simulations. Analogously to what we reported in §2.5, in order to study cosmic voids at both the small and the large scales, we would need *wide-* and *deep-field* surveys, i.e. large volumes enclosing a high tracer density. It is easily understandable that such requirements have entailed severe limits on the development of cosmic voids as a cosmological probe.

In recent years, scientific breakthroughs have made it possible to investigate voids more and more closely, leading to the development of several models and techniques to exploit the potentially highly-constraining power of different void statistics, such as: the *void-galaxy cross-correlation*, i.e. the void density profile (Nadathur et al., 2019; Voivodic et al., 2020; Correa et al., 2021; Hamaus et al., 2022), the *void size function* (Pollina et al., 2015; Sahlén et al., 2016; Verza et al., 2019; Contarini et al., 2019 and 2022), the *void lensing* (Krause et al., 2012; Sánchez et al., 2016; Baker et al., 2018; Kovács et al., 2022); the void shapes, i.e. the *geometrical* and *dynamic distortions* (Lee and Park, 2009; Lavaux and Wandelt, 2012; Hamaus et al., 2020).

Furthermore, we underline that cosmic voids are extremely sensitive to DE (Bos et al., 2012b; see references on the void shapes, to which the DE is strongly related) and neutrinos (Massara et al., 2015; Kreisch et al., 2019), since the fraction of these components is higher than in the collapsed structures. Let us also mention that cosmic voids are the perfect laboratories to investigate the MG theories because the gravitational potential is shallow and easy to model, and the screening mechanism operates only marginally within these objects (Clampitt et al., 2013; Cai et al., 2015; Barreira et al., 2015; Falck et al., 2018; Perico et al., 2019b). Notice that MG models have an effect on some observational properties; for example, they generally enhance the void expansion making the dynamical distortions become stronger, and produce modifications on the lensing signal around voids.

As an example of the void exploitation as a cosmological probe, we show in fig. 3.6 a comparison among the constraints on both $f\sigma_8$ and $D_\mathrm{A}H$ obtained from cosmic voids in the literature (the references and surveys employed are indicated in the legend). We recall that f is the growing factor, σ_8 the mass variance filtered on a radius of $8\ h^{-1}\mathrm{Mpc}$, D_A the angular diameter distance and H the Hubble parameter.

Finally, as previously mentioned, note that we can not only exploit the void statistics itself in a cosmological sense, but we can also take advantage of its combination with other probes. When the void and overdense structures analyses are merged, the constraints improve because we are drawing information from two different sides of our Universe.

The main aim of this Thesis is to make the void clustering become competitive with the aforementioned probes in the current cosmological panorama. Indeed, we developed a preliminary method to assess the cosmological constraining power of the void auto-correlation function. As anticipated in §3.2.3, we relied on the power spectrum model proposed by Chan et al. (2014) and we exploited its Fourier transform, combining its theoretical predictions with those of the VSF model (see §3.2.1). Being our model almost entirely based on first principles, we will show in chapter 5 how the void clustering can finally give its contribution to con-

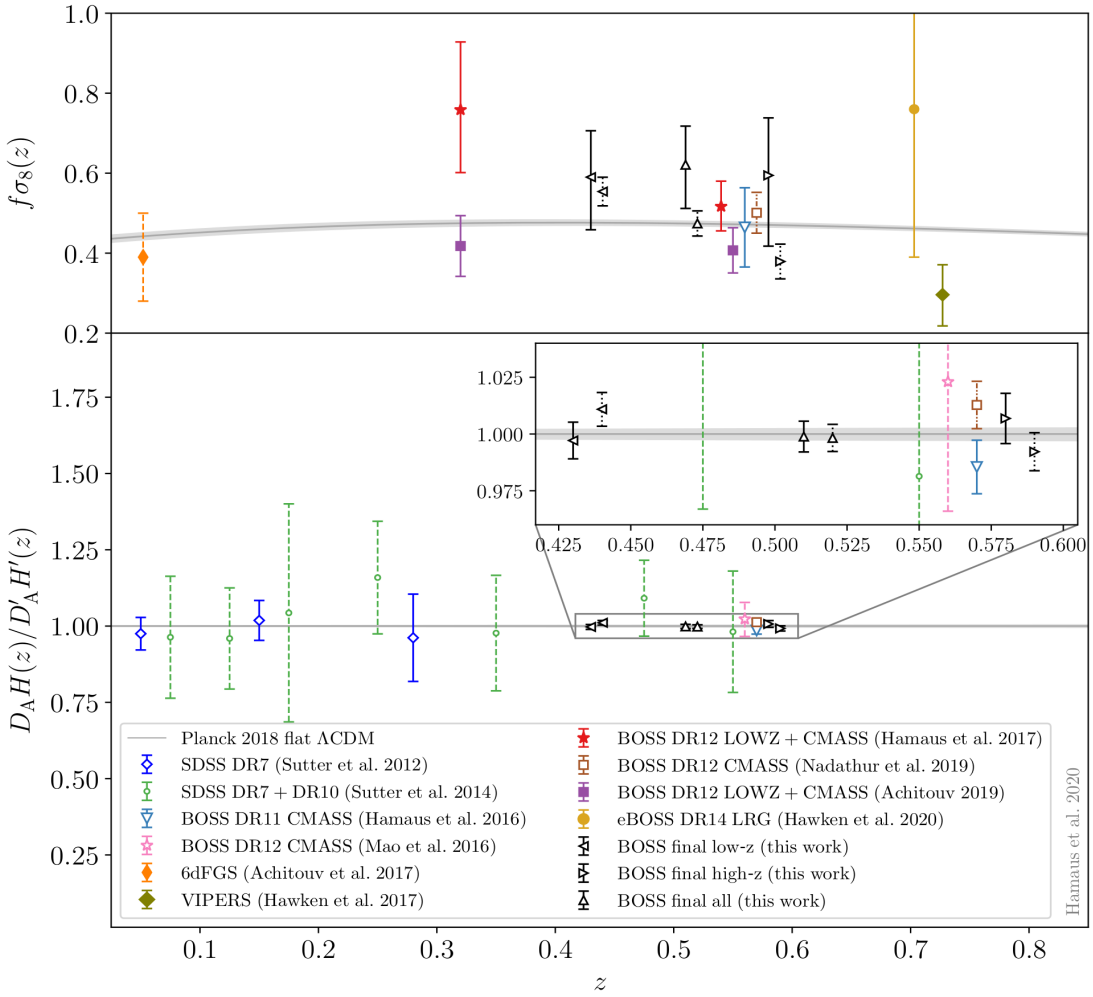

Figure 3.6: Constraints on $f\sigma_8$ and $D_A H$ from cosmic voids: a comparison among ΛCDM predictions and several measurements from real datasets. For graphic purposes, $D_A H$ is normalised to its reference value $D'_A H'$ (Planck Collaboration et al., 2020c). The filled markers refer to growth rate measurements without considering the *Alcock-Paczynski* effect (i.e. geometrical distortions), while the open markers include the AP test. Finally, the style of the error bars reflects the various degrees of assumptions made in the models: model-independent assumptions (solid error bars), calibrated on N-body simulations (dashed), calibrated on mock galaxy catalogues (dotted), calibrated on both simulations and mocks (dash-dotted). Credits to: Hamaus et al. (2020).

strain some cosmological parameters, such as the matter density parameter, $\Omega_{\rm m}$, the matter power spectrum normalization at $z = 0$, σ_8, and their derived parameter $S_8 \equiv \sigma_8\sqrt{\Omega_{\rm m}/0.3}$. To do this, we will use void catalogues properly prepared for this analysis, i.e. constructed by means of the cleaning algorithm presented in §4.3.2 to make them consistent with the theory of the VSF (i.e. the Vdn model).

Our work represents a key step towards a full cosmological usage of cosmic voids, since we propose a new pipeline to exploit for the first time the void clustering as cosmological probe.

Chapter 4

Data preparation

4.1 CosmoBolognaLib

The CosmoBolognaLib[1] (CBL hereafter) are a large set of *free software* C++/Python libraries for cosmological calculations, that have been developed by Marulli et al. (2016) to handle object catalogues of either observed or simulated data, with the main aim of numerically investigating the statistical properties of our Universe. It is thanks to the numerical tools provided by the CBL network that we have been able to carry out the cosmological analysis presented in this Thesis by means of: *(i)* the 2PCF measure, which relies on the Landy-Szalay estimator given by eq. (3.11); *(ii)* the Fourier transform of the power spectrum model (eq. 3.13) to get its corresponding real-space 2PCF; *(iii)* the algorithms required to perform Bayesian analyses, used to calibrate the void auto-correlation model and constrain the cosmological parameters; *(iv)* the cleaning algorithm to account only for properly re-scaled and non-overlapping voids, in agreement with the VSF theory; *(v)* the VSF measure and model both to verify the agreement of cleaned voids with the Vdn model and to include its theory in our 2PCF model; *(vi)* the HMF measure and model to study the properties of the halo catalogues from which the voids are identified.

Furthermore, let us point out here that, beyond the tools provided by the CBL, we also developed C++ and Python codes necessary for the implementation of the auto-correlation model presented in §3.2.3, with some additional corrections that will be outlined in CHAPTER 5. We also plan to include these codes in the environment of the CBL and deploy them within the next public version of the libraries.

4.2 DUSTGRAIN-*pathfinder* simulations

The suite of N-body simulations we consider to perform our analysis on cosmic voids is called DUSTGRAIN[2]-*pathfinder* (Giocoli et al., 2018). It arose with the aim of studying modified gravity in the form of $f(R)$ models, with and without massive neutrinos, as an alternative physical cause to the cosmological constant Λ for the late time accelerated expansion of the Universe.

[1] https://gitlab.com/federicomarulli/CosmoBolognaLib

[2] The acronym DUSTGRAIN stands for Dark Universe Simulations to Test GRAvity In the presence of Neutrinos.

These collisionless simulations trace the evolution of $768^3(\times 2)$ DM particles (and neutrinos) under the effect of gravity in a periodic cosmological box of $750\ h^{-1}\mathrm{Mpc}$ per side. The CDM particles are assumed to have a mass of $8.1 \cdot 10^{10}\ h^{-1}M_\odot$ in both the ΛCDM and $f(R)$ cosmologies without neutrinos. We will focus in this Thesis on the models that do not account for the presence of massive neutrinos. Moreover, the cosmological parameters, on which these simulations are based, are the ones provided by Planck Collaboration et al. (2016): $\Omega_\mathrm{m} = \Omega_\mathrm{CDM} + \Omega_\mathrm{b} + \Omega_\nu = 0.31345$, $\Omega_\Lambda = 0.68655$, $h = 0.6731$, $\mathcal{A}_\mathrm{s} = 2.199 \times 10^{-9}$ (corresponding to $\sigma_8 = 0.842$ for the ΛCDM simulation) and $n_\mathrm{s} = 0.9658$; see §1.4 for a description of these quantities. In tab. 4.1 we report the main parameters of these simulations.

The DUSTGRAIN-*pathfinder* simulations are performed through the MG-GADGET[3] code (Puchwein et al., 2013) to include the $f(R)$ gravity (see §1.4.2), in combination with a particle-based implementation to account for massive neutrinos (Viel et al., 2010). Furthermore, a *chameleon screening mechanism* (for further details see Khoury and Weltman, 2004) is taken into account in order to recover the GR predictions at small scales. The value of $|f_{\mathrm{R}0}|$ is set to be within the range $[10^{-6} - 10^{-4}]$, while the total mass of neutrinos span over $[0 - 0.3]$ eV. During the evolution of these simulations, a series of comoving snapshots has been produced, each one representing a comoving volume of $750^3\ h^{-3}\mathrm{Mpc}^3$, at a specific cosmological time in the history of our Universe (see e.g. fig. 4.1). For our analysis only four snapshots have been considered, corresponding to the redshifts $z = 0, 0.5, 1, 2$.

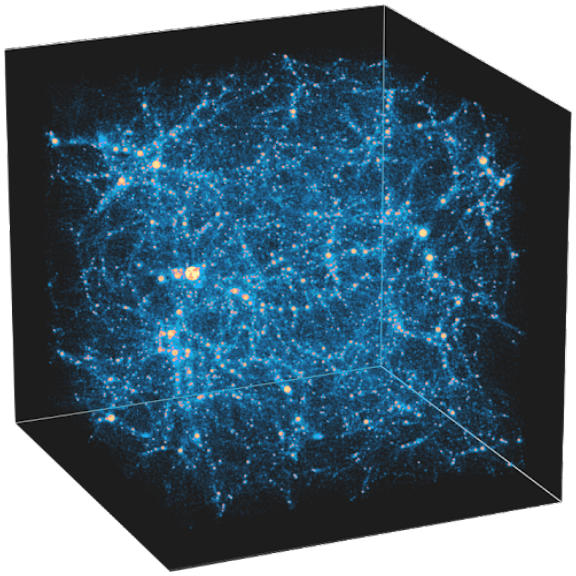

Figure 4.1: Graphical representation of the ΛCDM cosmological simulation of the DUSTGRAIN-*pathfinder*. 3-dimensional distribution of CDM particles (blue points) and haloes (yellow circles whose size is proportional to the halo mass) at $z = 0$. The comoving box has dimensions of $750\ h^{-1}\mathrm{Mpc}$ per side. Courtesy of Sofia Contarini.

These simulations have been extensively exploited to study the statistical properties of the overdense Universe, such as: the halo weak-lensing (Giocoli et al., 2018), the DM halo clustering (García-Farieta et al., 2019), the DM halo abundances (Hagstotz et al., 2019b), and

[3]MG-GADGET is an evolved version of the previous GR-based GADGET (Springel, 2005), developed to take into account modifications of gravity.

Simulation name	Gravity model	$f_{\rm R0}$	$\Omega_{\rm m}$	σ_8	S_8
ΛCDM	GR	-	0.31345	0.842	0.861
fR4	$f(R)$	-1×10^{-4}	0.31345	0.963	0.984
fR5	$f(R)$	-1×10^{-5}	0.31345	0.898	0.918
fR6	$f(R)$	-1×10^{-6}	0.31345	0.856	0.875

Table 4.1: Summary of relevant cosmological parameters of the DUSTGRAIN-*pathfinder* simulations used in this Thesis work. In the third column we report the value of the MG parameter $f_{\rm R0}$, while the fourth and fifth columns provide $\Omega_{\rm m}$ (i.e. the CDM density parameter) and σ_8 (i.e. the linear power spectrum normalization at $z = 0$), respectively. Finally, in the sixth column we provide the value of the derived parameter S_8.

the large-scale velocity field (Hagstotz et al., 2019a). Let us mention that the DUSTGRAIN-*pathfinder* have been also employed to test novel machine learning tecniques (Peel et al., 2019). By contrast, statistical studies of the underdense Universe are not so widespread. Both the void size function and the void density profile have already been addressed by Contarini et al. (2021) and, in order to extend this work to a still unexplored statistics with these simulations, we decided to devote this Thesis to the investigation of the void clustering properties.

4.2.1 Building up halo catalogues

As previously mentioned in §3.1, in order to identify the voids, a finding algorithm must be applied to the tracer catalogues. The DM particle distribution is known from the simulation, and so does its mean particle separation ($\mathrm{MPS} = n^{-1/3} = \sqrt[3]{V/N}$, where n is the tracer number density, V is the volume of the simulation box considered and N is the number of tracers), which is about $1.55\ h^{-1}\mathrm{Mpc}$. By contrast, the halo distribution must be recovered by means of a *halo finding* algorithm, together with the halo MPS, which is found to span over the range $[8.7 - 12.4]\ h^{-1}\mathrm{Mpc}$ from $z = 0$ to $z = 2$.

Over the years, many techniques have been developed to identify the collapsed DM structures in the underlying field of DM particles. For our analysis, the so-called DENHF algorithm (see e.g. Tormen et al., 2004) is applied to produce the halo catalogues at four different redshifts. This halo finding procedure is based on the *spherical overdensity* (SO) methodology presented by Press and Schechter (1974); hence, it defines spherical overdensities as regions surrounding the density peaks. The radius of these spheres corresponds to the distance within which the mean density enclosed can be expressed as $\Delta(z) = \Delta_{\rm c} \cdot \rho_{\rm crit}(z)$, where $\Delta_{\rm c}$ is the selected overdensity threshold and $\rho_{\rm crit}(z)$ is the already defined critical density of the Universe (see eq. 1.33). According to this method, haloes are considered as gravitationally bound structures: the most massive haloes (i.e. those having the highest density contrasts) are identified first, then the less massive haloes are reconstructed among the left DM particles. Note that the sub-haloes are not extracted by the DENHF algorithm.

Considering that typically $\Delta_{\rm c}$ is chosen to be 200 or 500 (namely, 200c and 500c halo cata-

logues)[4], it is possible to compute the halo mass through the following equation:

$$\frac{4}{3}\pi R_{\rm c}^3 \Delta_{\rm c} \rho_{\rm crit} = M_{\rm c} \ , \tag{4.1}$$

where $R_{\rm c}$ and $M_{\rm c}$ are the halo virial radius and mass respectively. Note that the 200c halo catalogues are best suited for our analysis, to ensure both a relevant void statistics and realistic modelling. The chosen approach is the same that we will adopt with real data in future works.

By selecting a $\Delta_{\rm c}$ threshold, we set a specific upper-limit to the halo mass. Furthermore, we also set a lower-limit to the halo mass by considering only haloes composed of 30 CDM particles at least, which corresponds to a minimum mass of $2.43 \times 10^{12}\ h^{-1}{\rm Mpc}$; i.e. we prevent contamination by spurious density fluctuations accounting only for statistically relevant objects. Let us underline that avoiding spurious overdensities (i.e. rejecting those haloes with $M_{\rm h} < 2.43 \times 10^{12}\ h^{-1}{\rm Mpc}$, in this case) is needed to properly exclude the smallest scales, where the spatial resolution of the simulation is not sufficient. Indeed, both the volume and the spatial resolution of the simulation from which we extract DM haloes are fundamental quantities. As already pointed out in §2.5, we generally cannot improve both because of computational limits: a great volume ensures a more robust statistics and enhances the probability of finding massive haloes and large voids, while a high spatial resolution implies a better sampling of the smallest scales. The DUSTGRAIN-*pathfinder* simulations have a relatively small volume (around $0.42\ h^{-3}{\rm Gpc}^3$) if compared to other simulations or future surveys[5], hence they do not enable us to sample extended voids, but they are suitable for the small-sized ones. Moreover, another strength of this suite of simulations is that it allows the study of alternative cosmological models.

Once the DENHF halo finder is applied in our analysis to extract the halo catalogues both in the ΛCDM and the $f(R)$ cosmologies, we perform a validation test of these catalogues before addressing the void statistical properties. While the HMF theory has been extensively modelled and validated by different authors (see e.g. Sheth et al., 2001; Tinker et al., 2008; Despali et al., 2016), its extension to MG scenarios is still a relatively new subject of study. In particular, Gupta et al. (2022) demonstrated that the HMF computed in the fR4, fR5 and fR6 modified gravity scenarios is characterized by a deviation from the ΛCDM HMF model. Such a deviation has been modelled by the authors with an additional Gaussian contribute, peaking at a mass scale which is characteristic for each $f(R)$ variant. As the strength of MG in the models increases[6], the deviation peak is found to be at higher masses: the fR6 HMF peaks at small masses, followed by the fR5 and the fR4 going towards higher masses. Notice that not only the peak position of the deviation varies, but also its height does, being greater as the MG

[4] According to Despali et al. (2016), the halo catalogues are generally built on 2000, 1000, 500 and 200 $\rho_{\rm c}$, and $200\rho_{\rm b}$, where $\rho_{\rm c}$ and $\rho_{\rm b}$ are referred to as the critical and background densities of the Universe, respectively. We underline that $200\rho_{\rm b}$ is motivated by the spherical collapse theory developed in an EdS universe and, together with 200 $\rho_{\rm c}$ is a quite popular choice (Tinker et al., 2008). Furthermore, note that, observationally, 200 $\rho_{\rm c}$ is often used to define galaxy cluster masses in optical surveys, while 500 $\rho_{\rm c}$ and higher overdensity values are used in X-ray analyses, and in all those observations that are able to resolve only the innermost parts of DM haloes and related clusters.

[5] For example, *Euclid* and LSST will be characterised by huge volumes of about $44\ h^{-3}{\rm Gpc}^3$ and $154\ h^{-3}{\rm Gpc}^3$, respectively.

[6] We recall that in the $f(R)$ models it is the absolute value of the $f_{\rm R0}$ parameter that encloses the information on the MG strength; it is assumed to be 10^{-4}, 10^{-5} and 10^{-6} for the fR4, fR5 and fR6 simulations, respectively.

acts harsher. This behaviour is attributed to the physics of the environmentally-dependent chameleon screening effect.

In the context of our Thesis work, it is important to account for these differences when applying the void finder to the halo catalogues. In fact, the void identification limits vary also according to the catalogue of haloes considered, and so do the void statistical properties. Therefore, we measure the halo mass function in the cosmological models adopted at four different redshifts (i.e. $z = 0, 0.5, 1, 2$; see §4.2). We compare these measurements with the theoretical predictions of the HMF model proposed by Tinker et al. (2008), assuming the cosmology associated to the ΛCDM. Our results are shown in fig. 4.2. In agreement with Gupta et al. (2022), we find in the $f(R)$ models a Gaussian-like shape as deviation from the HMF model computed in the ΛCDM scenario. This feature is particularly evident in the upper-left panel of fig. 4.2, which shows the comparison among the computed mass functions with respect to the ΛCDM at $z = 0$. The residuals highlight the existence of three Gaussian-like trends, with the peak position growing towards higher masses from the fR6 model to the fR4. Note that the trends we have already described and the differences among them tend to vanish when going towards $z = 2$. Indeed, the MG is expected to have a much greater influence at low redshift, after having had more time to evolve.

The peculiar behaviour of the HMF in $f(R)$ cosmologies affects the value of the halo MPS, since both these quantities are directly linked to the number density of haloes. The MPS is computed as the inverse cube root of the halo number density, thus it becomes smaller as the latter quantity increases. The whole information on the halo number density as a function of the halo mass can be derived from the HMF, which tells us that the halo samples are dominated by relatively small haloes, and that the number density decreases as the halo masses considered increase. Indeed, the less massive haloes are statistically more relevant than the massive ones. The halo number density at small masses and $z = 0$ is the highest in the fR6 cosmology, followed by those in the fR5, fR4 and ΛCDM cosmologies. As a consequence, we find an analogous, even if inverted, trend in the corresponding values of the MPS. Indeed, fig. 4.3 reveals that the overall MPS follows the predicted order at $z = 0$, and that its evolution with the redshift is non-trivial. These results are expected to be relevant in the context of the analysis of voids identified in the DM halo distribution (§5.4).

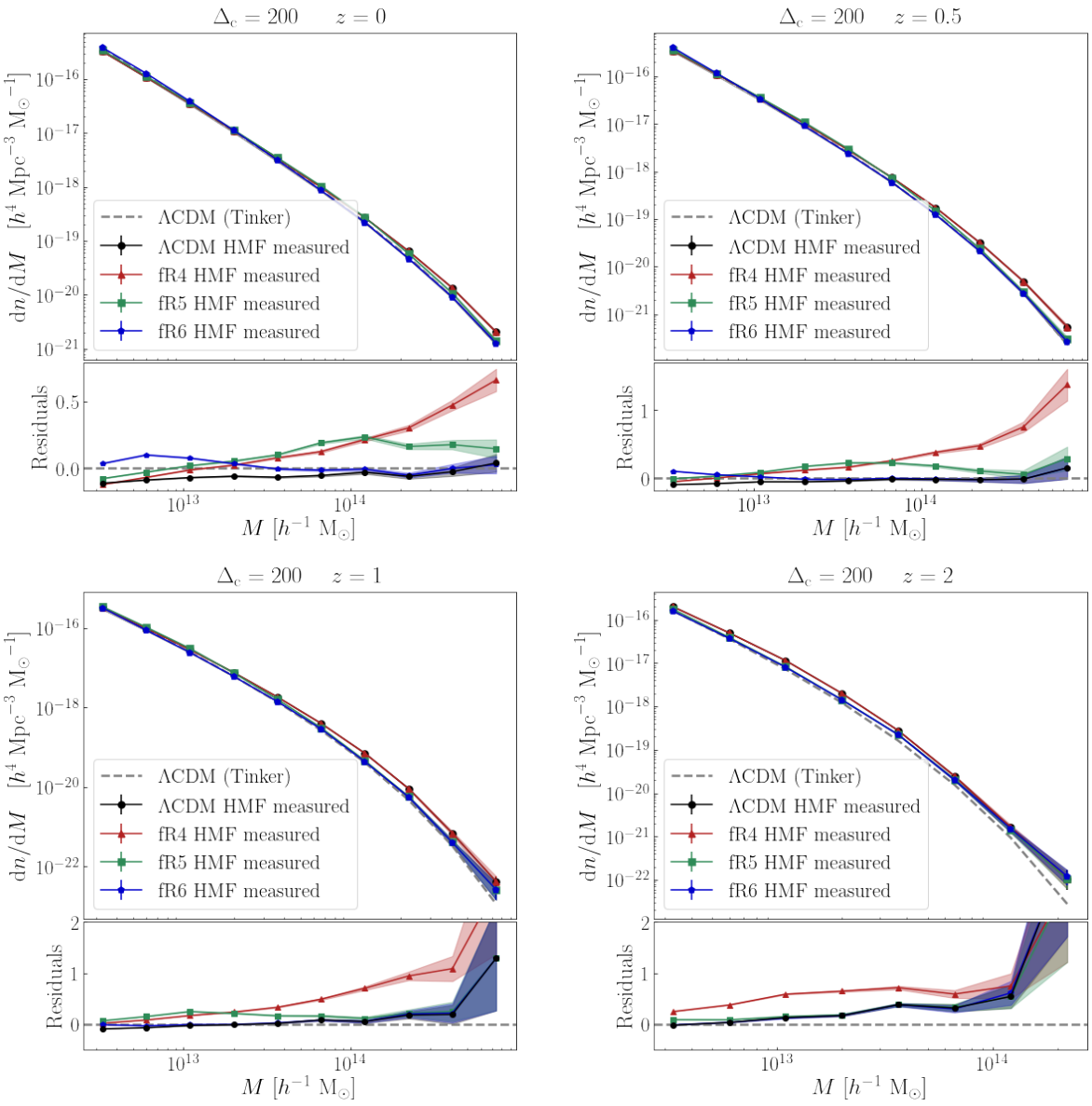

Figure 4.2: Mass abundances of 200c haloes in ΛCDM and $f(R)$ cosmologies at four different redshift: $z = 0$ (upper-left panel), $z = 0.5$ (upper-right panel), $z = 1$ (lower-left panel) and $z = 2$ (lower-right panel). In each figure, the dashed grey line represents the theoretical predictions (i.e. the HMF computed with the model of Tinker et al. (2008), reported in eq. 2.89) computed for the ΛCDM halo abundance. The HMF measurements in the ΛCDM, fR4, fR5 and fR6 cosmologies are identified by the black, red, green and blue dots, respectively. The shaded areas represent the Poissonian uncertainty on the measured halo mass counts. The coloured dots in the sub-panels of each plot refer to the residuals computed with respect to the ΛCDM HMF model as $(\mathrm{HMF}_{\mathrm{measured}} - \mathrm{HMF}_{\mathrm{model,\Lambda CDM}})/\mathrm{HMF}_{\mathrm{model,\Lambda CDM}}$. The errors (i.e. shaded areas) are computed dividing the Poissonian errors associated to the measured HMF by $\mathrm{HMF}_{\mathrm{model,\Lambda CDM}}$.

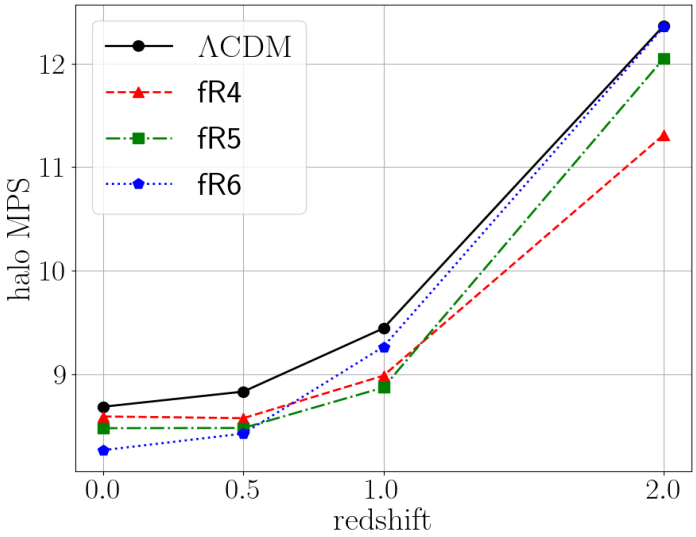

Figure 4.3: Halo MPS as a function of the redshift for the ΛCDM (black solid line), fR4 (red dashed), fR5 (green dot-dashed) and fR6 (blue dotted) cosmologies. At each redshift, the MPS values for the cosmological models analysed is a direct consequence of the specific behaviour of the corresponding measured HMF, reported in fig. 4.2.

4.3 Building up void catalogues

Since the DUSTGRAIN-*pathfinder* (§4.2) are N-body simulations, we can reconstruct a void catalogue from the distribution of either DM particles or DM haloes. Haloes are generally more clustered than the DM particles, and their number density is lower. Hence, the halo MPS is greater than the particle one. Given that when performing a statistical analysis on cosmic voids it is common practice to remove all the spurious voids smaller than about 2 MPS (or more), the DM particle field is more suitable than haloes to study small voids.

With the ultimate aim of exploiting the void clustering statistics, in the following sections we will first outline the void finder algorithm[7] used in this work and then proceed with a description of the void cleaner we apply to both DM particle and halo distributions in order to build our void catalogues (see forthcoming §4.3.1 and §4.3.2, respectively). Lastly, in §4.4 we will present the final void catalogues we consider to perform a reliable statistical analysis on the void clustering properties.

4.3.1 Void finding

From §3.1 we learnt how there exist several void finders based on different criteria. Let us now focus on the finder employed in this Thesis: the VIDE void finder (Sutter et al., 2015b), which

[7] See §3.1 for a general definition of the three most common categories of void finders.

relies on a geometrical criterion[8] to build void catalogues. VIDE is an improved version of ZOBOV[9], which finds underdensities in a 3D sample of particles, without making assumptions on the void shape and without free parameters. This void finding algorithm consists of three major steps:

1. The density field is sampled with the *Voronoi tessellation*: the finder associates to each tracer centre a cell of borders defined by those points that are closer to the considered centre than to any other tracer centre. To each *Voronoi cell* we associate a certain density, which corresponds to the inverse of the Voronoi-cell volume since it is assumed an equal weight for all the particles.

2. The second step is to search for local minima in the 3D density field, corresponding to those cells in which the density is lower than in all the surrounding adjacent cells. Once each minimum has been defined, the neighbouring cells are gradually merged. This procedure (see fig. 4.4) leads to the creation of the so-called *zones* and stops when a cell of lower density than that of the selected minimum is encountered.

3. At last, voids are defined via the *watershed algorithm* (see fig. 4.5; Platen et al., 2007). The zones are merged if the density of the ridge between them is lower than a fixed threshold, corresponding to 0.2 times the mean particle density of the sample. According to this algorithm, the cosmic voids are naturally arranged in a hierarchical structure, where the merging zones are referred to as *sub-voids*. As before, if going outwards with respect to the local minimum a more underdense cell is encountered, the process stops.

For each void identified by VIDE through the steps described above, it is possible to define its centre as the volume-weighted barycenter $\overline{X}$ of all the merging cells of which it is composed. $\overline{X}$ is defined by the following formula:

$$\overline{X} = \frac{\sum_{i=1}^{N} \bar{x}_i \, V_i}{\sum_{i=1}^{N} V_i} \,, \tag{4.2}$$

where $\bar{x}_i$ refers to the coordinates of the i-th tracer of the void considered and V_i is the volume of the Voronoi cell to which the tracer belongs. The sum $\sum_{i=1}^{N} V_i$ represents the total volume of the void V_v:

$$V_\mathrm{v} \equiv \sum_{i=1}^{N} V_i = \frac{4}{3}\pi \, r_\mathrm{v}^3 \,, \tag{4.3}$$

where r_v is the void radius, which is determined from the value of the void volume, assuming a spherical shape.

We apply the VIDE void finder both to DM particles[10] and halo catalogues, producing two main outputs: the so-called *trimmed* and *untrimmed* void catalogues, the former including only major parent voids while the latter accounting also for child voids (i.e. sub-voids).

[8] When geometrical criteria are considered, voids are identified as underdense regions composed of geometrical structures, such as spherical cells or polyhedra. These algorithms search for local density minima in the 3D matter field in order to recover the void positions and shapes.

[9] **ZOBOV** stands for ZOnes Bordering On Voidness; see Neyrinck (2008) for further details.

[10] Note that in the case of cosmic voids identified in the DM field, we randomly select a 25% sub-sample of the total number of particles, in order to reduce the computational time. This has no practical effects on the results.

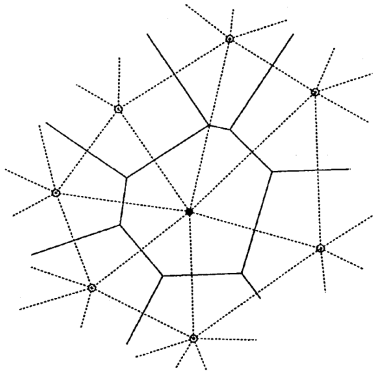

Figure 4.4: Graphical representation of the natural neighbours (whose centers are identified by the open circles) of a local density minimum (black dot). The solid black lines identify the Voronoi cells, while the dashed lines refer to the so-called *Delaunay triangles*, whose centres are defined as the vertices of the Voronoi diagram. Credits to: Platen et al. (2007).

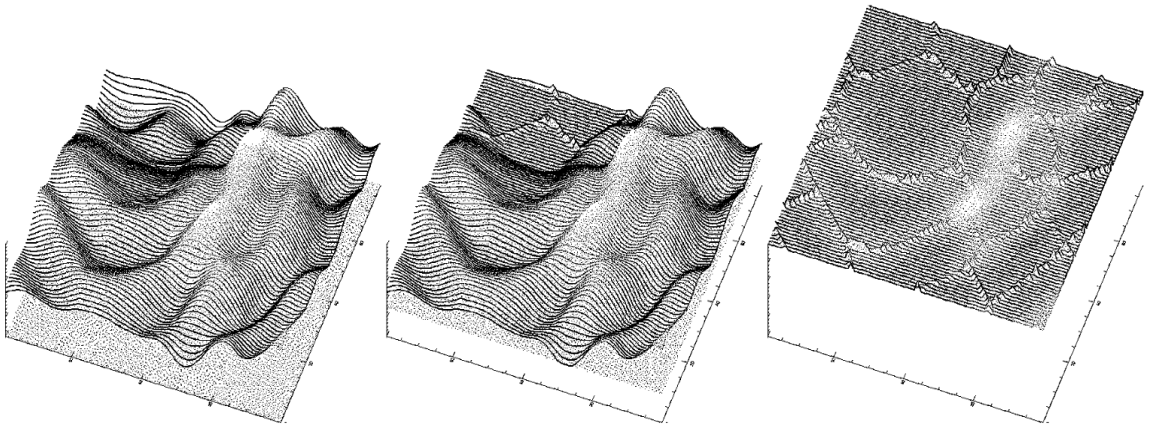

Figure 4.5: Graphical representation of the watershed technique. The shape of the density field is illustrated in the leftmost panel. Starting from the local minima, the surrounding underdense regions flood as the water level rises, and when the water that fills two adjacent basins is mixed, a "dam" is build (central panel). Finally, the entire surface is flooded, and a network of dams is constructed (right panel). This network defines the corresponding cosmic web. Credits to: Platen et al. (2007).

4.3.2 Void cleaning

With the purpose of exploiting cosmic voids for a reliable cosmological analysis, it is necessary that the void definition adopted is coherent when identifying them and when studying their statistical properties. The catalogue objects resulting from the finding algorithms can be selected on several bases. In the procedure presented here, the statistical models are required to be consistent with the basic theory of the void size function in order to set accurate constraints on the cosmological parameters. We do this by means of the cleaning algorithm introduced by Ronconi and Marulli (2017), implemented in the `CosmoBolognaLib` and constantly improved.

The cleaning algorithm depends only on the positions of the void centres and therefore it is applicable to any existing void finder, regardless its basic criterion of void identification. It consists of three main steps:

1. The spurious voids are excluded from the catalogue because of two main reasons: either their effective radius is out of the boundaries of the selected range $[R_{\rm min}, R_{\rm max}]$, or their central density[11] is found to be higher than $(1+\delta_{\rm v}^{\rm NL})\bar{\rho}$, where $\delta_{\rm v}^{\rm NL}$ is the nonlinear density threshold and $\bar{\rho}$ is the mean density of the sample considered. With this limit, the cloud-in-void process is taken into account.

2. A re-scaling of the void radius is performed: the centre of an ideal sphere is placed in the void centre and its radius is increased (or decreased) until the position at which the density contrast emerging from the void density profile equals the chosen threshold for the nonlinear density contrast $\delta_{\rm v}^{\rm NL}$.

3. In presence of overlapping[12] voids, the one with higher central density is excluded, accounting for the void-in-void process.

As it is evident from fig. 4.6, taken from Ronconi and Marulli (2017), while the original voids extracted with VIDE are not consistent with the theory of the void size function proposed by Jennings et al. (2013) (see §3.2.1), the cleaned voids are instead statistically in agreement with the model predictions. Something else that should be noted in fig. 4.6 is that the output of the cleaning procedure is characterised by lower void number counts than that produced by VIDE. This follows as a natural consequence of the three cleaning steps previously outlined, in which the spurious and overlapping voids are properly removed.

To sum up, the final effect of the cleaning procedure is a catalogue of both selected and re-shaped[13] voids defined as non-overlapping spheres in which the nonlinear density contrast equals a fixed value selected by the user, which can correspond e.g. to the shell-crossing value $\delta_{\rm v}^{\rm NL} = -0.795$. This value must be converted in linear theory in order to compute the model of the VSF. To do this, we can use the conversion proposed by Bernardeau (1994) (see forthcoming eq. 4.5). For example, the shell-crossing value in linear theory becomes $\delta_{\rm v}^{\rm L} = -2.71$. Given

[11] Note that the central density is computed within a sphere of radius 2 MPS from the centre, in order to avoid the shot noise related to the innermost regions.

[12] The term *overlapping* refers to a situation in which the distance between two void centres exceeds the sum of their radii.

[13] Note that even if each single void is not spherical but slightly elliptical (see e.g. Lavaux and Wandelt, 2012; Verza et al., 2019), the averaged void shape in real space is perfectly approximated by a sphere (see e.g. Hamaus et al., 2017; 2020; 2022).

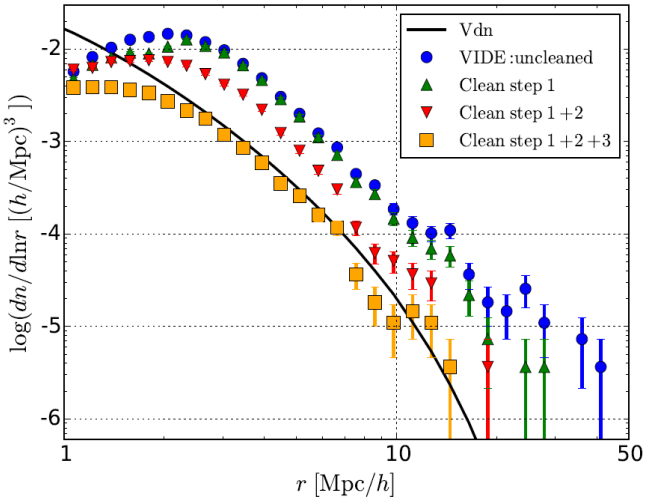

Figure 4.6: Effects of the cleaning procedure on the measured void size function with respect to the theoretical predictions (black solid line). The blue dots represent the size function computed for the original voids extracted with VIDE, while the yellow squares refer to the measured size function after the cleaning procedure. This analysis has been performed on a N-body simulation of $128\ h^{-1}\mathrm{Mpc}$ per side, which accounts for the presence of 256^3 CDM particles in a $\Lambda\mathrm{CDM}$ scenario. Credits to: Ronconi and Marulli (2017).

the close match between the VSF measured with the void sample selected by the cleaning algorithm and the theoretical one, we can conclude that this approach is extremely powerful because it allows us to directly compare the void statistics we want to investigate with the theoretical models of spherical evolution introduced in §2.3.2.

4.4 Cleaned void catalogues

Once the void catalogues are built both in the DM particle field and in the halo distribution, the cleaning algorithm (§4.3.2) is employed to ensure consistency with the theory of the VSF (i.e. Vdn model; Jennings et al., 2013). In particular, this procedure is applied to the untrimmed VIDE void catalogues (§4.3.1), by using the CBL catalogue constructors and functions.

As already clarified, from the cleaning procedure we get catalogues of both selected and re-shaped voids consisting of non-overlapping spheres embedding a fixed nonlinear density contrast $\delta_\mathrm{v}^\mathrm{NL}$. This value, and its linear counterpart $\delta_\mathrm{v}^\mathrm{L}$, are those that we used in both the Vdn model of the VSF and the power spectrum model introduced by Chan et al. (2014). In this context, let us point out that the threshold $\delta_\mathrm{v}^\mathrm{NL}$ can assume any reasonable value between -1 and 0. The only requirement to be satisfied is that the density contrast must be balanced between a value which is low enough to represent the interiors of cosmic voids, and a value which is high enough to sample spatially-resolved regions in both the DM particle field and halo distribution. It is also important to notice that, despite the measured VSF is well fitted by the Vdn model at any fixed $\delta_\mathrm{v}^\mathrm{NL}$, the value of this threshold affects the statistical relevance on the sample resulting from the cleaning procedure (Contarini et al., 2021). If $\delta_\mathrm{v}^\mathrm{NL}$ is particularly low, the re-scaling algorithm leads to small void radii, most of which are then removed according

to the tracer MPS (see §4.3). By contrast, if it is particularly high, voids are provided with large radii that are also removed from the cleaned catalogue because of their tendency to overlap.

In the next subsections we will show how the final void catalogues we obtained are in agreement with the Vdn model predictions for the void size function, in both the DM particle field and the halo distribution.

4.4.1 Voids in the dark matter field

To understand the effect of the void cleaning on the original catalogue produced by VIDE we show in fig. 4.7 a comparison of the VSF measured for both these catalogues at $z = 0$. As expected from §4.3.2, while the measured VSF of the cosmic voids identified by VIDE is not consistent with the Vdn theoretical predictions, the cleaned void catalogue fulfils the theoretical predictions quite accurately. As already pointed out concerning fig. 4.6, fig. 4.7 demonstrates that the cleaning procedure has two main effects on the starting catalogue. Indeed, not only the data become consistent with the VSF theory, but also the number density of voids decreases, leading to larger statistical uncertainties related to the void sample. For example, focusing on the measured ΛCDM VSF at redshift $z = 0$, we find that the number of objects of the VIDE catalogue is much greater than the number of objects after the cleaning algorithm is applied, being 273686 and 48776, respectively. We recall here that the smallest possible size of the voids considered must be at least two times the tracer MPS to avoid the spatial scales affected by a loss of void counts (see §4.2.1). The numbers of objects reported above are derived for voids larger than 2.5 MPS.

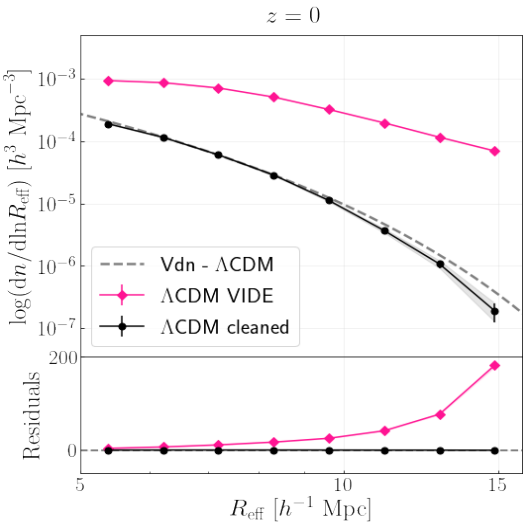

Figure 4.7: Comparison between the VSF measured for the original VIDE void catalogue (pink solid line) and for the cleaned void catalogue (black solid line) with respect to the Vdn model (grey dashed line). Both the measurements and the model are computed in the ΛCDM scenario at $z = 0$. The errorbars and relative shaded areas represent the Poissonian errors of the measured VSF. The residuals in the lower sub-panel are calculated as the difference of data points from the Vdn theoretical model, divided by the model. The associated errors are the Poissonian errors of the measured VSF normalized to the value of the model.

The same validity test on the cleaned catalogues with respect to the uncleaned ones has

been performed also in the other three redshifts considered (i.e. $0.5, 1, 2$). It results that the differences between the pre-cleaning and the post-cleaning measured VSF are similar or even greater as the redshift increases. Note that the cleaned catalogues and their relative VSF are prepared by considering thresholds $\delta_{\rm v}^{\rm NL}$ growing with redshift, i.e. $\delta_{\rm v}^{NL} = -0.795, -0.75, -0.7, -0.65$ at $z = 0, 0.5, 1, 2$, respectively. As already pointed out, we do this because, as the redshift increases, the voids become shallower, and this must be taken into account to afford the best compromise between sufficient statistics (high enough $\delta_{\rm v}^{\rm NL}$) and the identification of actual voids (low enough $\delta_{\rm v}^{\rm NL}$).

Having ascertained that the cleaned void catalogues are the ones we want to analyse for fundamental theoretical reasons, before proceeding with our analysis on the void clustering, we investigate how the VSF measured in $f(R)$ cosmologies varies with respect to the ΛCDM model. Our results are shown in fig. 4.8, from which it is possible to evaluate the differences of the number counts measured in the various cosmological scenarios. It emerges that, going from $z = 2$ to $z = 0$, the $\rm fR4$ VSF shows a slightly higher number of relatively large voids with respect to the other cases, and this can be justified since the gravity in this model is stronger than in any other model. Indeed, the MG enhances the void formation and expansion, since it makes the large-scale overdense structures evolving and clustering more rapidly.

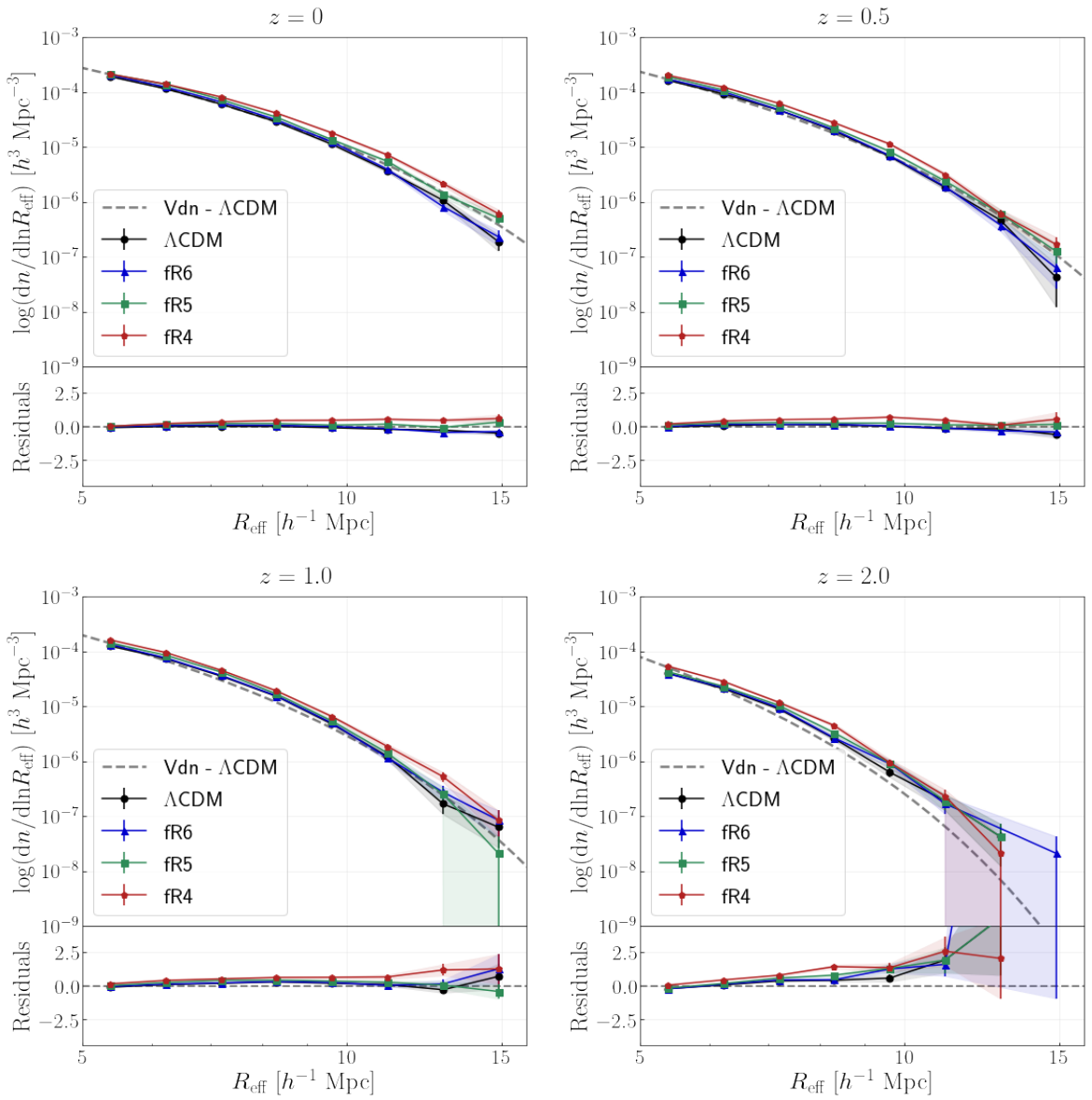

Figure 4.8: Comparison between the theoretical VSF of the ΛCDM model and the measured VSF at four different redshift, $z = 0, 0.5, 1, 2$, with corresponding thresholds $\delta_{\rm v}^{NL} = -0.795, -0.75, -0.7, -0.65$. The measurements are computed for voids identified in the DM particle field in the four cosmological scenarios considered: ΛCDM (black solid line), fR4 (red), fR5 (green), fR6 (blue). The residuals in the lower sub-panels are analogous to the ones reported in fig. 4.7.

4.4.2 Voids in the halo distribution

As mentioned at the beginning of §4.4, to properly re-scale voids through the cleaning procedure and to compute their theoretical VSF, it can be assumed any reasonable value for the nonlinear density contrast (i.e. $-1 < \delta_{\rm v}^{\rm NL} < 0$). Anyway, the theoretical model of the VSF is formulated for the total matter density field, which is represented by the DM particle field at first approximation. When dealing with biased tracers (i.e. DM haloes in the case of our analysis), the tracer bias plays a crucial role in determining the VSF and the void density profile, which is strongly related to the cleaning algorithm employed. In particular, assuming a cosmic void whose profile can be traced by both the DM particles and haloes, it turns out that the latter trace a deeper[14] density profile than the former. A possible solution to take this into account and to correctly predict the void abundance in the biased tracer field is to consider a bias-dependent underdensity threshold. The DM density field within cosmic voids is linearly related to the density field traced by the biased tracers (Pollina et al., 2017 and 2019), and we can write that $\delta_{\rm v,tr}^{\rm NL} = b\,\delta_{\rm v,DM}^{\rm NL}$, where b is the tracer bias. From this relation, it is evident that if $b > 1$ the resulting density contrast inside voids traced by overdensity tracers is very negative, and this would lead to re-scale voids to their innermost regions, where the Poisson noise dominates. From Contarini et al. (2019) it emerges that the tracer bias inside voids ($b_{\rm punct}$) is much higher than the large-scale tracer bias ($b_{\rm eff}$). Therefore, Contarini et al. (2019) proposed to follow the opposite approach, by selecting a physically reasonable threshold for the voids identified in the tracer distribution and then converting it to the corresponding value for voids identified in the DM field (i.e. unbiased tracers). The latter is then used in order to re-scale the theoretical VSF. Contarini et al. (2019) demonstrated that the relation between the DM density contrast inside cosmic voids ($\delta_{\rm v,DM}^{\rm NL}$) and the corresponding value in the tracer distribution ($\delta_{\rm v,tr}^{\rm NL}$) can be modelled with a linear relation[15] $\mathcal{F} = \mathcal{F}(b_{\rm eff})$ as:

$$\delta_{\rm v,DM}^{\rm NL} = \frac{\delta_{\rm v,tr}^{\rm NL}}{\mathcal{F}(b_{\rm eff})}\,, \tag{4.4}$$

where $b_{\rm eff}$ is referred to as the large-scale effective bias of the tracers considered. In practice, it is assumed that the voids are always the same, regardless of whether they are traced in either the DM particle field or the tracer distribution, and the theoretical Vdn model predictions are shifted towards greater radii by means of this calibrated relation. Note that, in order to exploit

[14] As already anticipated in §3.2.3, the void density profile is directly related to the void-tracer cross-correlation function. Since the biased tracers are more clustered than the unbiased DM particles, and their number density is lower, we actually count fewer pairs in the former case than in the latter. Therefore, both the cross-correlation signal and the density contrast are lower in the former case, at least in the innermost regions (see Contarini et al., 2019).

[15] According to the theory, we can use the ratio of the density profiles of the same voids, drawn from the DM particles and biased tracers, respectively, to calculate the tracer bias within cosmic voids. However, this method could not be applied to real data because we have no information on the true total matter density field. This leads to the need of calibrating a relation that allows us to derive the tracer bias inside voids ($b_{\rm punct}$) from the large-scale tracer bias ($b_{\rm eff}$). Note that the latter can be easily derived from the real data, e.g. from the tracer 2PCF. The relation resulting from this calibration is linear, and depends only on two parameters, namely $B_{\rm slope}$ and $B_{\rm offset}$, which are the slope and offset of the relationship, respectively. Lastly, in Contarini et al. (2022) it has been demonstrated that $\mathcal{F}(b_{\rm eff})$ is almost independent of Cosmology, but it depends on the nature of the considered tracer (e.g. galaxies, 200c haloes, 500c haloes, and so on).

the nonlinear threshold defined in eq. (4.4) to compute the theoretical VSF, we need to convert it to its linear value. To do this, we make use of a relation proposed by Bernardeau (1994):

$$\delta_{\rm v}^{L} = \mathcal{C}\left[1 - (1+\delta_{\rm v}^{NL})^{-1/\mathcal{C}}\right] , \tag{4.5}$$

where $\mathcal{C} = 1.594$. See the aforementioned paper for further details on this relation and the methods employed to obtain it.

For our analysis on cosmic voids identified in the DM haloes (see §5.4), we select the threshold $\delta_{\rm v,tr}^{\rm NL} = -0.5$, since it ensures the best compromise between the void sample statistical relevance and the agreement of the void counts with the theoretical VSF. Let us underline that, unlike the case of the voids identified in the DM particle field (i.e. where the threshold is set to be less negative as the redshift increases), in this case the nonlinear threshold $\delta_{\rm v,tr}^{\rm NL}$ remains the same at every redshift considered. This is justified by the fact that the tracer bias entering eq. (4.4) depends on the redshift and, in particular, it is higher as the redshift increases (see §2.4.2). Thus, it is itself able to select $\delta_{\rm v,DM}^{\rm NL}$ thresholds which are more negative at earlier ages of the Universe.

Finally, analogously to what we pointed out in §4.4.1, after the application of the cleaning algorithm to our void catalogues in order to make them consistent with the first principles of the Vdn model, the void number density decreases. For example, in the ΛCDM at $z = 0$, the number of voids of the sample selected (i.e. with radii greater than 2.5 MPS to avoid spurious objects) is 2213 and 947 for the untrimmed and cleaned catalogues, respectively. Fig. 4.9 shows how the cleaned void catalogues in both the ΛCDM and $f(R)$ cosmologies are described accurately enough by the Vdn model predictions.

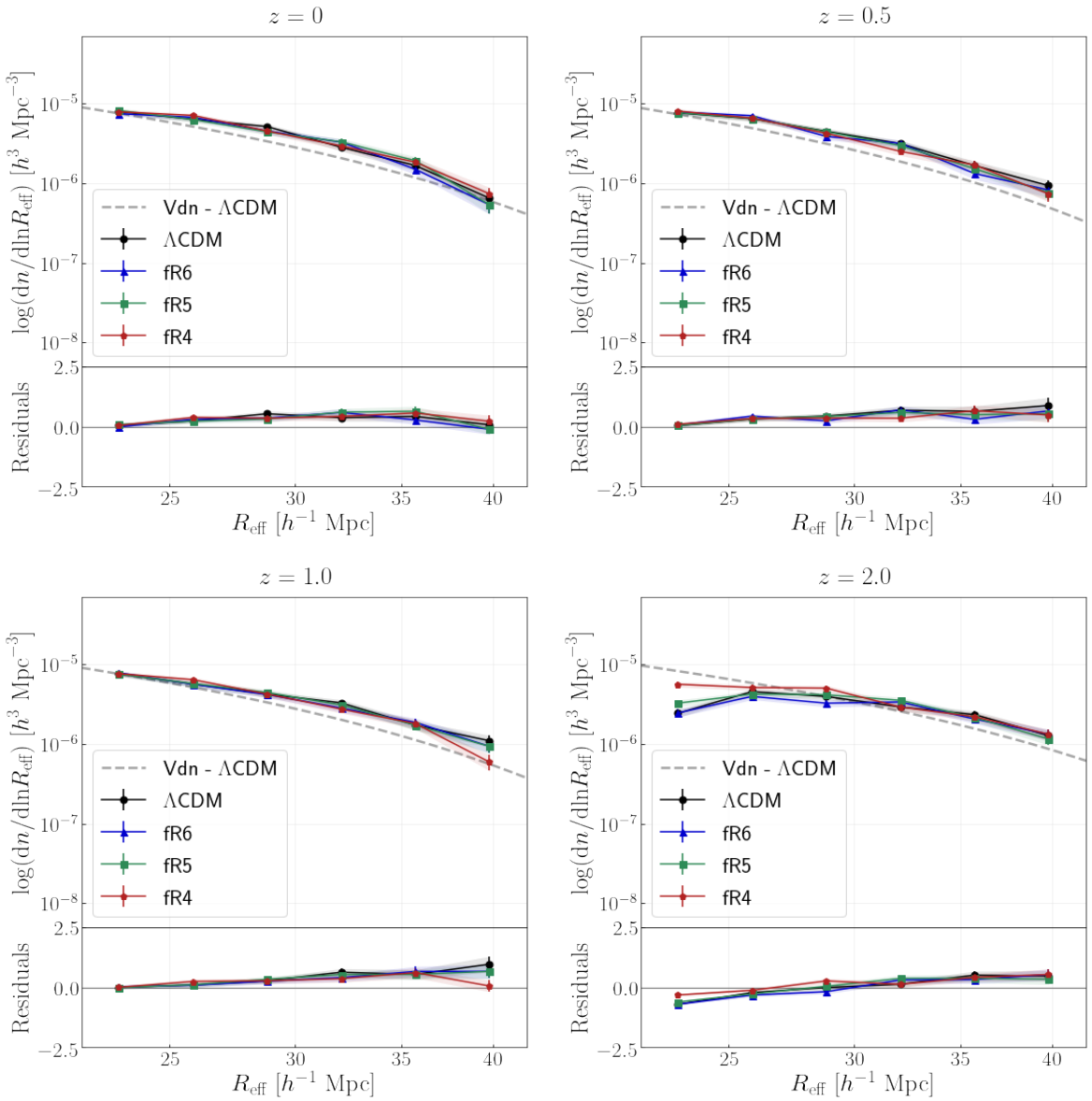

Figure 4.9: Comparison between the theoretical VSF of the ΛCDM model and the measured VSF at four different redshift, $z = 0, 0.5, 1, 2$, with corresponding threshold $\delta^{NL}_{\rm v,tr} = -0.5$. The measurements are obtained for voids identified in the halo distribution in the four cosmological scenarios considered: ΛCDM (black solid line), fR4 (red), fR5 (green), fR6 (blue). The residuals in the lower sub-panels are analogous to the ones reported in caption of fig. 4.7.

Chapter 5

The clustering of cosmic voids

A reliable cosmological exploitation of cosmic voids requires an accurate modelling of their statistical properties, and such model is more solid as its dependence on first principles becomes stronger. In this chapter we focus on the two-point statistics, in particular the auto-correlation function of cosmic voids (see §3.2.3), investigating void catalogues constructed from both the DM particle field and the halo distribution, within the DUSTGRAIN-*pathfinder* simulations. As already discussed in §3.1, void catalogues can be extracted by means of a finding algorithm that can be based on different criteria of void identification. The set of the void catalogues we analyse in this chapter is obtained using VIDE, a geometry-based finder that we described extensively in §4.3.1. Furthermore, a cleaning procedure (see §4.3.2) is employed in order to account only for non-overlapping and properly re-scaled voids; the results of the application of this algorithm are outlined in section §4.4. By doing this, our voids are defined as in the theoretical model of the VSF proposed by Jennings et al. (2013) (i.e. the Vdn model, see §3.2.1), which correctly accounts for both the void-in-cloud and void-in-void processes, in agreement with the excursion-set formalism (see §3.2.1). Indeed, the nonlinear threshold $\delta_{\rm v}^{\rm NL}$ and its linear counterpart defined by the spherical collapse model (see §2.3.2), is assumed to take on the same value in both the VSF model (eq. 3.7) and the void linear bias (eq. 3.17) that we use to model the 2PCF, making our analysis almost entirely grounded on theoretical prescriptions. We recall that $\delta_{\rm v}$ can take on any reasonable value as long as it accounts for both the spatial resolution and the overlapping phenomenon (see §4.4). Finally, note that also the linear critical threshold $\delta_{\rm c}^{\rm L}$ enters in our statistical analysis, and we assume for it the turn-around value defined by the spherical collapse model developed within the linear regime.

In §5.1 we introduce few relevant concepts in order to study cosmic voids identified in the DM field. We then investigate the void clustering properties within and beyond the ΛCDM scenario (see §5.2 and §5.3, respectively), discussing both the measure and modelling of the 2PCF. Furthermore, we assess the cosmological constraining power of the void 2PCF by means of a Bayesian analysis on our data. Lastly, in §5.4 we repeat the same analysis, investigating the clustering properties of the cosmic voids identified in the halo distribution.

5.1 Voids in the dark matter field

Starting from the cleaned void catalogues in the DM field presented in §4.4.1, we select sub-samples of voids such that an accurate modelling of the 2PCF can be performed. There are three main requirements to be satisfied in order to exploit the void 2PCF as a cosmological probe, which can be summarised as follows:

- the void 2PCF model requires in input both the void median radius and comoving number density and, to account for theoretical principles, these quantities can be modelled with the Vdn model, if the sample is properly cleaned (as explained in §4.4);
- given the low amplitude of the clustering signal, the statistics of the void sample considered must be high enough to allow precision on the data measurements and therefore on the modelling procedure;
- considering the extremely wide range of sizes over which cosmic voids span, together with the strong dependency of their properties on those sizes (see e.g. §3.2.2), for a proper modelling of these objects it is necessary to select void sub-samples that are similar enough to exhibit almost the same features.

It is easily noticeable how the second and third conditions tend towards opposite directions: the former requires object catalogues containing the maximum possible amount of data, while the latter naturally implies limited data samples. Therefore, the choice of the sub-catalogue to be considered for building and testing the model is defined as the best compromise between its statistical relevance and the similarity of the properties characterising its objects. According to this argument, among the whole sample of cleaned voids, we opt to account only for those with radii inside the range $[5 - 7.5]\ h^{-1}\mathrm{Mpc}$. For the sake of completeness, we mention that several tests have been performed in order to verify the stability of our results, such as considering a wider range for the selection of void radii and applying different binning strategies (e.g. logarithmic, equispaced and equipopulated binning). From our statistical analyses, the aforementioned range $[5 - 7.5]\ h^{-1}\mathrm{Mpc}$ is found to be the best compromise to perform a reliable modelling and an effective cosmological exploitation of the void clustering properties. Therefore, the results we will present in this chapter concern voids belonging to this radius bin, the properties of which are computed at $z = 0, 0.5, 1, 2$ in four different cosmological scenarios (i.e. $\Lambda\mathrm{CDM}$, fR4, fR5 and fR6). Finally, let us point out that there are three reasons why we are bound to study small voids[1]: *(i)* the DUSTGRAIN-*pathfinder* simulations have not a large enough volume, *(ii)* the voids are identified in the DM particle field, and *(iii)* the cleaning algorithm re-scales voids, also removing the overlaps.

In the next sections, we will first characterise the 2PCF in the $\Lambda\mathrm{CDM}$ scenario, addressing both its measure and modelling (§5.2) with the main aim of evaluating the constraining power of the void clustering as a cosmological probe. Then, we will compare the two-point statistics in the $f(R)$ models with the $\Lambda\mathrm{CDM}$ theoretical predictions (§5.3). Note that the latter has to be intended as a test to verify whether the data extracted from the $\Lambda\mathrm{CDM}$ simulation are consistent with those in MG simulations, in order to evaluate the potential disentangling power of the void clustering within the limits of the data sets we are analysing.

[1] As already mentioned in the Introduction, cosmic voids can vary in size from a few to over hundreds of Mpc.

5.2 Results within the Standard Model

With the aim of selecting properly the cosmic voids in the ΛCDM catalogues[2], we remove all the objects whose centre is less than 30 h^{-1}Mpc from the edge of the simulation boxes. As a consequence, the resulting volume that we consider in our analysis decreases from 750^3 $(h^{-1}\,\mathrm{Mpc})^3$ to 710^3 $(h^{-1}\,\mathrm{Mpc})^3$. Moreover, as anticipated, voids are selected according to their radius, excluding all those objects that are outside the interval $[5 - 7.5]$ h^{-1}Mpc. Note that the lower limit chosen for the void radii is more than two times larger than the MPS of the tracers (i.e. the DM particles), which corresponds to 1.55 h^{-1} Mpc.

In tab. 5.1 we summarise the relevant characteristics of our ΛCDM void sub-catalogues, computed from both the simulation samples and the theoretical VSF.

z	N_v		$\bar{n}_\mathrm{v}$ $[h^3\,\mathrm{Mpc}^{-3}]$		R_median $[h^{-1}\,\mathrm{Mpc}]$	
	simulation	model	simulation	model	simulation	model
0	18578	19755	5.19×10^{-5}	5.52×10^{-5}	5.86	5.83
0.5	15470	15570	4.32×10^{-5}	4.35×10^{-5}	5.84	5.79
1	11878	12477	3.32×10^{-5}	3.49×10^{-5}	5.84	5.77
2	3551	4177	9.92×10^{-6}	1.17×10^{-5}	5.79	5.67

Table 5.1: Summary of the main characteristics of the ΛCDM void sub-sample considered, i.e. the redshift z, the number of voids N_v, the void mean number density $\bar{n}_\mathrm{v}$ and the median radius R_median. The last three columns are split into two sub-columns, where the first refers to the quantities calculated directly from the simulations, while the second contains the quantities computed from the VSF theory.

5.2.1 Auto-correlation measure

As anticipated in §3.2.3, we rely on the LS estimator (eq. 3.11) to measure the 2PCF, which we compute in 20 radial separation logarithmic bins from 10 to 100 h^{-1}Mpc. We estimate the associated errors by means of the so-called *Bootstrap method*, constructing 100 realisations by resampling from the sub-catalogue, with replacement. Our results are reported in fig. 5.1, where we show the 2PCF measurements obtained at $z = 0, 0.5, 1, 2$.

5.2.2 Auto-correlation modelling

To model the 2PCF measurement shown in fig. 5.1 we rely on the power spectrum model proposed by Chan et al. (2014), that has been presented extensively in §3.2.3. However, differently from this paper, we rely also on the Vdn model of the VSF, with the aim of extracting reliable

[2]Let us clarify that the same procedure described in this subsection is applied also to the $f(R)$ simulations (see forthcoming §5.3).

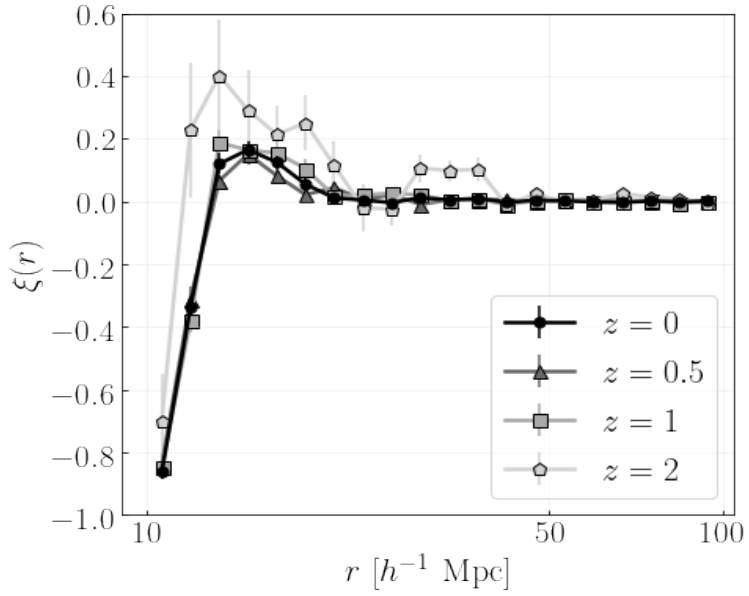

Figure 5.1: Void auto-correlation measure computed in the ΛCDM scenario at four different redshifts: $z = 0$ (black dots), $z = 0.5$ (dark grey triangles), $z = 1$ (grey squares) and $z = 2$ (light grey pentagons). The measurements are achieved by means of the LS estimator and the error bars represent the associated Bootstrap errors.

cosmological constraints. Indeed, both in the theoretical linear void bias, $b_1(R_\mathrm{v})$, and in the whole theory of the HS approximation, we exploit the Vdn model predictions to define both the median radius (R_median) and the mean number density ($\bar{n}_\mathrm{v}$), since it has been proven that the agreement of properly cleaned void samples with the VSF theory is robust (see fig. 4.8). The values of these quantities at all redshifts are reported in tab. 5.1.

Let us emphasise that the improvement we have made to the 2PCF model is of major cosmological importance, as referring to theoretical principles is crucial to realiably constrain the parameters on which the current model of our Universe is based. Considering instead the theoretical quantities, such as the void formation threshold (δ_v) and the void linear bias (b_1), as free parameters, results in the impossibility of exploiting the void clustering as a robust statistical probe.

Concerning the critical thresholds δ_c and δ_v, let us underline that the former is set to the spherical collapse value at the turn-around (i.e. $\delta_\mathrm{c}^\mathrm{L} = 1.06$), while the latter assumes different values at different redshifts, consistently with those used in the Vdn model. In particular, the threshold $\delta_\mathrm{v}^\mathrm{L}$ defined by the spherical collapse in linear theory is -2.71, and it becomes higher as the redshift increases. Indeed, considering that the cosmic voids are expected to exhibit a shallow density profile at earlier epochs, it is easily understandable that only few voids can be re-scaled by the cleaning procedure to enclose such a density contrast (i.e. the deepest ones). Therefore, it is necessary to modulate this threshold across cosmic epochs so as to enlarge the sample of cleaned voids and decrease the shot noise. We recall here that this choice does not affect the Vdn model predictions as far as the considered threshold is used coherently in both the cleaning procedure and in the computation of the theoretical VSF. Notice that, since the cleaning procedure is built to re-scale voids in a nonlinear framework (see §4.3.2), we need

also to account for the corresponding nonlinear thresholds $\delta_{\rm v}^{\rm NL}$. A conversion relation between the linear and the nonlinear regimes has been introduced by Bernardeau (1994) (eq. 4.5). A summary of all these threshold values can be found in tab. 5.2.

Once the decisions on these theoretical variables are made, we proceed by testing the formula of the void power spectrum model proposed by Chan et al. (2014) in Fourier space. This is done in order to verify the theoretical formulas implemented with our methods, before moving to real space and reconstructing the 2PCF model that we aim to investigate. The results obtained from the implementation of eq. (3.13) at redshift $z = 0$ are shown in fig. 5.2. The same validity test of the theoretical formula of the void power spectrum is performed at all redshifts, but only $z = 0$ is reported for simplicity.

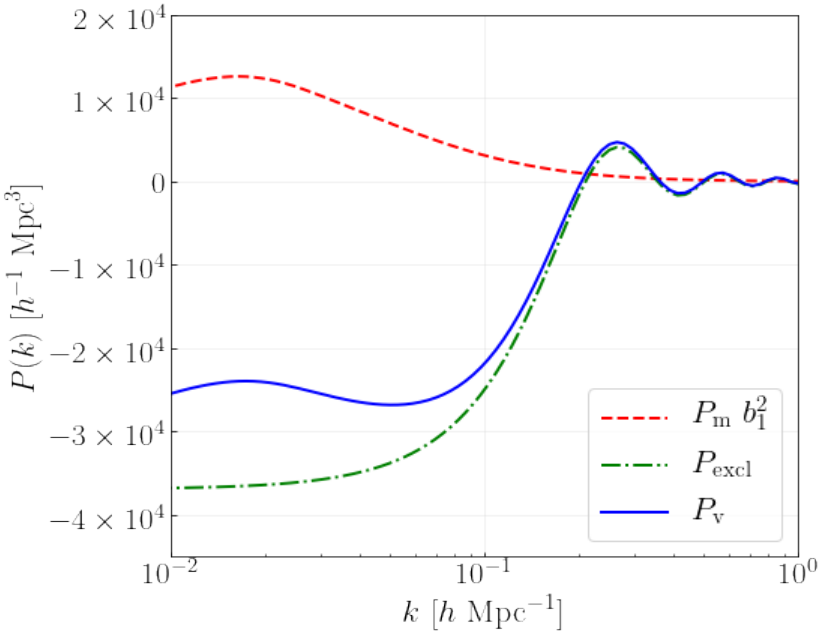

Figure 5.2: Model of the void power spectrum resulting from eq. (3.13) in the ΛCDM cosmological model at $z = 0$: $P_{\rm m}b_1^2$ (red dashed line) is the matter power spectrum re-scaled by the square of the theoretical linear bias of cosmic voids (see eq. 3.17), $P_{\rm excl}$ (green dash-dotted line) is the void exclusion term and $P_{\rm v}$ (blue solid line) is the resulting void power spectrum.

As predicted by the theory of the HS (see §3.2.3), fig. 5.2 shows the effects of the exclusion term ($P_{\rm excl}$) on the DM power spectrum normalised with the squared linear bias ($P_{\rm m}b_1^2$): the introduction of oscillations at large k modes (i.e. small physical scales) and the lowering of the DM power spectrum at small k modes (i.e. large physical scales). Both these effects make the void power spectrum behave as represented by the blue solid line. Note that both the colours and line-styles chosen for this representation are the same as those used by Chan et al. (2014), to allow a direct comparison with fig. 3.5. Let us also emphasise that the y-scales characterising the power spectrum are different in these two figures. The reason is that a different normalisation for $P(k)$ has been used in Chan et al. (2014), which consists of adding a multiplicative factor $(2\pi)^{-3}$. Finally, note that both the DM power spectrum ($P_{\rm m}$) and the mass variance ($\sigma_{\rm M}$) entering the theoretical void bias (eq. 3.17) are computed by means of the CBL libraries presented in §4.1, through the EISENSTEIN-HU Boltzmann solver.

Being the model of the void power spectrum successfully tested, we proceed with its conversion to the real-space 2PCF. To do this, we exploit the Fast Fourier Transform method implemented in the `fftlog`[3] class of the CBL, which consents to directly perform the Fourier transform of any given input functional form.

First of all, we stress the fact that, with the current theory, we can only afford to model the 2PCF after the peak around $15\ h^{-1}\mathrm{Mpc}$ (see fig. 5.1), since at smaller separations the signal is dominated by some effects related to the void density profile that are not yet well understood. Furthermore, to properly fit both the peak height and position of the 2PCF measure, we found that it is necessary to add a multiplicative factor to the median radius that enters the theory of the HS. Indeed, the HS model approximates the void shape and size as if one were analysing a void population formed by identical spherical objects. It is important to emphasise, once again, that the properties of cosmic voids vary depending on their dimension. To take this into account, we express the radius of the HS theory as a function of a free parameter, that we call $\mathcal{C}_{\mathrm{R}}$, as follows:

$$R = \mathcal{C}_{\mathrm{R}} \cdot R_{\mathrm{median}} \ , \tag{5.1}$$

where R_{median} is the median radius of the voids in the interval $[5 - 7.5]\ h^{-1}\mathrm{Mpc}$, computed by means of the theoretical VSF. Then, we calibrate the model through a Bayesian Markov Chain Monte Carlo (MCMC) statistical analysis of the measured 2PCF. According to the so-called *Bayes theorem*, for a given dataset $\mathcal{D}$, the distribution of a set of model parameters Θ is provided by the so-called *posterior probability*, which can be expressed as follows:

$$\mathcal{P}(\Theta|\mathcal{D}) \propto \mathcal{L}(\mathcal{D}|\Theta)p(\Theta) \ , \tag{5.2}$$

where $\mathcal{L}(\mathcal{D}|\Theta)$ is the *likelihood* (i.e. a conditional probability expressed as a function of its second argument, while the first one is kept fixed) and $p(\Theta)$ refers to the *prior distribution* (i.e. the prior knowledge on the analyzed parameters). We sample the posterior distribution of the free parameter ($\mathcal{C}_{\mathrm{R}}$), assuming a Gaussian likelihood and a uniform prior. The values of $\mathcal{C}_{\mathrm{R}}$ resulting from this calibration procedure at the four considered redshifts are then inserted in the theoretical formulation of our model when performing the Bayesian analysis to extract the cosmological constraints. A summary of the $\mathcal{C}_{\mathrm{R}}$ parameter values is reported in tab. 5.2, while in fig. 5.3 we present the best-fit models of the measured 2PCF at $z = 0, 0.5, 1, 2$. A complete discussion on both the origin of this factor and its evolution with redshift will be addressed in future works.

5.2.3 Constraining the cosmological parameters

Holding the $\mathcal{C}_{\mathrm{R}}$ parameter fixed at its maximum posterior value (see tab. 5.2), we then run the MCMC again in order to sample the posterior distribution of the cosmological parameters Ω_{m} and σ_8. Note that Gaussian likelihoods and uniform priors are also assumed in this case. Our results are reported in fig. 5.4 and fig. 5.5, where we show the contour plots obtained from the Bayesian analysis that has been performed within each redshift, and combining all

[3] To verify that the `fftlog` method works properly, it was first applied to the DM power spectrum alone, since it is better understood than the void power spectrum we are modelling in this thesis. From this test, we obtained the expected outcome.

z	$\delta_{\rm v}^{\rm L}$	$\delta_{\rm v}^{\rm NL}$	$\mathcal{C}_{\rm R}$
0	-2.71	-0.795	1.13
0.5	-2.21	-0.75	1.12
1	-1.80	-0.7	1.19
2	-1.49	-0.65	1.22

Table 5.2: Summary of the linear and nonlinear thresholds of void formation ($\delta_{\rm v}$), and of the calibrated values of $\mathcal{C}_{\rm R}$ at four different redshift ($z = 0, 0.5, 1, 2$).

the redshifts together, respectively. Moreover, in tab. 5.3 we show the values and associated uncertainties of the constrained cosmological parameters within the ΛCDM scenario. These values have to be compared with those provided by Planck Collaboration et al. (2016) and used to build the DUSTGRAIN-*pathfinder* simulations, which are reported in tab. 4.1. It emerges from our analysis how the constrained parameters we get from both each single redshift and their combination, accounting for the 2PCF model presented in §3.2.3, are consistent within the errors with those of the analysed simulations.

z	$\Omega_{\rm m}$	σ_8	S_8
0	$0.38^{+0.14}_{-0.14}$	$0.84^{+0.12}_{-0.08}$	$0.94^{+0.08}_{-0.11}$
0.5	$0.31^{+0.17}_{-0.14}$	$0.84^{+0.09}_{-0.09}$	$0.83^{+0.11}_{-0.13}$
1	$0.41^{+0.13}_{-0.12}$	$0.81^{+0.10}_{-0.18}$	$0.87^{+0.12}_{-0.07}$
2	$0.26^{+0.11}_{-0.07}$	$0.85^{+0.10}_{-0.12}$	$0.77^{+0.06}_{-0.05}$
combined	$0.36^{+0.07}_{-0.07}$	$0.83^{+0.05}_{-0.05}$	$0.90^{+0.06}_{-0.06}$

Table 5.3: Summary of the cosmological constraints and relative uncertainties emerging from the Bayesian analysis we performed on each redshift ($z = 0, 0.5, 1, 2$) and on their combination within the ΛCDM scenario. We recall that the corresponding true values of the cosmological parameters assumed by the DUSTGRAIN-*pathfinder* ΛCDM simulations are the following: $\Omega_{\rm m} = 0.31345$, $\sigma_8 = 0.842$ and $S_8 = 0.861$.

Let us point out here the main reasons why we opt to constrain specifically $\Omega_{\rm m}$ and σ_8. These cosmological parameters taken together define the most famous degeneracy of the ΛCDM model, i.e. the so-called S_8 degeneracy, where S_8 is defined as $S_8 = \sigma_8\sqrt{\Omega_{\rm m}/0.3}$. Therefore, setting constraints on them helps to brake this degeneracy, by defining the lower and upper limits in the parameter space. Indeed, ideally, without performing an appropriate Bayesian analysis on the theoretical model of the considered statistics, such parameters could take on, in pairs, any value, as far as a decreasing $\Omega_{\rm m}$ is counterbalanced by an increasing σ_8,

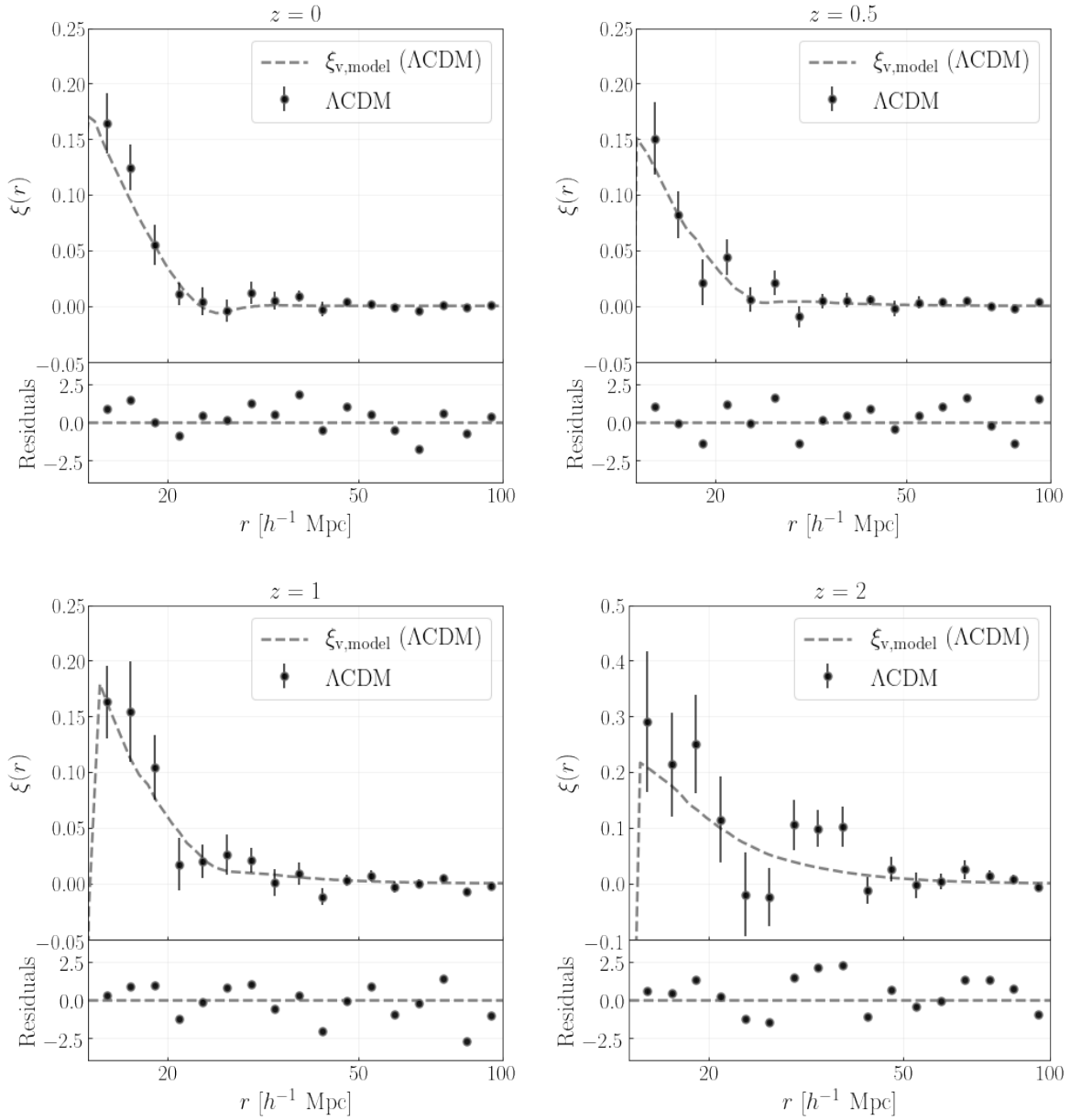

Figure 5.3: Upper sub-panels: best-fit model (grey dashed line) of the 2PCF measure (black dots) after the calibration of the HS radius. The black error bars are the Bootstrap errors associated with the measured 2PCF. Lower sub-panels: residuals of the measured clustering profile, computed as the ratio between the difference $2\mathrm{PCF}_{\rm data} - 2\mathrm{PCF}_{\rm model}$ and the Bootstrap errors of the data.

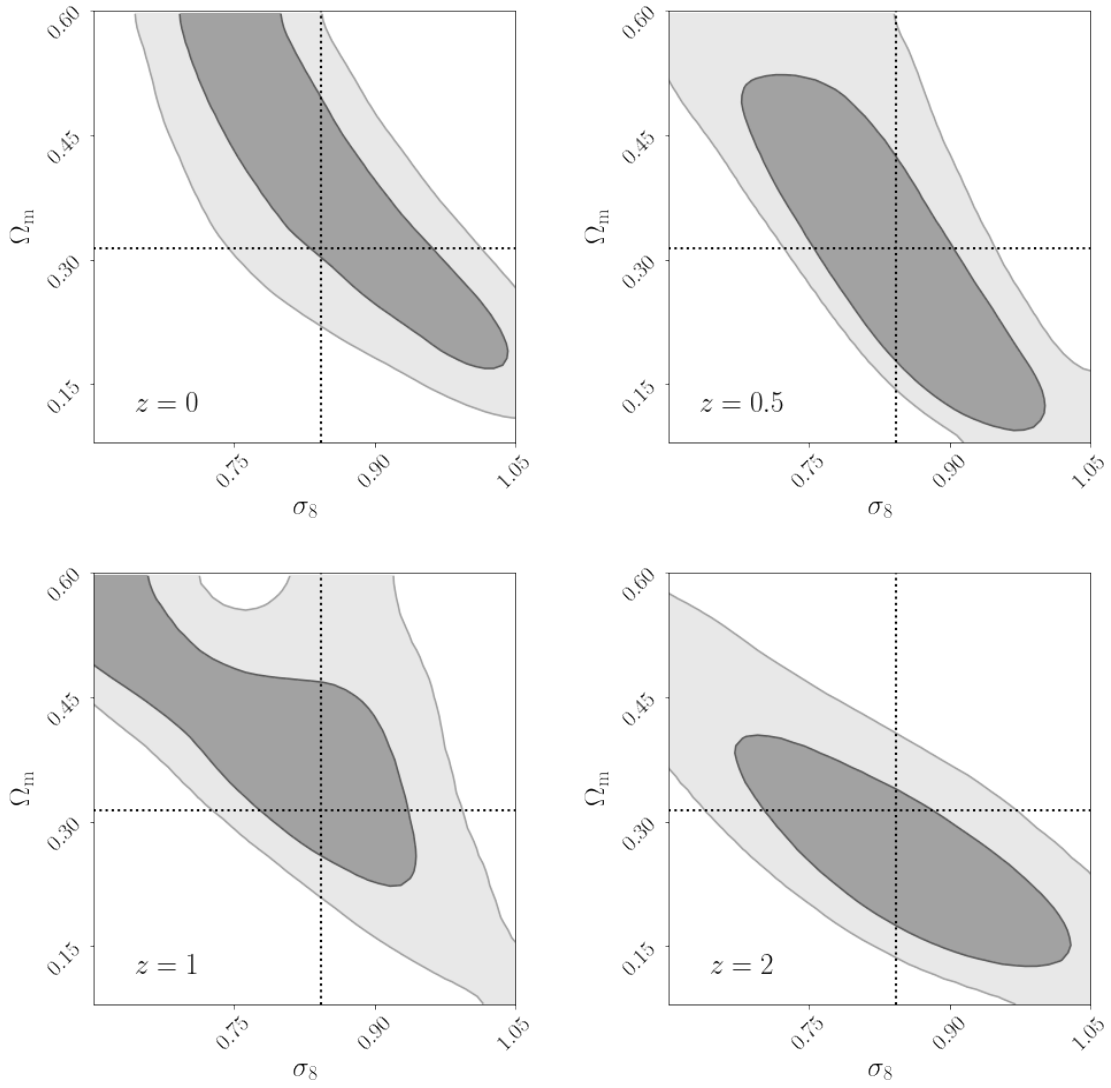

Figure 5.4: Comparison between the 68% (dark grey) and 95% (light grey) confidence levels computed with the void auto-correlation function at $z = 0$ (upper-left panel), $z = 0.5$ (upper-right panel), $z = 1$ (lower-left panel) and $z = 2$ (lower-right panel). The dotted black lines represent the truth values of $\Omega_{\rm m}$ and σ_8 assumed by the DUSTGRAIN-*pathfinder* simulations (see tab. 4.1).

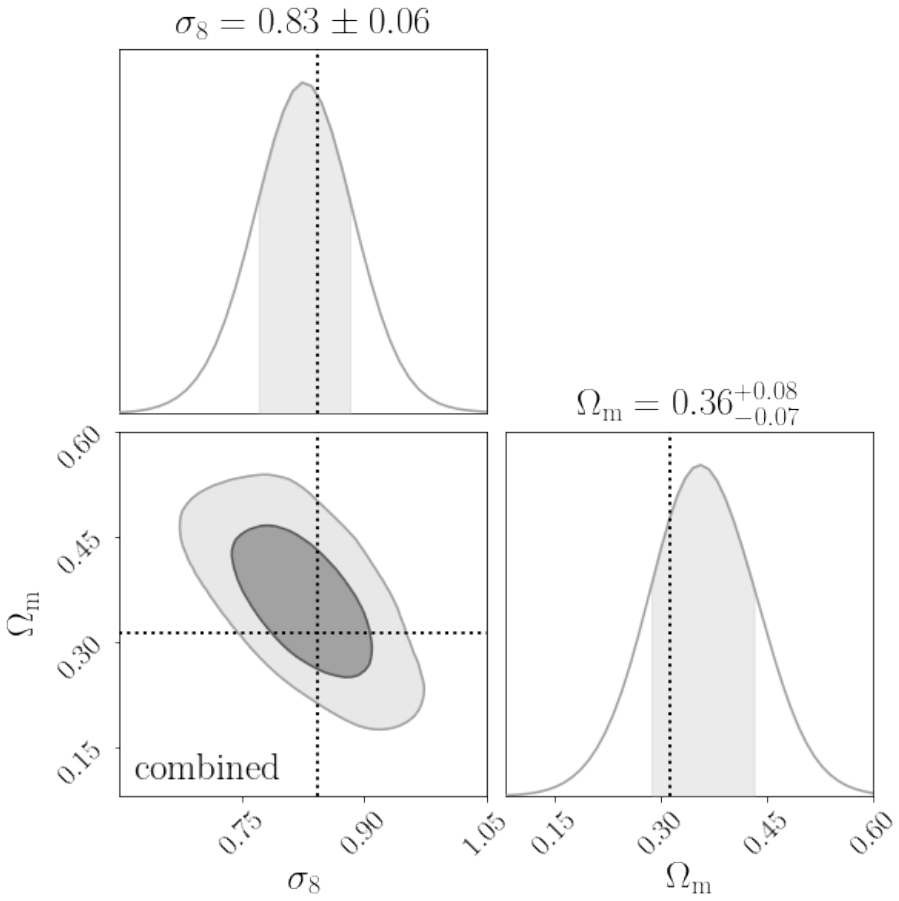

Figure 5.5: Combined posterior probability distribution of the cosmological parameters, Ω_m and σ_8, obtained from the 2PCF model at four redshift ($z = 0, 0.5, 1, 2$) together. The dark and light areas represent the 1σ (68%) and 2σ (95%) confidence regions, respectively. The dotted black lines represent the truth values on Ω_m and σ_8 assumed by the DUSTGRAIN-*pathfinder* simulations (see tab. 4.1). Finally, in the top of each column is reported the median of the posterior distributions with its associated errors.

or viceversa. Furthermore, among the ΛCDM parameters presented in §1.4, we exclude $\Omega_{\rm b}$ (i.e. the baryonic matter density parameter) since it has already been extensively studied in the literature, which provided us with rather tight constraints[4]. Lastly, we have ruled out the possibility of constraining the DE parameters. Indeed, on the one hand, Ω_Λ (i.e. the cosmological constant density parameter) is related to the constraints on $\Omega_{\rm m}$, since we are assuming a flat Universe, and thus $\Omega_{\rm tot} = \Omega_{\rm m} + \Omega_\Lambda = 1$. On the other hand, the w_0 and w_a parameters that account for possible forms of DE beyond the cosmological constant (see §1.4.1) are proven to be sensitive to the shape and size of cosmic voids rather than to their clustering properties. In fact, we recall that the 2PCF we are studying depends almost exclusively on the position (and number) of void centres.

In fig. 5.6 we show a graphical representation of the 2PCF model variations when different values of $\Omega_{\rm m}$ and σ_8 are considered, at $z = 0$. For each parameter value, the quantities $R_{\rm median}$ and $\bar{n}_{\rm v}$ are recomputed from the theoretical VSF. To perform this test and clarify the 2PCF model dependence on the analysed cosmological parameters, we assumed a flat-universe hypothesis, so that the cosmological constant energy density parameter (Ω_Λ) is derived according to each value of $\Omega_{\rm m}$, in order to recover $\Omega_{\rm tot} = \Omega_{\rm m} + \Omega_\Lambda = 1$. Notice that we have reported only $z = 0$ for the sake of brevity, but the cosmological information is derived from all the other redshifts as well.

[4]For example, the $\Omega_{\rm b}$ parameter was constrained from the theory of the primordial nucleosynthesis (Schramm, 1982) and from the CMB (Lineweaver et al., 1997), but also other probes and observables have been exploited (see e.g. Steigman et al., 1999).

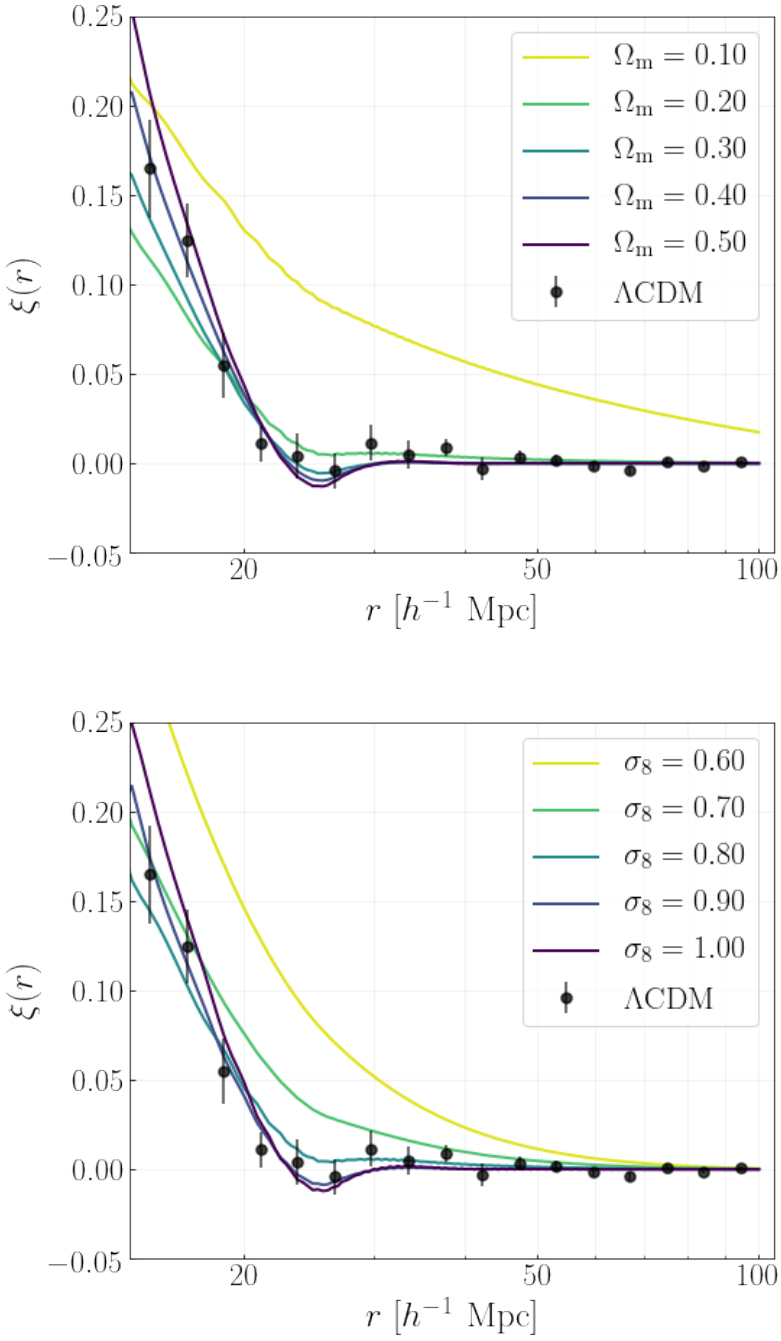

Figure 5.6: Graphical representation of how the 2PCF model varies according to different values of both Ω_m (upper panel) and σ_8 (lower panel) at $z = 0$. Note that theoretical model parameters, R_median and $\bar{n}_\mathrm{v}$ are computed for each couple of Ω_m and σ_8.

5.3 Results beyond the Standard Model

With the aim of initiating the exploitation of void clustering for cosmological purposes, we now proceed by testing the MG in the context of the void auto-correlation function, exploiting the DUSTGRAIN-*pathfinder* simulations which include the $f(R)$ models. We develop a preliminary investigation on possible dependencies of the considered two-point statistics on the background Cosmology. As already mentioned, the one reported in §5.2 is the very first cosmological analysis developed on void clustering. This section has then to be intended only as an initial step towards a full understanding of the potential role of the void auto-correlation function in discriminating between different cosmological scenarios, beyond the well-known ΛCDM.

We perform the same logical steps as presented in §5.2, comparing the measured 2PCF with the model validated within the ΛCDM simulation. Note that both the same void radius bin and sample selection criteria have been adopted. Firstly, we measure the real-space 2PCF in the $f(R)$ cosmological scenarios (i.e. fR4, fR5 and fR6) by means of the LS estimator (see eq. 3.11). Our results are reported in fig. 5.7, which shows the comparison between the calibrated ΛCDM model and the void clustering measurements obtained in MG scenarios. Then, we calibrate the 2PCF model function with respect to each measured $f(R)$ 2PCF, considering $\mathcal{C}_{\rm R}$ as a free parameter. We account for the void-formation linear and nonlinear thresholds specified in tab. 5.2, and assume for $R_{\rm median}$ and $\bar{n}_{\rm v}$ the quantities computed from the theoretical Vdn model of the VSF, within the Standard Cosmological Model (see tab. 5.1). The values of $\mathcal{C}_{\rm R}$ resulting from this calibration procedure at each redshift and for each cosmological scenario are summarized in tab. 5.4.

	$\mathcal{C}_{\rm R}$		
z	fR4	fR5	fR6
0	1.17	1.13	1.12
0.5	1.13	1.13	1.13
1	1.13	1.07	1.02
2	1.15	1.30	1.22

Table 5.4: Summary of the $\mathcal{C}_{\rm R}$ values resulting from the calibration performed by means of the MCMC with respect to the measured $f(R)$ 2PCF at four redshifts ($z = 0, 0.5, 1, 2$).

Finally, starting from the values of $\mathcal{C}_{\rm R}$ reported in tab. 5.4, we run the MCMC once again in order to constrain the cosmological parameters ($\Omega_{\rm m}$ and σ_8), by applying the fitting procedure to the 2PCF measured in MG cosmologies for each simulation snapshot considered (i.e. $z = 0, 0.5, 1, 2$). Note that the Bayesian analysis is performed with the same characteristics of that described in §5.2, i.e. Gaussian likelihood and uniform prior distributions. As done before, the resulting values for $\Omega_{\rm m}$ and σ_8 have to be compared with those assumed by the DUSTGRAIN-*pathfinder* simulations, in each cosmological framework (see tab. 4.1). Our results at $z = 0$

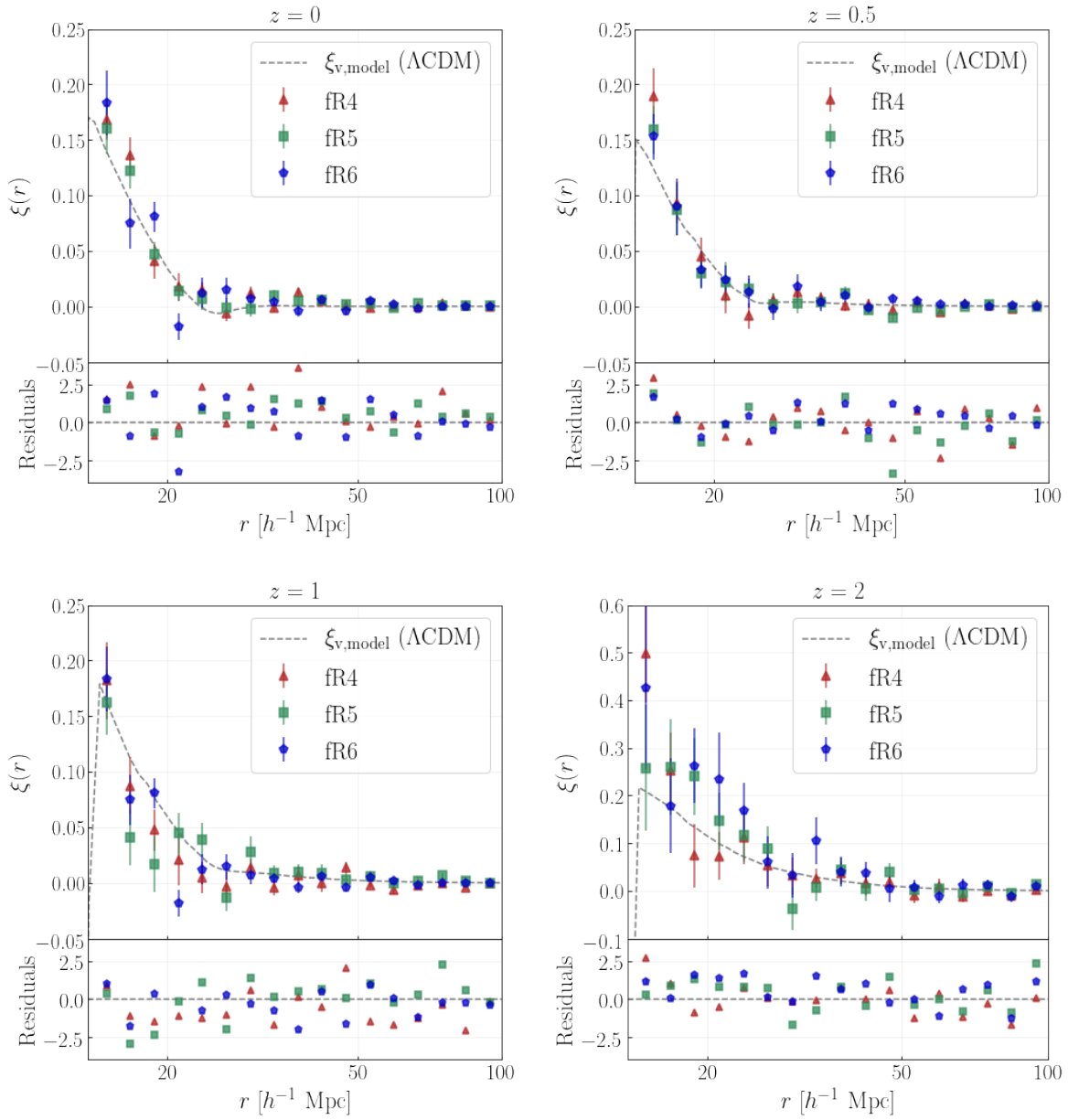

Figure 5.7: Upper sub-panels: comparison between the ΛCDM model (grey dashed line) and the 2PCF estimations in fR4 (red triangles), fR5 (green squares) and fR6 (blue pentagons) cosmologies. The error bars and residuals are defined as in the caption of fig. 5.3.

are reported in fig. 5.8, where we show the $\Omega_{\rm m} - \sigma_8$ contours obtained from the fitting of the $f(R)$ 2PCF with respect to those presented in the upper-left panel of fig. 5.4 (i.e. grey contours associated to the ΛCDM scenario). The same analysis has been performed also at $z = 0.5, 1, 2$, but we chose not to include them for simplicity. Indeed, as already clarified, the MG effects are significant at redshifts close to zero, and hence we do expect to see the greatest differences with respect to the ΛCDM both data and model at $z \sim 0$. Moreover, in figs. 5.9, 5.10 and 5.11, we show the $\Omega_{\rm m} - \sigma_8$ contours resulting from the combination of the entire set of considered redshifts. Finally, note that all the values obtained for the constrained cosmological parameters in the fR4, fR5 and fR6 scenarios are reported in tab. 5.5.

This analysis, which has been performed by comparing the ΛCDM auto-correlation model with the 2PCF measured in $f(R)$-based simulations, has been designed in order to understand whether the clustering statistics depends on the eventual presence of MG in our Universe. In particular, we wonder whether, assuming the model we introduced in §3.2.3, we are able to recover the values of $\Omega_{\rm m}$ and σ_8 of the simulations (see tab. 4.1) even in the case of MG cosmologies. As already underlined, the void clustering statistics has not yet been addressed with cosmological purposes in the literature. Thus, it has been not even employed in an attempt to discriminate between the well-known ΛCDM model and other feasible models, which suggest valid alternative to the cosmological constant for the late-time accelerated expansion of the Universe (see §1.4).

Within the limits of the DUSTGRAIN-*pathfinder* simulations we considered, our results clearly demonstrate how the method developed in this Thesis is robust as far as the strength of the MG model taken into account is relatively feeble. Indeed, both in the fR5 and fR6 simulations, the values of $\Omega_{\rm m}$ and σ_8 estimated from the void 2PCF assuming ΛCDM are totally consistent, within the 1σ confidence level, with those of the analysed simulations. Let us emphasize that the parameter values assumed by the fR5 and fR6 simulations are found to be also inside the 1σ contours associated to the ΛCDM scenario[5] (see figs. 5.10 and 5.11). Hence, we are unable to distinguish whether a model considers MG or not, but we can state that the method we have developed is robust: regardless of the background cosmology, applying 2PCF model built for a ΛCDM universe, we find values of $\Omega_{\rm m}$ and σ_8 that are compatible with expectations.

By contrast, for stronger modifications of gravity, as in the fR4 cosmological model, our method fails to predict the correct cosmological parameter values. In fact, from fig. 5.9, it is evident that the fR4 true values are not included in the 2σ fR4 contours. Though the reduced χ^2 of the model fitting is approximately equal to 1[6], we can conclude that, for high values of the $f_{\rm R0}$ parameter (i.e. $f_{\rm R0} \gtrsim 10^{-4}$), the void clustering statistics is enough itself to discriminate between ΛCDM and MG universes. For a proper modelling of the fR4 2PCF we need to consider additional parameters (such as $f_{\rm R0}$) in our likelihood. In other words, if the Universe was described by a fR4 cosmology, we would be able to realise it simply by means of the void 2PCF statistics. Indeed, by applying the model we developed in the ΛCDM framework, we would not find cosmological constraints on $\Omega_{\rm m}$ and σ_8 that are compatible with those already extracted in the literature from other probes. Let us point out that, in order to develop a robust

[5] Notice that the offset of the true values and contours of $f(R)$ cosmologies with respect to those of the ΛCDM tends to increase as the $f_{\rm R0}$ MG parameter becomes higher (i.e. going from fR6 towards fR5).

[6] Note that the fitting procedure performed with our ΛCDM model function provides good agreement (i.e. $\tilde{\chi}^2 \simeq 1$) in all the cosmological models analysed in this Thesis work.

theory of the void clustering and understand its results, it is important to make use of the present knowledge on the properties of our Universe. In fact, while the void clustering statistics is a novel cosmological probe that has yet to be properly tested, the constraints coming from other probes, such as the CMB or the galaxy clustering, are already considered to be reliable.

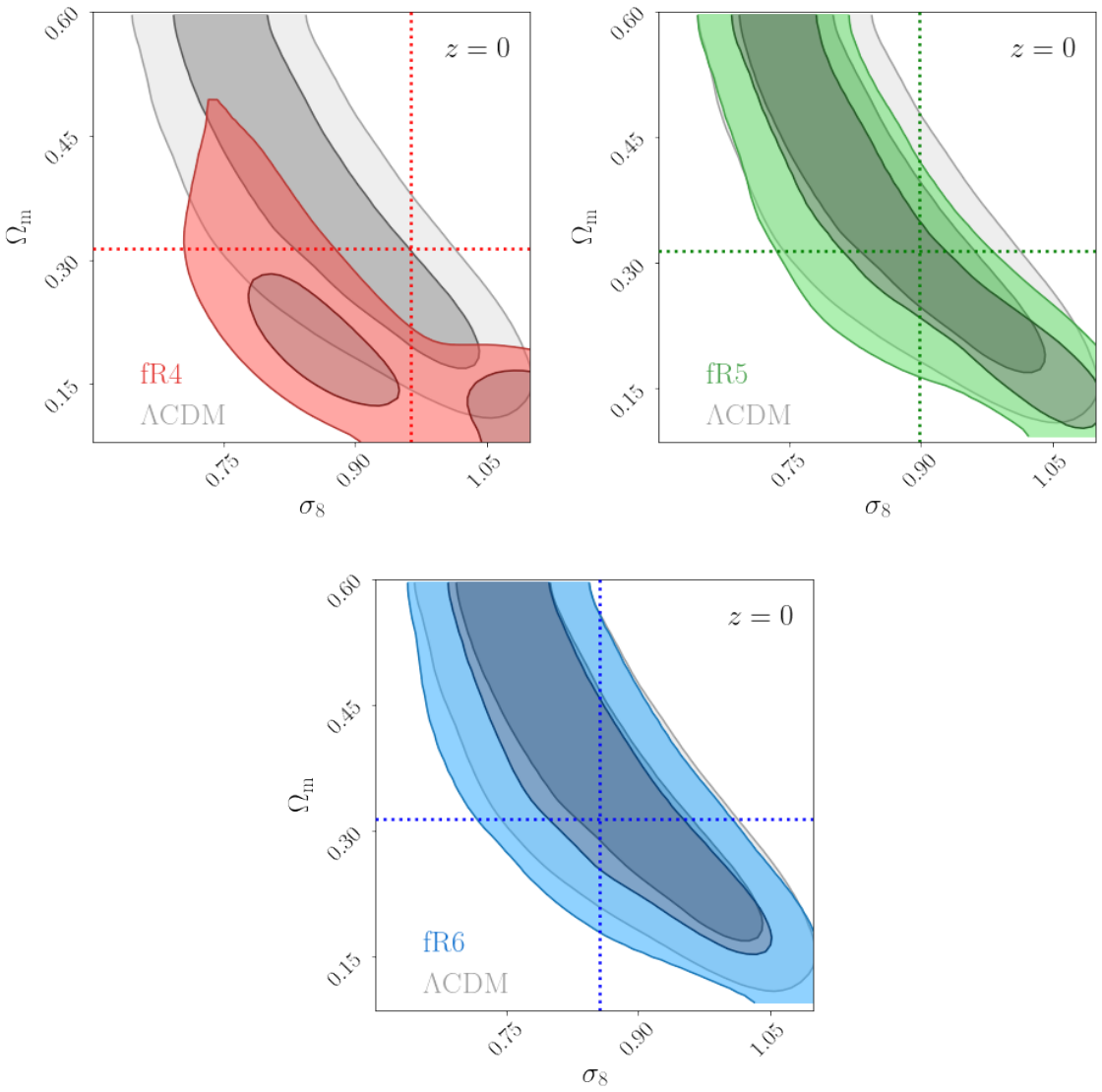

Figure 5.8: Comparison between the 68% (dark shades) and 95% (light shades) confidence levels computed with the void auto-correlation function at $z = 0$ in $f(R)$ scenarios of MG with respect to the ΛCDM grey contours presented in the upper-left panel of fig. 5.4. The dotted lines represent the truth values of Ω_m and σ_8 assumed by the DUSTGRAIN-*pathfinder* simulations for the $f(R)$ cosmologies (see tab. 4.1). The fR4, fR5 and fR6 are associated to the red, green and blue colours, respectively.

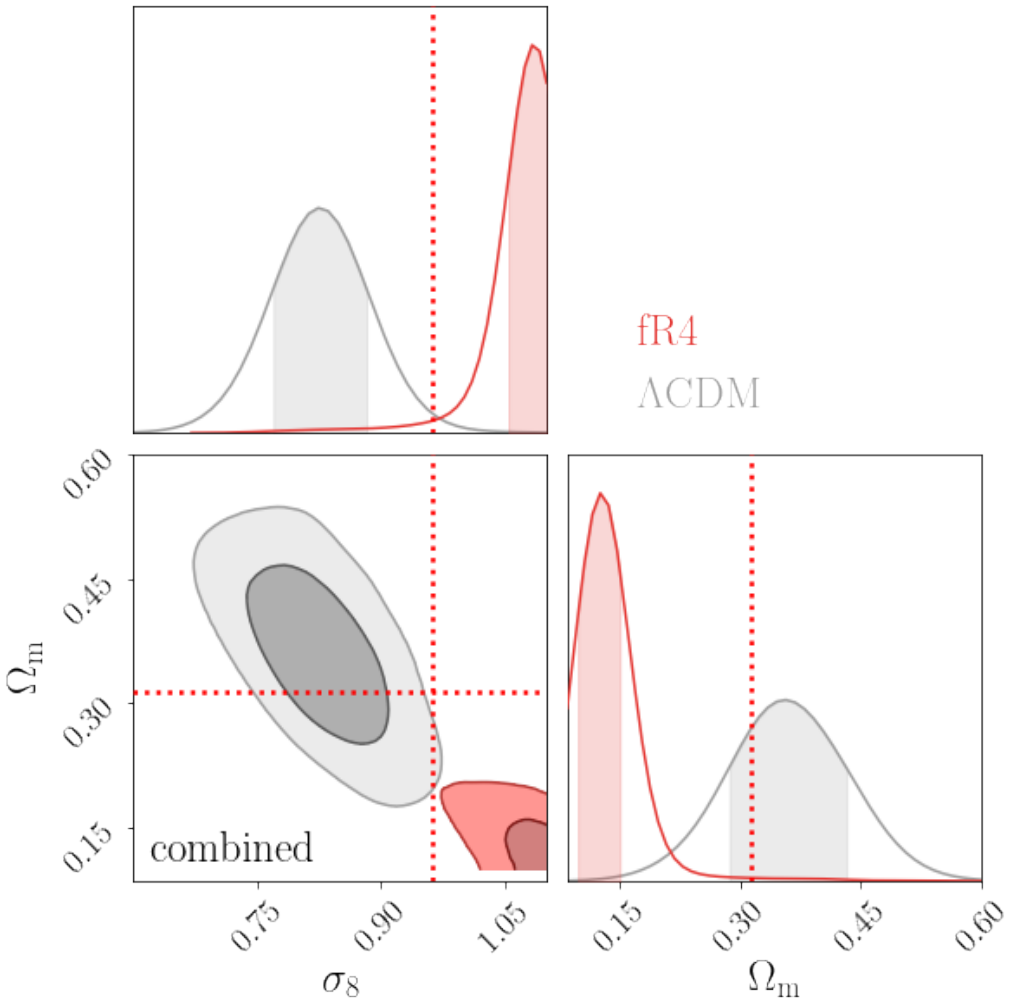

Figure 5.9: Combined posterior probability distribution of the cosmological parameters, Ω_m and σ_8, obtained for the fR4 data from the ΛCDM model at four redshift ($z = 0, 0.5, 1, 2$) taken together. The dark and light red areas represent the 68% and 95% confidence regions, respectively. The dotted red lines indicate the truths values of Ω_m and σ_8 assumed by the fR4 DUSTGRAIN-*pathfinder* simulations (see tab. 4.1). Note that the dark and light gray contours represent the combined posterior probability distribution obtained for the ΛCDM 2PCF (see fig. 5.5).

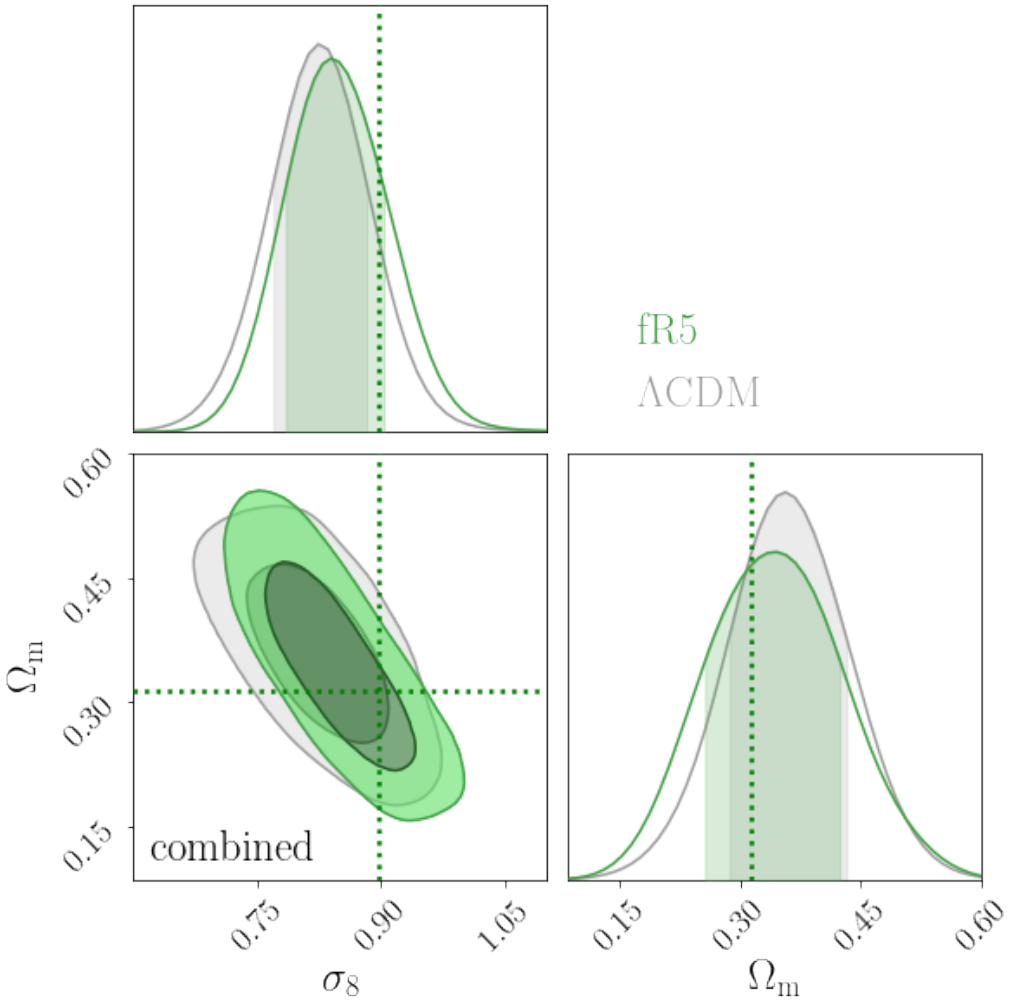

Figure 5.10: As fig. 5.9 but for the fR5 data.

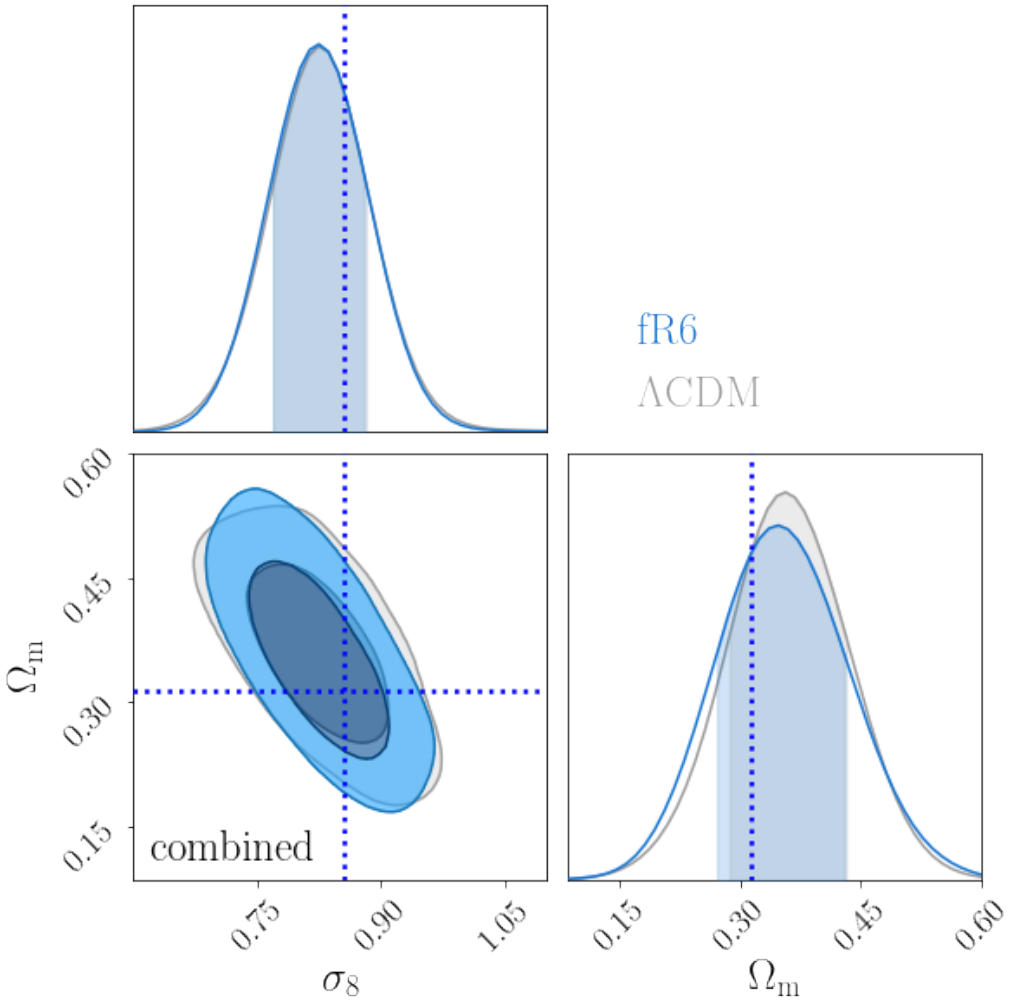

Figure 5.11: As fig. 5.9 but for the fR6 data.

	fR4			fR5			fR6		
z	$\Omega_{\rm M}$	σ_8	S_8	$\Omega_{\rm M}$	σ_8	S_8	$\Omega_{\rm M}$	σ_8	S_8
0	$0.14^{+0.12}_{-0.04}$	$0.99^{+0.13}_{-0.18}$	$0.68^{+0.07}_{-0.04}$	$0.34^{+0.17}_{-0.15}$	$0.84^{+0.17}_{-0.09}$	$0.90^{+0.10}_{-0.12}$	$0.37^{+0.15}_{-0.14}$	$0.83^{+0.13}_{-0.08}$	$0.92^{+0.09}_{-0.12}$
0.5	$0.41^{+0.13}_{-0.15}$	$0.90^{+0.08}_{-0.05}$	$1.04^{+0.12}_{-0.16}$	$0.44^{+0.10}_{-0.12}$	$0.84^{+0.06}_{-0.06}$	$0.98^{+0.10}_{-0.10}$	$0.31^{+0.13}_{-0.10}$	$0.85^{+0.06}_{-0.06}$	$0.85^{+0.14}_{-0.11}$
1	$0.39^{+0.13}_{-0.16}$	$0.96^{+0.08}_{-0.08}$	$1.06^{+0.17}_{-0.17}$	$0.25^{+0.14}_{-0.08}$	$0.88^{+0.05}_{-0.08}$	$0.80^{+0.10}_{-0.11}$	$0.44^{+0.11}_{-0.12}$	$0.77^{+0.09}_{-0.09}$	$0.90^{+0.06}_{-0.05}$
2	$0.49^{+0.08}_{-0.11}$	$0.62^{+0.12}_{-0.07}$	$0.79^{+0.06}_{-0.05}$	$0.40^{+0.11}_{-0.10}$	$0.71^{+0.13}_{-0.11}$	$0.80^{+0.07}_{-0.05}$	$0.35^{+0.10}_{-0.08}$	$0.70^{+0.11}_{-0.10}$	$0.73^{+0.05}_{-0.04}$
combined	$0.13^{+0.02}_{-0.01}$	$1.08^{+0.02}_{-0.03}$	$0.71^{+0.04}_{-0.03}$	$0.34^{+0.08}_{-0.08}$	$0.85^{+0.06}_{-0.05}$	$0.90^{+0.06}_{-0.06}$	$0.35^{+0.08}_{-0.07}$	$0.83^{+0.05}_{-0.05}$	$0.89^{+0.06}_{-0.06}$

Table 5.5: Summary of the cosmological constraints and relative uncertainties emerging from the Bayesian analysis we performed on each redshift and on their combination beyond the ΛCDM scenario, i.e. in the fR4, fR5 and fR6 cosmologies. We recall that the corresponding true values of the cosmological parameters assumed by the DUSTGRAIN-*pathfinder* $f(R)$ simulations are the following (see tab. 4.1): $\Omega_{\rm m}({\rm fR4}) = 0.31345$, $\sigma_8({\rm fR4}) = 0.963$ and $S_8({\rm fR4}) = 0.984$; $\Omega_{\rm m}({\rm fR5}) = 0.31345$, $\sigma_8({\rm fR5}) = 0.898$ and $S_8({\rm fR5}) = 0.918$; $\Omega_{\rm m}({\rm fR6}) = 0.31345$, $\sigma_8({\rm fR6}) = 0.856$ and $S_8({\rm fR6}) = 0.875$.

5.4 Voids in the halo distribution

In §5.1 we focused on cosmic voids extracted from the DM particle distribution, but we can also investigate those emerging from the DM halo distribution[7]. In the latter case, the requirements to be satisfied in order to deal with the void clustering properties and their modelling, are exactly the same as those reported at the beginning of §5.1: *(I)* the void 2PCF model requires in input both the void median radius and comoving number density, and these quantities can be modelled with the Vdn model to account for theoretical principles, if properly cleaned voids are considered (see §4.4); *(II)* the statistics of the sample considered must be high enough to provide precision on the measurements and, therefore, precision on the modelling; *(III)* the range of the considered void radii must be rather narrow, in order to avoid contamination due to the mixing of different information associated with different void sizes.

As anticipated, cosmic voids identified in the halo distribution are larger than those identified in the DM particle field. Furthermore, while the number of DM particles is always the same[8] in the DUSTGRAIN-*pathfinder* simulations, the number of haloes among which we identify voids changes according to the redshift considered. Indeed, a greater number of haloes is found at lower redshift, where the small-scale gravitational interaction has had more time to create DM particle aggregations. Let us also mention that the number of haloes is expected to vary also according to the cosmological model we consider (i.e. ΛCDM and $f(R)$ scenarios), since the overdensity clustering properties depend on whether the MG is taken into account. Therefore, in order to perform a fair analysis, ensuring the conservation of the void considered percentage at each redshift and for each cosmology, we decide to select void sub-samples on the basis of the halo MPS (see §4.2.1). According to this argument, once both the void finding and cleaning procedures are applied to the halo catalogues, we opt to account only for voids with radii included in the range $[2.5 - 5.5]$ MPS, in order to avoid spurious underdensities and exclude too large voids. We underline that many tests[9] have been performed to establish this selection of voids, which turned out to be the best achievable compromise between sample statistics, agreement with the theoretical VSF (see fig. 4.9), and similar enough radii to study the void clustering properties. Lastly, as it is done for voids identified in the DM particle distribution, we remove all those objects whose centre is less than $30\ h^{-1}\mathrm{Mpc}$ from the edge of the simulation boxes. In tab. 5.6 we summarise the relevant characteristics of our ΛCDM void sub-catalogues at each redshift, computed both directly from the sample and from the theoretical Vdn model of the VSF.

The auto-correlation measure of cosmic voids in DM haloes is performed by means of the LS estimator (eq. 3.11) and, in order to build the 2PCF model, we use the theoretical quantities derived from the VSF (see tab. 5.6), and adopt the nonlinear threshold $\delta_{\mathrm{v,DM}}^{\mathrm{NL}} = -0.5$ weighted for the tracer bias (see §4.4.2). The corresponding linear thresholds of void formation from which we compute the 2PCF model in the biased tracers at $z = 0, 0.5, 1, 2$ are $\delta_{\mathrm{v,tr}}^{\mathrm{NL}} = -0.54, -0.42, -0.32, -0.19$, respectively.

[7] The other underdensity tracers (i.e. galaxies) cannot be exploited in our work since the DUSTGRAIN-*pathfinder* do not include baryonic matter yet.

[8] We recall that for the whole analysis presented in §5.1, only a 25% randomly selected sample of DM particles is considered, in order to reduce the computational time.

[9] In particular, we tested different mass cuts on the halo catalogues (see §4.2.1) and different thresholds of void formation.

z	$N_{\rm v}$		$\bar{n}_{\rm v}$ $[h^3\,{\rm Mpc}^{-3}]$		$R_{\rm median}$ $[h^{-1}\,{\rm Mpc}]$	
	simulation	model	simulation	model	simulation	model
0	939	823	2.62×10^{-6}	2.30×10^{-6}	27.50	26.92
0.5	888	728	2.48×10^{-6}	2.04×10^{-6}	27.74	27.07
1	708	577	1.98×10^{-6}	1.61×10^{-6}	29.39	28.72
2	251	204	7.01×10^{-7}	5.71×10^{-7}	37.32	36.43

Table 5.6: Summary of the main characteristics of the ΛCDM sub-sample considered, i.e. the redshift z, the number of voids $N_{\rm v}$, the void mean number density $\bar{n}_{\rm v}$ and the median radius $R_{\rm median}$. The last three columns are split into two sub-columns, where the first refers to the quantities calculated directly from the sample, while the second contains the quantities computed from the theory of the VSF.

Although we have shown in §5.1 that our 2PCF model works well for the voids identified in DM particles, the situation is different for voids identified in the halo distribution. The MCMC do not give statistically significant limits on the free parameter ($\mathcal{C}_{\rm R}$) value, which would be necessary in to proceed with the Bayesian analysis that allows us to constrain the $\Omega_{\rm m}$ and σ_8 cosmological parameters. This is due to the fact that, after the application of all the aforementioned criteria to obtain a void selected sample in accordance with theoretical principles, the resulting statistics of cosmic voids in the halo distribution is rather poor (i.e. the error bars associated with our measurements are too large with respect to the clustering signal itself). Indeed, not only the considered DUSTGRAIN-*pathfinder* simulations are rather small for this study, and consequently better suited to analyse the statistical properties of small voids instead of large voids, but we must also consider the additional loss of counts resulting from the cleaning procedure, which is a necessary step to be consistent with the assumptions of the VSF model. Let us underline that another consequence of such a low statistics is that we cannot properly compare the ΛCDM results with those obtained in the presence of MG.

Our results are reported in fig. 5.12 and 5.13. The former shows the comparison between the measured 2PCF within and beyond the Standard Cosmological Model. Notice that no trend is found in the clustering of voids measured in different cosmologies, contrary to the expectations related to the halo MPS we presented in §4.2.1. This can be caused by two main reasons: we do not know yet all the possible outcomes of the cleaning procedure in the context of the void clustering statistics, and the uncertainties on our data are definitely too large, with respect to the effective signal, to make proper comparisons. Figure 5.13 shows instead possible alternative 2PCF models for the void clustering in the ΛCDM scenario, which result from different values of the free parameter $\mathcal{C}_{\rm R}$. As anticipated, we cannot recover robust enough estimates of the $\mathcal{C}_{\rm R}$ from the posterior distribution, and hence we prefer just to highlight a reasonable range of values for which the predictions of our 2PCF model could be in agreement with the measurements.

Focusing on the void clustering estimation in the ΛCDM cosmological scenario at $z = 0$

(upper-left panel in fig. 5.13), we stress the fact that, even if for separations greater than $\simeq 100\ h^{-1}\mathrm{Mpc}$ the dark violet model (i.e. $\mathcal{C}_{\mathrm{R}} = 1$) seems to accurately describe the measured black dots, at smaller separations the data are not adequately reproduced by any curve. Moreover, being the signal consistent with zero at scales greater than $100\ h^{-1}\mathrm{Mpc}$, we have no clue on how to use the void clustering statistics to extract cosmological constraints. Note that for increasing redshifts (i.e. $z = 0.5, 1, 2$) the statistics becomes even worse, and almost the whole clustering signal turns out to be compatible with zero.

To sum up, given the insufficient dimensions of the considered simulations with respect to the typical large dimensions of cosmic voids extracted from the DM halo distribution, we conclude that the analysis performed in §5.1 cannot be successfully applied also in this case. The investigation of such voids is left for future works, by considering both larger simulations and real data catalogues.

Let us emphasise that, since the two-point statistics depends mainly on the centre positions, we expect to be able to model the auto-correlation function of voids identified in the halo distribution through the same theoretical formulas as those implemented in the dark matter field, at least at first approximation. Indeed, the real underdensities of our Universe are unique in the total dark matter field, and even if we trace them by means of biased collapsed objects, their true centres are immutable, beyond all the issues related to both the spatial resolution and the shot noise of the employed void finder. The only void feature that changes is the density profile (both slope and depth) and, with it, the density contrast enclosed within the void radius. However, this variation is already included properly in the extended theory of the Vdn model proposed by Contarini et al. (2019) and Contarini et al. (2022).

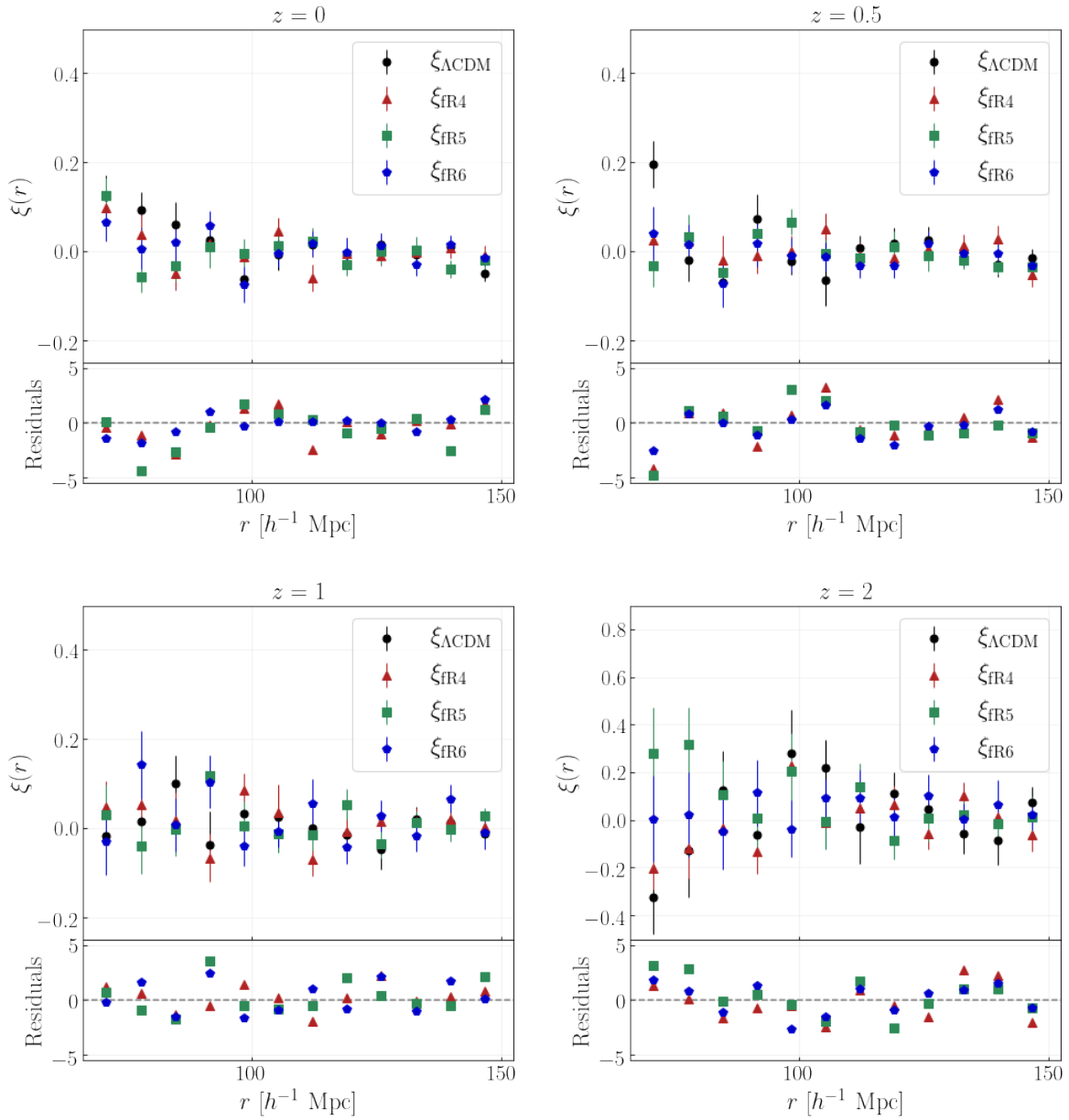

Figure 5.12: Comparison between the auto-correlation function measured in different cosmological scenarios at four different redshifts ($z = 0, 0.5, 1, 2$). The black dots represent the ΛCDM 2PCF, while the red triangles, green squares and blue pentagons refer to the fR4, fR5 and fR6, respectively. The error bars are the Bootstrap errors associated with the measured 2PCF. Lower sub-panels: residuals of the measured clustering profile, computed as the ratio between the difference $2\mathrm{PCF}_{\mathrm{data},\Lambda\mathrm{CDM}} - 2\mathrm{PCF}_{data,f(R)}$ and the Bootstrap errors of the $f(R)$ data.

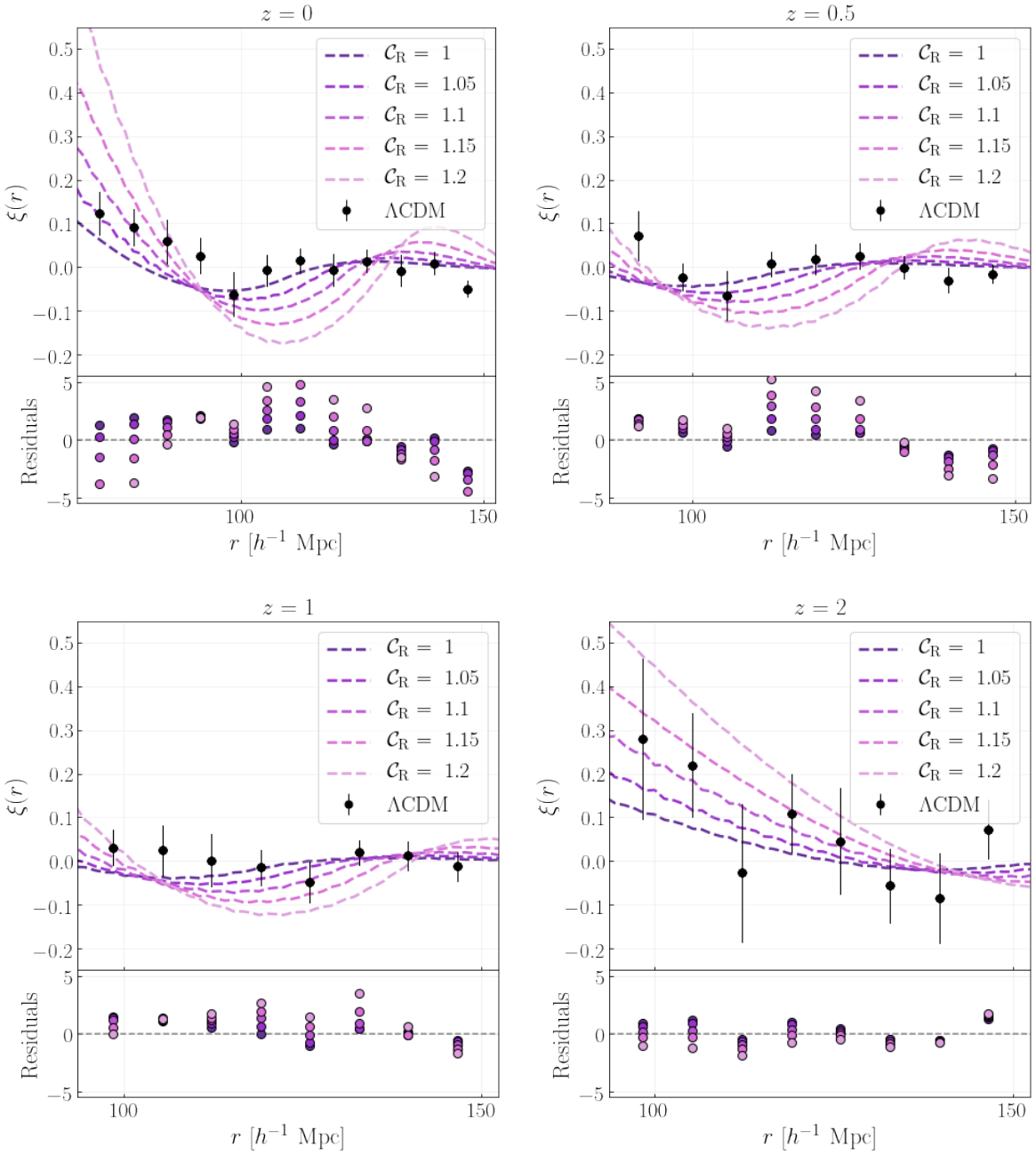

Figure 5.13: Upper sub-panels: 2PCF model (coloured dashed lines) hypothesised starting from the ΛCDM measure (black dots) for different feasible values of $\mathcal{C}_R$ (i.e. $\mathcal{C}_R = 1, 1.05, 1.1, 1.15, 1.2$). The black error bars are the Bootstrap errors associated with the measured 2PCF. Lower sub-panels: residuals of the measured clustering profile, computed as the ratio between the difference $2\mathrm{PCF}_{\mathrm{data}} - 2\mathrm{PCF}_{\mathrm{model}}$ and the Bootstrap errors of the data.

Chapter 6

Discussion and conclusions

In this chapter we outline the main highlights of this Master Thesis, beginning with a brief recapitulation of the general context in which our work originated, proceeding with a schematic summary of both the results and procedures employed, and finally presenting possible future developments of our analysis (see forthcoming §6.1, §6.2 and §6.3, respectively). In particular, we focus on the relevance of cosmic voids as cosmological probes, especially underlying the potential powerful role that their clustering statistics can have in the current cosmological framework.

6.1 The scientific problem

As already clarified, the ΛCDM model (extensively described in §1.3) is widely accepted as the Standard Cosmological Model, since it is the one that provides the best predictions of the large-scale properties of the Universe. Indeed, this model has been constantly tested in the literature by means of increasingly precise measurements, leading to a quite good agreement between real data and theoretical prescriptions. According to this model, our Universe is based on General Relativity and the Cosmological Principle, and therefore it can be modelled as an expanding spacetime that behaves following the FLRW metric (§1.1.1). It is assumed the existence of two so-called *dark components*, namely cold dark matter and dark energy, whose properties and behaviour are far to be completely understood.

Over the years, in order to solve the main issues emerging within this cosmological framework, the scientific community has developed both wide and deep field surveys, which have been able to constrain the ΛCDM parameters with astonishing precision, mapping the distribution of the luminous objects that trace the underlying total matter field. It is due to this increasing precision that observational tensions have arisen among the constraints obtained from different cosmological probes. As mentioned in §1.4, such tensions emerge when comparing the so-called high and low redshift probes, referring to the CMB anisotropies and the statistical properties of collapsed objects in the local Universe, respectively.

Focusing on the present day large-scale structure, since it is in this context that our work can be included, let us underline that galaxy clusters (and relative dark matter haloes) evolving from the positive Gaussian fluctuations of the primordial density field, are the largest existing

virialized structures of the Universe. Therefore, their statistics turns out to be an extremely powerful probe to constrain the cosmological parameters. We refer especially to their number counts, density profiles and clustering. Likewise, we can exploit the same statistical properties of cosmic voids, which are their negative counterparts, evolving instead from the negative initial perturbations. Despite the identification of the underdense regions is non-trivial[1], it is very important to build the theoretical basis for studying these objects, as they have many advantageous characteristics for their exploitation with cosmological purposes. First of all, they do not need to be modelled dealing with all the complications related to the nonlinear regime, and this is thanks to the physical barrier $\delta = -1$, which makes their evolution undergo only a mildly nonlinear regime. Moreover, they tend towards sphericity as they evolve and, being almost baryon-free, they are much less affected by the effects of micro-physics processes. All these three characteristics ensure that the void formation and evolution should be easier to model than the overdense counterparts. Moreover, void interiors are very useful for astrophysical studies on the formation of galaxies and their evolution. Indeed, while addressing these aspects in high-density environments is non-trivial, isolated galaxies in underdense regions allow us to do so, since their evolution is almost entirely driven by in-situ processes. Finally, cosmic voids are classified as extremely suitable laboratories to investigate neutrinos, dark energy and modified gravity, thanks to their emptiness and shallow gravitational potentials. Despite all these favourable characteristics, cosmic voids are still not widely comprehended and the route towards their full cosmological exploitation is still a long way off.

The aim of this Thesis is to develop a theoretically robust method to handle the void clustering properties with cosmological purposes. Indeed, while the two-point statistics has already been extensively treated for overdense collapsed objects, for underdensities no modelling based entirely on theoretical principles has yet been presented in the literature. Our work is a first key step towards the effective employment of the void auto-correlation function for cosmological purposes, which has turned out to be an extremely powerful probe to constrain the cosmological parameters describing our Universe. Thus, we base our model function on the first principles of the void size function (i.e. Vdn model), preparing catalogues to be analysed in accordance with these same principles. By doing this, we aim at actively participating in the ongoing research of the best cosmological model to describe our Universe. Let us highlight that, despite all the problems that still exist regarding both the void identification and definition, the statistics of their number counts has now reached a high degree of maturity in the literature. Thus, it can be reliably used as a theoretically motivated basis for our studies.

[1]We recall that, being the cosmic voids defined as devoid of matter that do not emit themselves, we must recover both their shape and centre positions from the distribution of the luminous biased tracers. The only exception in which we can find voids directly in the DM field is when analysing simulations, because in this case the DM particle distribution is known by construction.

6.2 Procedure and relevant results

In this Thesis, we exploited the void clustering statistics in three main ways: *(I)* to constrain the ΛCDM cosmological parameters, especially $\Omega_{\rm m}$ and σ_8, by fitting the measured void auto-correlation with a 2PCF model function; *(II)* to evaluate both the robustness of our model when different cosmological scenarios are considered, and the potential constraining power of the two-point statistics of cosmic voids in discriminating between the standard ΛCDM and the $f(R)$ modified gravity models; *(III)* to investigate the overall evolution of the auto-correlation of voids identified in the halo distributions. Note that the latter analysis is meant as a first step towards future application of the void clustering statistics to real data catalogues.

To extract our data, we made use of high-resolution N-body simulations, namely the DUSTGRAIN-*pathfinder*, which are characterized by a volume of $750^3\ h^{-3}{\rm Mpc}^3$, and by a quite high number of DM particles (768^3). With the intention of studying the void clustering properties both in the DM particle field and in the halo distribution, we extracted the DM halo catalogues by means of the DENHF halo finder at $z = 0, 0.5, 1, 2$. Once the tracer catalogues had been defined, we identified cosmic voids by means of the VIDE void finder in both the aforementioned cases, and then proceeded with the application of the cleaning algorithm, which is meant to exclude spurious underdensities, re-scale the void radii to a defined density threshold, and finally remove the overlapping. Let us emphasize, once again, that this is done in order to make our void samples consistent with the assumptions made when predicting the theoretical void size function through the Vdn model.

We then implemented a model to describe the void clustering properties, improving the void power spectrum model introduced by Chan et al. (2014) by accounting only of cleaned voids, in order to use properly the theoretical quantities of $R_{\rm median}$, $\bar{n}_{\rm v}$, $\delta_{\rm v}$ and $\delta_{\rm c}$ (i.e. the median void radius and number density, and the thresholds of void and overdense structures formation, respectively). Our model enabled us to fit the data quite well ($\tilde{\chi}^2 \simeq 1$), as far as the $\mathcal{C}_{\rm R}$ free parameter is considered in the HS theory. Once the model was calibrated by establishing a value of $\mathcal{C}_{\rm R}$ through the MCMC, we run them again to constrain the cosmological parameters, namely $\Omega_{\rm m}$ and σ_8. This procedure has been applied to cosmic voids identified both in the ΛCDM and $f(R)$ cosmologies. Our findings are the following:

- within the ΛCDM simulation, despite the necessary calibration of $\mathcal{C}_{\rm R}$, the 2PCF model works properly, and sets reliable constraints on the cosmological parameters, which are in agreement with the true values of the simulation;

- as long as the effects of modified gravity are modest, the model built in the ΛCDM framework is also suitable for the $f(R)$ simulations (in particular, fR5 and fR6), and extracts constraints that are compatible at 1σ with the true values of the corresponding simulation; when instead the modified gravity becomes stronger, the contours are not consistent with the true values of the cosmological parameters assumed by the DUSTGRAIN-*pathfinder* fR4 simulation.

Therefore, for minor modifications of gravity, the void clustering properties can still be described by ΛCDM 2PCF model, providing cosmological parameters whose values are totally in agreement both with those of the DUSTGRAIN-*pathfinder* simulations. We can conclude that,

in these cases, our method is robust. For stronger levels of modified gravity, the model is not suitable anymore, and it predicts $\Omega_{\rm m}$ and σ_8 values that do not match those of the $\rm fR4$ simulations. Hence, in order to properly model the modified gravity contribution, some additional parameters must be considered ($|f_{\rm R0}|$, in this case).

By contrast, from the cosmic voids identified in the halo distribution we have not yet extracted any cosmological information. The statistical relevance of our void samples is quite poor, and the signal is almost consistent to zero within the errors. Since the two-point statistics depends the most on void centres, we do expect that, with better suited catalogues, we will be able to properly model the auto-correlation of these voids by means of the same model adopted for voids identified in the dark matter particle field. Let us emphasise that our statistical constraining power will improve when considering both larger and high-resolution simulations and surveys.

To perform our analysis we made use of classes and functions implemented in the CBL, together with some C++/Python codes we built to model the void 2PCF and related statistics (i.e. the halo MPS and MF).

6.3 Future perspectives

Our studies are of enormous importance in the current cosmological framework, since for the very first time we have been able to investigate the constraining power of the void clustering statistics on the main cosmological parameters ($\Omega_{\rm m}$ and σ_8). With the aim of overcoming some still physically unexplained limitations of our model (e.g. the origin and redshift evolution of the calibrated $\mathcal{C}_{\rm R}$ parameter), we will make use of larger and higher-resolution simulations. First of all, we will analyse the DUSTGRAIN (Baldi, 2020), an improved version of their *pathfinder* precursors. These simulations have a large comoving box side of $2\ h^{-1}\ {\rm Gpc}$ and a relatively high resolution, given that the number of particles is $2048^3(\times 2)$ CDM particles (and neutrinos). Having these simulations a volume about 20 times greater than the DUSTGRAIN-*pathfinder*, they will help us to study the modified gravity $f(R)$ models in more detail, and therefore to verify if the void clustering statistics is an effectively suitable probe to discriminate among $f(R)$ and $\Lambda{\rm CDM}$ cosmologies. Then, we aim also at investigating hydrodynamical simulations, in order to evaluate the possible effects of the baryonic matter in the void auto-correlation function. This will allow us to both investigate the voids in the DM field with more precision and analyse the larger voids found in the biased tracer distribution. We also intend to exploit the current observational surveys (e.g. BOSS) and provide forecasts for future missions (e.g. Euclid, LSST), analysing the angular void clustering properties of real data as well. Thus, the overall result of employing such simulations is a significant increase in void number counts, and consequently, a much higher statistics, thanks to which we could manage to definitely improve our analysis and relative cosmological outcomes. Note that the resulting constraints extracted from the void clustering statistics will be also combined with those emerging from other cosmological probes (e.g. void and cluster number counts and density profiles, weak lensing analyses, Ly-α forest, CMB, and many others).

Finally, we will construct our void two-point model function within the next publicly available version of the CBL.

Bibliography

Alcock, C. et al. (Oct. 2001). "The MACHO Project: Microlensing Detection Efficiency". In: *The Astrophysical Journal Supplement Series* 136.2, pp. 439–462. DOI: 10.1086/322529.

Amendola, L. et al. (2013). "Cosmology and Fundamental Physics with the Euclid Satellite". In: *Living Reviews in Relativity*. DOI: 10.12942/lrr-2013-6.

Amendola, L. et al. (Apr. 2018). "Cosmology and fundamental physics with the Euclid satellite". In: *Living Reviews in Relativity* 21.1. DOI: 10.1007/s41114-017-0010-3 (cit. on pp. 30, 61).

Bacon, R. et al. (Mar. 2021). "The MUSE Extremely Deep Field: The cosmic web in emission at high redshift". In: *Astronomy & Astrophysics* 647, A107. DOI: 10.1051/0004-6361/202039887 (cit. on p. 35).

Bagla, J.S. and T. Padmanabhan (Aug. 1997). "Cosmological N-body simulations". In: *Pramana* 49, p. 161. DOI: 10.1007/BF02845853 (cit. on p. 60).

Bai, Y., A. J. Long, and S. Lu (Sept. 2020). "Tests of Dark MACHOs: lensing, accretion, and glow". In: *Journal of Cosmology and Astroparticle Physics* 2020.09, pp. 044–044. DOI: 10.1088/1475-7516/2020/09/044 (cit. on p. 29).

Baker, T. et al. (July 2018). "Void lensing as a test of gravity". In: *Physical Review D* 98.2. DOI: 10.1103/physrevd.98.023511 (cit. on p. 75).

Baldi, M. (May 2012). "The CoDECS project: a publicly available suite of cosmological N-body simulations for interacting dark energy models". In: *Monthly Notices of the Royal Astronomical Society* 422.2, pp. 1028–1044. DOI: 10.1111/j.1365-2966.2012.20675.x (cit. on p. 61).

— (Jan. 2020). "DUSTGRAIN Follow Up report". In: *Mem. Societa Astronomica Italiana* 91, p. 197 (cit. on p. 126).

Baldi, M. and F. Villaescusa-Navarro (2016). "Cosmic Degeneracies II: Structure formation in joint simulations of Warm Dark Matter and $f(R)$ gravity". In: DOI: 10.48550/ARXIV.1608.08057.

Baldi, M. et al. (Mar. 2014). "Cosmic degeneracies – I. Joint N-body simulations of modified gravity and massive neutrinos". In: *Monthly Notices of the Royal Astronomical Society* 440.1, pp. 75–88. DOI: 10.1093/mnras/stu259 (cit. on p. 30).

Barnes, J. and P. Hut (Dec. 1986). "A hierarchical $\mathcal{O}(NlogN)$ force-calculation algorithm". In: *Nature* 324.6096, pp. 446–449. DOI: 10.1038/324446a0 (cit. on p. 60).

Barreira, A. et al. (Aug. 2015). "Weak lensing by voids in modified lensing potentials". In: *Journal of Cosmology and Astroparticle Physics* 2015.08, pp. 028–028. DOI: 10.1088/1475-7516/2015/08/028 (cit. on p. 75).

Beisbart, C. (2009). "Can We Justifiably Assume the Cosmological Principle in Order to Break Model Underdetermination in Cosmology?" In: *Journal for General Philosophy of Science / Zeitschrift für allgemeine Wissenschaftstheorie* 40.2, pp. 175–205. URL: http://www.jstor.org/stable/20722507 (cit. on p. 8).

Bernardeau, F. (Nov. 1994a). "The effects of smoothing on the statistical properties of large-scale cosmic fields." In: *Astronomy and Astrophysics* 291, pp. 697–712 (cit. on p. 71).

— (May 1994b). "The Nonlinear Evolution of Rare Events". In: *Astrophysical Journal* 427, p. 51. DOI: 10.1086/174121 (cit. on pp. 88, 94, 101).

Blumenthal, G. R. et al. (Apr. 1992). "The Largest Possible Voids". In: *The Astrophysical Journal* 388, p. 234. DOI: 10.1086/171147 (cit. on p. 4).

Bolejko, K. et al. (Jan. 2013). "Anti-lensing: The Bright Side of Voids". In: *Physical Review Letters* 110.2. DOI: 10.1103/physrevlett.110.021302.

Bond, J.R. et al. (Oct. 1991). "Excursion Set Mass Functions for Hierarchical Gaussian Fluctuations". In: *The Astrophysical Journal* 379, p. 440. DOI: 10.1086/170520 (cit. on p. 63).

Bos, E. G. P. et al. (Sept. 2012a). "The darkness that shaped the void: dark energy and cosmic voids". In: *Monthly Notices of the Royal Astronomical Society* 426.1, pp. 440–461. DOI: 10.1111/j.1365-2966.2012.21478.x.

Bos, E. G. P. et al. (Oct. 2012b). "The darkness that shaped the void: dark energy and cosmic voids". In: *Monthly Notices of the Royal Astronomical Society* 426.1, pp. 440–461. DOI: 10.1111/j.1365-2966.2012.21478.x (cit. on p. 75).

Brandt, T. D. (June 2016). "Constraints on MACHO Dark Matter from compact stellar systems in ultra-faint dwarf galaxies". In: *The Astrophysical Journal* 824.2, p. L31. DOI: 10.3847/2041-8205/824/2/l31.

Brax, P. and P. Valageas (July 2013). "Impact on the power spectrum of screening in modified gravity scenarios". In: *Physical Review D* 88.2. DOI: 10.1103/physrevd.88.023527 (cit. on p. 32).

— (July 2014). "K-mouflage cosmology: The background evolution". In: *Physical Review D* 90.2. DOI: 10.1103/physrevd.90.023507.

Cai, Y.-C., N. Padilla, and B. Li (June 2015). "Testing gravity using cosmic voids". In: *Monthly Notices of the Royal Astronomical Society* 451.1, pp. 1036–1055. DOI: 10.1093/mnras/stv777 (cit. on p. 75).

Carr, B. and F. Kuhnel (2021). *Primordial Black Holes as Dark Matter Candidates*. DOI: 10.48550/ARXIV.2110.02821 (cit. on p. 29).

Carson, Z. and K. Yagi (2021). "Testing General Relativity with Gravitational Waves". In: *Handbook of Gravitational Wave Astronomy*, p. 9. DOI: 10.1007/978-981-15-4702-7_41-1.

Casado, J. (Jan. 2020). "Linear expansion models vs. standard cosmologies: a critical and historical overview". In: *Astrophysics and Space Science* 365.1, p. 16. DOI: 10.1007/s10509-019-3720-z (cit. on p. 25).

Castorina, E. et al. (July 2015). "DEMNUni: the clustering of large-scale structures in the presence of massive neutrinos". In: *Journal of Cosmology and Astroparticle Physics* 2015.07, pp. 043–043. DOI: 10.1088/1475-7516/2015/07/043 (cit. on p. 3).

Cautun, M. et al. (July 2014). "Evolution of the cosmic web". In: *Monthly Notices of the Royal Astronomical Society* 441.4, pp. 2923–2973. DOI: 10.1093/mnras/stu768 (cit. on p. 3).

Cautun, M. et al. (May 2018). "The Santiago-Harvard-Edinburgh-Durham void comparison - I. SHEDding light on chameleon gravity tests". In: *Monthly Notices of the Royal Astronomical Society* 476.3, pp. 3195–3217. DOI: 10.1093/mnras/sty463. arXiv: 1710.01730 [astro-ph.CO] (cit. on p. 62).

Chan, K. C., N. Hamaus, and M. Biagetti (June 2019). "Constraint of void bias on primordial non-Gaussianity". In: *Physical Review D* 99.12. DOI: 10.1103/physrevd.99.121304.

Chan, K. C. et al. (Jan. 2020). "Measurement of Void Bias Using Separate Universe Simulations". In: *The Astrophysical Journal* 889.2, p. 89. DOI: 10.3847/1538-4357/ab64ec.

Chan, K.C., N. Hamaus, and V. Desjacques (Nov. 2014). "Large-scale clustering of cosmic voids". In: *Physical Review D* 90.10. DOI: 10.1103/physrevd.90.103521 (cit. on pp. 1, 70, 71, 73, 75, 89, 99, 101, 125).

Chapline, G. F. and P. H. Frampton (Nov. 2016). "A new direction for dark matter research: intermediate-mass compact halo objects". In: *Journal of Cosmology and Astroparticle Physics* 2016.11, pp. 042–042. DOI: 10.1088/1475-7516/2016/11/042.

Clampitt, J., Y.-C. Cai, and B. Li (May 2013). "Voids in modified gravity: excursion set predictions". In: *Monthly Notices of the Royal Astronomical Society* 431.1, pp. 749–766. DOI: 10.1093/mnras/stt219 (cit. on p. 75).

Clampitt, J. and B. Jain (Oct. 2015). "Lensing measurements of the mass distribution in SDSS voids". In: *Monthly Notices of the Royal Astronomical Society* 454.4, pp. 3357–3365. DOI: 10.1093/mnras/stv2215.

Clampitt, J., B. Jain, and C. Sánchez (Jan. 2016). "Clustering and bias measurements of SDSS voids". In: *Monthly Notices of the Royal Astronomical Society* 456.4, pp. 4425–4431. DOI: 10.1093/mnras/stv2933 (cit. on p. 69).

Clifton, T. et al. (Mar. 2012). "Modified gravity and cosmology". In: *Physics Reports* 513.1, pp. 1–189. DOI: 10.1016/j.physrep.2012.01.001.

Coil, A.L. (2013). "The Large-Scale Structure of the Universe". In: *Planets, Stars and Stellar Systems*. Springer Netherlands, pp. 387–421. DOI: 10.1007/978-94-007-5609-0_8 (cit. on p. 4).

Coles, P. and B. Jones (Jan. 1991). "A lognormal model for the cosmological mass distribution". In: *Monthly Notices of the Royal Astronomical Society* 248, pp. 1–13. DOI: 10.1093/mnras/248.1.1 (cit. on p. 46).

Coles, P. and F. Lucchin (2002). *Cosmology. The Origin and Evolution of Cosmic Structure*. 2nd ed. John Wiley Sons Inc (cit. on pp. 7, 12, 21, 59).

Contarini, S. et al. (July 2019). "Cosmological exploitation of the size function of cosmic voids identified in the distribution of biased tracers". In: *Monthly Notices of the Royal Astronomical Society* 488.3, pp. 3526–3540. DOI: 10.1093/mnras/stz1989 (cit. on pp. 1, 2, 4, 75, 93, 119).

Contarini, S. et al. (Apr. 2021). "Cosmic voids in modified gravity models with massive neutrinos". In: *Monthly Notices of the Royal Astronomical Society* 504.4, pp. 5021–5038. DOI: 10.1093/mnras/stab1112 (cit. on pp. 4, 81, 89).

Contarini, S. et al. (May 2022). “Euclid: Cosmological forecasts from the void size function”. In: *arXiv e-prints* (cit. on pp. 1, 2, 75, 93, 119).

Correa, C. M. et al. (Jan. 2021). “Redshift-space effects in voids and their impact on cosmological tests. Part I: the void size function”. In: *Monthly Notices of the Royal Astronomical Society* 500.1, pp. 911–925. DOI: 10.1093/mnras/staa3252 (cit. on p. 75).

Crocce, M. et al. (Apr. 2010). “Simulating the Universe with MICE: the abundance of massive clusters”. In: *Monthly Notices of the Royal Astronomical Society* 403.3, pp. 1353–1367. DOI: 10.1111/j.1365-2966.2009.16194.x (cit. on p. 58).

Davari, Z., V. Marra, and M. Malekjani (Nov. 2019). “Cosmological constrains on minimally and non-minimally coupled scalar field models”. In: *Monthly Notices of the Royal Astronomical Society*. DOI: 10.1093/mnras/stz3096 (cit. on p. 31).

Davies, C. T., M. Cautun, and B. Li (July 2018). “Weak lensing by voids in weak lensing maps”. In: *Monthly Notices of the Royal Astronomical Society: Letters* 480.1, pp. L101–L105. DOI: 10.1093/mnrasl/sly135.

— (Oct. 2019). “Cosmological test of gravity using weak lensing voids”. In: *Monthly Notices of the Royal Astronomical Society* 490.4, pp. 4907–4917. DOI: 10.1093/mnras/stz2933.

Davies, C. T. et al. (Aug. 2021a). “Constraining cosmology with weak lensing voids”. In: *Monthly Notices of the Royal Astronomical Society*. DOI: 10.1093/mnras/stab2251 (cit. on p. 62).

— (2021b). “Cosmological forecasts with the clustering of weak lensing peaks”. In: DOI: 10.48550/ARXIV.2110.10164.

Davis, M. et al. (May 1985). “The evolution of large-scale structure in a universe dominated by cold dark matter”. In: *Astrophysical Journal* 292, pp. 371–394. DOI: 10.1086/163168.

Dawson, K. S. et al. (Jan. 2013). “The Baryon Oscillation Spectroscopic Survey of SDSS-III”. In: *Astronomical Journal* 145.1, p. 10. DOI: 10.1088/0004-6256/145/1/10 (cit. on p. 61).

de Cruz Pérez, J. (May 2021). “Implications of Dynamical Dark Energy in the expansion of the Universe and the Structure Formation”. In: *arXiv e-prints*. arXiv: 2105.14800 (cit. on p. 33).

de Sitter, W. (July 1916a). “On Einstein’s Theory of Gravitation and its Astronomical Consequences. First Paper”. In: *Monthly Notices of the Royal Astronomical Society* 76.9, pp. 699–728. DOI: 10.1093/mnras/76.9.699.

— (Dec. 1916b). “On Einstein’s Theory of Gravitation and its Astronomical Consequences. Second Paper.” In: *Monthly Notices of the Royal Astronomical Society* 77.2, pp. 155–184. DOI: 10.1093/mnras/77.2.155.

— (Nov. 1917). “On Einstein’s Theory of Gravitation and its Astronomical Consequences. Third Paper.” In: *Monthly Notices of the Royal Astronomical Society* 78.1, pp. 3–28. DOI: 10.1093/mnras/78.1.3 (cit. on p. 17).

Delva, P. et al. (Dec. 2018). “Gravitational Redshift Test Using Eccentric Galileo Satellites”. In: *Physical Review Letters* 121.23. DOI: 10.1103/physrevlett.121.231101 (cit. on p. 26).

Dentler, Mona et al. (2021). *Fuzzy Dark Matter and the Dark Energy Survey Year 1 Data*. DOI: 10.48550/ARXIV.2111.01199. URL: https://arxiv.org/abs/2111.01199 (cit. on p. 29).

Desjacques, V., D. Jeong, and F. Schmidt (Feb. 2018). "Large-scale galaxy bias". In: *Physics Reports* 733, pp. 1–193. DOI: 10.1016/j.physrep.2017.12.002 (cit. on p. 74).

Despali, G et al. (Mar. 2016). "The universality of the virial halo mass function and models for non-universality of other halo definitions". In: *Monthly Notices of the Royal Astronomical Society* 456.3, pp. 2486–2504. DOI: 10.1093/mnras/stv2842 (cit. on pp. 58, 82).

Di Valentino, E. et al. (Sept. 2021). "Snowmass2021 - Letter of interest cosmology intertwined II: The hubble constant tension". In: *Astroparticle Physics* 131, p. 102605. DOI: 10.1016/j.astropartphys.2021.102605 (cit. on p. 30).

Dijkstra, M. (Oct. 2014). "Lyα Emitting Galaxies as a Probe of Reionisation". In: *Publications of the Astronomical Society of Australia* 31, e040, e040. DOI: 10.1017/pasa.2014.33 (cit. on p. 3).

Dolag, Klaus (Aug. 2015). "The Magneticum Simulations, from Galaxies to Galaxy Clusters". In: *IAU General Assembly*. Vol. 29, p. 2250156 (cit. on p. 61).

Efstathiou, G. and S. Gratton (May 2020). "The evidence for a spatially flat Universe". In: *Monthly Notices of the Royal Astronomical Society: Letters* 496.1, pp. L91–L95. DOI: 10.1093/mnrasl/slaa093 (cit. on p. 44).

Efstathiou, G. et al. (Feb. 1985). "Numerical techniques for large cosmological N-body simulations". In: *The Astrophysical Journal Supplement* 57, pp. 241–260. DOI: 10.1086/191003 (cit. on p. 60).

Einstein, A. (Jan. 1915). "Zur allgemeinen Relativitätstheorie". In: *Sitzungsberichte der Königlich Preußischen Akademie der Wissenschaften (Berlin)*, pp. 778–786 (cit. on p. 8).

— (Jan. 1917). "Kosmologische Betrachtungen zur allgemeinen Relativitätstheorie". In: *Sitzungsberichte der Königlich Preußischen Akademie der Wissenschaften (Berlin)*, pp. 142–152 (cit. on p. 16).

Eisenstein, D. J. and W. Hu (Mar. 1998). "Baryonic Features in the Matter Transfer Function". In: *Astrophysical Journal* 496.2, pp. 605–614. DOI: 10.1086/305424 (cit. on p. 70).

Ellis, R. S. (2010). "Gravitational lensing: a unique probe of dark matter and dark energy". In: *Phil. Trans. R. Soc. A.* URL: http://doi.org/10.1098/rsta.2009.0209 (cit. on p. 29).

Elyiv, A. et al. (Mar. 2015). "Cosmic voids detection without density measurements". In: *Monthly Notices of the Royal Astronomical Society* 448.1, pp. 642–653. DOI: 10.1093/mnras/stv043 (cit. on p. 62).

Elyiv, A.A. et al. (July 2013). "Low-density structures in the Local Universe. II. Nearby cosmic voids". In: *Astrophysical Bulletin*. DOI: 10.1134/S199034131301001X (cit. on p. 62).

Etherington, I.M.H. (Jan. 1933). "On the Definition of Distance in General Relativity." In: *Philosophical Magazine* 15.18, p. 761 (cit. on p. 15).

Euclid Collaboration et al. (Oct. 2020). "Euclid preparation. VII. Forecast validation for Euclid cosmological probes". In: *Astronomy & Astrophysics* 642, A191. DOI: 10.1051/0004-6361/202038071 (cit. on p. 61).

Falck, B. et al. (Apr. 2018). "Using voids to unscreen modified gravity". In: *Monthly Notices of the Royal Astronomical Society* 475.3, pp. 3262–3272. DOI: 10.1093/mnras/stx3288 (cit. on p. 75).

Finelli, F. et al. (Jan. 2016). "Supervoids in the WISE-2MASS catalogue imprinting cold spots in the cosmic microwave background". In: *Monthly Notices of the Royal Astronomical Society* 455.2, pp. 1246–1256. DOI: 10.1093/mnras/stv2388 (cit. on p. 67).

Forero-Romero, J. E. et al. (July 2009). "A dynamical classification of the cosmic web". In: *Monthly Notices of the Royal Astronomical Society* 396.3, pp. 1815–1824. DOI: 10.1111/j.1365-2966.2009.14885.x (cit. on p. 62).

Friedmann, A. (Jan. 1922). "Über die Krümmung des Raumes". In: *Zeitschrift fur Physik* 10, pp. 377–386. DOI: 10.1007/BF01332580 (cit. on p. 16).

FUCHS, B. (May 2003). "CONSTRAINTS ON THE DECOMPOSITION OF THE ROTATION CURVES OF SPIRAL GALAXIES". In: *The Identification of Dark Matter*. WORLD SCIENTIFIC. DOI: 10.1142/9789812791313_0010.

Fuchs, B. (2000). *The Amount of Dark Matter in Spiral Galaxies*. DOI: 10.48550/ARXIV.ASTRO-PH/0010358 (cit. on p. 29).

Fukuda, Y. et al. (Aug. 1998). "Evidence for Oscillation of Atmospheric Neutrinos". In: *Physical Review Letters* 81.8, pp. 1562–1567. DOI: 10.1103/PhysRevLett.81.1562 (cit. on p. 31).

García-Farieta, J.E. et al. (July 2019). "Clustering and redshift-space distortions in modified gravity models with massive neutrinos". In: *Monthly Notices of the Royal Astronomical Society* 488.2, pp. 1987–2000. DOI: 10.1093/mnras/stz1850 (cit. on pp. 3, 80).

García, R. and E. Rozo (Nov. 2019). "Halo exclusion criteria impacts halo statistics". In: *Monthly Notices of the Royal Astronomical Society* 489.3, pp. 4170–4175. DOI: 10.1093/mnras/stz2458 (cit. on p. 71).

Giocoli, C., M. Baldi, and L. Moscardini (Dec. 2018). "Weak lensing light-cones in modified gravity simulations with and without massive neutrinos". In: *Monthly Notices of the Royal Astronomical Society* 481.2. DOI: 10.1093/mnras/sty2465 (cit. on pp. 30, 61, 79, 80).

Giocoli, C. et al. (July 2015). "Disentangling dark sector models using weak lensing statistics". In: *Monthly Notices of the Royal Astronomical Society* 452.3, pp. 2757–2772. DOI: 10.1093/mnras/stv1473.

Green, J. et al. (Aug. 2012). "Wide-Field InfraRed Survey Telescope (WFIRST) Final Report". In: *arXiv e-prints* (cit. on p. 61).

Griest, K. (June 1993). "The Search for the Dark Matter: WIMPs and MACHOs". In: *Annals of the New York Academy of Sciences* 688.1, pp. 390–407. DOI: 10.1111/j.1749-6632.1993.tb43912.x.

Gunn, J. E. and J. R. Gott (Aug. 1972). "On the Infall of Matter Into Clusters of Galaxies and Some Effects on Their Evolution". In: *Astrophysical Journ* 176, p. 1. DOI: 10.1086/151605 (cit. on p. 47).

Gupta, S. et al. (Feb. 2022). "Universality of the halo mass function in modified gravity cosmologies". In: *Physical Review D* 105.4. DOI: 10.1103/physrevd.105.043538 (cit. on pp. 82, 83).

Guth, A. H. (Jan. 1981). "Inflationary universe: A possible solution to the horizon and flatness problems". In: *Physical Review D* 23.2, pp. 347–356. DOI: 10.1103/PhysRevD.23.347.

— (2004). "Inflation". In: *Measuring and Modeling the Universe*. Ed. by W.L. Freedman (Cambridge: Cambridge Univ. Press). Vol. 2. Carnegie Observatories Astrophysics Series. URL:

https://sites.astro.caltech.edu/~ccs/Ay21/guth_inflation.pdf (cit. on p. 37).

Hagstotz, S. et al. (Sept. 2019a). "Breaking cosmic degeneracies: Disentangling neutrinos and modified gravity with kinematic information". In: *Astronomy & Astrophysics* 629, A46. DOI: 10.1051/0004-6361/201935213 (cit. on p. 81).

Hagstotz, S. et al. (July 2019b). "Joint halo-mass function for modified gravity and massive neutrinos - I. Simulations and cosmological forecasts". In: *Monthly Notices of the Royal Astronomical Society* 486.3, pp. 3927–3941. DOI: 10.1093/mnras/stz1051 (cit. on p. 80).

Hamaus, N. (2017). *COSMIC VOIDS - Lecture notes for the Lecture Series on Cosmology, held on June 29th 2017 at MPA in Garching*.

Hamaus, N., P. M. Sutter, and B. D. Wandelt (2014a). "Modeling cosmic void statistics". In: DOI: 10.48550/ARXIV.1409.7621.

— (June 2014b). "Universal Density Profile for Cosmic Voids". In: *Physical Review Letters* 112.25. DOI: 10.1103/physrevlett.112.251302 (cit. on pp. 67, 68).

Hamaus, N. et al. (Jan. 2014c). "Cosmology with Void-Galaxy Correlations". In: *Physical Review Letters* 112.4. DOI: 10.1103/physrevlett.112.041304 (cit. on p. 74).

Hamaus, N. et al. (Dec. 2014d). "Testing cosmic geometry without dynamic distortions using voids". In: *Journal of Cosmology and Astroparticle Physics* 2014.12, pp. 013–013. DOI: 10.1088/1475-7516/2014/12/013.

— (Nov. 2015). "Probing cosmology and gravity with redshift-space distortions around voids". In: *Journal of Cosmology and Astroparticle Physics* 2015.11, 036, p. 036. DOI: 10.1088/1475-7516/2015/11/036 (cit. on p. 74).

Hamaus, N. et al. (Aug. 2016). "Constraints on Cosmology and Gravity from the Dynamics of Voids". In: *Phys. Rev. Lett.* 117 (9), p. 091302. DOI: 10.1103/PhysRevLett.117.091302.

Hamaus, N. et al. (July 2017). "Multipole analysis of redshift-space distortions around cosmic voids". In: *Journal of Cosmology and Astroparticle Physics* 2017.07, pp. 014–014. DOI: 10.1088/1475-7516/2017/07/014 (cit. on p. 88).

Hamaus, N. et al. (Dec. 2020). "Precision cosmology with voids in the final BOSS data". In: *Journal of Cosmology and Astroparticle Physics* 2020.12, pp. 023–023. DOI: 10.1088/1475-7516/2020/12/023 (cit. on pp. 75, 76, 88).

Hamaus, N. et al. (Feb. 2022). "Euclid: Forecasts from redshift-space distortions and the Alcock-Paczynski test with cosmic voids". In: *Astronomy and Astrophysics* 658, A20. DOI: 10.1051/0004-6361/202142073 (cit. on pp. 75, 88).

Hansen, J. P. and I. McDonald (2006). *Theory of Simple Liquids*. Academic Press, Amsterdam (cit. on p. 72).

Hatfield, P.W. et al. (Apr. 2018). "The environment and host haloes of the brightest z ∼ 6 Lyman-break galaxies". In: *Monthly Notices of the Royal Astronomical Society* 477.3, pp. 3760–3774. DOI: 10.1093/mnras/sty856.

Heavens, A. et al. (Sept. 2017). "No Evidence for Extensions to the Standard Cosmological Model". In: *Physical Review Letters* 119.10. DOI: 10.1103/physrevlett.119.101301 (cit. on p. 3).

Hockney, R. W. and J. W. Eastwood (1981). *Computer Simulation Using Particles* (cit. on p. 60).

Hogg, D.W. and D. Foreman-Mackey (May 2018). "Data Analysis Recipes: Using Markov Chain Monte Carlo". In: *The Astrophysical Journal Supplement Series* 236.1, p. 11. DOI: 10.3847/1538-4365/aab76e.

Hu, W., R. Barkana, and A. Gruzinov (Aug. 2000). "Fuzzy Cold Dark Matter: The Wave Properties of Ultralight Particles". In: *Physical Review Letters* 85.6, pp. 1158–1161. DOI: 10.1103/physrevlett.85.1158 (cit. on p. 29).

Hu, W. and I. Sawicki (Sept. 2007). "Models of f(R) cosmic acceleration that evade solar system tests". In: *Physical Review D* 76.6. DOI: 10.1103/physrevd.76.064004 (cit. on pp. 32, 33).

Hubble, E. (Mar. 1929). "A Relation between Distance and Radial Velocity among Extra-Galactic Nebulae". In: *Proceedings of the National Academy of Science* 15.3, pp. 168–173. DOI: 10.1073/pnas.15.3.168 (cit. on p. 11).

Icke, V. (Jan. 1984). "Voids and filaments". In: *Monthly Notices of the Royal Astronomical Society* 206.1, 1P–3P. DOI: 10.1093/mnras/206.1.1P (cit. on p. 61).

Jamieson, D. and M. Loverde (Dec. 2019). "Separate universe void bias". In: *Physical Review D* 100.12. DOI: 10.1103/physrevd.100.123528.

Jenkins, A. et al. (Feb. 2001). "The mass function of dark matter haloes". In: *Monthly Notices of the Royal Astronomical Society* 321.2, pp. 372–384. DOI: 10.1046/j.1365-8711.2001.04029.x (cit. on p. 58).

Jennings, E., Y. Li, and W. Hu (July 2013). "The abundance of voids and the excursion set formalism". In: *Monthly Notices of the Royal Astronomical Society* 434.3, pp. 2167–2181. DOI: 10.1093/mnras/stt1169 (cit. on pp. 1, 66, 70, 88, 89, 97).

Joyce, A. et al. (Mar. 2015). "Beyond the cosmological standard model". In: *Physics Reports* 568, pp. 1–98. DOI: 10.1016/j.physrep.2014.12.002.

Kaiser, N. (Sept. 1984). "On the spatial correlations of Abell clusters." In: *Astrophysical Journal Letters* 284, pp. L9–L12. DOI: 10.1086/184341 (cit. on p. 56).

Kerscher, M., I. Szapudi, and A. S. Szalay (May 2000). "A Comparison of Estimators for the Two-Point Correlation Function". In: *Astrophysical Journal, Letters* 535.1, pp. L13–L16. DOI: 10.1086/312702 (cit. on p. 69).

Khoury, J. and A. Weltman (Feb. 2004). "Chameleon cosmology". In: *Physical Review D* 69.4, p. 044026. DOI: 10.1103/PhysRevD.69.044026 (cit. on p. 80).

Kobayashi, T. et al. (Dec. 2017). "Lyman-α constraints on ultralight scalar dark matter: implications for the early and late universe". In: *Physical Review D* 96.12. DOI: 10.1103/physrevd.96.123514 (cit. on p. 30).

Komatsu, E. et al. (Jan. 2011). "Seven-Year Wilkinson Microwave Anisotropy Probe (WMAP) observations: cosmological interpretation". In: *The Astrophysical Journal Supplement Series* 192.2, p. 18. DOI: 10.1088/0067-0049/192/2/18 (cit. on p. 30).

Kovács, A. et al. (Feb. 2022). "The DES view of the Eridanus supervoid and the CMB cold spot". In: *Monthly Notices of the Royal Astronomical Society* 510.1, pp. 216–229. DOI: 10.1093/mnras/stab3309 (cit. on p. 75).

Krause, E. et al. (Dec. 2012). "The weight of emptiness: the gravitational lensing signal of stacked voids". In: *The Astrophysical Journal* 762.2, p. L20. DOI: 10.1088/2041-8205/762/2/l20 (cit. on p. 75).

Kreisch, C. D. et al. (July 2019). "Massive neutrinos leave fingerprints on cosmic voids". In: *Monthly Notices of the Royal Astronomical Society* 488.3, pp. 4413–4426. DOI: 10.1093/mnras/stz1944 (cit. on pp. 69, 75).

Kreisch, C. D. et al. (2021). "The GIGANTES dataset: precision cosmology from voids in the machine learning era". In: DOI: 10.48550/ARXIV.2107.02304.

Lambiase, G. et al. (Feb. 2019). "Testing dark energy models in the light of σ_8 tension". In: *European Physical Journal C* 79.2, p. 141. DOI: 10.1140/epjc/s10052-019-6634-6 (cit. on p. 30).

Landy, S. D. and A. S. Szalay (July 1993). "Bias and Variance of Angular Correlation Functions". In: *The Astrophysical Journal* 412, p. 64. DOI: 10.1086/172900 (cit. on p. 69).

Lares, M. et al. (Apr. 2017). "The sparkling Universe: clustering of voids and void clumps". In: *Monthly Notices of the Royal Astronomical Society* 468.4, pp. 4822–4830. DOI: 10.1093/mnras/stx825.

Laureijs, R. et al. (Oct. 2011). "Euclid Definition Study Report". In: *arXiv e-prints* (cit. on p. 61).

Lavaux, G. and B. D. Wandelt (Apr. 2010). "Precision cosmology with voids: definition, methods, dynamics". In: *Monthly Notices of the Royal Astronomical Society* 403.3, pp. 1392–1408. DOI: 10.1111/j.1365-2966.2010.16197.x (cit. on p. 62).

— (July 2012). "Precision cosmography with stacked voids". In: *The Astrophysical Journal* 754.2, p. 109. DOI: 10.1088/0004-637x/754/2/109 (cit. on pp. 75, 88).

Lee, J. and D. Park (May 2009). "Constraining the Dark Energy Equation of State with Cosmic Voids". In: *Astrophysical Journal, Letters* 696.1, pp. L10–L12. DOI: 10.1088/0004-637X/696/1/L10 (cit. on p. 75).

Lewis, A., A. Challinor, and A. Lasenby (Aug. 2000). "Efficient Computation of Cosmic Microwave Background Anisotropies in Closed Friedmann-Robertson-Walker Models". In: *Astrophysical Journal* 538.2, pp. 473–476. DOI: 10.1086/309179 (cit. on p. 70).

Li, Z., P. Wu, and H. Yu (Feb. 2011). "COSMOLOGICAL-MODEL-INDEPENDENT TESTS FOR THE DISTANCE–DUALITY RELATION FROM GALAXY CLUSTERS AND TYPE Ia SUPERNOVA". In: *The Astrophysical Journal* 729.1, p. L14. DOI: 10.1088/2041-8205/729/1/l14 (cit. on p. 15).

Liang, Y. et al. (Apr. 2016). "Measuring baryon acoustic oscillations from the clustering of voids". In: *Monthly Notices of the Royal Astronomical Society* 459.4, pp. 4020–4028. DOI: 10.1093/mnras/stw884.

Liao, K. (Nov. 2019). "The Cosmic Distance Duality Relation with Strong Lensing and Gravitational Waves: An Opacity-free Test". In: *The Astrophysical Journal* 885.1, p. 70. DOI: 10.3847/1538-4357/ab4819 (cit. on p. 15).

Linde, A. (2007). "Inflationary Cosmology". In: *Inflationary Cosmology*. Springer Berlin Heidelberg, pp. 1–54. DOI: 10.1007/978-3-540-74353-8_1 (cit. on p. 38).

Lineweaver, C. et al. (Jan. 1997). "Constraints on h, Ω_b and λ_O from cosmic microwave background observations". In: *Astronomy Astrophysics* 322, pp. 365–374 (cit. on p. 107).

Lorenz, C. S., E. Calabrese, and D. Alonso (Aug. 2017). "Distinguishing between neutrinos and time-varying dark energy through cosmic time". In: *Physical Review D* 96.4, p. 043510. DOI: 10.1103/PhysRevD.96.043510 (cit. on p. 30).

LSST Dark Energy Science Collaboration (Nov. 2012). "Large Synoptic Survey Telescope: Dark Energy Science Collaboration". In: *arXiv e-prints* (cit. on p. 61).

Mandelbaum, R. et al. (Apr. 2013). "Cosmological parameter constraints from galaxy–galaxy lensing and galaxy clustering with the SDSS DR7". In: *Monthly Notices of the Royal Astronomical Society* 432.2, pp. 1544–1575. DOI: 10.1093/mnras/stt572 (cit. on p. 30).

Marulli, F., A. Veropalumbo, and M. Moresco (Jan. 2016). "CosmoBolognaLib: C++ libraries for cosmological calculations". In: *Astronomy and Computing* 14, pp. 35–42. DOI: 10.1016/j.ascom.2016.01.005 (cit. on pp. 4, 79).

Marulli, F. et al. (Oct. 2012). "Cosmology with clustering anisotropies: disentangling dynamic and geometric distortions in galaxy redshift surveys". In: *Monthly Notices of the Royal Astronomical Society* 426.3, pp. 2566–2580. DOI: 10.1111/j.1365-2966.2012.21875.x (cit. on p. 3).

Marulli, F. et al. (Mar. 2017). "Redshift-space distortions of galaxies, clusters and AGN:" in: *Astronomy & Astrophysics* 599, A106. DOI: 10.1051/0004-6361/201526885 (cit. on p. 3).

Marulli, F. et al. (Nov. 2018). "The XXL Survey. XVI. The clustering of X-ray selected galaxy clusters at z 0.3". In: *Astronomy & Astrophysics* 620, A1. DOI: 10.1051/0004-6361/201833238.

Marulli, F. et al. (Oct. 2021). "C^3 Cluster Clustering Cosmology I. New Constraints on the Cosmic Growth Rate at $z \sim 0.3$ from Redshift-space Clustering Anisotropies". In: *Astrophysical Journal* 920.1, p. 13. DOI: 10.3847/1538-4357/ac0e8c.

Massara, E. et al. (Nov. 2015). "Voids in massive neutrino cosmologies". In: *Journal of Cosmology and Astroparticle Physics* 2015.11, pp. 018–018. DOI: 10.1088/1475-7516/2015/11/018 (cit. on pp. 69, 75).

Melchior, P. et al. (Apr. 2014). "First measurement of gravitational lensing by cosmic voids in SDSS". In: *Monthly Notices of the Royal Astronomical Society* 440.4, pp. 2922–2927. DOI: 10.1093/mnras/stu456.

Meszaros, P. (Dec. 1974). "The behaviour of point masses in an expanding cosmological substratum." In: *Astronomy and Astrophysics* (cit. on pp. 45, 54).

Micheletti, D. et al. (Oct. 2014). "The VIMOS Public Extragalactic Redshift Survey. Searching for cosmic voids". In: *Astronomy & Astrophysics* 570, A106. DOI: 10.1051/0004-6361/201424107 (cit. on p. 62).

Misner, C.W., Thorne K.S., and J.A. Wheeler (1973). *Gravitation*. W.H. Freeman and Company, San Francisco (cit. on p. 8).

Mo, H. J. and S. D. M. White (Sept. 1996). "An analytic model for the spatial clustering of dark matter haloes". In: *Monthly Notices of the Royal Astronomical Society* 282.2, pp. 347–361. DOI: 10.1093/mnras/282.2.347 (cit. on p. 56).

Mohajan, H. (Nov. 2017). "A Brief Analysis of de Sitter Universe in Relativistic Cosmology". In: *JOURNAL OF SCIENTIFIC ACHIEVEMENTS* 2, pp. 1–17 (cit. on p. 17).

Mukherjee, S., B. D. Wandelt, and J. Silk (Mar. 2021). "Testing the general theory of relativity using gravitational wave propagation from dark standard sirens". In: *Monthly Notices of the Royal Astronomical Society* 502.1, pp. 1136–1144. DOI: 10.1093/mnras/stab001 (cit. on p. 26).

Nadathur, S. et al. (June 2015). "Self-similarity and universality of void density profiles in simulation and SDSS data". In: *Monthly Notices of the Royal Astronomical Society* 449.4, pp. 3997–4009. DOI: 10.1093/mnras/stv513 (cit. on p. 67).

Nadathur, S. et al. (July 2019). "Beyond BAO: Improving cosmological constraints from BOSS data with measurement of the void-galaxy cross-correlation". In: *Physical Review D* 100.2, p. 023504. DOI: 10.1103/PhysRevD.100.023504 (cit. on p. 75).

Nadolny, T. et al. (Nov. 2021). "A new way to test the Cosmological Principle: measuring our peculiar velocity and the large-scale anisotropy independently". In: *Journal of Cosmology and Astroparticle Physics* 2021.11, p. 009. DOI: 10.1088/1475-7516/2021/11/009 (cit. on p. 8).

Nelson, D. et al. (May 2019). "The IllustrisTNG simulations: public data release". In: *Computational Astrophysics and Cosmology* 6.1, p. 2. DOI: 10.1186/s40668-019-0028-x (cit. on p. 61).

Neyrinck, M. C. (June 2008). "ZOBOV: a parameter-free void-finding algorithm". In: *Monthly Notices of the Royal Astronomical Society* 386.4, pp. 2101–2109. DOI: 10.1111/j.1365-2966.2008.13180.x (cit. on pp. 62, 86).

Nezbeda, I. (Feb. 1974). "Analytic solution of Percus-Yevick equation for fluid of hard spheres". In: *Czechoslovak Journal of Physics - CZECH J PHYS* 24, pp. 55–62. DOI: 10.1007/BF01596443.

Norberg, P. et al. (June 2009). "Statistical analysis of galaxy surveys - I. Robust error estimation for two-point clustering statistics". In: *Monthly Notices of the Royal Astronomical Society* 396.1, pp. 19–38. DOI: 10.1111/j.1365-2966.2009.14389.x (cit. on p. 3).

Novosyadlyj, B. and M. Tsizh (Mar. 2017). "Voids in the Cosmic Web as a probe of dark energy". In: *Condensed Matter Physics* 20.1, p. 13901. DOI: 10.5488/cmp.20.13901 (cit. on p. 3).

Paczyński, B. (Sept. 1996). "Gravitational microlensing in the local group". In: *Annual Review of Astronomy and Astrophysics* 34.1, pp. 419–459. DOI: 10.1146/annurev.astro.34.1.419 (cit. on p. 29).

Pan, Supriya et al. (Nov. 2019). "Interacting scenarios with dynamical dark energy: Observational constraints and alleviation of the H_0". In: *Physical Review D* 100.10. DOI: 10.1103/physrevd.100.103520 (cit. on p. 30).

Peebles, P. J. E. and M. G. Hauser (Nov. 1974). "Statistical Analysis of Catalogs of Extragalactic Objects. III. The Shane-Wirtanen and Zwicky Catalogs". In: *Astrophysical Journal, Supplement* 28, p. 19. DOI: 10.1086/190308 (cit. on p. 69).

Peel, A. et al. (July 2019). "Distinguishing standard and modified gravity cosmologies with machine learning". In: *Physical Review D* 100.2, p. 023508. DOI: 10.1103/PhysRevD.100.023508 (cit. on p. 81).

Perico, E. L. D. et al. (Nov. 2019a). "Cosmic voids in modified gravity scenarios". In: *Astronomy & Astrophysics* 632, A52. DOI: 10.1051/0004-6361/201935949.

— (Dec. 2019b). "Cosmic voids in modified gravity scenarios". In: *Astronomy and Astrophysics* 632, A52. DOI: 10.1051/0004-6361/201935949 (cit. on p. 75).

Perlmutter, S. et al. (June 1999). "Measurements of Ω and Λ from 42 High-Redshift Supernovae". In: *The Astrophysical Journal* 517.2, pp. 565–586. DOI: 10.1086/307221 (cit. on pp. 4, 20).

Pisani, A., P.M. Sutter, and B.D. Wandelt (June 2015a). "Mastering the effects of peculiar velocities in cosmic voids". In: *arXiv e-prints*, arXiv:1506.07982, arXiv:1506.07982. eprint: 1506.07982 (astro-ph.CO).

Pisani, A. et al. (Oct. 2015b). "Counting voids to probe dark energy". In: *Physical Review D* 92.8, 083531. DOI: 10.1103/PhysRevD.92.083531.

Pisani, A. et al. (2019). "Cosmic voids: a novel probe to shed light on our Universe". In: DOI: 10.48550/ARXIV.1903.05161 (cit. on pp. 4, 61).

Planck Collaboration et al. (2016). "Planck 2015 results - XIII. Cosmological parameters". In: *Astronomy & Astrophysics* 594, A13. DOI: 10.1051/0004-6361/201525830 (cit. on pp. 80, 103).

Planck Collaboration et al. (2020a). "Planck 2018 results - I. Overview and the cosmological legacy of Planck". In: *Astronomy & Astrophysics* 641, A1. DOI: 10.1051/0004-6361/201833880.

Planck Collaboration et al. (2020b). "Planck 2018 results - V. CMB power spectra and likelihoods". In: *Astronomy & Astrophysics* 641, A5. DOI: 10.1051/0004-6361/201936386.

Planck Collaboration et al. (Sept. 2020c). "Planck 2018 results. VI. Cosmological parameters". In: *Astronomy & Astrophysics* 641, A6. DOI: 10.1051/0004-6361/201833910 (cit. on pp. 3, 26, 30, 54, 76).

Platen, E., R. van de Weygaert, and B.J.T. Jones (Sept. 2007). "A cosmic watershed: the WVF void detection technique". In: *Monthly Notices of the Royal Astronomical Society* 380.2, pp. 551–570. DOI: 10.1111/j.1365-2966.2007.12125.x (cit. on pp. 4, 62, 86, 87).

Pollina, G. et al. (Nov. 2015). "Cosmic voids in coupled dark energy cosmologies: the impact of halo bias". In: *Monthly Notices of the Royal Astronomical Society* 455.3, pp. 3075–3085. DOI: 10.1093/mnras/stv2503 (cit. on p. 75).

Pollina, G. et al. (Apr. 2017). "On the linearity of tracer bias around voids". In: *Monthly Notices of the Royal Astronomical Society* 469.1, pp. 787–799. DOI: 10.1093/mnras/stx785 (cit. on p. 93).

Pollina, G. et al. (May 2019). "On the relative bias of void tracers in the Dark Energy Survey". In: *Monthly Notices of the Royal Astronomical Society* 487.2, pp. 2836–2852. DOI: 10.1093/mnras/stz1470 (cit. on p. 93).

Press, W. H. and P. Schechter (Feb. 1974). "Formation of Galaxies and Clusters of Galaxies by Self-Similar Gravitational Condensation". In: *Astrophysical Journal* 187, pp. 425–438. DOI: 10.1086/152650 (cit. on pp. 57, 81).

Puchwein, E., M. Baldi, and V. Springel (Nov. 2013). "Modified-Gravity-GADGET: a new code for cosmological hydrodynamical simulations of modified gravity models". In: *Monthly Notices of the Royal Astronomical Society* 436.1, pp. 348–360. DOI: 10.1093/mnras/stt1575 (cit. on p. 80).

Rassat, A. et al. (Aug. 2014). "Planck CMB anomalies: astrophysical and cosmological secondary effects and the curse of masking". In: *Journal of Cosmology and Astroparticle Physics* 2014.08, pp. 006–006. DOI: 10.1088/1475-7516/2014/08/006 (cit. on p. 3).

Riess, A.G. et al. (Sept. 1998). "Observational Evidence from Supernovae for an Accelerating Universe and a Cosmological Constant". In: *The Astrophysical Journal* 116.3, pp. 1009–1038. DOI: 10.1086/300499 (cit. on pp. 4, 20, 30).

Ronconi, T. and F. Marulli (Oct. 2017). "Cosmological exploitation of cosmic void statistics". In: *Astronomy & Astrophysics* 607, A24. DOI: 10.1051/0004-6361/201730852 (cit. on pp. 63, 88, 89).

Ronconi, T. et al. (Aug. 2019). "Cosmic voids uncovered – first-order statistics of depressions in the biased density field". In: *Monthly Notices of the Royal Astronomical Society* 488.4, pp. 5075–5084. DOI: 10.1093/mnras/stz2115.

Roszkowski, L., E. M. Sessolo, and S. Trojanowski (May 2018). "WIMP dark matter candidates and searches—current status and future prospects". In: *Reports on Progress in Physics* 81.6, p. 066201. DOI: 10.1088/1361-6633/aab913 (cit. on p. 29).

Ryden, B. (2016). *Introduction to Cosmology*. Cambridge University Press (cit. on p. 55).

Sahlén, M. and J. Silk (May 2018). "Cluster-void degeneracy breaking: Modified gravity in the balance". In: *Physical Review D* 97.10, 103504, p. 103504. DOI: 10.1103/PhysRevD.97.103504.

Sahlén, M., Í. Zubeldıa, and J. Silk (Mar. 2016). "Cluster-Void Degeneracy Breaking: Dark Energy, Planck, and the Largest Cluster and Void". In: *Astrophysical Journal, Letters* 820.1, p. L7. DOI: 10.3847/2041-8205/820/1/L7 (cit. on p. 75).

Sakstein, J. and M. Trodden (Apr. 2020). "Early Dark Energy from Massive Neutrinos as a Natural Resolution of the Hubble Tension". In: *Physical Review Letters* 124.16, p. 161301. DOI: 10.1103/PhysRevLett.124.161301 (cit. on p. 30).

Sánchez, A.G. (Dec. 2020). "Arguments against using h^{-1} Mpc units in observational cosmology". In: *Physical Review D* 102.12, p. 123511. DOI: 10.1103/PhysRevD.102.123511 (cit. on p. 12).

Sánchez, C. et al. (Oct. 2016). "Cosmic voids and void lensing in the Dark Energy Survey Science Verification data". In: *Monthly Notices of the Royal Astronomical Society* 465.1, pp. 746–759. DOI: 10.1093/mnras/stw2745 (cit. on pp. 62, 75).

Schaye, J. et al. (Jan. 2015). "The EAGLE project: simulating the evolution and assembly of galaxies and their environments". In: *Monthly Notices of the Royal Astronomical Society* 446.1, pp. 521–554. DOI: 10.1093/mnras/stu2058 (cit. on p. 61).

Schmidt, B.P. et al. (Nov. 1998). "The High-Z Supernova Search: Measuring Cosmic Deceleration and Global Curvature of the Universe Using Type IA Supernovae". In: *The Astrophysical Journal* 507.1, pp. 46–63. DOI: 10.1086/306308 (cit. on p. 4).

Schneider, P. (2006). "Weak Gravitational Lensing". In: *Saas-Fee Advanced Courses*. Springer Berlin Heidelberg, pp. 269–451. DOI: 10.1007/978-3-540-30310-7_3.

Schramm, D. N. (Oct. 1982). "Constraints on the Density of Baryons in the Universe". In: *Philosophical Transactions of the Royal Society of London Series A* 307.1497, pp. 43–53. DOI: 10.1098/rsta.1982.0099 (cit. on p. 107).

Schuster, N. et al. (Dec. 2019). "The bias of cosmic voids in the presence of massive neutrinos". In: *Journal of Cosmology and Astroparticle Physics* 2019.12, pp. 055–055. DOI: 10.1088/1475-7516/2019/12/055.

Schwarz, D.J. (Sept. 2009). "Thoughts on the Cosmological Principle". In: *Fundamental Interactions*. WORLD SCIENTIFIC, pp. 267–276. DOI: 10.1142/9789814277839_0015 (cit. on p. 8).

Secrest, N.J. et al. (Feb. 2021). "A Test of the Cosmological Principle with Quasars". In: *The Astrophysical Journal Letters* 908.2, p. L51. DOI: 10.3847/2041-8213/abdd40 (cit. on pp. 8, 10).

Sereno, M. et al. (Apr. 2015). "New constraints on σ_8 from a joint analysis of stacked gravitational lensing and clustering of galaxy clusters". In: *Monthly Notices of the Royal Astronomical Society* 449.4, pp. 4147–4161. DOI: 10.1093/mnras/stv280 (cit. on p. 3).

Shafieloo, A. and C. Clarkson (Apr. 2010). "Model independent tests of the standard cosmological model". In: *Physical Review D* 81.8. DOI: 10.1103/physrevd.81.083537 (cit. on p. 3).

Sheth, R. K. and G. Tormen (Sept. 1999). "Large-scale bias and the peak background split". In: *Monthly Notices of the Royal Astronomical Society* 308.1, pp. 119–126. DOI: 10.1046/j.1365-8711.1999.02692.x (cit. on p. 70).

Sheth, R. K. and R. van de Weygaert (May 2004). "A hierarchy of voids: much ado about nothing". In: *Monthly Notices of the Royal Astronomical Society* 350.2, pp. 517–538. DOI: 10.1111/j.1365-2966.2004.07661.x (cit. on pp. 64, 65, 71).

Sheth, R.K., H.J. Mo, and G. Tormen (May 2001). "Ellipsoidal collapse and an improved model for the number and spatial distribution of dark matter haloes". In: *Monthly Notices of the Royal Astronomical Society* 323.1, pp. 1–12. DOI: 10.1046/j.1365-8711.2001.04006.x (cit. on p. 82).

Sheth, R.K. and G. Tormen (Jan. 2002). "An excursion set model of hierarchical clustering: ellipsoidal collapse and the moving barrier". In: *Monthly Notices of the Royal Astronomical Society* 329.1, pp. 61–75. DOI: 10.1046/j.1365-8711.2002.04950.x (cit. on p. 57).

Snedden, A. et al. (Nov. 2015). "Star formation and gas phase history of the cosmic web". In: *Monthly Notices of the Royal Astronomical Society* 455.3, pp. 2804–2825. DOI: 10.1093/mnras/stv2421 (cit. on p. 35).

Sola Peracaula, Joan, Javier de Cruz Perez, and Adria Gomez-Valent (June 2016). "Dynamical dark energy versus Λ =const. in light of observations". In: *arXiv e-prints*. arXiv: 1606.00450 (cit. on p. 31).

Speagle, J.S. (2019). "A Conceptual Introduction to Markov Chain Monte Carlo Methods". In: DOI: 10.48550/ARXIV.1909.12313.

Spolyar, D., M. Sahlén, and J. Silk (Dec. 2013). "Topology and Dark Energy: Testing Gravity in Voids". In: *Physical Review Letters* 111.24. DOI: 10.1103/physrevlett.111.241103.

Springel, V. (Dec. 2005). "The cosmological simulation code GADGET-2". In: *Monthly Notices of the Royal Astronomical Society* 364.4, pp. 1105–1134. DOI: 10.1111/j.1365-2966.2005.09655.x (cit. on p. 80).

Springel, V. et al. (June 2005). "Simulations of the formation, evolution and clustering of galaxies and quasars". In: *Nature* 435.7042, pp. 629–636. DOI: 10.1038/nature03597.

Steigman, G., N. Hata, and J. E. Felten (Jan. 1999). "Nonnucleosynthetic Constraints on the Baryon Density and Other Cosmological Parameters". In: *Astrophysical Journal* 510.2, pp. 564–575. DOI: 10.1086/306589 (cit. on p. 107).

Steiner, F. (Dec. 2007). "Solution of the Friedmann equation determining the time evolution, acceleration and the age of the Universe". In: URL: https://www.uni-ulm.de/fileadmin/website_uni_ulm/nawi.inst.260/paper/08/tp08-7.pdf (cit. on p. 50).

Suto, Y., K. Sato, and H. Sato (May 1984). "Expansion of Voids in a Matter-Dominated Universe". In: *Progress of Theoretical Physics* 71.5, pp. 938–945. DOI: 10.1143/PTP.71.938.

Sutter, P.M. et al. (Oct. 2014a). "A measurement of the Alcock-Paczyński effect using cosmic voids in the SDSS". In: *Monthly Notices of the Royal Astronomical Society* 443.4, pp. 2983–2990. DOI: 10.1093/mnras/stu1392.

Sutter, P.M. et al. (June 2014b). "Sparse sampling, galaxy bias, and voids". In: *Monthly Notices of the Royal Astronomical Society* 442.1, pp. 462–471. DOI: 10.1093/mnras/stu893.

Sutter, P.M. et al. (Jan. 2015a). "On the observability of coupled dark energy with cosmic voids". In: *Monthly Notices of the Royal Astronomical Society* 446, pp. L1–L5. DOI: 10.1093/mnrasl/slu155.

Sutter, P.M. et al. (Mar. 2015b). "VIDE: The Void IDentification and Examination toolkit". In: *Astronomy and Computing* 9. DOI: 10.1016/j.ascom.2014.10.002 (cit. on pp. 62, 85).

Szapudi, I. and A. S. Szalay (Feb. 1998). "A New Class of Estimators for the N-Point Correlations". In: *The Astrophysical Journal* 494.1, pp. L41–L44. DOI: 10.1086/311146 (cit. on p. 74).

Szapudi, I. et al. (Apr. 2015). "Detection of a supervoid aligned with the cold spot of the cosmic microwave background". In: *Monthly Notices of the Royal Astronomical Society* 450.1, pp. 288–294. DOI: 10.1093/mnras/stv488 (cit. on p. 4).

Tikhonov, A. V. and I. D. Karachentsev (Dec. 2006). "Minivoids in the Local Volume". In: *The Astrophysical Journal* 653.2, pp. 969–976. DOI: 10.1086/508981 (cit. on p. 4).

Tinker, J. et al. (Dec. 2008). "Toward a Halo Mass Function for Precision Cosmology: The Limits of Universality". In: *Astrophysical Journal* 688.2, pp. 709–728. DOI: 10.1086/591439 (cit. on pp. 58, 82–84).

Tormen, G., L. Moscardini, and N. Yoshida (June 2004). "Properties of cluster satellites in hydrodynamical simulations". In: *Monthly Notices of the Royal Astronomical Society* 350.4, pp. 1397–1408. DOI: 10.1111/j.1365-2966.2004.07736.x (cit. on p. 81).

Torquato, S. (2001). *Random Heterogeneous Materials: Mi- crostructure and Macroscopic Properties*. Springer-Verlag, New York (cit. on p. 72).

Tsujikawa, S. (Oct. 2013). "Quintessence: a review". In: *Classical and Quantum Gravity* 30.21, p. 214003. DOI: 10.1088/0264-9381/30/21/214003 (cit. on p. 31).

Tutusaus, I. et al. (Nov. 2020). "Euclid: The importance of galaxy clustering and weak lensing cross-correlations within the photometric Euclid survey". In: *Astronomy & Astrophysics* 643, A70. DOI: 10.1051/0004-6361/202038313 (cit. on p. 3).

van de Weygaert, R. and E. Platen (2011). "Cosmic voids: Structure, dynamics and galaxies". In: *International Journal of Modern Physics: Conference Series*. DOI: 10.1142/S2010194511000092.

van de Weygaert, R. and W. Schaap (2009). "The Cosmic Web: Geometric Analysis". In: *Data Analysis in Cosmology*. Ed. by V. J. Martínez et al. Vol. 665, pp. 291–413. DOI: 10.1007/978-3-540-44767-2_11 (cit. on p. 3).

van de Weygaert, R. and E. van Kampen (July 1993). "Voids in gravitational instability scenarios – I. Global density and velocity fields in an Einstein–de Sitter universe". In: *Monthly Notices of the Royal Astronomical Society* 263.2, pp. 481–526. DOI: 10.1093/mnras/263.2.481.

Vankov, A. A. (2010). *General Relativity Problem of Mercury's Perihelion Advance Revisited.* DOI: 10.48550/ARXIV.1008.1811 (cit. on p. 26).

Vanzella, E. et al. (Mar. 2020). "Candidate Population III stellar complex at z = 6.629 in the MUSE Deep Lensed Field". In: *Monthly Notices of the Royal Astronomical Society: Letters* 494.1, pp. L81–L85. DOI: 10.1093/mnrasl/slaa041.

Veropalumbo, A. et al. (June 2014). "An improved measurement of baryon acoustic oscillations from the correlation function of galaxy clusters at z $\sim$ 0.3". In: *Monthly Notices of the Royal Astronomical Society* 442.4, pp. 3275–3283. DOI: 10.1093/mnras/stu1050.

— (Feb. 2016). "Measuring the distance–redshift relation with the baryon acoustic oscillations of galaxy clusters". In: *Monthly Notices of the Royal Astronomical Society* 458.2, pp. 1909–1920. DOI: 10.1093/mnras/stw306.

Verza, G. et al. (Dec. 2019). "The void size function in dynamical dark energy cosmologies". In: *Journal of Cosmology and Astroparticle Physics* 2019.12, p. 040. DOI: 10.1088/1475-7516/2019/12/040 (cit. on pp. 75, 88).

Viel, M., M. G. Haehnelt, and V. Springel (June 2010). "The effect of neutrinos on the matter distribution as probed by the intergalactic medium". In: *Journal of Cosmology and Astroparticle Physics* 2010.6, p. 015. DOI: 10.1088/1475-7516/2010/06/015 (cit. on p. 80).

Vielzeuf, P. et al. (Oct. 2020). "Dark Energy Survey Year 1 results: the lensing imprint of cosmic voids on the cosmic microwave background". In: *Monthly Notices of the Royal Astronomical Society* 500.1, pp. 464–480. DOI: 10.1093/mnras/staa3231.

Villaescusa-Navarro, F. et al. (Sept. 2020). "The Quijote Simulations". In: *Astrophysical Journal, Supplement* 250.1, p. 2. DOI: 10.3847/1538-4365/ab9d82 (cit. on p. 61).

Voivodic, R., H. Rubira, and M. Lima (Oct. 2020). "The Halo Void (Dust) Model of large scale structure". In: *Journal of Cosmology and Astroparticle Physics* 2020.10, p. 033. DOI: 10.1088/1475-7516/2020/10/033 (cit. on p. 75).

Weinberg, D.H. et al. (May 2003). "The Lyman-α Forest as a Cosmological Tool". In: *The Emergence of Cosmic Structure*. Ed. by Stephen H. Holt and Christopher S. Reynolds. Vol. 666. American Institute of Physics Conference Series, pp. 157–169. DOI: 10.1063/1.1581786 (cit. on p. 3).

Weinberg, S. (Jan. 1989). "The cosmological constant problem". In: *Reviews of Modern Physics* 61.1, pp. 1–23. DOI: 10.1103/RevModPhys.61.1 (cit. on p. 28).

Wheeler, J.A. and K.W. Ford (1998). *Geons, Black Holes and Quantum Foam: A Life in Physics.* New York: Norton. (cit. on p. 8).

White, Martin (Apr. 2005). "Reducing the shear". In: *Astroparticle Physics* 23.3, pp. 349–354. DOI: 10.1016/j.astropartphys.2005.01.008.

Will, C.M. (June 2015). "The 1919 measurement of the deflection of light". In: *Classical and Quantum Gravity* 32.12, p. 124001. DOI: 10.1088/0264-9381/32/12/124001 (cit. on p. 26).

Young, S. and M. Musso (Nov. 2020). "Application of peaks theory to the abundance of primordial black holes". In: *Journal of Cosmology and Astroparticle Physics* 2020.11. DOI: 10.1088/1475-7516/2020/11/022 (cit. on p. 46).

Zel'dovich, Y. B. (Mar. 1970). "Gravitational instability: An approximate theory for large density perturbations." In: *Astronomy and Astrophysics* 5, pp. 84–89 (cit. on p. 46).

Zeldovich, Y.B. (Jan. 1972). "A hypothesis, unifying the structure and the entropy of the Universe". In: *Monthly Notices of the Royal Astronomical Society* 160, 1P. DOI: 10.1093/mnras/160.1.1P.

Zivick, P. et al. (June 2015). "Using cosmic voids to distinguish f(R) gravity in future galaxy surveys". In: *Monthly Notices of the Royal Astronomical Society* 451.4, pp. 4215–4222. DOI: 10.1093/mnras/stv1209.

Zwicky, F. (Oct. 1937). "On the Masses of Nebulae and of Clusters of Nebulae". In: *The Astrophysical Journal* 86, p. 217. DOI: 10.1086/143864 (cit. on p. 29).